MULTI-ACTION NITRIC OXIDE-RELEASE SYSTEMS FOR BIOMEDICAL APPLICATIONS

Sara Elizabeth Maloney

A dissertation submitted to the faculty at the University of North Carolina at Chapel Hill in partial fulfillment for the degree of Doctor of Philosophy in the Department of Chemistry (Analytical Division).

Chapel Hill
2021

Approved by:

Mark H. Schoenfisch

Jeffrey E. Dick

Leslie M. Hicks

Robert Maile

Shannon M. Wallet

ABSTRACT

Sara Elizabeth Maloney: Multi-action nitric oxide-release systems for biomedical applications
(Under the direction of Mark H. Schoenfisch)

Antibiotic-resistant bacterial infections pose a significant threat to global health. Limitations in treating resistant, biofilm-based, and polymicrobial infections necessitate the development of novel antimicrobial agents that limit the potential for resistance. Nitric oxide (NO), an endogenous signaling molecule, is involved in a host of physiological properties, including the eradication of foreign pathogens. As NO also possesses roles in modulating inflammation, angiogenesis, and thrombosis, it represents an attractive molecule for the multimodal treatment of chronic wound and catheter-based infections.

Hyaluronic acid (HA), a biopolymer involved in endogenous wound healing, was modified with a series of alkylamines to store and release NO, with release kinetics dependent upon the alkylamine structure. The NO-releasing HA derivatives exhibited broad-spectrum antibacterial efficacy against a range of wound pathogens, including *Pseudomonas aeruginosa* and *Staphylococcus aureus*. The biopolymers also exhibited antibiofilm action against *P. aeruginosa* biofilms. Nitric oxide-releasing HA was evaluated using an infected murine model and proved beneficial in accelerating wound healing and reducing bacterial burden.

Two glycosaminoglycans, HA and chondroitin sulfate (CS), were derivatized with alkylamines to form NO donors and compared regarding their wound healing properties. Both NO-releasing glycosaminoglycans exhibited bactericidal activity against antibiotic-susceptible

and multi-drug resistant strains of *P. aeruginosa* and *S. aureus*. The alkylamine identity, glycosaminoglycan identity, and NO-release capability were all found to influence skin cell proliferation and adhesion to the extracellular matrix. Owing to NO's anti-inflammatory properties, the NO-releasing glycosaminoglycans were found to mitigate activation of inflammatory pathways via Toll-like receptor 4. Comparison in an infected murine model demonstrated that NO-releasing CS outperformed HA in accelerating wound closure, with success attributed to both NO and the CS backbone.

Nitric oxide-releasing hemodialysis catheter lock solutions were prepared using low molecular weight NO donors with different NO-release profiles. Slow, sustained release of NO from the catheter surface was found to be superior to high NO flux in preventing bacterial and protein adhesion as well as removing pre-adhered bacteria from the surface, indicating the potential for this system to act as both a preventative and treatment strategy. Minimal toxicity of the catheter lock solutions was discovered toward mammalian cells.

To my parents –
for your love, support, and confidence that I would someday change the world

ACKNOWLEDGEMENTS

This dissertation was made possible through the support of many people. First, I would like to thank my graduate research advisor, Dr. Mark Schoenfisch, for always seeing what I was capable of, even when I couldn't. He was always there to push me to grow as a scientist, but always knew exactly when he had to switch gears and go into "dad mode" to deal with whatever crisis I was having that day. No matter what, I knew he always had my back, and for that, I am so grateful. I would also like to thank my undergraduate research advisor, Dr. Shannon Stitzel. Being a research scientist was never part of my plan, but when she asked me to join her research lab, I agreed. What started as a boost to my resume became something I was truly passionate about, and I would've never found that without her encouragement and support. Most people are lucky if they have one amazing research advisor. I have been so lucky to have two.

I would also like to thank my research collaborators. Dr. Rob Maile and Dr. Shannon Wallet taught me so much about wound healing and offered continuous support over many years of my grad school career. Through in vitro experiments and in vivo studies, Shannon was right by my side to make sure I had the data I needed to write this dissertation, even if it meant giving up her weekend to help me prove that the experiment itself didn't work and that it wasn't just me. I would also like to thank Dr. Prabir Roy-Chaudhury, who provided helpful insight and direction regarding the catheter work presented in this dissertation.

My ability to write this dissertation was supported by so many helpful professors I have met along the way. My love of chemistry was cultivated through learning experiences and interactions with many professors in Towson's chemistry program. As such, I would like to thank

Dr. Ryan Casey, Dr. Kelly Elkins, Dr. Mary Sajini Devadas, Dr. Ellen Hondrogiannis, and Dr. Beth Kautzman for all of their support early on in my chemistry career. At UNC, I had the opportunity to learn from and be supported by Dr. Jeffrey Dick, Dr. Jim Jorgenson, Dr. Gary Glish, and Dr. Leslie Hicks. They created an exceptional support system for me in the analytical division of UNC's Chemistry department.

Of course, this dissertation would not have been possible without the support from both past and present members of the Schoenfisch lab. When I first joined the lab in 2016, Shaylyn Walter made sure I was integrated into the lab seamlessly. I don't think she realizes just how important this was to me, and I am so thankful for her years of friendship. Dr. Mona Ahonen, the other half of the dream team, has always been right by my side. I am so thankful for her friendship and support throughout the years. I would like to extend a huge thanks to Dr. Evan Feura. From offering sage scientific wisdom, to letting me vent about every experiment gone wrong, to dealing with every life crisis that came up, he was always there for me when I needed him. I am thankful for Dr. Kaitlyn Rouillard and her years of being my bodyguard, shoulder to cry on, partner-in-crime, and best friend. I would also like to thank Dr. James Taylor. His selflessness and caring for others made him an amazing lab mate, and I will forever remember all of the times he dropped everything to make sure I was okay. I would like to extend a thank you to past lab members, Dr. Robert Soto, Dr. Dakota Suchyta, Dr. Micah Brown, Dr. Lei Yang, Dr. Jackson Hall, Dr. Maggie Malone-Povolny, Brian Tran, and Dr. Feichen Yang. I learned so much from each one of you, and I thank you for all for your advice and support. Thank you to the current lab members, Dr. Ivie Conlon, Taron Bradshaw, Kyle Nguyen, Sami Picciotti, Sarah Nagy, and Courtney Johnson, for making the remainder of my grad school experience full of antics and much less boring. A special thank you goes to Dr. Chris Broberg for all of his microbiology wisdom and being a great friend,

and to Quincy Grayton, who somehow managed to take on all of my lab responsibilities in addition to her own to keep things going smoothly after I'm gone. I have also had the pleasure of working with two incredible undergraduate students, Kyle McGrath and Daniel Soliman. Thank you so much for your hard work and dedication, and I know you will both succeed in whatever you do.

Finally, I need to thank my family and friends for their love and support through the years. Dr. Tessa Moyer, Dr. Tavleen Kochar, and Olivia Sanchez-Felix were the best squad I could've hoped for to make it through all of my graduate coursework. I am also so thankful that grad school introduced me to my best friend, Chad Lloyd. With him by my side, I knew I could make it through even the toughest of days. I would also like to thank Dr. Kathleen Nevins for being an amazing mentor and friend. To my best friend over the past 20+ years, Niki Stein, I send a huge thank you for always being there for me and being my biggest fan, no matter what.

I could not have made it this far without the support from my family. To my parents, Carolyn and Jim Maloney, thank you for giving me all of the tools I needed to succeed on this journey and for always being there for me. I believe I am the luckiest person alive to have them as my parents. I would like to thank my big sister and other half, Katie Maloney, for teaching me everything she learned in school when she learned it, even if it was 5 years ahead of what I should've been learning. She likes to think all of our basement school sessions are the reason I've made it here, and I don't think we have sufficient evidence to say she's not, so thank you. Lastly, I would like to thank my fiancé, Greyson Norcross. Through every up and down of grad school, he's been there to celebrate with me or make me feel better. I am thankful every day that I had you by my side through this journey. To my entire family, thank you, and I love you.

TABLE OF CONTENTS

LIST OF TABLES

LIST OF FIGURES

LIST OF ABBREVIATIONS AND SYMBOLS

$[NO]_{max}$	Maximum instantaneous nitric oxide concentration
$[NO]_t$	Total nitric oxide
$[NO]_{t,4h}$	Total nitric oxide released over 4 hours
%	Percent
°C	Degree(s) Celsius
<	Less than
>	Greater than
~	Approximately
≤	Less than or equal to
≥	Greater than or equal to
±	Standard deviation of the mean
×*g*	Times the force of gravity
$	U.S. dollar(s)
A. baumannii	*Acinetobacter baumannii*
Abs	Absorbance
agr	Accessory gene regulator
AHL	*N*-acylhomoserine lactone
ANOVA	Analysis of variance
Ar	Argon
ATCC	American Type Culture Collection
atm	Atmosphere(s)
ATR	Attenuated total reflection

AV	Arteriovenous
BSA	Bovine serum albumin
C. albicans	*Candida albicans*
CDC	Centers for Disease Control
CFU	Colony forming unit(s)
CHNS	Carbon hydrogen nitrogen sulfur analysis
cm	Centimeter(s)
cm^{-1}	Wavenumber(s)
cm^2	Centimeters squared
CO_2	Carbon dioxide
CS	Chondroitin sulfate
CSA	Chondroitin-4-sulfate
CSC	Chondroitin-6-sulfate
CT	Cycle threshold
Cyclic di-GMP	Bis-(3'-5')-cyclic dimeric guanosine monophosphate
d	Day(s)
Da	Dalton(s)
Đ	Dispersity
DAF-2 DA	4,5-diaminofluorescein diacetate
DBHD	Dibutylhexanediamine
DETA	Diethylenetriamine
DFU	Diabetic foot ulcer
DMEM	Dulbecco's modified Eagle's medium

DNA	Deoxyribonucleic acid
DPTA	Bis(3-aminopropyl)amine
DS	Dermatan sulfate
E. coli	*Escherichia coli*
E. faecalis	*Enterococcus faecalis*
e.g.	Exempli gratia (for example)
ECM	Extracellular matrix
EDC	1-ethyl-3-(3-dimethylaminopropyl)carbodiimide hydrochloride
ELSD	Evaporative light scattering detector
eNOS	Endothelial nitric oxide synthase
EPS	Exopolysaccharide
et al.	Et alia (and others)
FBS	Fetal bovine serum
FDA	Food and Drug Administration
FTIR	Fourier transform infrared spectroscopy
g	Gram(s)
GAG	Glycosaminoglycan
GlcA	D-glucuronic acid
GlcNAc	*N*-acetyl-D-glucosamine
GPC	Gel permeation chromatography
GSNO	*S*-nitrosoglutathione
h	Hour(s)
HA	Hyaluronic acid

HA50	50 kilodalton hyaluronic acid
HA6	6 kilodalton hyaluronic acid
HA90	90 kilodalton hyaluronic acid
HBOT	Hyperbaric oxygen therapy
HCl	Hydrochloric acid
HDF	Human dermal fibroblast
HEDA	*N*-(2-hydroxyethyl)ethylenediamine
HEK	Human epidermal keratinocyte
HGF	Human gingival fibroblast
HNO_2	Nitrous acid
HOK	Human oral keratinocyte
HPLC	High performance liquid chromatography
HS	Heparan sulfate
i.e.	Id est (that is)
IC_{50}	Inhibitory concentration in 50% of the population
IL	Interleukin
IMP	Integral membrane protein
iNOS	Inducible nitric oxide synthase
kDa	Kilodalton(s)
kg	Kilogram(s)
KS	Keratin sulfate
L	Liter(s)
LC/MS	Liquid chromatography mass spectrometry

LPS	Lipopolysaccharide
M	Molar
MALS	Multi-angle light scattering
MBC_{4h}	Minimum bactericidal concentration at 4 hours
$MBEC_{24h}$	Minimum biofilm eradication concentration at 24 hours
MDa	Megadalton(s)
MDR-PA	Multidrug-resistant *Pseudomonas aeruginosa*
mg	Milligram(s)
MHB	Mueller Hinton II broth
MHz	Megahertz
MIC_{24h}	Minimum inhibitory concentration at 24 hours
min	Minute(s)
mL	Milliliter(s)
mM	Millimolar
mm	Millimeter(s)
mm Hg	Millimeter of mercury
MMP	Matrix metalloprotease
mol	Mole(s)
MRSA	Methicillin-resistant *Staphylococcus aureus*
MSD	Mass spectrometer detector
MTS	3-(4,5-dimethylthiazol-2-yl)-5-(3-carboxymethoxyphenyl)-2-(4-sulfophenyl)-2H-tetrazolium inner salt
MW	Molecular weight
M_w	Weight-average molecular weight

MΩ	Megaohm(s)
N_2	Nitrogen gas
N_2O_3	Dinitrogen trioxide
Na_2EDTA	Ethylenediaminetetraacetic acid disodium salt dihydrate
NaN_3	Sodium azide
$NaNO_3$	Sodium nitrate
NaOH	Sodium hydroxide
NaOMe	Sodium methoxide
NF-κB	Nuclear factor kappa B
ng	Nanogram(s)
NHS	*N*-hydroxysuccinimide
NIH	National Institutes of Health
nM	Nanomolar
nm	Nanometer(s)
NMR	Nuclear magnetic resonance
nNOS	Neuronal nitric oxide synthase
NO	Nitric oxide
NO_2	Nitrogen dioxide
NO_2^-	Nitrite
NOA	Nitric oxide analyzer
NONOate	*N*-diazeniumdiolate
NOS	Nitric oxide synthase
NPWT	Negative-pressure wound therapy
O_2	Oxygen

O_2^-	Superoxide
OD	Optical density
OMP	Outer membrane protein
$OONO^-$	Peroxynitrite
P. aeruginosa	*Pseudomonas aeruginosa*
PAPA	*N*-propyl-1,3-propanediamine
PBS	Phosphate buffered saline
PEG	Poly(ethylene glycol)
pH	-Log of proton concentration
pM	Picomolar
pmol	Picomole(s)
PMS	Phenazine methosulfate
ppb	Parts per billion
ppm	Parts per million
PROLI	Proline
PS	Penicillin streptomycin
psig	Pounds per square inch gauge
PTFE	Polytetrafluoroethylene
PVA	Poly(vinyl alcohol)
qPCR	Quantitative polymerase chain reaction
QS	Quorum sensing
rEGF	Human recombinant epidermal growth factor
RHAMM	Receptor for HA-mediated motility

RNS	Reactive nitrogen species
ROS	Reactive oxygen species
rpm	Revolutions per minute
rRNA	Ribosomal ribonucleic acid
RSNO	*S*-nitrosothiol
s	Second(s)
S. aureus	*Staphylococcus aureus*
S. epidermidis	*Staphylococcus epidermidis*
SDS	Sodium dodecyl sulfate
SEAP	Secreted embryonic alkaline phosphatase
SFM	Serum-free medium
SNAC	*S*-nitroso-*N*-acetylcysteine
SNAP	*S*-nitrosopenicillamine
spp.	Several species
STZ	Streptozotocin
SWF	Simulated wound fluid
$t_{1/2}$	Half-life
t[NO]	Total NO release
$t[NO]_{theor}$	Theoretical NO total
$t[NO]_{72h}$	72 h total NO release
t_d	Duration
TDC	Tunneled dialysis catheter
TGF-α	Transforming growth factor alpha

TLR	Toll-like receptor
TNF-α	Tumor necrosis factor alpha
TSA	Tryptic soy agar
TSB	Tryptic soy broth
UV-Vis	Ultraviolet-Visible
V	Volt(s)
v/v	Volume to volume ratio
v/v/v	Volume to volume to volume ratio
vol%	Volume percent
wt%	Weight percent
µg	Microgram(s)
µL	Microliter(s)
µM	Micromolar
µm	Micrometer(s)
µmol	Micromole(s)

CHAPTER 1: CHALLENGES OF TREATING BACTERIAL INFECTIONS

1.1. Bacterial infections

Bacterial infections, especially those that do not respond to traditional antibiotic therapies, pose a tremendous threat to global health. Treatment with conventional antibiotics fails when bacteria develop resistance to specific antibiotic agents, as is the case for multidrug-resistant *Pseudomonas aeruginosa* and methicillin-resistant *Staphylococcus aureus* (MRSA), both of which are currently reported as serious threats by the Centers for Disease Control (CDC).[1,2] The formation of biofilms, which are cooperative communities of bacteria encased in a protective exopolysaccharide (EPS) matrix, provides an alternative or additional route to evading eradication by antibiotics, as bacteria within the biofilm are significantly more difficult to treat due to protection afforded by the EPS matrix.[3,4] Further, most bacterial infections are not a result of a single bacterial species, but instead, are a conglomeration of multiple bacterial species, each of which may require treatment with different antibiotic agents.[5–7] In developing new prevention and treatment strategies for bacterial infections, specifically those residing adjacent to or on biotic surfaces (e.g., chronic wound infections) and on biomedical devices (e.g., hemodialysis catheter infections), it is imperative to first consider the challenges in managing antibiotic resistant, biofilm-based, and polymicrobial infections.

1.1.1. Antibiotic resistance mechanisms

Antibiotics exert activity against bacteria by disrupting either a specific cellular component (e.g., cell membrane) or biosynthetic pathway (e.g., cell membrane synthesis, protein synthesis, nucleic acid synthesis).[8] However, resistance mechanisms have been discovered for nearly all antibiotics developed to date.[2] Two pathogens, *Acinetobacter baumannii* and *Mycobacterium tuberculosis*, have already produced globally resistant strains.[9] While these two pathogens represent just a small fraction of existing bacteria, they highlight the evolving nature of the antibiotic resistance crisis. As antibiotics continue to be incorrectly prescribed, over-prescribed, and heavily used in the livestock industry, which indirectly leads to human consumption, threats of antibiotic resistance will only worsen.[2] Potentiating this issue, pharmaceutical industries have either stopped or slowed their research and development of new antibiotics as a result of economic and regulatory obstacles. When new antibiotics are discovered, they are often saved as the last line of defense in order to prevent the development of resistance, even though resistance is understood to be inevitable.[2,9,10] Understanding the causes and mechanisms behind bacterial resistance is necessary in order to design antimicrobial agents that are not rendered ineffective by such developments.

Certain bacteria species are innately resistant to one or more classes of antimicrobial agents.[11] This innate resistance is most commonly seen in Gram-negative bacteria, as they are intrinsically less permeable to many antibiotics due to the presence of an outer phospholipid bilayer (Figure 1.1).[12,13] However, the ramifications of acquired resistance are of much greater concern than those of innate resistance.[11] Acquired resistance can occur spontaneously through a genetic mutation, allowing treatment with the antibiotic agent to eradicate all susceptible bacteria, leaving behind only the resistant bacteria to proliferate and thrive.[2,14] This process can lead to the

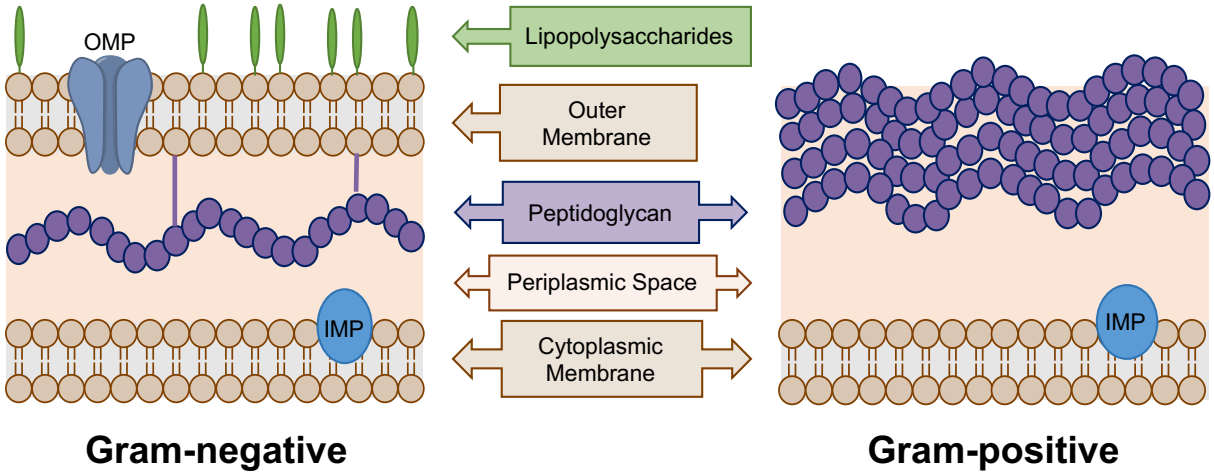

Figure 1.1 Depiction of Gram-negative and Gram-positive cell envelopes: OMP = outer membrane protein (e.g., porin); IMP = integral membrane protein.

development of a particular strain of resistant bacteria, but acquired resistance can also be transferred among different species of bacteria through horizontal gene transfer, generating multiple resistant bacterial species from a single mutation.[2,11,14,15]

Resistant bacterial strains (both Gram-positive and Gram-negative) have reduced susceptibility to antimicrobial agents through multiple mechanisms, including intracellular drug removal via efflux pumps, modified or protected drug target sites, and drug inactivation via production of inactivating enzymes.[16] Bacterial species produce efflux pumps, which may be substrate-specific or have broad activity.[12,14] Efflux pumps actively transport antibiotic agents out of the cell prior to the antibiotic reaching its target site and are a major contributor to intrinsic resistance in Gram-negative bacteria.[11,12] Alternatively, bacteria may acquire genes that encode enzymes (e.g., β-lactamases) that inactivate certain antibiotics before they are able to exert their effect.[11,14] These enzymes inactivate antibiotics via the addition of specific chemical moieties (e.g., phosphorylation, acetylation, or adenylation) or by destruction (e.g., hydrolysis).[14,17] Lastly, bacteria can evolve to either protect the target site (i.e., where the antibiotic binds) by blocking access to the site or altering the site to decrease the binding affinity of the antibiotic.[11,12,14] Several mechanisms exist for these processes, such as the production of altered cell membranes that no longer contain the binding site of the antibiotic or mutations that lead to downregulated porin genes, limiting access of antibiotics to intracellular targets.[11] Target site changes are among the most common mechanisms of resistance, affecting several classes of antibiotics.[14]

1.1.2. Biofilm formation

In addition to the potential for acquired resistance through the described mechanisms, the propensity of bacteria to exist in biofilms rather than in their planktonic form confers additional

resistance to conventional antibiotics. Biofilms are aggregates of microorganisms embedded within a self-produced EPS matrix that are adherent to each other and/or a surface.[18] The National Institutes of Health (NIH) estimates that more than 80% of persistent bacterial infections are caused by biofilms, highlighting the need for therapies targeted at biofilm disruption and eradication.[3]

Adherent biofilms, or those attached to biotic or abiotic surfaces, are formed through multiple processes (Figure 1.2A).[19,20] On surfaces, biofilm formation is initiated by reversible adhesion or adsorption, where the bacteria population (single- or multi-species) remains in an equilibrium between adhered and suspended cells.[21,22] Attached cells begin to produce an EPS matrix due to the stimulation of membrane-bound sensory proteins, allowing for the development of cell-to-cell bridges that bind the cells to each other and the surface, resulting in irreversible attachment.[22] Irreversibly-bound bacteria begin to grow and divide, forming microcolonies.[15,22,23] Production of the EPS matrix continues, leading to large bacterial aggregates called towers.[23] Of note, the EPS matrix is primarily composed of water (~98%) with solid components including polysaccharides (e.g., alginate), extracellular DNA, proteins, and lipids.[3,15,18,19,24] Biofilm dispersal occurs when bacteria return to a planktonic state due to internal or external stimuli (e.g., expression of virulence factors, enzymatic degradation of EPS, cyclic di-GMP concentration).[19,23] Bacteria can be released via three major dispersal methods: swarming dispersal, where individual bacterial cells are released; clumping dispersal, where aggregates of bacteria are shed as clumps; and, surface dispersal, where biofilm structures move across surfaces.[15,22,25] Released planktonic bacteria are then able to colonize new surfaces, restarting the biofilm formation process.

An important distinction must be made between biofilms that are on the surface of abiotic medical implants versus those associated with biotic surfaces. For medical devices or implants,

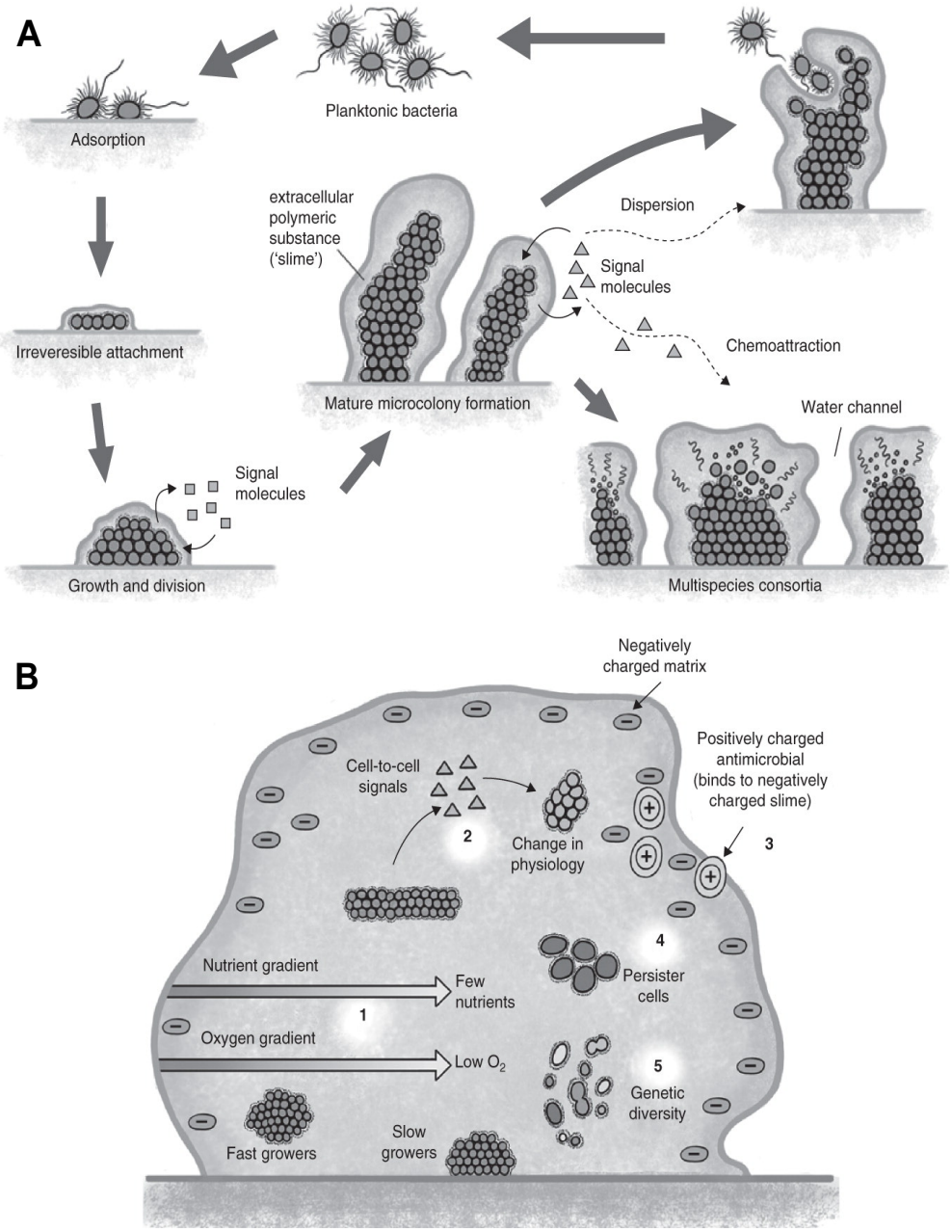

Figure 1.2 (A) Growth and development of biofilms. Planktonic bacteria go through a cycle of reversible adherence, tight adherence, and microcolony formation under regulation of specific cell-cell communication. The center figure shows microcolony formation seen in biofilms. The lower right figure demonstrates polymicrobial biofilms formed through specific cell-cell signaling and attraction. The upper right figure demonstrates the mechanism of biofilm spread where cells become motile, swim away as a planktonic population, and again repeat the cycle. **(B)** Multifactorial mechanisms that contribute to antibiotic tolerance developed within a biofilm. Reprinted with permission from Ceri et al. Copyright 2010, Taylor & Francis.

adhered biofilms represent a significant challenge.[23] However, in the context of chronic wounds or cystic fibrosis, for example, bacterial aggregates have been found adjacent to biotic surfaces in the exudate of chronic wounds or in the mucus layer of the lungs rather than directly attached to the tissue.[26,27] Studies have demonstrated that planktonic aggregates of *P. aeruginosa* possess similar properties, including dispersal mechanisms and production of the EPS matrix, to traditionally adherent biofilms and are therefore classified as non-adherent biofilms.[28,29] For the purposes of this dissertation research, both adherent and non-adherent biofilms are utilized where appropriate.

1.1.3. Protective mechanisms of biofilms

The formation of a biofilm almost always leads to a large increase in antibiotic resistance.[16,30] However, the aforementioned mechanisms of antibiotic resistance, such as efflux pumps, inactivating enzymes, and target modifications, are not fully responsible for the resistance observed with biofilm-based bacteria. When bacteria are dispersed from biofilms in their planktonic form, they typically become susceptible to antibiotic agents that they were resistant to in their biofilm form, suggesting that the resistance of biofilm-based bacteria is not due to mutations but instead is environmentally controlled.[4] Proposed mechanisms of biofilm resistance include chemical gradients, cell-to-cell communication, protection by the EPS matrix, adaptive stress responses, and genetic diversity.[20]

The EPS matrix hinders the diffusion of nutrients and gases into the biofilm, preventing deeply embedded bacteria from growing and dividing as actively as bacteria at the surface (Figure 1.2B, label #1).[20,31] Nutrient and gas gradients can lead to slowed, anaerobic growth or metabolic inactivation.[16,31,32] Even in a single species biofilm, a significant amount of heterogeneity is found

with respect to growth rates.[32] Decreased growth rates can have devastating effects for antibiotic efficacy, as many antibiotics, such as penicillins, require active bacterial growth to be effective.[32] Reduced growth rates also decrease the rate at which antibiotics are taken into the bacteria, thus reducing the inactivation kinetics of the drug.[15,33] Not only do these chemical gradients affect the growth of cells, indirectly resulting in decreased antibiotic efficacy, they can also directly impact the ability of the antibiotic to exert its target action. For example, oxygen availability is known to modulate aminoglycoside efficacy.[4,32] Local accumulation of acidic waste products can lead to pH differences throughout the biofilm, which is also known to negatively impact the activity of certain antibiotics.[4,32]

Bacteria embedded within biofilms communicate with each other via quorum sensing (Figure 1.2B, label #2). Quorum sensing allows bacteria to alter their gene expression profile and physiological processes as a result of population density and environmental changes.[19,31] This communication allows the bacteria to survive collectively as a community. For example, bacteria can suppress the expression of virulence factors until the bacteria reach a high enough density to prevent the host from clearing a growing biofilm and overcome the host immune system.[31] Quorum sensing mechanisms have been discovered in both Gram-negative and Gram-positive bacteria species. Many Gram-negative bacteria communicate by signaling of *N*-acylhomoserine lactone (AHL), which coordinates behavior during invasion and colonization.[3,34] On the other hand, Gram-positive bacteria can signal using various mechanisms, such as small peptides or exploitation of the accessory gene regulator (agr).[3,34] Regardless of mechanistic pathway, this cell-to-cell communication confers a strong advantage to biofilms in evading antibiotic therapy by facilitating advantageous changes in gene expression and physiological processes.

Antibiotics and host immune cells are often trapped by the EPS matrix and unable to diffuse through the biofilm to reach the bacterial cells (Figure 1.2B, label #3).[16,20,31,32] Charged components in the EPS matrix (e.g., polysaccharides, glycoproteins, etc.) can bind antibiotics, preventing further diffusion and action.[19,20] For example, the EPS matrix of *P. aeruginosa* has been shown to bind tobramycin.[15,35] The EPS matrix can also slow diffusion by limiting the rate of transport through the biofilm, though a decrease in mobility is insufficient to explain the high level of antibiotic resistance common to biofilms.[15,32,36] A combination of decreased antibiotic diffusion in addition to inactivation and sequestration of antibiotics by EPS matrix components is hypothesized to partially explain biofilm resistance.

Bacteria are equipped with many stress responses that facilitate adaptation to environmental factors, including abrupt temperature changes, oxidative stress, and starvation.[32] Nutrient- and oxygen-limited zones, such as those present deep in the biofilm, provide necessary environmental cues for bacteria to upregulate their stress responses and switch their metabolic pathways from growth to persistence (Figure 1.2B, label #4). This phenotype allows for persistence in the presence of antibiotics for prolonged periods.[19,31] While persisters constitute a relatively low fraction of the population, they have entered a protected (i.e., dormant) state and are proposed to contribute to broad-spectrum resistance.[32]

In addition to the four described protective mechanisms for biofilm-based infections, genetic diversity is hypothesized to further contribute to resistance in biofilms (Figure 1.2B, label #5).[5,19,20] Biofilms have high bacterial cell densities (typically 10^8 to 10^{11} cells g^{-1} wet weight) and are usually comprised of many species.[18] The genetic diversity between the multitude of bacterial species within these biofilms makes treatment with single-mechanism antibiotics difficult. As such, a more detailed investigation of polymicrobial infections will be presented below.

1.1.4. Polymicrobial infections

Polymicrobial infections are acute or chronic infections caused by various combinations of viruses, bacteria, fungi, and parasites.[5] For the purposes of this dissertation work, the focus will remain on multi-species bacterial infections. Polymicrobial infections are believed to be initiated in three distinct manners: (1) the presence of one microorganism generates a niche for other pathogenic microorganisms to colonize; (2) the presence of one microorganism predisposes the host to colonization by other microorganisms; or, (3) two or more non-pathogenic microorganisms together cause disease.[5] Regardless of formation mechanism, polymicrobial infections are often worse than single-species infections and lead to increased disease severity, enhanced bacterial persistence, and increased antibiotic resistance.[6] These complications are often due to interactions between bacterial species. For example, *S. aureus* can act either cooperatively or competitively with other bacteria, with either mechanism leading to a difference in behavior. For example, bacterial species *Haemophilus influenzae* often reach higher colony densities when cultured with *S. aureus* due to the available of nutrients provided by *S. aureus*.[37] In competitive interactions, such as those with *P. aeruginosa*, *S. aureus* employs defensive strategies for its survival, which leads to altered morphology, antibiotic resistance, and increased virulence. As a result, polymicrobial infections containing *S. aureus* exhibit enhanced disease severity.[37]

Chronic wounds have been used as a means to study the incidence of polymicrobial infections. Soft tissue infections, such as those found in chronic wounds, are often polymicrobial.[6,38–40] In one study of diabetic foot wounds, only ~6% contained no bacteria while ~16% consisted of a single bacterial species. In contrast, ~53% wounds had two to four species with ~30% showing five or more bacterial species.[39,41] A different study of chronic venous leg ulcers found that ~94% of the wounds contained more than one bacterial species, ~50% had four

to six species, and ~39% had more than six species. The mean number of bacterial species identified per chronic wound was reported as 6.3.[7] These results strongly demonstrate the need for considering polymicrobial infections when designing antibacterial agents.

Traditional antibiotic therapies target individual causative agents (e.g., single bacteria species) without consideration for the effect on a polymicrobial infection or on other members of a microbial community.[5] A major challenge in clinical care is the accurate and rapid detection of the bacteria species comprising a biofilm, making prescribing the appropriate antibiotic regimen difficult.[31] These shortcomings necessitate the development of broad-spectrum drugs that simultaneously eradicate both the Gram-negative and Gram-positive bacteria found in biofilms without relying on testing strategies to accurately determine which bacteria are present prior to treatment.[31]

1.1.5. Infection in chronic wounds

Chronic wounds affect approximately 6.5 million patients in the United States alone, with an estimated $25 billion spent annually on the treatment of chronic wounds.[42] This great humanistic and financial burden demands the development of novel treatment agents for chronic wound healing. As mentioned above, the vast majority of these wounds are infected with one or more bacterial species,[7,39,41] making antibacterial activity a central objective of these new treatments. However, infection is typically not the sole cause of wound chronicity, necessitating a thorough understanding of wound-healing mechanisms, complications, and the pitfalls of current treatment strategies for the development of a novel, multi-action therapeutic.

Healthy wound healing consists of four main phases: hemostasis, inflammation, proliferation, and remodeling (Figure 1.3).[43,44] The first phase of wound healing, hemostasis,

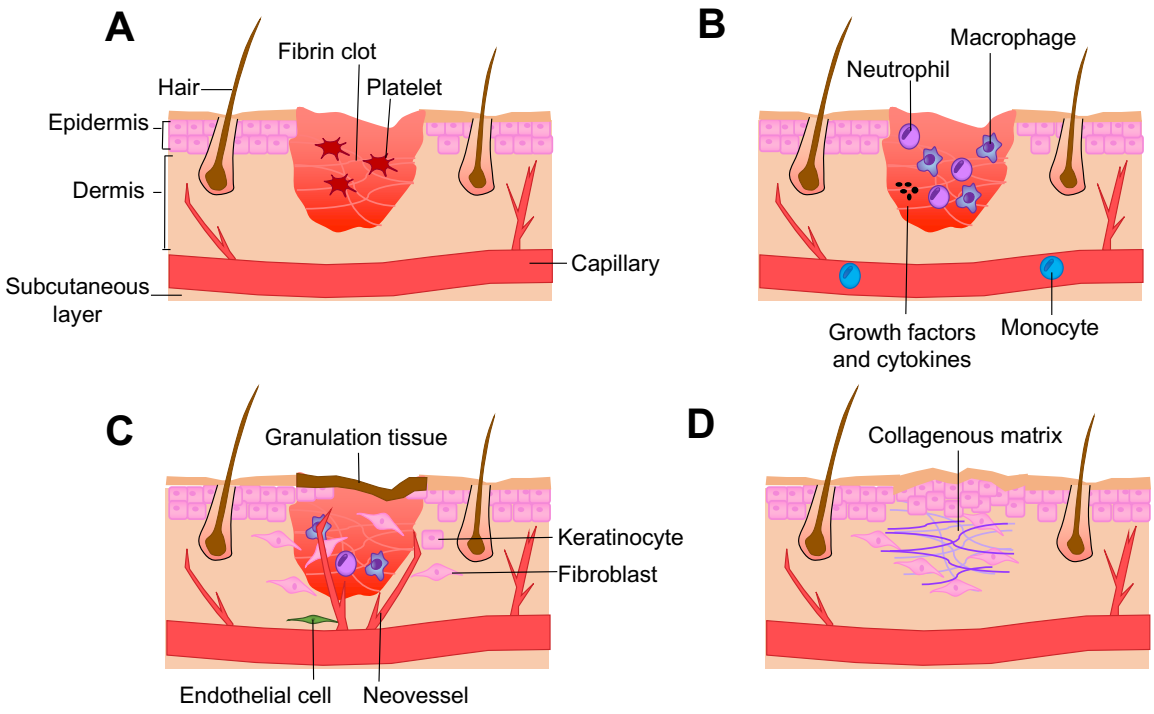

Figure 1.3 Healthy wound healing pathway, consisting of **(A)** hemostasis, **(B)** inflammation, **(C)** proliferation, and **(D)** remodeling phases.

begins immediately following injury and is characterized by the formation of a blood clot by local vasculature constriction, platelet degranulation, and fibrin activation.[45] The subsequent stage, inflammation, facilitates the removal of tissue debris and invading pathogens through matrix metalloprotease (MMP)-mediated phagocytosis and reactive oxygen species (ROS) released by infiltrating neutrophils, lymphocytes, and macrophages.[46,47] After infection clearance, the wound moves on to the proliferation phase of healing. The release of growth factors stimulates the generation of new tissue through mechanisms such as angiogenesis, formation of type III collagen and granulation tissue by fibroblasts, and deposition of a provisional extracellular matrix (ECM) by MMPs.[45,47,48] In the final phase, remodeling, the new tissue formed in the proliferation phase matures, the type III collagen deposited in the wound turns to type I (restoring to the initial collagen content), and the vascular density of the wound decreases from the high levels found in the proliferation phase.[45,47]

In acute/healthy healing, the four stages complete within 4-12 weeks, and the healed tissue closely resembles pre-wounded tissue.[47,49] However, many factors can prevent completion of this wound healing pathway, leading to wound chronicity. In such wounds, tissue enters a state of pathologic inflammation that results in protracted or incomplete healing.[45,47] Persistent stimuli at the wound site (e.g., repeated tissue trauma, pressure points) can cause cutaneous tissue to break down with the damaged tissue becoming a medium for bacterial growth.[50] Chronic wounds are often found to be hypoxic (<20 mm Hg oxygen) due to disruption of the vasculature in the surrounding tissue.[51] Oxygen is necessary for many processes in wound healing, including epithelialization, angiogenesis, and collagen dposition.[52] In situations of low oxygen tension, there will be more necrotic tissue to facilitate bacterial growth. A primary mechanism in the immune system for combatting these microbes (i.e., via reactive oxygen species) is thus compromised.[47]

A major factor for wound chronicity is infection and biofilm formation. Incomplete clearance of bacteria elongates the inflammation stage of wound healing, leading to biofilm formation.[3,43] Chronic wound infections are directly correlated with biofilms, whereas only ~6% of acute wounds are shown to have biofilms.[53] Biofilms have been found to cause chronic inflammation.[54,55] Predominant bacterial species of chronic wound infections include *S. aureus* (found in 40-90% of chronic wounds), *Enterococcus faecalis* (found in ~70% of chronic wounds), *P. aeruginosa* (found in 20-50% of chronic wounds), *Staphylococcus epidermidis* (found in 40-50% of chronic wounds), and *Escherichia coli* (found in ~30% of chronic wounds).[7,41] The polymicrobial nature of chronic wound infections allows for the exchange of genetic material between bacteria species, promoting the development of antibiotic resistance. Of the many bacteria present in chronic wounds, *P. aeruginosa* has been described as being almost impossible to eradicate with antibiotics.[3,56] Infections with *P. aeruginosa* typically show altered levels of MMPs. While MMPs are necessary to remove devitalized tissue and facilitate the proliferation phase, an elevated level of MMPs can impair the wound healing process.[3] Infection leads to devastating outcomes for wound healing and should thus be of central importance in developing a wound therapeutic.

Systemic factors that induce tissue hypoxia or leave one vulnerable to infection often result in the formation of chronic wounds. Conditions reported to correspond with poor wound healing outcomes include malnutrition, senescence, stress, obesity, alcoholism, cancer, immunodeficiency, and ischemia.[43,45] Diabetes is a group of metabolic diseases that through dysregulation of blood glucose levels contributes to the greatest number of chronic wounds via complex physiological processes.[43,57] For example, frequent states of hyperglycemia can cause increased glycation end-products, leading to a high concentration of reactive nitrogen species

(RNS) and ROS.[58] Reactive oxygen and nitrogen species are essential to wound healing in that they allow for the clearance of pathogens and dead tissue. In excess concentrations though, they prevent the transition from the inflammation to the proliferation phases of wound healing.[48,51] Those afflicted with diabetes also have an impaired ability to fight infection, resulting in failure to clear invading pathogens.[59] These complications lead to elongated or arrested wound healing timelines.

Current chronic wound therapies fail to address both infection and impaired host wound healing, such as in the case of diabetes. Standard wound care consists of debridement, infection control, and wound dressings.[60] Surgical debridement involves the removal of nonviable wound tissue, as necrotic tissue impairs or impedes keratinocyte migration over the wound bed and serves as a breeding ground for infection.[47,61] Surgical debridement is rapid and effective, but can also damage viable tissue.[61] Antimicrobial agents are equally crucial for controlling infection. For localized infections, typical treatments include topical antimicrobials (e.g., triple antibiotic ointment), dilute vinegar, or silver-containing wound dressings.[47,61,62] Physicians prefer not to use systemic antibiotics due to concerns over generating bacterial resistance. However, topical antibiotics, such as neomycin and gentamicin, often cause allergic contact dermatitis in chronic wounds.[61,62] Thus, systemic antibiotics are still used, but most published guidelines for clinical use are based on expert opinion rather than evidence-based conclusions.[62] The inconsistencies in infection control are clearly a motivation for developing new antibacterial agents with broad-spectrum activity and reduced off-target side effects (e.g., contact dermatitis or toxicity to the host). Wound dressings are frequently employed to maintain a moist wound bed and protect the wound from infection.[61] However, the frequent removal of wound dressings can cause trauma to newly developed tissue formed under the dressing.[63] Presently used standards of care (i.e., debridement,

antibacterial agents, and wound dressings) have been shown to be only marginally effective on biofilm-infected wounds.[55]

In order to address missing aspects of the standard wound treatment regimen, adjuvant therapies have been presented. For example, growth factor therapies have been proposed. However, in an environment where so many factors are deficient and dysregulated, replacing one of them through growth factor supplementation is insufficient to rescue the wound chronicity.[47] As such, results have been modest, and general acceptance of this therapy is hesitant.[47] Negative-pressure wound therapy (NPWT) is another alternative technique, wherein a wound dressing is utilized with an applied vacuum to remove excess fluid and promote wound healing.[61] Treatment with NPWT has shown evidence of reduced edema, reduction in wound size, and angiogenesis stimulation, but its effect on infection is unclear. Some studies have reported no difference in bacterial load compared to wounds treated with gauze whereas others show that NPWT can reduce rates of infection.[47,61] Hyperbaric oxygen therapy (HBOT) involves the application of oxygen at high pressure to the wound to counteract tissue hypoxia.[44] HBOT currently requires full-body exposure as localized oxygen delivery has not shown to be effective. Positive mechanisms have been proposed to occur through this treatment, including promotion of fibroblast proliferation and stimulated angiogenesis, but it is debatable whether these mechanisms have been shown in practice.[47] Full-body HBOT can lead to off-target side effects, including myopia, oxygen toxicity in the brain, and pneumothorax. Currently, HBOT is only available in limited settings.[43,47,61] Skin grafts or bioprosthetic skin substitutes are another option for treatment, but potential risks exist for rejection and hypersensitivity. As well, the grafts themselves are very costly.[47] While many therapies have been proposed and evaluated, none sufficiently fill the void of treating impaired host immune processes and clearing infection within a single therapy.

1.1.6. Infection resulting from the use of hemodialysis catheters

Many biomedical devices and implants fail due to the formation of biofilms on their surfaces. As opposed to chronic wound infections found associated with tissue, these biofilm infections are attached to the device or implant itself. Biofilms are responsible for the persistence of implant-related infections and are a source of bacterial dissemination to other sites. As described previously, host immune responses and conventional antibiotics are often ineffective against biofilm-based bacteria. Chronic inflammation is associated with untreated infection.[23] In developing new therapies for catheter-related infections, catheter complications and current therapies must be first understood.

Hemodialysis is a long-term renal-replacement therapy. The primary goal of hemodialysis is to transport solutes such as urea from blood into the dialysate and bicarbonate from the dialysate into the blood.[64,65] A buildup of waste products (e.g., urea) increases the likelihood of hospitalization or death. As such, patients typically undergo hemodialysis three times per week to prevent a buildup of waste products in the blood.[64] Three major strategies exist for hemodialysis access: tunneled dialysis catheters (TDCs), arteriovenous (AV) fistulas, and AV grafts (Figure 1.4). Tunneled dialysis catheters (Figure 1.4A and B) are an essential part of dialysis access despite their shortcomings.[66] TDCs are most often used for temporary access in patients who are in need of an AV fistula or AV graft but must start dialysis before the graft/fistula matures.[65,66] The creation of an AV fistula (Figure 1.4C) is the first choice option, though patients may require 1-4 months with a TDC prior to fistula maturation.[65,66] An AV fistula has the lowest infection rate of the access types and has fewer problems with thrombosis.[65,66] Larger vein sizes correlate to increased success and long-term use; thus, some patients with smaller veins are unable to use an AV fistula.[66] For patients without an adequate vein for an AV fistula, an AV graft (Figure 1.4D)

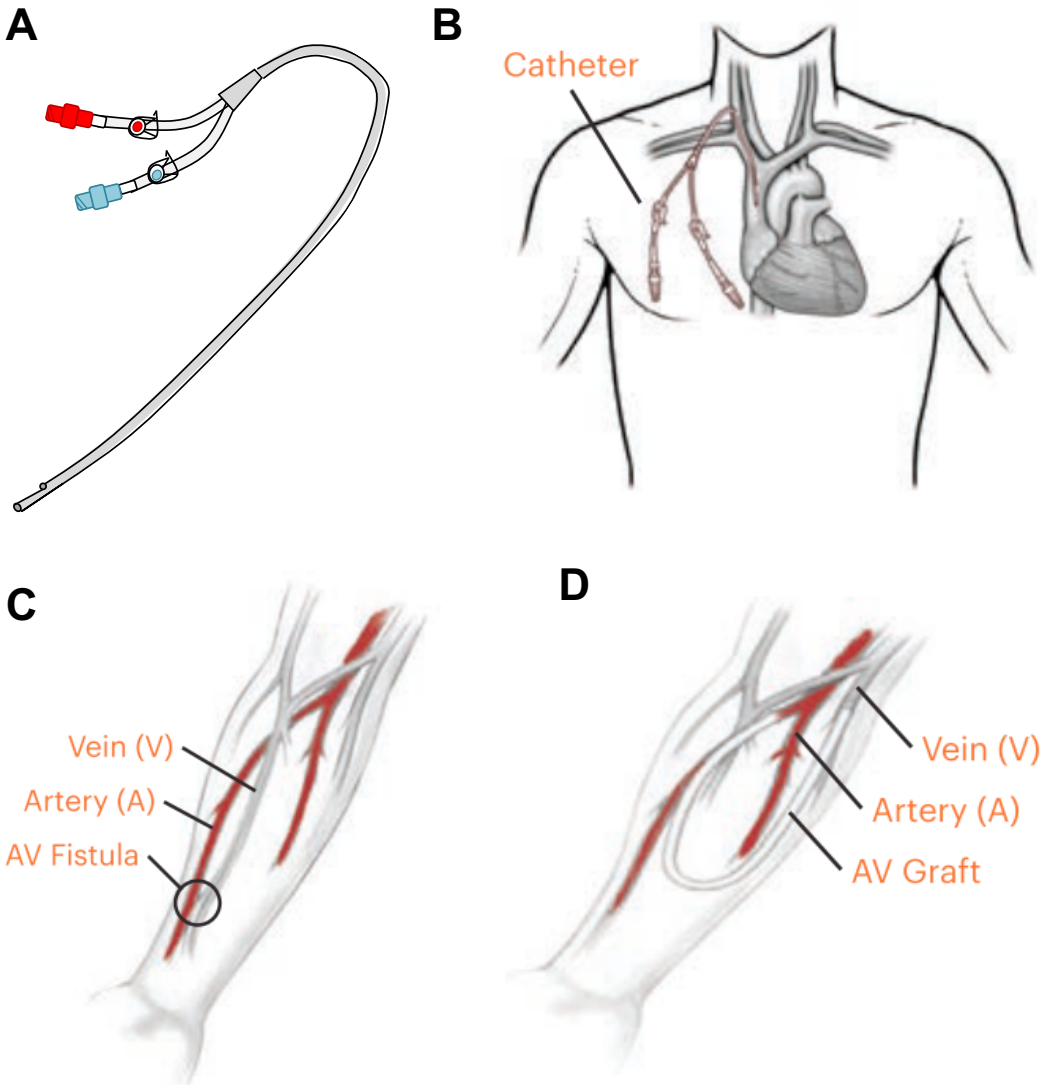

Figure 1.4 Hemodialysis access options including **(A, B)** tunneled dialysis catheters, **(C)** arteriovenous fistulas, and **(D)** arteriovenous grafts. (**B-D**) Reprinted with permission from the National Kidney Foundation, Inc. Produced by the National Kidney Foundation, Inc. All rights reserved.

may be suitable. However, these grafts have at least a 2-week lead time before use. They are also not as durable as fistulas and are more prone to infection and thrombosis complications.[65] In cases where fistulas or grafts are not possible, TDCs are used for long-term hemodialysis access.[65] The main benefit of TDCs is that they may be used immediately upon placement; however, they are the most prone to infection compared to other access options, thrombus formation can block blood flow, and stenosis is another problem encountered.[65] Regardless of eventual access type, 80% of dialysis patients in the United States begin with a TDC.[66] Mitigating complications associated with TDCs is therefore an essential area of research.

Tunneled dialysis catheters suffer from a host of complications, including infection, thrombosis, and stenosis. Infection is the second leading cause of mortality in dialysis patients, accounting for 15-20% of all deaths.[66,67] Upon placement, the bare catheter surface is rapidly covered with ECM proteins and immune protein components. This protein coating then facilitates adhesion of bacteria to the surface.[23,33] For example, *S. aureus* adheres to proteins such as fibronectin, fibrinogen, and laminin.[33] Colonization of the catheter and biofilm formation can occur within three days of catheter placement.[33] Organisms that colonize the TDC typically originate from the skin insertion site or the catheter hub.[33,68] Gram-positive bacteria account for 61-95% of all catheter-related bacteremias, with *S. aureus*, *S. epidermidis*, and *E. faecalis* being frequently isolated. Gram-negative bacteria, such as *P. aeruginosa*, *E. coli*, and *Klebsiella spp.*, are increasing in frequency and account for up to 45% of bacteremias.[15,69,70] Once a biofilm has formed on the catheter surface, antimicrobial treatment without catheter removal generally fails to eradicate the infection.[71] The inability to clear biofilm-based infection is unsurprising as the protective mechanisms conferred on biofilms render traditional antibiotics ineffective in clearing catheter-related infections. Not only does infection lead to catheter failure and subsequent removal,

catheter-related infections are associated with an increased risk of myocardial infarction, heart failure, peripheral vascular disease, and stroke.[69] Thus, both prevention and treatment strategies for catheter-related infections remain highly relevant to catheter use.

Thrombosis presents significant challenges in maintaining hemodialysis access through a TDC. Catheter blood flow problems that occur rapidly after placement are likely due to catheter position; however, blood flow problems that occur later are usually related to thrombosis or stenosis.[72] Rapid protein adhesion to the catheter surface not only serves as a breeding ground for infection but also triggers a coagulation cascade when activated platelets bind to fibrinogen on the catheter surface. Fibrinogen forms insoluble fibrin, which traps red blood cells, resulting in the formation of a thrombus.[73] Thrombus formation occurs in 33-59% of indwelling catheters, but only a small percentage of patients develop clinical concerns.[68] Thrombi can form external to the catheter via central vein thrombosis, where thrombosis occurs in the vein itself, and mural thrombosis, where a thrombus is attached to the wall of the vessel/atrium and the tip of the catheter. Internal thrombi include intraluminal thrombosis where the thrombus forms within the lumen, catheter tip thrombosis where a thrombus forms at the side holes of the catheter tip, and fibrin sheath thrombus where fibrin surrounds the catheter and can occlude the catheter tip.[72] Depending on the location of the thrombus, blood flow through the catheter can be affected. Lastly, stenosis, or narrowing of blood vessels, caused by TDCs can lead to varying degrees of occlusion, also preventing blood flow and leading to catheter failure.[68,74]

Current therapies for treating catheter complications (i.e., infection, thrombosis, stenosis) are aimed at addressing a single issue, not all three simultaneously. For infection, antibiotics or antiseptics are typically used as a first attempt, either topically or within the catheter itself.[33] Topical antibiotics have not been shown to decrease catheter-related bloodstream infections, may

increase the rate of infection by fungi, and have a chance of promoting the development of antibiotic resistance.[33,75] Catheters can be impregnated with antimicrobial agents, such as chlorhexidine, silver sulfadiazine, minocycline, and rifampin, which may reduce the rate of catheter-related bloodstream infections.[75] However, the utility of antimicrobial-impregnated catheters is debated, especially due to the potential to cause antibiotic resistance. Use of these catheters is indicated only for select clinical situations according to the CDC.[68] Lock solutions, which are placed into the catheter in between dialysis sessions, can also be filled with antibiotics. While benefits have been seen with this method, such as bacterial killing as well as preventing catheter-related bacteremia and sepsis, concerns related to antibiotic resistance are still present. Further, leakage of the antibiotics via the catheter tip can cause localized toxicity.[69,76,77] Regardless of treatment method, catheter salvage rates are poor (25-30%) with antibiotic treatment alone.[66] Catheter removal is indicated in multiple scenarios: (1) in cases where catheter infection is associated with bacteremia; (2) if there is no clinical improvement within 72 h following broad-spectrum systemic antibiotics; or, (3) if infections are related to MRSA, *P. aeruginosa*, or a fungal species.[66,78] Preventative strategies in addition to non-antibiotic-based treatment strategies are urgently needed to prevent catheter removal and subsequent surgery to insert a replacement catheter as a response to infection.

As a preventative measure for thrombosis, anticoagulants are routinely administered, with heparin being the most common. Systemic heparin administration can lead to hemorrhage and thrombocytopenia (i.e., low blood platelet count), but localized release can be employed without major side effects.[73] Heparin is often included within the lock solution placed in the catheter between dialysis sessions.[72] Unfortunately, heparin may promote biofilm formation as an unintended side effect.[78] Thrombolytic agents and catheter aspiration have been utilized in

declotting hemoaccess, but central vein thrombosis and mural thrombi are often treated via catheter removal and anticoagulation agents.[66,72] As a strong relationship between thrombosis and sepsis has been reported,[79] novel preventative measures that do not rely on catheter removal are necessary.

Lastly, preventative and treatment measures for stenosis are often overlooked. Central vein stenosis can be treated via angioplasty of the stenosis; however, recurrent stenosis may require stent placement.[66,74] The long-term benefits of endovascular procedures are modest and not durable, and surgical options are usually limited and a last resort.[74,80,81] Avoiding the use of TDCs continues to be the best strategy for preventing stenosis but is often not possible.[80] Overall, it can be seen that the current regimens are insufficient to prevent and treat complications associated with TDCs, even with only focusing on a single issue (i.e., infection, thrombosis, or stenosis). The development of a therapeutic strategy that can address all three complications simultaneously is of critical need.

1.2. Nitric oxide

Nitric oxide (NO) is an endogenous signaling molecule involved in a host of physiological processes. It has essential roles in wound healing,[45,82,83] neurotransmission,[84–86] inflammation,[87] vasodilation,[88,89] angiogenesis,[90–92] and the immune response.[87,93] The multifaceted roles of nitric oxide have motivated numerous investigations into the effect of exogenous NO therapy. In the context of infection prevention and treatment associated with both biotic and abiotic surfaces, the capacity for NO to act as an antibacterial and antibiofilm agent is motivation for utilizing NO-based strategies. This section will consider the physiological roles of endogenous NO, strategies

for delivering exogenous NO, and the potential for NO to serve as a preventative and/or treatment strategy for wound and catheter-related infections.

1.2.1. Physiological roles of nitric oxide

Nitric oxide is produced endogenously via the oxidation of L-arginine to L-citrulline by a family of enzymes called the nitric oxide synthases (NOS).[94] There are three NOS isoforms that produce NO at concentrations relevant for their intended role. Endothelial NOS (eNOS) and neuronal NOS (nNOS) are constitutively expressed in endothelial and neuronal cells, respectively, and catalyze low level (pM-nM) NO generation involved in signaling.[95] The concentrations generated by eNOS and nNOS correspond to anti-inflammatory processes.[87,92] Inducible NOS (iNOS) is an inducible isoform that can be activated in immune cells, such as neutrophils and macrophages. This isoform produces high levels of NO (nM-μM) in response to acute inflammatory stimuli (e.g., invading pathogens, pro-inflammatory cytokines) and is responsible for pro-inflammatory and antimicrobial actions.[87,92,96] Of note, certain diseases, such as diabetes, are characterized by abnormal NO production, correlating to an impaired immune system.[87]

One of NO's most important roles is its ability to function as a broad-spectrum antibacterial agent. Nitric oxide exerts its antibacterial action through multiple mechanisms, including nitrosative and oxidative pathways (Figure 1.5).[97] Reaction with extracellular oxygen lead to the production of dinitrogen trioxide, a reactive species that can facilitate thiol nitrosation and DNA deamination. Intracellular superoxide also reacts with NO to form peroxynitrite, which results in DNA cleavage, tyrosine nitrosation, and membrane destruction via lipid peroxidation.[93,98–100] Not only are these mechanisms effective against planktonic bacteria, these processes also work against biofilms. Nitric oxide can facilitate biofilm dispersal at pM-nM concentrations and complete

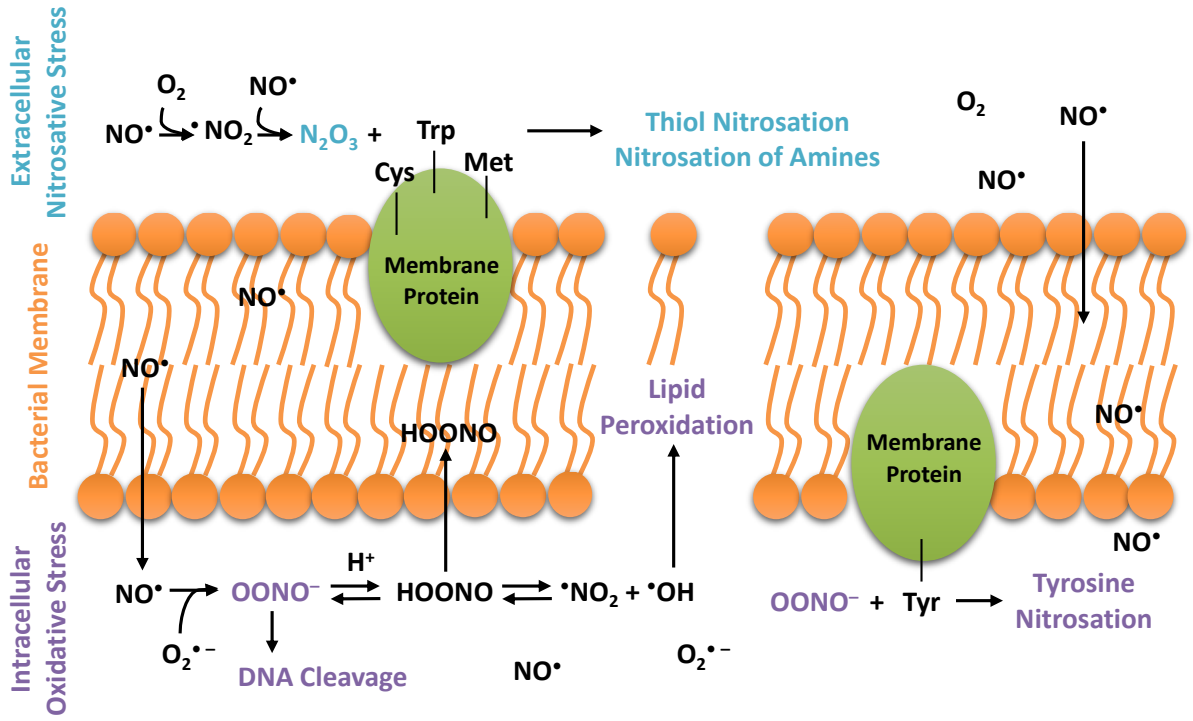

Figure 1.5 Proposed mechanisms of the multi-mechanistic killing pathways of NO and its byproducts through nitrosative and oxidative stresses.

eradication at μM-mM concentrations.[101–103] While potent against bacteria, eukaryotic cells have evolved mechanisms to scavenge these reactive species (e.g., superoxide neutralization via superoxide dismutase), minimizing their impact on the host cells.[104] Of importance, nitric oxide has not been observed to generate bacterial resistance and is unlikely to due to its multiple mechanisms of action.[105,106]

Nitric oxide also has important roles in vascular homeostasis, or the maintenance of vascular function over time while adapting to persistent environmental stimuli.[107] Angiogenesis, or the formation of new blood vessels, requires NO produced by eNOS.[90,91] Nitric oxide-modulated processes include endothelial cell survival, proliferation, migration, and interaction with the ECM.[90,91,108] Confirming the important roles of NO in angiogenesis, it has been determined that treatment with agents that increase NO synthesis enhance angiogenesis. Contrarily, the use of NOS inhibitors seemingly blocks angiogenesis.[90,108]

Other noteworthy roles of NO involve the modulation of inflammation and thrombosis. Nitric oxide cannot be definitively classified as a pro- or anti-inflammatory molecule, as its actions are largely dependent on cellular context and NO concentration.[109,110] The role of NO is nonspecific and not receptor-mediated, resulting in regulation of the activity, growth, and death of many immune and inflammatory cells, including macrophages, lymphocytes, mast cells, and neutrophils.[111] Nitric oxide also regulates cytokines that initiate inflammation. There is a large body of evidence supporting NO's role in several inflammatory disorders.[109,112,113] Similarly, thrombosis is highly affected by NO concentration. Endothelial cells that line the inner wall of blood vessels produce NO via eNOS with a surface flux of 0.5-4 x 10^{10} mol cm^{-2} min^{-1} to prevent platelet activation and control the balance between thrombosis and hemorrhage.[73] An NO

deficiency has been reported to facilitate platelet aggregation and thrombus formation, demonstrating the necessity of NO to mitigate thrombosis.[114,115]

1.2.2. Nitric oxide donors and donor scaffolds

Due to the multifaceted roles of endogenous NO, strategies to harness exogenous NO for a myriad of biomedical applications have been investigated. The direct use of gaseous NO is hindered by its short half-life (seconds) and high reactivity (e.g., formation of NO_2 from reaction with O_2), complicating localized delivery.[116] In addition, gaseous NO treatments are limited to hospital settings where there can be constant oversight.[103,117] For example, systemic toxicity can occur when NO is inhaled at 40 ppm or when a reactive NO byproduct, NO_2, is inhaled at 1.5 ppm.[118] As a means to mitigate challenges associated with gaseous NO, NO donors capable of storing and releasing NO are frequently employed.[119,120] These molecules release NO through unique decomposition methods forming a dissolved gas, allowing for more control in effectively delivering NO to the desired physiological target.[120] While many classes of NO donors have been explored,[119] this section will focus on the two classes of NO donors that have been most widely utilized in antibacterial and antibiofilm treatment strategies for both biotic and abiotic surface-related infections.

S-nitrosothiols (RSNOs) are a class of NO donors found endogenously in the form of nitrosated cysteine and glutathione.[121] *S*-nitrosothiol NO donors can also be formed exogenously through the nitrosation of thiol groups using nitrosating agents (e.g., NO_2^-, NO_2, N_2O_3).[122] Nitric oxide is released from RSNOs following multiple decomposition mechanisms (Figure 1.6A), including photothermal degradation via homolytic cleavage of the S-N bond, liberating one mole of NO per thiol group.[119,123] An additional mechanism involves the catalytic decomposition of

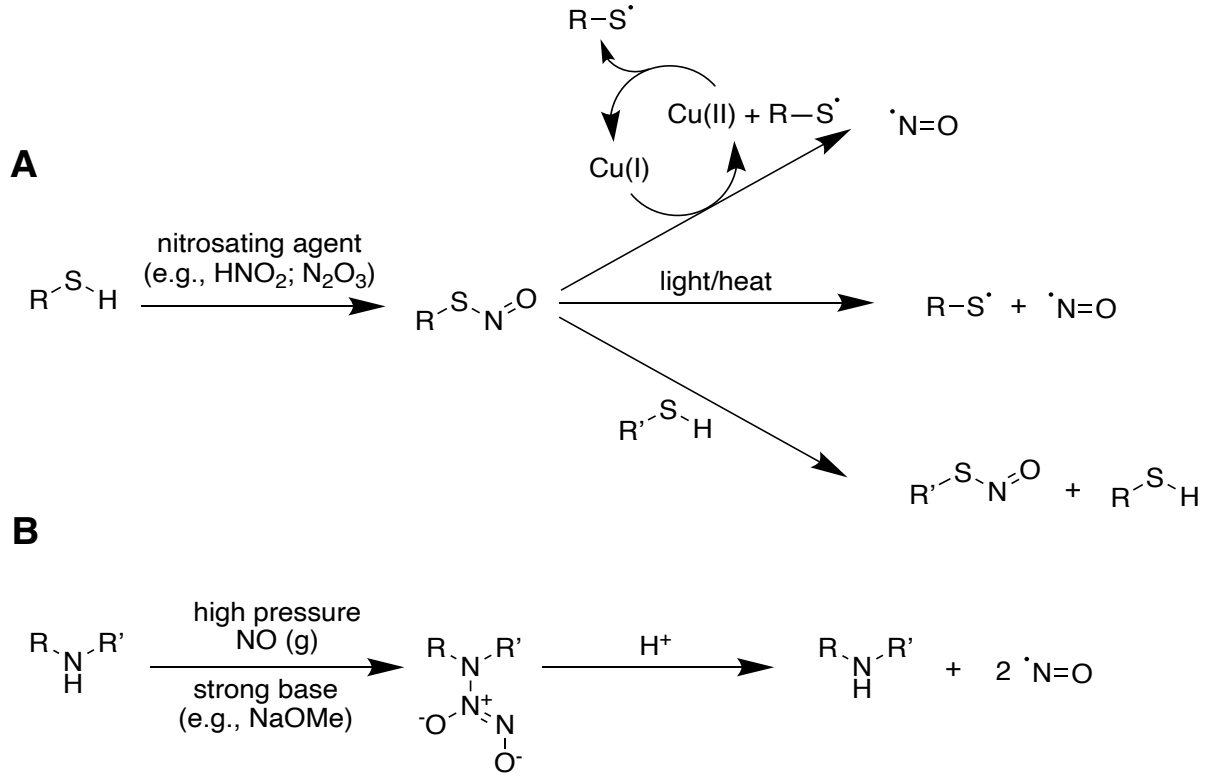

Figure 1.6 Nitric oxide storage and release mechanisms of **(A)** *S*-nitrosothiol and **(B)** *N*-diazeniumdiolate NO donors. *S*-nitrosothiols form on thiol groups upon nitrosation via nitrosating agents and can break down via copper-mediated decomposition, undergo homolytic cleavage via light or heat, or transnitrosylate other thiols. *N*-diazeniumdiolate NO donors form on secondary amines when exposed to high pressure gaseous NO under basic conditions and release via a proton-initiated mechanism.

RSNOs by copper and other transition metals; however, low copper levels are found endogenously, implicating photothermal methods as the primary mechanism for releasing NO in vivo.[119,124,125] Diverse release kinetics are possible depending on the structure of the RSNO (e.g., primary versus tertiary thiol) and degree of exposure to external release triggers.[119,123] Unfortunately, instability due to light and heat exposure may lead to premature NO release and concerns for storage in clinical scenarios, as these NO donors must be stored in dark, cold environments.

Another class of NO donors includes *N*-diazeniumdiolates (NONOates), which form selectively on secondary amines upon exposure to high pressure gaseous NO under sufficiently basic conditions. Two moles of NO can be stored per secondary amine with NO released through a spontaneous proton-initiated breakdown mechanism under physiological conditions following first-order kinetics (Figure 1.6B).[126,127] The release of NO from these donors is influenced by both environmental factors (e.g., temperature or pH) and the structure of the NO donor molecule. Under physiological conditions (i.e., pH 7.4, 37 °C, 0.1 M phosphate buffer), NO-release half-lives of small molecule NONOates range from 2 s with NONOate-modified proline (PROLI/NO) to 20 h with NONOate-modified diethylenetriamine (DETA/NO).[127] While PROLI/NO does not contain any chemical functional groups to stabilize the net negative NONOate, DETA/NO has two positively charged terminal primary amines that provide such stabilization, leading to extended-release properties.[127–129] With increased stabilization of the NONOate, NO is released more slowly from the NO donor. Due to the release mechanisms of NO from NONOates, these NO donors must be stored under anhydrous conditions but are otherwise stable for extended periods.

Small molecule NO donors, such as *S*-nitrosoglutathione (GSNO) or DETA/NO, are capable of NO storage and release with high payloads of NO per unit mass. However, the release of NO from these donors is often not well-controlled (i.e., rapid breakdown of NO donor prior to

localization), and the donor or precursor (upon NO release) can diffuse away from the site of interest. In the case of NONOates, amine-containing donors can be cytotoxic and therefore cause off-target toxicity.[100,120] The use of macromolecular NO donor scaffolds has been found to ameliorate these concerns, facilitating increased localization, biocompatibility, and antibacterial action.[120,130] Hetrick et al. first confirmed that NO-releasing silica was less cytotoxic to mammalian cells than low molecular weight NO donor PROLI/NO at their respective bactericidal doses.[100]

An approach to prepare NO-releasing macromolecules involves the encapsulation of small molecule NO donors within a scaffold, such as a liposome.[131,132] Nitric oxide donor-containing liposomes have proven useful in storing their NO payload until reaching the desired target, where a change in pH upon arrival at an acidic cancerous site triggered the release of NO from within the scaffold.[132] Alternatively, small molecule NO donors can be covalently bound to the scaffold structure (e.g., biopolymers, dendrimers, silica nanoparticles).[120] Modifying the scaffold with NO donors allows for enhanced control over the NO-release properties and therapeutic utility.[45] The main challenge in direct NO loading on a macromolecular scaffold involves low NO payloads per unit mass due to the greater overall mass, increased steric hindrance, and reduced access to NO loading sites, all of which prohibit NO donor formation on every thiol or secondary amine present.[120] As such, the choice to utilize a macromolecular scaffold or directly use a small molecule NO donor is highly dependent on the intended application. In cases where a high NO payload is most beneficial and off-target toxicity is not a major concern, small molecule NO donors may be favorable. In other scenarios, where toxicity and localization are more important than high payloads per unit mass, employing a macromolecular NO donor scaffold could be advantageous. These considerations have justified the development of a wide range of NO donor molecules and

scaffolds, each demonstrating their own benefits and challenges for intended biomedical applications.

1.2.3. Nitric oxide as an antibacterial wound healing agent

Insufficient endogenous NO levels, such as those common to certain disease states (e.g., diabetes), are implicated in the failure of the wound healing process.[45] Previous reports described wound healing in iNOS knockout mice and how cutaneous wound healing was severely impaired in the total absence of iNOS-derived NO production.[133] On the contrary, excessively elevated levels of NO result in tissue damage, highlighting the need for closely monitoring released NO concentrations and properties from designed therapeutics.[45] In the wound environment, NO is produced at greater levels by iNOS during the inflammatory phase and at lesser eNOS-derived levels during the proliferation and maturation phases (Figure 1.7),[134] indicating the dichotomous concentration ranges that must be considered when developing exogenous therapies. Due to NO's influential roles in healthy wound healing, including its antimicrobial action, inflammation modulation, and vascular homeostasis maintenance, numerous therapies based on NO delivery have been investigated for the treatment of chronic wounds.[45]

The most straightforward way to deliver NO to a wound is via direct exposure to gaseous NO. High pressures of oxygen are used for HBOT therapy; thus, NO can be used in place of oxygen for direct administration to the wound without needing a carrier.[44] In one study, Miller et al. treated a patient's chronic diabetic foot ulcer (DFU) that had persisted for over 2 years. For 14 d, the wound was continuously exposed to 200 ppm NO using a hyperbaric boot. On day 14, the surface area of the wound was down by 70%, and complete healing was observed after 26 weeks.[135] While this treatment was effective, continuous treatments of this type are not practical for clinical

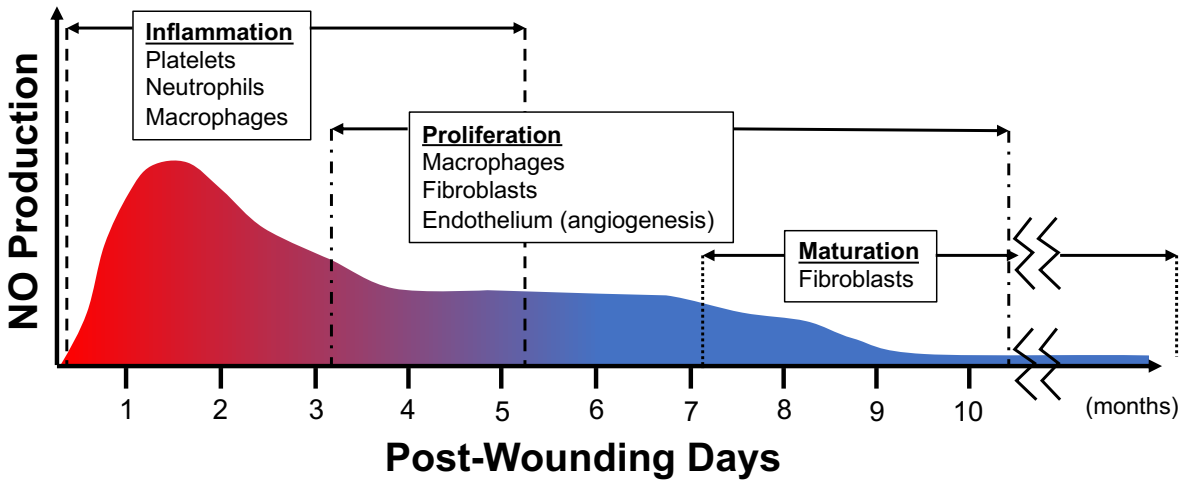

Figure 1.7 Temporal production of NO over the days following wound healing overlaid with the phases of wound healing and the cell populations most relevant to each phase.

translation to a wide patient population. As such, intermittent strategies have been investigated. Exposures of *S. aureus*-infected rabbit wounds to 200 ppm NO for 8 h facilitated improved collagen deposition and reduced bacterial loads by 1-log after just 3 days of treatment.[136] Gaseous NO was found to be safely dosed at 5, 25, 75, and 200 ppm for 8 h, but 8-h exposure to >200 ppm NO resulted in decreased cell viability and immune cell proliferation, suggesting an upper limit to exposure concentrations/durations.[137] Higher NO concentrations have successfully been used for shorter exposures (i.e., 500 ppm for 60 s once daily) without reported adverse effects, wherein wounded rats showed reduced hypoxia and infection, increased angiogenesis, and more rapid recovery times.[138]

These studies have implicated NO as an effective wound healing agent, but localized delivery via NO donors over gaseous NO therapy may provide an avenue that could more easily be translated to an at-home, patient-applied therapy. Both RSNO- and NONOate-based therapies have been evaluated for their antibacterial and wound healing efficacy.[45] Kim et al. developed chitosan films doped with small molecule NO donor GSNO.[139] This wound dressing reduced bacterial viability of *P. aeruginosa* and *S. aureus* by 2- and 1-log, respectively. A rat wound model further demonstrated that the GSNO-doped chitosan films accelerated wound healing and increased collagen fiber content.[139] In a series of studies, pluronic-F127 hydrogels were developed that encapsulated GSNO and *S*-nitroso-*N*-acetylcysteine (SNAC).[140] Initial in vivo studies involved application of the NO-loaded hydrogels to the forearms of humans, confirming that there was elevated dermal blood flow for at least 3 h following application.[141] Follow-on studies involved the application of two doses of GSNO-loaded hydrogels (23 mM and 230 mM GSNO) to the skin of healthy and diabetic rats. The 230 mM GSNO-loaded hydrogel doubled the perfusion of blood in both normal and diabetic rats.[142] Lastly, NO-releasing pluronic-F127 hydrogels were

used to treat excisional wounds in a rat model. Most favorable healing outcomes were observed when the wounds were treated during both the inflammatory and proliferation phases.[143]

The use of small molecule NONOate donors has also yielded success. Dashti et al. added DETA/NO powder directly to the wounds of streptozotocin-induced diabetic rats, where accelerated wound closure was observed.[144] In a different study by Brisbois et al., wound dressings were doped with NONOate-loaded dibutylhexanediamine (DBHD/N_2O_2) and evaluated against infected murine burn wounds. Treatment with DBHD/N_2O_2 wound dressings decreased *A. baumannii* burden by ~4 logs, highlighting NO's exceptional role in antibacterial action for wound infections.[145] *N*-diazeniumdiolate NO donors have also been covalently linked to polymer scaffolds in the development of wound therapies. Acrylonitrile-based terpolymers were covalently bound with NONOates and electrospun to prepare non-woven fibrous wound dressings.[146] Evaluation in an in vivo excisional mouse wound model displayed enhanced closure on day 14 when treated with NO versus a control dressing. Confirming NO's role in vascular homeostasis, a greater capillary density was found with NO treatment. Additionally, a marked upregulation of NO-induced gene expression (e.g., eNOS) was evident within 30 min of treatment.[146] In a different approach, Masters et al. coupled an NONOate NO donor to poly(vinyl alcohol) (PVA) hydrogels.[147] A significant increase in collagen content was found following treatment of diabetic mouse wounds, with a noted concentration dependence where greater doses of NO led to more collagen.[147]

A common factor in the above studies is that NO-based therapies enhance wound healing via increasing angiogenesis and collagen content, faster wound closure, and lower bacterial burden. Clearly, NO is a beneficial wound healing agent. My dissertation research aims to develop a bioactive macromolecular backbone for NO delivery to potentially further enhance wound

healing. Targeting wound healing applications, the glycosaminoglycan (GAG) family represents an attractive series of macromolecular backbones for NO storage and delivery.

Glycosaminoglycans (Figure 1.8) are unbranched polysaccharides that fall into four main categories: (1) hyaluronic acid (HA), (2) chondroitin sulfate (CS) and dermatan sulfate (DS), (3) heparan sulfate (HS) and heparin, and (4) keratan sulfate (KS).[148,149] These biopolymers are major constituents of the ECM found in epithelial, connective, and nervous tissues of vertebrates.[148,150] All of the GAGs are characterized by the same structure of disaccharide units, containing an amino sugar (*N*-acetyl-D-galactosamine or *N*-acetyl-D-glucosamine), usually sulfated, and a uronic sugar (glucuronic acid or iduronic acid) or galactose.[148,150] Hyaluronic acid is the only GAG that is not naturally sulfated but is found at much greater molecular weights (≤ 10 MDa) than the other GAGs (≤ 50 kDa).[150,151] All GAGs are negatively charged due to their carboxyl and/or sulfate groups.[148] Sulfated GAGs are structurally heterogeneous in their disaccharide composition, sulfation pattern and degree, and chain length, giving them diverse in vivo properties.[149]

Heparin and HS are most studied for their anticoagulant activity and prevention of thrombosis.[152] Keratan sulfate is mainly found in the cornea where it is involved in maintenance of corneal transparency. It is also important to note that KS is the least understood GAG at this time.[152] Dermatan sulfate, a stereoisomer of CS, has strong antithrombotic activity similar to heparin and HS.[152,153] However, two major drawbacks of DS include its relatively short half-life and low bioavailability when compared to heparin.[152] It is hypothesized that DS may be involved in wound healing, as it is a major constituent of the skin and influences coagulation, immune defense, and cell growth. However, these roles have not yet been fully characterized.[154] Hyaluronic acid is the major GAG found in fetal wounds whereas CS is the major GAG found in adult wounds,

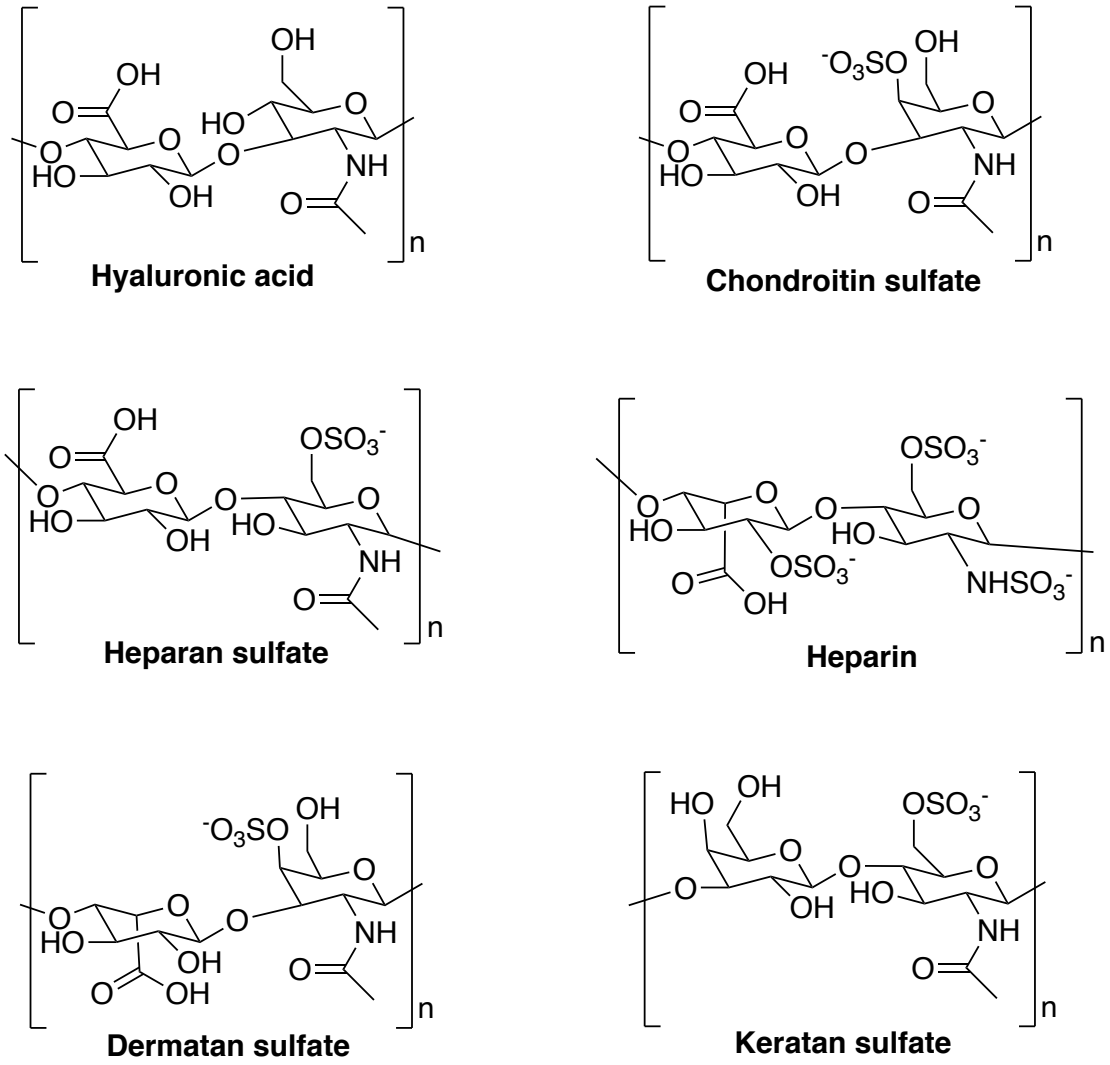

Figure 1.8 Structures of disaccharides forming the various GAG species. Of note, sulfation pattern varies for the sulfated GAGs. An example sulfation pattern is presented.

implicating their significance in the wound healing process.[155] Much of my work in developing a novel wound therapy focuses on HA and CS.

Hyaluronic acid is composed of alternating D-glucuronic acid and *N*-acetyl-D-glucosamine residues.[150,151] Approximately 50% of the total HA in the human body resides in the skin, both in the dermis and epidermis.[150,156] Most important to this research, HA is involved in many processes related to wound healing. Hyaluronic acid acts as a signaling molecule dependent on molecular weight, location, and cell-specific factors.[150] High molecular weight HA (≥ 1 MDa) is expressed in healthy tissue signaling for immunosuppressive, anti-inflammatory, and anti-angiogenic mechanisms.[151,157] Under times of inflammatory stress, endogenous HA is degraded to lower molecular weight HA (< 800 kDa), which signals for immunostimulatory, pro-inflammatory, and angiogenic activities.[150,151,157] These molecular weight-dependent signals give HA the ability to contribute to each stage of wound healing (Figure 1.9).

During hemostasis, HA (> 400 kDa) is released to prompt the deposition of fibrinogen and the formation of a clot.[156,158] During inflammation, the secretion of inflammatory cytokines signals for degradation of high molecular weight HA to low molecular weight HA, which recruits leukocytes, monocytes, and lymphocytes to the wound cite. Toll-like receptors TLR2 and TLR4 interact with low molecular weight HA to express TNF-α and interleukins (e.g., IL-6, IL-8, and IL-1β).[156,158] Subsequently, HA is further degraded into oligosaccharides that reduce the inflammatory response and guide proliferative activity.[156] During proliferation, HA oligosaccharides guide fibroblast migration and proliferation (leading to wound contraction), foster angiogenesis, facilitate collagen deposition, and interact with CD44 receptors on keratinocytes to regulate the re-epithelialization process.[156,158] Lastly, HA oligosaccharides

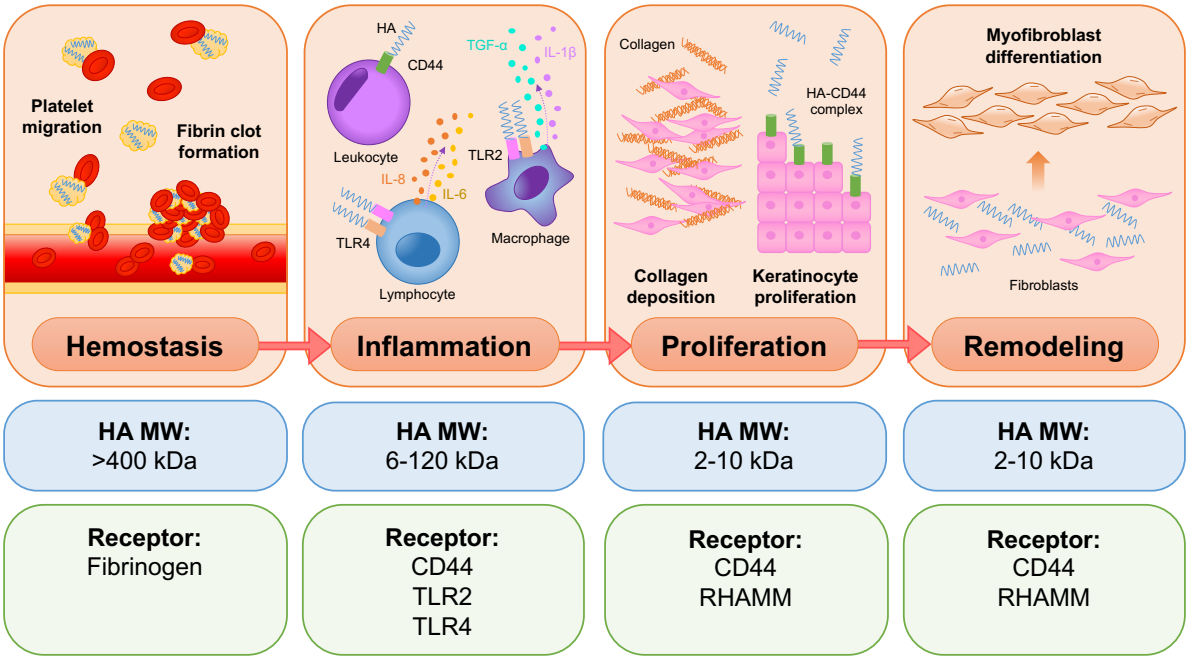

Figure 1.9 Roles of HA in the wound healing process dependent on the molecular weight of HA. Abbreviations include molecular weight, MW; toll-like receptors 2 and 4; TLR2 and TLR4; transforming growth factor α, TGF-α; interleukins 1β, 6, and 8, IL-1β, IL-6, and IL-8; receptor for HA-mediated motility, RHAMM.

promote the differentiation of fibroblasts to myofibroblasts, promoting wound contraction and maturation of collagen from type III to type I.[156]

Due to HA's prominent roles in wound healing, numerous studies have investigated the treatment of wounds with exogenous HA. Studies involving exogenous HA treatment for wound healing have demonstrated increased fibroblast proliferation, migration, and adhesion to the wound site, enhanced collagen production, and improvement and acceleration of wound closure and re-epithelialization.[150] Topical treatment with HA oligosaccharides (1-7 kDa) in mice and rats was found to increase wound healing rates, angiogenesis, collagen deposition, and endothelial cell proliferation.[159–161] When incorporated in wound dressings and hydrogels, HA reduced healing time and helped retain moisture, alleviate inflammation, and relieve scar formation.[162,163] These promising results indicate that HA would be well served as a macromolecular vehicle for NO delivery for wound healing applications.

Due to the similarity in structures between HA and CS as well as CS's large concentration in adult wounds, CS may represent another attractive vehicle for NO delivery for wound therapy. Contrary to HA's molecular weight-specific interactions, CS's interactions are not significantly impacted by CS molecular weight, which is typically ~20 kDa in animal tissue.[164] Chondroitin sulfate is composed of alternating glucuronic acid and *N*-acetyl-D-galactosamine residues, which can be sulfated at multiple positions.[165] Polysaccharides isolated from animal tissue are predominantly composed of chondroitin-4-sulfate (CSA) and chondroitin-6-sulfate (CSC), sulfated in the 4 and 6 position of *N*-acetyl-D-galactosamine residues, respectively.[166] The sulfation pattern of CS, rather than its molecular weight, is important in controlling the specific molecular interactions of CS both in vitro and in vivo.[148,165]

Chondroitin sulfate is widely distributed throughout the human body with important roles in the regulation of growth factors, cytokines, and chemokines dependent on its sulfation pattern.[148] Regarding cellular growth and movement, CS decelerates keratinocyte migration and proliferation, increases fibroblast proliferation and migration, increases or decreases fibroblast adhesion, and stimulates chondrocyte proliferation.[166–170] Derivatives of CS also exhibit anti-inflammatory properties, inhibiting the release and/or activity of MMPs, ROS, lysosomal enzymes, and hyaluronidase.[170–172] Chondroitin sulfate is able to diminish NF-κB activation and nuclear translocation in chondrocytes.[173] Of note, activation of NF-κB is a key component in the inflammatory process and has a role in many inflammatory diseases. The role of CS in NF-κB activation has raised the hypothesis that CS might be able to treat diseases that have a strong inflammatory component.[173] Thus, the main applications for CS to date have involved the treatment of osteoarthritis and other conditions that might utilize CS's anti-inflammatory actions. However, more relevant areas of interest include tissue regeneration and engineering applications.[148]

A number of wound dressings have been prepared using CS. In a study by Kirker et al., wounds treated with CS films showed more vascular tissue by day 10. A significant increase in re-epithelialization was found in wounds treated with the CS films versus controls.[174] Chondroitin sulfate-based hydrogels have also been evaluated. For example, Gilbert et al. reported on the treatment of maxillary sinus mucosa wounds in rabbits with a CS hydrogel and demonstrated accelerated wound healing. The authors attributed the better healing to the CS hydrogel's resemblance to the ECM, which could serve as a repository for cytokines and growth factors as well as provide structural framework for infiltrating fibroblasts.[175] Lastly, GAG-containing (HA or CS) electrospun nanofibers were evaluated for skin tissue regeneration applications by

Bhowmick et al.[172,176] These fibers, regardless of GAG identity, were found to stimulate cellular performance and accelerate epidermal and dermal regeneration.[172,176]

Substantial evidence has been described in the literature that the two GAGs presented herein, HA and CS, have important roles related to wound healing. Further, preliminary reports have utilized HA or CS as an active ingredient for wound therapy with promising results. Due to the wound healing actions of HA and CS, they represent an attractive biopolymer backbone for storage and delivery of NO, as once the NO is released, the backbone itself may remain bioactive. The structures of HA and CS (Figure 1.8) contain multiple functional groups (e.g., primary and secondary alcohols, carboxylic acids) that are easily modified to incorporate *N*-diazeniumdiolate NO donor precursor structures (e.g., secondary amines). The combination of NO's antimicrobial, inflammation modulatory, and angiogenic properties with the wound healing benefits of HA or CS has the potential to generate a multi-action therapeutic aimed at treating infected wounds.

1.2.4. Nitric oxide therapies for mitigating hemodialysis catheter infection and failure

While initial studies have demonstrated NO therapies as an attractive option for preventing and treating infections related to hemodialysis catheter use, most reported systems do not exhibit NO-release durations sufficient for long-term applications. Hou et al. reported modifying the surface of the catheter with an NO-releasing polymer brush.[177] Active release of NO persisted for 15 d with both in vitro and in vivo (murine and porcine) models showing strong antibacterial activity (i.e., 4-log reduction in MRSA viability).[177] While useful for short-term catheterization, long-term applications (i.e., months or longer) are not yet available using this method, as it is not possible to replace the NO source once the NO payload has been released. Another strategy involves impregnating/infusing catheters with small molecule NO donors. Central venous

catheters were fabricated containing DBHD/N_2O_2, with PLGA added to alter NO release by controlling PLGA hydrolysis. Active NO release was observed for at least 14 d with in vivo testing in rabbits demonstrating decreased thrombus size and decreased bacterial adhesion by 95%.[178] Multiple NO-releasing catheter systems have been evaluated using small molecule NO donor *S*-nitroso-*N*-acetylpenicillamine (SNAP), either by fabricating catheters from polymers mixed with SNAP or swelling pre-formed catheters to include SNAP. Reported NO release durations from SNAP-impregnated catheters range from 1-60 d.[179–182] These studies reported antibiofilm action against *S. epidermidis*,[179] *S. aureus*,[180–182] *P. aeruginosa*,[179,180,182] and *E. coli*,[181] stating 1- to 3-log reductions in bacterial/biofilm viability. In addition, in vivo studies in rabbits resulted in thrombus reduction by 96%.[179] SNAP has also been embedded within a polymer and the polymer/SNAP mixture used to fill one lumen of a dual-lumen catheter, restricting vascular access to a single lumen. This study demonstrated a 97% reduction in *E. coli* and *S. aureus* biofilm viability in vitro as well as an 85% reduction in thrombus size in vivo.[183] Unfortunately, these methods all utilize non-renewable NO sources, limiting their functional lifetime to the length of achievable NO release, which for most of the described studies, is approximately 2 weeks.

Two recent studies have investigated the use of renewable NO sources for fabricating NO-releasing catheters. Doverspike et al. achieved a replenishable NO-releasing catheter system by developing a small, NO-releasing insert that attaches to the catheter hub cap and is replaced every 48-72 h, when NO release is exhausted. In vivo experiments in a sheep model demonstrated reduced bacterial counts by 3-5 logs in the hub region but only 2-3 logs in the inner lumen.[184] By attaching the NO-releasing device to only the hub region, the amount of NO that diffuses along the length of the catheter, through the clamped portion to the tip, is unclear but relevant as the catheter tip is often the site of occlusive thrombosis.

An alternative approach to developing a renewable NO catheter system is to utilize an NO-releasing lock solution that fills both catheter lumens between dialysis sessions. Kumar et al. previously reported on an *S*-nitroso-*N*-acetyl-L-cysteine ethyl ester lock solution that releases NO for at least 18 h. In vitro, the researchers observed a 3-log reduction in *S. aureus* and *E coli* adhesion but did not evaluate the effects on thrombosis or stenosis.[185] While this report demonstrates the benefits of an NO-releasing lock solution, future utility clearly necessitates the use of longer NO-releasing systems, as lock solutions are replaced every 48-72 h in the clinic. The NO release must thus be maintained above a certain threshold for at least 72 h to maintain efficacy between treatments.

Nitric oxide-releasing lock solutions remain a promising avenue to pursue for catheter NO release, particularly if such solutions can easily be incorporated within current dialysis regimens, maximizing potential for clinical translation. Further, the NO donor itself does not need to provide localization, as NO will diffuse through the catheter surface[183–185] and not contact blood or tissue in great quantities, mitigating concerns over toxicity. As such, the use of small molecule NONOate NO donors that provide high NO payloads per mass of NO donor may prove ideal. As the exact role of NO flux (i.e., concentration, release profile) from the catheter surface has yet to be elucidated, small molecule NONOate donors represent ideal tools to evaluate the role of NO-release properties (e.g., payload, flux) and durability of NO for reducing on infection, thrombosis, and stenosis.

1.3. Summary of dissertation research

The goal of my dissertation research was to develop multi-action NO-release systems capable of preventing and treating infections, as well as associated complications, of biotic and

abiotic surfaces. Chronic wound infections were chosen as a representative infection associated with biotic surfaces (i.e., wound tissue). The combination of a bioactive macromolecular scaffold with NO addressed both clearing infection and promoting host wound healing. Hemodialysis catheter-related infections were chosen as a representative infection associated with abiotic surfaces (i.e., the catheter surface). Nitric oxide's ability to reduce bacterial and platelet adhesion as well as stenosis were all harnessed to cultivate a triple-action strategy. Both multi-action NO release systems were evaluated in vitro and in vivo to elucidate their potential in infection control for wound and catheter systems. Specifically, my research aimed to:

1. Synthesize NO-releasing glycosaminoglycans as a function of molecular weight and sulfation pattern that exhibit tunable NO-release properties;
2. Assess the in vitro antibacterial and antibiofilm properties of NO-releasing glycosaminoglycans against common wound pathogens;
3. Evaluate the wound healing potential of NO-releasing glycosaminoglycans using in vitro wound healing assays containing human fibroblasts or keratinocytes and in vivo infected murine wound models;
4. Develop NO-releasing lock solutions for hemodialysis catheters with tunable NO payloads and flux profiles;
5. Investigate the ability of NO-releasing lock solutions to reduce infection, thrombosis, and stenosis using both in vitro and in vivo porcine models.

In this introductory chapter, I sought to describe how bacteria evade conventional antibiotic treatments through acquired antibiotic resistance, biofilm formation, and the propensity to exist in polymicrobial communities. The limited success of antibiotics and associated therapies in treating

chronic wound infections and those associated with hemodialysis catheters has motivated the development of novel therapeutics, including NO-releasing strategies with antibacterial, antibiofilm, inflammation modulatory, angiogenic, anti-thrombosis, and anti-stenosis properties. Previous NO-release systems for treating both wound infections and catheter infections were described, along with their limitations. The synthesis and characterization of novel NO-releasing HA derivatives with tunable NO-release properties will be presented in Chapter 2. With antibacterial action against a broad spectrum of chronic wound pathogens as well as promising preliminary results in promoting wound healing in infected mice, the application of NO-releasing glycosaminoglycans as wound healing agents will be discussed in Chapter 3. Briefly, the use of NO-releasing HA and CS derivatives for inhibiting and eradicating bacteria common infections along with in vitro skin cell toxicity profiles, and effect on fibroblast and keratinocyte adhesion, proliferation, and migration are detailed. The efficacy of NO-releasing GAGs in promoting more rapid wound closure are demonstrated in a murine infection model. In Chapter 4, the development of extended-use NO-releasing lock solutions are described for use in hemodialysis catheters. The NO-release properties are varied to determine the effect on in vitro bacterial adhesion and removal, protein adhesion, and mammalian cell toxicity. Lastly, Chapter 5 provides a final summary of my dissertation research and describes future areas for investigation related to the biomedical applications of multi-action NO-releasing systems.

REFERENCES

(1) US Department of Health and Human Services. *Antibiotic Resistance Threats in the United States*; 2019.

(2) Ventola, C. L. The Antibiotic Resistance Crisis: Part 1: Causes and Threats. *Pharm. Ther.* **2015**, *40*, 277–283.

(3) Bjarnsholt, T.; Kirketerp-Møller, K.; Jensen, P. Ø.; Madsen, K. G.; Phipps, R.; Krogfelt, K.; Høiby, N.; Givskov, M. Why Chronic Wounds Will Not Heal: A Novel Hypothesis. *Wound Repair Regen.* **2008**, *16*, 2–10.

(4) Stewart, P. S.; Costerton, J. W. Antibiotic Resistance of Bacteria in Biofilms. *Lancet* **2001**, *358*, 135–138.

(5) Brogden, K. A.; Guthmiller, J. M.; Taylor, C. E. Human Polymicrobial Infections. *Lancet* **2005**, *365*, 253–255.

(6) Murray, J. L.; Connell, J. L.; Stacy, A.; Turner, K. H.; Whiteley, M. Mechanisms of Synergy in Polymicrobial Infections. *J. Microbiol.* **2014**, *52*, 188–199.

(7) Gjødsbøl, K.; Christensen, J. J.; Karlsmark, T.; Jørgensen, B.; Klein, B. M.; Krogfelt, K. A. Multiple Bacterial Species Reside in Chronic Wounds: A Longitudinal Study. *Int. Wound J.* **2006**, *3*, 225–231.

(8) Kapoor, G.; Saigal, S.; Elongavan, A. Action and Resistance Mechanisms of Antibiotics: A Guide for Clinicians. *J. Anaesthesiol. Clin. Pharmacol.* **2017**, *33*, 300–305.

(9) Lewis, K. Recover the Lost Art of Drug Discovery. *Nature* **2012**, *485*, 439–440.

(10) Norrby, S. R.; Nord, C. E.; Finch, R. Lack of Development of New Antimicrobial Drugs: A Potential Serious Threat to Public Health. *Lancet Infect. Dis.* **2005**, *5*, 115–119.

(11) Tenover, F. C. Mechanisms of Antimicrobial Resistance in Bacteria. *Am. J. Med.* **2006**, *119*.

(12) Blair, J. M. A.; Webber, M. A.; Baylay, A. J.; Ogbolu, D. O.; Piddock, L. J. V. Molecular Mechanisms of Antibiotic Resistance. *Nat. Rev. Microbiol.* **2015**, *13*, 42–51.

(13) Silhavy, T. J.; Kahne, D.; Walker, S. The Bacterial Cell Envelope. *Cold Spring Harb Perspect Biol* **2010**, *2*, 1–16.

(14) Munita, J. M.; Arias, C. A. Mechanisms of Antibiotic Resistance. *Virulence Mech. Bact. Pathog.* **2016**, No. 6, 481–511.

(15) Donlan, R. M. Biofilm Formation: A Clinically Relevant Microbiological Process. *Clin. Infect. Dis.* **2001**, *33*, 1387–1392.

(16) Smith, A. W. Biofilms and Antibiotic Therapy: Is There a Role for Combating Bacterial Resistance by the Use of Novel Drug Delivery Systems? *Adv. Drug Deliv. Rev.* **2005**, *57*, 1539–1550.

(17) Nikaido, H. Multidrug Resistance in Bacteria. *Annu. Rev. Biochem.* **2009**, *78*, 119–146.

(18) Flemming, H. C.; Wingender, J.; Szewzyk, U.; Steinberg, P.; Rice, S. A.; Kjelleberg, S. Biofilms: An Emergent Form of Bacterial Life. *Nat. Rev. Microbiol.* **2016**, *14*, 563–575.

(19) Yin, W.; Wang, Y.; Liu, L.; He, J. Biofilms: The Microbial "Protective Clothing" in Extreme Environments. *Int. J. Mol. Sci.* **2019**, *20*, 3423.

(20) Ceri, H.; Olson, M. E.; Turner, R. J. Needed, New Paradigms in Antibiotic Development. *Expert Opin. Pharmacother.* **2010**, *11*, 1233–1237.

(21) Dunne, W. M. Bacterial Adhesion: Seen Any Good Biofilms Lately? *Clin. Microbiol. Rev.* **2002**, *15*, 155–166.

(22) Lindsay, D.; von Holy, A. Bacterial Biofilms within the Clinical Setting: What Healthcare Professionals Should Know. *J. Hosp. Infect.* **2006**, *64*, 313–325.

(23) Arciola, C. R.; Campoccia, D.; Montanaro, L. Implant Infections: Adhesion, Biofilm Formation and Immune Evasion. *Nat. Rev. Microbiol.* **2018**, *16*, 397–409.

(24) Frieri, M.; Kumar, K.; Boutin, A. Antibiotic Resistance. *J. Infect. Public Health* **2017**, *10*, 369–378.

(25) Hall-Stoodley, L.; Costerton, J. W.; Stoodley, P. Bacterial Biofilms: From the Natural Environment to Infectious Diseases. *Nat. Rev. Microbiol.* **2004**, *2*, 95–108.

(26) Percival, S. L.; McCarty, S. M.; Lipsky, B. Biofilms and Wounds: An Overview of the Evidence. *Adv. Wound Care* **2015**, *4*, 373–381.

(27) Davis, S. C.; Ricotti, C.; Cazzaniga, A.; Welsh, E.; Eaglstein, W. H.; Mertz, P. M. Microscopic and Physiologic Evidence for Biofilm-Associated Wound Colonization in Vivo. *Wound Repair Regen.* **2008**, *16*, 23–29.

(28) Alhede, M.; Kragh, K. N.; Qvortrup, K.; Allesen-Holm, M.; van Gennip, M.; Christensen, L. D.; Jensen, P. Ø.; Nielsen, A. K.; Parsek, M.; Wozniak, D.; Molin, S.; Tolker-Nielsen, T.; Høiby, N.; Givskov, M.; Bjarnsholt, T. Phenotypes of Non-Attached Pseudomonas Aeruginosa Aggregates Resemble Surface Attached Biofilm. *PLoS One* **2011**, *6*.

(29) Schleheck, D.; Barraud, N.; Klebensberger, J.; Webb, J. S.; McDougald, D.; Rice, S. A.; Kjelleberg, S. Pseudomonas Aeruginosa PAO1 Preferentially Grows as Aggregates in Liquid Batch Cultures and Disperses upon Starvation. *PLoS One* **2009**, *4*.

(30) Coquet, L.; Junter, G. A.; Jouenne, T. Resistance of Artificial Biofilms of Pseudomonas Aeruginosa to Imipenem and Tobramycin. *J. Antimicrob. Chemother.* **1998**, *42*, 755–760.

(31) Buch, P. J.; Chai, Y.; Goluch, E. D. Treating Polymicrobial Infections in Chronic Diabetic Wounds. *Clin. Microbiol. Rev.* **2019**, *32*, e0009.

(32) Stewart, P. S. Mechanisms of Antibiotic Resistance in Bacterial Biofilms. *Int. J. Med. Microbiol.* **2002**, *292*, 107–113.

(33) Donlan, R. M.; Costerton, J. W. Biofilms: Survival Mechanisms of Clinically Relevant Microorganisms. *Clin. Microbiol. Rev.* **2002**, *15*, 167–193.

(34) Costerton, J. W.; Montanaro, L.; Arciola, C. R. Biofilm in Implant Infections: Its Production and Regulation. *Int. J. Artif. Organs* **2005**, *28*, 1062–1068.

(35) Hoyle, B. D.; Wong, C. K.; Costerton, J. W. Disparate Efficacy of Tobramycin on Ca(2+)-, Mg(2+)-, and HEPES-Treated Pseudomonas Aeruginosa Biofilms. *Can. J. Microbiol.* **1992**, *38*, 1214–1218.

(36) Suci, P. A.; Mittelman, M. W.; Yu, F. P.; Geesey, G. G. Investigation of Ciprofloxacin Penetration into Pseudomonas Aeruginosa Biofilms. *Antimicrob. Agents Chemother.* **1994**, *38*, 2125–2133.

(37) Nair, N.; Biswas, R.; Götz, F.; Biswas, L. Impact of Staphylococcus Aureus on Pathogenesis in Polymicrobial Infections. *Infect. Immun.* **2014**, *82*, 2162–2169.

(38) Percival, S. L.; Thomas, J. G.; Williams, D. W. Biofilms and Bacterial Imbalances in Chronic Wounds: Anti-Koch. *Int. Wound J.* **2010**, *7*, 169–175.

(39) Peters, B. M.; Jabra-Rizk, M. A.; O'May, G. A.; William Costerton, J.; Shirtliff, M. E. Polymicrobial Interactions: Impact on Pathogenesis and Human Disease. *Clin. Microbiol. Rev.* **2012**, *25*, 193–213.

(40) Price, L. B.; Liu, C. M.; Melendez, J. H.; Frankel, Y. M.; Engelthaler, D.; Aziz, M.; Bowers, J.; Rattray, R.; Ravel, J.; Kingsley, C.; Keim, P. S.; Lazarus, G. S.; Zenilman, J. M. Community Analysis of Chronic Wound Bacteria Using 16S RRNA Gene-Based Pyrosequencing: Impact of Diabetes and Antibiotics on Chronic Wound Microbiota. *PLoS One* **2009**, *4*, e6462.

(41) Citron, D. M.; Goldstein, E. J. C.; Merriam, C. V.; Lipsky, B. A.; Abramson, M. A. Bacteriology of Moderate-to-Severe Diabetic Foot Infections and in Vitro Activity of Antimicrobial Agents. *J. Clin. Microbiol.* **2007**, *45*, 2819–2828.

(42) Sen, C. K.; Gordillo, G. M.; Roy, S.; Kirsner, R.; Lambert, L.; Hunt, T. K.; Gottrup, F.; Gurtner, G. C.; Longaker, M. T. Human Skin Wounds: A Major and Snowballing Threat to Public Health and the Economy. *Wound Repair Regen.* **2009**, *17*, 763–771.

(43) Guo, S.; DiPietro, L. A. Factors Affecting Wound Healing. *J. Dent. Res.* **2010**, *89*, 219–229.

(44) Mathieu, D. *Handbook on Hyperbaric Medicine*; Springer, 2006.

(45) Malone-Povolny, M. J.; Maloney, S. E.; Schoenfisch, M. H. Nitric Oxide Therapy for Diabetic Wound Healing. *Adv. Healthc. Mater.* **2019**, *8*, 1801210.

(46) Mast, B. A.; Schultz, G. S. Interactions of Cytokines, Growth Factors, and Proteases in Acute and Chronic Wounds. *Wound Repair Regen.* **1996**, *4*, 411–420.

(47) Han, G.; Ceilley, R. Chronic Wound Healing: A Review of Current Management and Treatments. *Adv. Ther.* **2017**, *34*, 599–610.

(48) Campos, A. C. L.; Groth, A. K.; Branco, A. B. Assessment and Nutritional Aspects of Wound Healing. *Curr. Opin. Clin. Nutr. Metab. Care* **2008**, *11*, 281–288.

(49) Järbrink, K.; Ni, G.; Sönnergren, H.; Schmidtchen, A.; Pang, C.; Bajpai, R.; Car, J. The Humanistic and Economic Burden of Chronic Wounds: A Protocol for a Systematic Review. *Syst. Rev.* **2017**, *6*, 1–7.

(50) Stechmiller, J. K.; Childress, B.; Cowan, L. Arginine Supplementation and Wound Healing. **2005**, No. February 2005, 52–61.

(51) Tandara, A. A.; Mustoe, T. A. Oxygen in Wound Healing - More than a Nutrient. *World J. Surg.* **2004**, *28*, 294–300.

(52) Castilla, D. M.; Liu, Z.-J.; Velazquez, O. C. Oxygen: Implications for Wound Healing. *Adv. Wound Care* **2012**, *1*, 225–230.

(53) James, G. A.; Swogger, E.; Wolcott, R.; Pulcini, E. D.; Secor, P.; Sestrich, J.; Costerton, J. W.; Stewart, P. S. Biofilms in Chronic Wounds. *Wound Repair Regen.* **2008**, *16*, 37–44.

(54) Chen, L.; Wen, Y. M. The Role of Bacterial Biofilm in Persistent Infections and Control Strategies. *Int. J. Oral Sci.* **2011**, *3*, 66–73.

(55) Percival, S. L.; Hill, K. E.; Williams, D. W.; Hooper, S. J.; Thomas, D. W.; Costerton, J. W. A Review of the Scientific Evidence for Biofilms in Wounds. *Wound Repair Regen.* **2012**, *20*, 647–657.

(56) Kirketerp-Møller, K.; Jensen, P.; Fazli, M.; Madsen, K. G.; Pedersen, J.; Moser, C.; Tolker-Nielsen, T.; Høiby, N.; Givskov, M.; Bjarnsholt, T. Distribution, Organization, and Ecology of Bacteria in Chronic Wounds. *J. Clin. Microbiol.* **2008**, *46*, 2717–2722.

(57) Olokoba, A. B.; Obateru, O. A.; Olokoba, L. B. Type 2 Diabetes Mellitus: A Review of Current Trends. *Oman Med. J.* **2012**, *27*, 269–273.

(58) Bansal, S.; Siddarth, M.; Chawla, D.; Banerjee, B. D.; Madhu, S. V.; Tripathi, A. K. Advanced Glycation End Products Enhance Reactive Oxygen and Nitrogen Species Generation in Neutrophils in Vitro. *Mol. Cell. Biochem.* **2012**, *361*, 289–296.

(59) Hirsch, T.; Spielmann, M.; Zuhaili, B.; Koehler, T.; Fossum, M.; Steinau, H. U.; Yao, F.; Steinstraesser, L.; Onderdonk, A. B.; Eriksson, E. Enhanced Susceptibility to Infections in a Diabetic Wound Healing Model. *BMC Surg.* **2008**, *8*, 1–8.

(60) Markova, A.; Mostow, E. N. US Skin Disease Assessment: Ulcer and Wound Care. *Dermatol. Clin.* **2012**, *30*, 107–111.

(61) Powers, J. G.; Higham, C.; Broussard, K.; Phillips, T. J. Chronic Wound Care and Management. *J. Am. Acad. Dermatol.* **2016**, *74*, 607–625.

(62) Siddiqui, A. R.; Bernstein, J. M. Chronic Wound Infection: Facts and Controversies. *Clin. Dermatol.* **2010**, *28*, 519–526.

(63) Hollinworth, H.; Collier, M. Nurses' Views about Pain and Trauma at Dressing Changes: Results of a National Survey. *J. Wound Care* **2013**, *9*, 369–373.

(64) Himmelfarb, J.; Ikizler, T. A. Hemodialysis. *N. Engl. J. Med.* **2010**, *363*, 1833–1845.

(65) National Kidney Foundation. *Hemodialysis Access: What You Need to Know*; 2006.

(66) Dougherty, M. J.; Troutman, D. A.; Maloni, K. C. Management of Difficult Dialysis Access Issues for Dialysis Patients. *Adv. Surg.* **2019**, *53*, 83–101.

(67) Delistefani, F.; Wallbach, M.; Müller, G. A.; Koziolek, M. J.; Grupp, C. Risk Factors for Catheter-Related Infections in Patients Receiving Permanent Dialysis Catheter. *BMC Nephrol.* **2019**, *20*, 1–7.

(68) Kusminsky, R. E. Complications of Central Venous Catheterization. *J. Am. Coll. Surg.* **2007**, *204*, 681–696.

(69) Barraclough, K. A.; Hawley, C. M.; Playford, E. G.; Johnson, D. W. Prevention of Access-Related Infection in Dialysis. *Expert Rev. Anti. Infect. Ther.* **2009**, *7*, 1185–1200.

(70) Costerton, A. J. W.; Stewart, P. S.; Greenberg, E. P. Bacterial Biofilms : A Common Cause of Persistent Infections Published by : American Association for the Advancement of Science Linked References Are Available on JSTOR for This Article : Bacterial Bioflims : A Common Cause of Persistent Infections. *Science (80-.).* **1999**, *284*, 1318–1322.

(71) Goto, T.; Nakame, Y.; Nishida, M.; Ohi, Y. In Vitro Bactericidal Activities of Betalactamases, Amikacin, and Fluoroquinolones against Pseudomonas Aeruginosa Biofilm in Artificial Urine. *Urology* **1999**, *53*, 1058–1062.

(72) Schwab, S. J.; Beathard, G. The Hemodialysis Catheter Conundrum: Hate Living with Them, but Can't Live without Them. *Kidney Int.* **1999**, *56*, 1–17.

(73) Wo, Y.; Brisbois, E. J.; Bartlett, R. H.; Meyerhoff, M. E. Recent Advances in Thromboresistant and Antimicrobial Polymers for Biomedical Applications: Just Say Yes to Nitric Oxide (NO). *Biomater. Sci.* **2016**, *4*, 1161–1183.

(74) Agarwal, A. K. Central Vein Stenosis: Current Concepts. *Adv. Chronic Kidney Dis.* **2009**, *16*, 360–370.

(75) McGee, D. C.; Gould, M. K. Preventing Complications of Central Venous Catheterization. *N. Engl. J. Med.* **2003**, *348*, 1123–1133.

(76) Poole, C. V.; Carlton, D.; Bimbo, L.; Allon, M. Treatment of Catheter-Related Bacteraemia with an Antibiotic Lock Protocol: Effect of Bacterial Pathogen. *Nephrol. Dial. Transplant.* **2004**, *19*, 1237–1244.

(77) Betjes, M. G. H.; van Agteren, M. Prevention of Dialysis Catheter-Related Sepsis with a Citrate-Taurolidine-Containing Lock Solution. *Nephrol. Dial. Transplant.* **2004**, *19*, 1546–1551.

(78) Ramanathan, V.; Darouiche, R. O. Prevention and Management of Hemodialysis Catheter Infections. *Expert Rev. Anti. Infect. Ther.* **2012**, *10*, 1447–1455.

(79) Raad, I. I.; Luna, M.; Khalil, S. A. M.; Costerton, J. W.; Lam, C.; Bodey, G. P. The Relationship Between the Thrombotic and Infectious Complications of Central Venous Catheters. *JAMA J. Am. Med. Assoc.* **1994**, *271*, 1014–1016.

(80) Yevzlin, A. S. Hemodialysis Catheter-Associated Central Venous Stenosis. *Semin. Dial.* **2008**, *21*, 522–527.

(81) Bakken, A. M.; Protack, C. D.; Saad, W. E.; Lee, D. E.; Waldman, D. L.; Davies, M. G. Long-Term Outcomes of Primary Angioplasty and Primary Stenting of Central Venous Stenosis in Hemodialysis Patients. *J. Vasc. Surg.* **2007**, *45*, 776–783.

(82) Luo, J. D.; Chen, A. F. Nitric Oxide: A Newly Discovered Function on Wound Healing. *Acta Pharmacol. Sin.* **2005**, *26*, 259–264.

(83) Rizk, M.; Witte, M. B.; Barbul, A. Nitric Oxide and Wound Healing. *World J. Surg.* **2004**, *28*, 301–306.

(84) Bredt, D. S.; Hwang, P. M.; Snyder, S. H. Localization of Nitric Oxide Synthase Indicating a Neural Role for Nitric Oxide. *Nature* **1990**, *347*, 768–770.

(85) Snyder, S. H. Nitric Oxide: First in a New Class of Neurotransmitters. *Science (80-.).* **1992**, *257*, 494–496.

(86) Garthwaite, J. Concepts of Neural Nitric Oxide-Mediated Transmission. *Eur. J. Neurosci.* **2008**, *27*, 2783–2802.

(87) Nathan, C. F.; Hibbs, J. B. Role of Nitric Oxide Synthesis in Macrophage Antimicrobial Activity. *Curr. Opin. Immunol.* **1991**, *3*, 65–70.

(88) Loscalzo, J.; Welch, G. Nitric Oxide and Its Role in the Cardiovascular System. *Prog. Cardiovasc. Dis.* **1995**, *38*, 87–104.

(89) Walford, G.; Loscalzo, J. Nitric Oxide in Vascular Biology. *J. Thromb. Haemost.* **2003**, *1*, 2112–2118.

(90) Cooke, J. P. NO and Angiogenesis. *Atheroscler. Suppl.* **2003**, *4*, 53–60.

(91) Morbidelli, L.; Donnini, S.; Ziche, M. Role of Nitric Oxide in the Modulation of Angiogenesis. *Curr. Pharm. Des.* **2005**, *9*, 521–530.

(92) Donnini, S.; Ziche, M. Constitutive and Inducible Nitric Oxide Synthase: Role in Angiogenesis. *Antioxidants Redox Signal.* **2002**, *4*, 817–823.

(93) Carpenter, A. W.; Schoenfisch, M. H. Nitric Oxide Release: Part II. Therapeutic Applications. *Chem. Soc. Rev.* **2012**, *41*, 3742–3752.

(94) Bredt, D. S.; Snyder, S. H. Isolation of Nitric Oxide Synthetase, a Calmodulin-Requiring Enzyme. *Proc. Natl. Acad. Sci. U. S. A.* **1990**, *87*, 682–685.

(95) Knowles, R. G.; Moncada, S. Nitric Oxide Synthases in Mammals. *Biochem. J.* **1994**, *298*, 249–258.

(96) Förstermann, U.; Sessa, W. C. Nitric Oxide Synthases: Regulation and Function. *Eur. Heart J.* **2012**, *33*, 829–837.

(97) Wink, D. A.; Mitchell, J. B. Chemical Biology of Nitric Oxide: Insights into Regulatory, Cytotoxic, and Cytoprotective Mechanisms of Nitric Oxide. *Free Radic. Biol. Med.* **1998**, *25*, 434–456.

(98) Fang, F. C. Antimicrobial Reactive Oxygen and Nitrogen Species: Concepts and Controversies. *Nat. Rev. Microbiol.* **2004**, *2*, 820–832.

(99) Möller, M. N.; Li, Q.; Lancaster, J. R.; Denicola, A. Acceleration of Nitric Oxide Autoxidation and Nitrosation by Membranes. *IUBMB Life* **2007**, *59*, 243–248.

(100) Hetrick, E. M.; Shin, J. H.; Stasko, N. A.; Johnson, C. B.; Wespe, D. A.; Holmuhamedov, E.; Schoenfisch, M. H. Bactericidal Efficacy of Nitric Oxide-Releasing Silica Nanoparticles. *ACS Nano* **2008**, *2*, 235–246.

(101) Barraud, N.; Kelso, M.; Rice, S.; Kjelleberg, S. Nitric Oxide: A Key Mediator of Biofilm Dispersal with Applications in Infectious Diseases. *Curr. Pharm. Des.* **2014**, *21*, 31–42.

(102) Neufeld, B. H.; Reynolds, M. M. Critical Nitric Oxide Concentration for Pseudomonas Aeruginosa Biofilm Reduction on Polyurethane Substrates. *Biointerphases* **2016**, *11*, 1–8.

(103) Schairer, D. O.; Chouake, J. S.; Nosanchuk, J. D.; Friedman, A. J. The Potential of Nitric Oxide Releasing Therapies as Antimicrobial Agents. *Virulence* **2012**, *3*, 271–279.

(104) Fang, F. C. Antimicrobial Actions of Reactive Oxygen Species. *MBio* **2011**, *2*, 1–6.

(105) Privett, B. J.; Broadnax, A. D.; Bauman, S. J.; Riccio, D. A.; Schoenfisch, M. H. Examination of Bacterial Resistance to Exogenous Nitric Oxide. *Nitric Oxide* **2012**, *26*, 169–173.

(106) Rouillard, K. R.; Novak, O. P.; Pistiolis, A. M.; Yang, L.; Ahonen, M. J. R.; McDonald, R. A.; Schoenfisch, M. H. Exogenous Nitric Oxide Improves Antibiotic Susceptibility in Resistant Bacteria. *ACS Infect. Dis.* **2021**, *7*, 23–33.

(107) Marsboom, G.; Rehman, J. Hypoxia Signaling in Vascular Homeostasis. *Physiology* **2018**, *33*, 328–337.

(108) Ziche, M.; Morbidelli, L. Nitric Oxide and Angiogenesis. *J. Neurooncol.* **2000**, *50*, 139–148.

(109) Cirino, G.; Distrutti, E.; Wallace, J. L. Nitric Oxide and Inflammation. *Inflamm. Allergy - Drug Targets* **2006**, *5*, 115–119.

(110) Guzik, T. J.; Korbut, R.; Adamek-Guzik, T. Nitric Oxide and Superoxide in Inflammation and Immune Regulation. *J. Physiol. Pharmacol.* **2003**, *54*, 469–487.

(111) Coleman, J. W. Nitric Oxide in Immunity and Inflammation. *Int. Immunopharmacol.* **2001**, *1*, 1397–1406.

(112) Kobayashi, Y. The Regulatory Role of Nitric Oxide in Proinflammatory Cytokine Expression during the Induction and Resolution of Inflammation. *J. Leukoc. Biol.* **2010**, *88*, 1157–1162.

(113) Ajuebor, M. N.; Virág, L.; Flower, R. J.; Perretti, M.; Szabó, C. Role of Inducible Nitric Oxide Synthase in the Regulation of Neutrophil Migration in Zymosan-Induced Inflammation. *Immunology* **1998**, *95*, 625–630.

(114) Loscalzo, J.; Freedman, J.; Inbal, A.; Keaney, J. F.; Michelson, A. D.; Vita, J. A. Nitric Oxide Insufficiency and Arterial Thrombosis. *Trans. Am. Clin. Climatol. Assoc.* **2000**, *111*, 158–163.

(115) Freedman, J. E.; Loscalzo, J. Nitric Oxide and Its Relationship to Thrombotic Disorders. *J. Thromb. Haemost.* **2003**, *1*, 1183–1188.

(116) Miller, O. I.; Celermajer, D. S.; Deanfield, J. E.; Macrae, D. J. Guidelines for the Safe Administration of Inhaled Nitric Oxide. *Arch. Dis. Child.* **1994**, *70*, 47–49.

(117) Yang, Y.; Qi, P. K.; Yang, Z. L.; Huang, N. Nitric Oxide Based Strategies for Applications of Biomedical Devices. *Biosurface and Biotribology* **2015**, *1*, 177–201.

(118) Weinberger, B.; Laskin, D. L.; Heck, D. E.; Laskin, J. D. The Toxicology of Inhaled Nitric Oxide. *Toxilogical Sci.* **2001**, *59*, 5–16.

(119) Wang, P. G.; Xian, M.; Tang, X.; Wu, X.; Wen, Z.; Cai, T.; Janczuk, A. J. Nitric Oxide Donors: Chemical Activities and Biological Applications. *Chem. Rev.* **2002**, *102*, 1091–1134.

(120) Riccio, D. A.; Schoenfisch, M. H. Nitric Oxide Release: Part I. Macromolecular Scaffolds. *Chem. Soc. Rev.* **2012**, *41*, 3731–3741.

(121) Zhang, Y.; Hogg, N. S-Nitrosothiols: Cellular Formation and Transport. *Free Radic. Biol. Med.* **2005**, *38*, 831–838.

(122) Williams, D. L. H. The Chemistry of S-Nitrosothiols. *Acc. Chem. Res.* **1999**, *32*, 869–876.

(123) Singh, R. J.; Hogg, N.; Joseph, J.; Kalyanaraman, B. Mechanism of Nitric Oxide Release from S -Nitrosothiols. *J. Biol. Chem.* **1996**, *271*, 18596–18603.

(124) Dicks, A. P.; Williams, D. L. H. Generation of Nitric Oxide from S-Nitrosothiols Using Protein-Bound Cu2+ Sources. *Chem. Biol.* **1996**, *3*, 655–659.

(125) Catalani, S.; Paganelli, M.; Gilberti, M. E.; Rozzini, L.; Lanfranchi, F.; Padovani, A.; Apostoli, P. Free Copper in Serum: An Analytical Challenge and Its Possible Applications. *J. Trace Elem. Med. Biol.* **2018**, *45*, 176–180.

(126) Hrabie, J. A.; Keefer, L. K. Chemistry of the Nitric Oxide-Releasing Diazeniumdiolate ("nitrosohydroxylamine") Functional Group and Its Oxygen-Substituted Derivatives. *Chem. Rev.* **2002**, *102*, 1135–1154.

(127) Keefer, L. K. Fifty Years of Diazeniumdiolate Research: From Laboratory Curiosity to Broad-Spectrum Biomedical Advances. *ACS Chem. Biol.* **2011**, *6*, 1147–1155.

(128) Hrabie, J. A.; Klose, J. R.; Wink, D. A.; Keefer, L. K. New Nitric Oxide-Releasing Zwitterions Derived from Polyamines. *J. Org. Chem.* **1993**, *58*, 1472–1476.

(129) Ahonen, M. J. R.; Suchyta, D. J.; Zhu, H.; Schoenfisch, M. H. Nitric Oxide-Releasing Alginates. *Biomacromolecules* **2018**, *19*, 1189–1197.

(130) Yang, L.; Feura, E. S.; Ahonen, M. J. R.; Schoenfisch, M. H. Nitric Oxide–Releasing Macromolecular Scaffolds for Antibacterial Applications. *Adv. Healthc. Mater.* **2018**, *7*, 1–18.

(131) Suchyta, D. J.; Schoenfisch, M. H. Controlled Release of Nitric Oxide from Liposomes. *ACS Biomater. Sci. Eng.* **2017**, *3*, 2136–2143.

(132) Suchyta, D. J.; Schoenfisch, M. H. Encapsulation of N-Diazeniumdiolates within Liposomes for Enhanced Nitric Oxide Donor Stability and Delivery. *Mol. Pharm.* **2015**, *12*, 3569–3574.

(133) Kitano, T.; Yamada, H.; Kida, M.; Okada, Y.; Saika, S.; Yoshida, M. Impaired Healing of a Cutaneous Wound in an Inducible Nitric Oxide Synthase-Knockout Mouse. *Dermatol. Res. Pract.* **2017**, *2017*, 1–11.

(134) Efron, D. T.; Most, D.; Barbul, A. Role of Nitric Oxide in Wound Healing. *Curr. Opin. Clin. Nutr. Metab. Care* **2000**, *3*, 197–204.

(135) Miller, C. C.; Miller, M. K.; Ghaffari, A.; Kunimoto, B. Treatment of Chronic Nonhealing Leg Ulceration with Gaseous Nitric Oxide: A Case Study. *J. Cutan. Med. Surg.* **2004**, *8*, 233–238.

(136) Ghaffari, A.; Jalili, R.; Ghaffari, M.; Miller, C.; Ghahary, A. Efficacy of Gaseous Nitric Oxide in the Treatment of Skin and Soft Tissue Infections. *Wound Repair Regen.* **2007**, *15*, 368–377.

(137) Moeen Rezakhanlou, A.; Miller, C.; McMullin, B.; Ghaffari, A.; Garcia, R.; Ghahary, A. Gaseous Nitric Oxide Exhibits Minimal Effect on Skin Fibroblast Extracellular Matrix Gene Expression and Immune Cell Viability. *Cell Biol. Int.* **2011**, *35*, 407–415.

(138) Shekhter, A. B.; Serezhenkov, V. A.; Rudenko, T. G.; Pekshev, A. V.; Vanin, A. F. Beneficial Effect of Gaseous Nitric Oxide on the Healing of Skin Wounds. *Nitric Oxide* **2005**, *12*, 210–219.

(139) Kim, J. O.; Noh, J. K.; Thapa, R. K.; Hasan, N.; Choi, M.; Kim, J. H.; Lee, J. H.; Ku, S. K.; Yoo, J. W. Nitric Oxide-Releasing Chitosan Film for Enhanced Antibacterial and in Vivo Wound-Healing Efficacy. *Int. J. Biol. Macromol.* **2015**, *79*, 217–225.

(140) Shishido, S. M.; Seabra, A. B.; Loh, W.; De Oliveira, M. G. Thermal and Photochemical Nitric Oxide Release from S-Nitrosothiols Incorporated in Pluronic F127 Gel: Potential Uses for Local and Controlled Nitric Oxide Release. *Biomaterials* **2003**, *24*, 3543–3553.

(141) Seabra, A. B.; Fitzpatrick, A.; Paul, J.; De Oliveira, M. G.; Weller, R. Topically Applied S-Nitrosothiol-Containing Hydrogels as Experimental and Pharmacological Nitric Oxide Donors in Human Skin. *Br. J. Dermatol.* **2004**, *151*, 977–983.

(142) Seabra, A. B.; Pankotai, E.; Fehér, M.; Somlai, Á.; Kiss, L.; Bíró, L.; Szabó, C.; Kollai, M.; De Oliveira, M. G.; Lacza, Z. S-Nitrosoglutathione-Containing Hydrogel Increases Dermal Blood Flow in Streptozotocin-Induced Diabetic Rats. *Br. J. Dermatol.* **2007**, *156*, 814–818.

(143) Amadeu, T. P.; Seabra, A. B.; de Oliveira, M. G.; Monte-Alto-Costa, A. Nitric Oxide Donor Improves Healing If Applied on Inflammatory and Proliferative Phase. *J. Surg. Res.* **2008**, *149*, 84–93.

(144) Dashti, N.; Ansari, M.; Shabani, M.; Vardasti, S.; Mirsalehian, A. The Effect of Nitric Oxide Donor in Diabetic Wound Healing. *Iran. J. Public Health* **2003**, *32*, 59–63.

(145) Brisbois, E. J.; Bayliss, J.; Wu, J.; Major, T. C.; Xi, C.; Wang, S. C.; Bartlett, R. H.; Handa, H.; Meyerhoff, M. E. Optimized Polymeric Film-Based Nitric Oxide Delivery Inhibits Bacterial Growth in a Mouse Burn Wound Model. *Acta Biomater.* **2014**, *10*, 4136–4142.

(146) Lowe, A.; Bills, J.; Verma, R.; Lavery, L.; Davis, K.; Balkus, K. J. Electrospun Nitric Oxide Releasing Bandage with Enhanced Wound Healing. *Acta Biomater.* **2015**, *13*, 121–130.

(147) Masters, K. S. B.; Leibovich, S. J.; Belem, P.; West, J. L.; Poole-Warren, L. A. Effects of Nitric Oxide Releasing Poly(Vinyl Alcohol) Hydrogel Dressings on Dermal Wound Healing in Diabetic Mice. *Wound Repair Regen.* **2002**, *10*, 286–295.

(148) Schiraldi, C.; Cimini, D.; De Rosa, M. Production of Chondroitin Sulfate and Chondroitin. *Appl. Microbiol. Biotechnol.* **2010**, *87*, 1209–1220.

(149) Scharnweber, D.; Hübner, L.; Rother, S.; Hempel, U.; Anderegg, U.; Samsonov, S. A.; Pisabarro, M. T.; Hofbauer, L.; Schnabelrauch, M.; Franz, S.; Simon, J.; Hintze, V. Glycosaminoglycan Derivatives: Promising Candidates for the Design of Functional Biomaterials. *J. Mater. Sci. Mater. Med.* **2015**, *26*.

(150) Fallacara, A.; Baldini, E.; Manfredini, S.; Vertuani, S. Hyaluronic Acid in the Third Millennium. *Polymers* **2018**, *10*, 701.

(151) Aya, K. L.; Stern, R. Hyaluronan in Wound Healing: Rediscovering a Major Player. *Wound Repair Regen.* **2014**, *22*, 579–593.

(152) Volpi, N. Therapeutic Applications of Glycosaminoglycans. *Curr. Med. Chem.* **2006**, *13*, 1799–1810.

(153) Soares Da Costa, D.; Reis, R. L.; Pashkuleva, I. Sulfation of Glycosaminoglycans and Its Implications in Human Health and Disorders. *Annu. Rev. Biomed. Eng.* **2017**, *19*, 1–26.

(154) Trownbridge, J. M.; Gallo, R. L. Dermatan Sulfate: New Functions from an Old Glycosaminoglycan. *Glycobiology* **2002**, *12*, 117R-125R.

(155) Melrose, J. Glycosaminoglycans in Wound Healing. *Bone Tissue Regen. Insights* **2016**, *7*,

29–50.

(156) Yang, H.; Song, L.; Zou, Y.; Sun, D.; Wang, L.; Yu, Z.; Guo, J. Role of Hyaluronic Acids and Potential as Regenerative Biomaterials in Wound Healing. *ACS Appl. Bio Mater.* **2021**, *4*, 311-324.

(157) Hussain, Z.; Thu, H. E.; Katas, H.; Nasir, S.; Bukhari, A.; Bukhari, S. N. A. Hyaluronic Acid-Based Biomaterials: A Versatile and Smart Approach to Tissue Regeneration and Treating Traumatic, Surgical, and Chronic Wounds. *Polym. Rev.* **2017**, *57*, 594–630.

(158) Graça, M. F. P.; Miguel, S. P.; Cabral, C. S. D.; Correia, I. J. Hyaluronic Acid — Based Wound Dressings : A Review. *Carbohydr. Polym.* **2020**, *241*, 116364.

(159) Gao, F.; Liu, Y.; He, Y.; Yang, C.; Wang, Y.; Shi, X.; Wei, G. Hyaluronan Oligosaccharides Promote Excisional Wound Healing through Enhanced Angiogenesis. *Matrix Biol.* **2010**, *29*, 107–116.

(160) Tolg, C.; Telmer, P.; Turley, E. Specific Sizes of Hyaluronan Oligosaccharides Stimulate Fibroblast Migration and Excisional Wound Repair. *PLoS One* **2014**, *9*, 1–10.

(161) Sattar, A.; Rooney, P.; Kumar, S.; Pye, D.; West, D. C.; Scott, I.; Ledger, P. Application of Angiogenic Oligosaccharides of Hyaluronan Increases Blood Vessel Numbers in Rat Skin. *J. Invest. Dermatol.* **1994**, *103*, 576–579.

(162) Vazquez, J. R.; Short, B.; Findlow, A. H.; Nixon, B. P.; Boulton, A. J. M.; Armstrong, D. G. Outcomes of Hyaluronan Therapy in Diabetic Foot Wounds. *Diabetes Res. Clin. Pract.* **2003**, *59*, 123–127.

(163) Hong, L.; Shen, M.; Fang, J.; Wang, Y.; Bao, Z.; Bu, S.; Zhu, Y. Hyaluronic Acid (HA)-Based Hydrogels for Full-Thickness Wound Repairing and Skin Regeneration. *J. Mater. Sci. Mater. Med.* **2018**, *29*, 1–11.

(164) Zhao, L.; Liu, M.; Wang, J.; Zhai, G. Chondroitin Sulfate-Based Nanocarriers for Drug / Gene Delivery. *Carbohydr. Polym.* **2015**, *133*, 391–399.

(165) Mikami, T.; Kitagawa, H. Biosynthesis and Function of Chondroitin Sulfate. *Biochim. Biophys. Acta - Gen. Subj.* **2013**, *1830*, 4719–4733.

(166) Corsuto, L.; Rother, S.; Koehler, L.; Bedini, E.; Moeller, S.; Schnabelrauch, M.; Hintze, V.; Schiraldi, C.; Scharnweber, D. Sulfation Degree Not Origin of Chondroitin Sulfate Derivatives Modulates Keratinocyte Response. *Carbohydr. Polym.* **2018**, *191*, 53–64.

(167) Kwon, H. J.; Han, Y. Chondroitin Sulfate-Based Biomaterials for Tissue Engineering. *Turkish J. Biol.* **2016**, *40*, 290–299.

(168) Zou, X. H.; Foong, W. C.; Cao, T.; Bay, B. H.; Ouyang, H. W.; Yip, G. W. Chondroitin

Sulfate in Palatal Wound Healing. *J. Dent. Res.* **2004**, *83*, 880–885.

(169) Zou, X. H.; Jiang, Y. Z.; Zhang, G. R.; Jin, H. M.; Hieu, N. T. M.; Ouyang, H. W. Specific Interactions between Human Fibroblasts and Particular Chondroitin Sulfate Molecules for Wound Healing. *Acta Biomater.* **2009**, *5*, 1588–1595.

(170) Lamari, F. N. The Potential of Chondroitin Sulfate as a Therapeutic Agent. *Connect. Tissue Res.* **2008**, *49*, 289–292.

(171) Iovu, M.; Dumais, G.; du Souich, P. Anti-Inflammatory Activity of Chondroitin Sulfate. *Osteoarthr. Cartil.* **2008**, *16*, 14–18.

(172) Pal, D.; Saha, S. Chondroitin: A Natural Biomarker with Immense Biomedical Applications. *RSC Adv.* **2019**, *9*, 28061–28077.

(173) Vallières, M.; du Souich, P. Modulation of Inflammation by Chondroitin Sulfate. *Osteoarthr. Cartil.* **2010**, *18*, 18–23.

(174) Kirker, K. R.; Luo, Y.; Nielson, J. H.; Shelby, J.; Prestwich, G. D. Glycosaminoglycan Hydrogel Films as Bio-Interactive Dressings for Wound Healing. *Biomaterials* **2002**, *23*, 3661–3671.

(175) Gilbert, M. E.; Kirker, K. R.; Gray, S. D.; Ward, P. D.; Szakacs, J. G.; Prestwich, G. D.; Orlandi, R. R. Chondroitin Sulfate Hydrogel and Wound Healing in Rabbit Maxillary Sinus Mucosa. *Laryngoscope* **2004**, *114*, 1406–1409.

(176) Bhowmick, S.; Rother, S.; Zimmermann, H.; Lee, P. S.; Moeller, S.; Schnabelrauch, M.; Koul, V.; Jordan, R.; Hintze, V.; Scharnweber, D. Biomimetic Electrospun Scaffolds from Main Extracellular Matrix Components for Skin Tissue Engineering Application – The Role of Chondroitin Sulfate and Sulfated Hyaluronan. *Mater. Sci. Eng. C* **2017**, *79*, 15–22.

(177) Hou, Z.; Wu, Y.; Xu, C.; Reghu, S.; Shang, Z.; Chen, J.; Pranantyo, D.; Marimuth, K.; De, P. P.; Ng, O. T.; Pethe, K.; Kang, E. T.; Li, P.; Chan-Park, M. B. Precisely Structured Nitric-Oxide-Releasing Copolymer Brush Defeats Broad-Spectrum Catheter-Associated Biofilm Infections in Vivo. *ACS Cent. Sci.* **2020**, *6*, 2031–2045.

(178) Brisbois, E. J.; Major, T. C.; Goudie, M. J.; Meyerhoff, M. E.; Bartlett, R. H.; Handa, H. Attenuation of Thrombosis and Bacterial Infection Using Dual Function Nitric Oxide Releasing Central Venous Catheters in a 9 Day Rabbit Model. *Acta Biomater.* **2016**, *44*, 304–312.

(179) Wo, Y.; Brisbois, E. J.; Wu, J.; Li, Z.; Major, T. C.; Mohammed, A.; Wang, X.; Colletta, A.; Bull, J. L.; Matzger, A. J.; Xi, C.; Bartlett, R. H.; Meyerhoff, M. E. Reduction of Thrombosis and Bacterial Infection via Controlled Nitric Oxide (NO) Release from S-Nitroso-N-Acetylpenicillamine (SNAP) Impregnated CarboSil Intravascular Catheters. *ACS Biomater. Sci. Eng.* **2017**, *3*, 349–359.

(180) Goudie, M. J.; Pant, J.; Handa, H. Liquid-Infused Nitric Oxide-Releasing (LINORel) Silicone for Decreased Fouling, Thrombosis, and Infection of Medical Devices. *Sci. Rep.* **2017**, *7*, 1–13.

(181) Pant, J.; Goudie, M. J.; Chaji, S. M.; Johnson, B. W.; Handa, H. Nitric Oxide Releasing Vascular Catheters for Eradicating Bacterial Infection. *J. Biomed. Mater. Res. - Part B Appl. Biomater.* **2018**, *106*, 2849–2857.

(182) Homeyer, K. H.; Goudie, M. J.; Singha, P.; Handa, H. Liquid-Infused Nitric-Oxide-Releasing Silicone Foley Urinary Catheters for Prevention of Catheter-Associated Urinary Tract Infections. *ACS Biomater. Sci. Eng.* **2019**, *5*, 2021–2029.

(183) Brisbois, E. J.; Kim, M.; Wang, X.; Mohammed, A.; Major, T. C.; Wu, J.; Brownstein, J.; Xi, C.; Handa, H.; Bartlett, R. H.; Meyerhoff, M. E. Improved Hemocompatibility of Multilumen Catheters via Nitric Oxide (NO) Release from S-Nitroso-N-Acetylpenicillamine (SNAP) Composite Filled Lumen. *ACS Appl. Mater. Interfaces* **2016**, *8*, 29270–29279.

(184) Doverspike, J. C.; Mack, S. J.; Luo, A.; Stringer, B.; Reno, S.; Cornell, M. S.; Rojas-Pena, A.; Wu, J.; Xi, C.; Yevzlin, A.; Meyerhoff, M. E. Nitric Oxide-Releasing Insert for Disinfecting the Hub Region of Tunnel Dialysis Catheters. *ACS Appl. Mater. Interfaces* **2020**, *12*, 44475–44484.

(185) Kumar, R.; Massoumi, H.; Chug, M. K.; Brisbois, E. J. S-Nitroso- N-Acetyl- l -Cysteine Ethyl Ester (SNACET) Catheter Lock Solution to Reduce Catheter-Associated Infections. *ACS Appl. Mater. Interfaces* **2021**, *13*, 25813–25824.

CHAPTER 2: NITRIC OXIDE-RELEASING HYALURONIC ACID AS AN ANTIBACTERIAL AGENT FOR WOUND THERAPY[1]

2.1. Introduction

In response to tissue injury, wound healing proceeds through four overlapping phases: hemostasis, inflammation, proliferation, and remodeling.[1] While the exact timeline of wound healing is dependent upon multiple factors (e.g., wound location, severity), acute wounds make progress toward closure without significant intervention. However, some wounds stall in a state of inflammation for extended or indefinite amounts of time, often as a result of disease and persistent stimuli such as repetitive tissue trauma or pressure, and are commonly referred to as chronic wounds.[2–4] Chronic wounds affect up to 6.5 million people in the United States and may lead to amputations and even mortality if not resolved.[5,6]

Underlying diseases and conditions that affect the host immune response by altering inflammatory cell migration or cell signaling (e.g., diabetes, malnutrition) are often associated with chronic wound development.[2,7] The delayed healing associated with chronic wounds is frequently initiated or exacerbated by persistent bacterial infections.[2,3] Indeed, approximately 45% of chronic wounds are associated with infection.[8] The bacterial burden within these wounds is often polymicrobial, making it difficult to clear the wound of foreign pathogens with single-mechanism antibiotics.[9,10] Biofilm formation, wherein cooperative communities of bacteria secrete a

[1] This chapter was adapted from an article that was published in *Biomacromolecules*. The original citation is as follows: Maloney, S. E.; McGrath, K. V.; Ahonen, M. J. R.; Soliman, D. S.; Feura, E. S.; Hall, H. R.; Wallet, S. M.; Maile, R.; Schoenfisch, M. H. *Biomacromolecules* **2021**, *22*, 867-879.

protective exopolysaccharide (EPS) matrix, further decreases the efficacy of antibiotic treatment as well as the host immune response. Bacteria within the biofilms often demonstrate reduced metabolic activity, decreasing the efficacy of many antibiotics that target metabolism. Furthermore, the viscous EPS matrix limits the diffusion of antibiotics and immune cells to the bacteria, preventing clearance of the infection.[3,11] The emergence of bacterial strains that are resistant to conventional antibiotics limits the use of these agents in controlling infection, motivating the need for alternative antimicrobial agents that are unlikely to foster resistance.[12]

Nitric oxide (NO), an endogenous signaling molecule, represents an attractive wound-healing therapeutic due to its ability to mitigate infection and modulate the type of inflammation that promotes chronic wound development. Nitric oxide exerts broad-spectrum antibacterial activity via multiple mechanisms including the formation of reactive byproducts (e.g., peroxynitrite, dinitrogen trioxide) that initiate DNA cleavage, thiol nitrosation, and destruction of bacterial membranes through lipid peroxidation.[13–15] Of importance, bacterial resistance to NO has yet to be observed[16] and is unlikely to occur due to these multiple mechanisms of bactericidal action.[13,16,17] An additional benefit of NO-releasing therapies for the treatment of chronic wounds stems from the intrinsic role of NO in wound healing. Nitric oxide, which is produced endogenously by a family of enzymes known as nitric oxide synthases (NOS), exhibits concentration-dependent functions related to wound healing.[4,18] High concentrations of nitric oxide (nM-μM) concomitant with inflammation in the wound environment facilitate bacterial eradication. Over time, lower levels of NO (pM-nM) produced by endothelial nitric oxide synthase (eNOS) regulate other aspects of wound healing, including collagen synthesis, angiogenesis, and inflammatory cell proliferation, phenotype, and function.[18–22] Certain conditions, such as diabetes, alter endogenous NO production and, as a result, impair several aspects of the wound healing

processes.[7,23] Exogenous and tunable NO therapy thus represents a novel way to mitigate these complications by stimulating wound healing as well as clearing infection.

Due to NO's high reactivity in biological media and short half-life[24], strategies have been developed to deliver exogenous NO by way of chemical NO donors. *N*-diazeniumdiolate NO donors have garnered much interest due to their spontaneous release of NO under physiological conditions, with NO-release kinetics dependent upon the NO donor precursor structure.[25,26] Conjugation of NO donors onto macromolecular scaffolds, such as silica nanoparticles[13,27,28], dendrimers[29,30], and biopolymers[31,32], have become an attractive alternative to small molecule NO donors as they enable targeted delivery opportunities and enhanced control over NO-release kinetics.[15,33,34] Further, these macromolecular scaffolds are easily incorporated within conventional wound therapies and dressings (e.g., hydrogels[35–37], creams[38–40], films[35,41,42], and fibers[43]) in order to facilitate topical NO delivery to the site of a wound. Treatment of wounds with NO has been shown to accelerate wound closure[35,36,38–41,43], enhance wound hydration[36], eradicate chronic wound pathogens[40,42], and increase capillary density[36,43] and collagen deposition.[35,37] Biopolymers are a particularly advantageous system for wound-healing applications due to their inherent water solubility, low toxicity, and biodegradability.

Hyaluronic acid (HA), an endogenous biopolymer composed of alternating D-glucuronic acid and *N*-acetyl-D-glucosamine residues, represents a promising NO delivery scaffold as it is already involved as a signaling molecule for wound healing.[44] High molecular weight HA (≥1 MDa) is expressed in healthy tissue and exhibits immunosuppressive, anti-inflammatory, and anti-angiogenic mechanisms.[44,45] Under inflammatory stress, endogenous HA is enzymatically degraded to lower molecular weights (1-800 kDa) that signal for immunostimulatory, pro-inflammatory, and angiogenic activity.[44,45] As a consequence of these properties, HA has been

used in a wide range of biomedical applications, including tissue engineering[46,47], drug delivery[48–51], and wound healing.[52–57] Several studies have investigated whether the beneficial properties associated with endogenous HA translate to exogenous HA therapy. For example, wounded diabetic mice systemically injected with high molecular weight HA (e.g., 4 MDa) demonstrated improved healing and improved mechanical properties of the healed skin.[52] Topical treatment with HA oligosaccharides (e.g., 1-7 kDa) in mice and rats has been found to increase wound healing rates, angiogenesis, collagen deposition, and endothelial cell proliferation.[53–55] Wound dressings, ointments, and hydrogels containing HA have demonstrated enhanced wound healing properties, such as increased fibroblast proliferation, alleviated inflammation, increased moisture, and improved skin regeneration.[56–58] In addition to the native state benefits of HA, the biopolymer backbone also allows for versatile chemical modification at available carboxylic acid and primary and secondary alcohol functional groups. Given HA's unique properties in tissue repair and the potential to add NO donor functionality to leverage NO's multifaceted roles in wound healing, NO-releasing HA represents a favorable antibacterial therapeutic for chronic wounds.

Herein, we describe the modification of 6 and 90 kDa HA with alkylamine moieties for subsequent *N*-diazeniumdiolation to produce a new type of NO-releasing biopolymer. The two molecular weights were specifically chosen to investigate a range of low molecular weight HA biopolymers, as low molecular weight HA is known to stimulate tissue regeneration.[44,59] The selected alkylamine groups used for modification have been described previously to confer diverse NO-release kinetics.[60,61] The effects of HA molecular weight and NO-release properties on antibacterial activity were evaluated using drug-susceptible and drug-resistant bacteria common to chronic wounds. In addition, the antibiofilm efficacy was evaluated using susceptible and

multidrug-resistant *Pseudomonas aeruginosa*. Toxicity to mammalian cells was assessed as a function of the HA biopolymer and NO-release properties using murine fibroblasts as a representative cell type in the wound environment. *In vitro* enzymatic degradation of control (unmodified and amine-modified) HA and NO-releasing HA was performed using bovine testicular hyaluronidase to ensure that altering the HA structure did not change the biodegradation potential of the biopolymer.

2.2. Materials and methods

2.2.1. Materials

Extra-low (80-110 kDa; HA90) and ultra-low (<6 kDa; HA6) molecular weight hyaluronic acid were purchased from Lotioncrafter (Eastsound, WA). Bis(3-aminopropyl)amine (DPTA), diethylenetriamine (DETA), *N*-propyl-1,3-propanediamine (PAPA), *N*-(2-hydroxyethyl)ethylenediamine (HEDA), 1-ethyl-3-(3-dimethylaminopropyl)carbodiimide hydrochloride (EDC), *N*-hydroxysuccinimide (NHS), neomycin sulfate, phenazine methosulfate (PMS), hyaluronidase (from bovine testes, Type I-S), ethylenediaminetetraacetic acid disodium salt dihydrate (Na_2EDTA), and qPCR primers for *Pseudomonas aeruginosa* quantification were purchased from MilliporeSigma (St. Louis, MO). 3-(4,5-dimethylthiazol-2-yl)-5-(3-carboxymethoxyphenyl)-2-(4-sulfophenyl)-2H-tetrazolium inner salt (MTS) was purchased from BioVision (Milpitas, CA). Trypsin, penicillin streptomycin (PS), fetal bovine serum (FBS), Dulbecco's modified Eagle's medium (DMEM), water (HPLC), acetonitrile (HPLC, ≥99.9%), and common laboratory salts and solvents were purchased from Thermo Fisher Scientific (Fair Lawn, NJ). Unless otherwise specified, all reagents were used as received without further purification. DNeasy Blood and Tissue Kit was purchased from Qiagen (Hilden, Germany). iQ SYBR Green

Supermix was purchased from Bio-Rad Laboratories, Inc. (Hercules, CA). Tryptic soy broth (TSB) and tryptic soy agar (TSA) were obtained from Becton, Dickinson, and Company (Franklin Lakes, NJ). L929 murine fibroblasts (ATCC CCL1) were obtained from the UNC Tissue Culture Facility (Chapel Hill, NC). Human gingival fibroblasts (HGF), human oral keratinocytes (HOK), fibroblast medium, and oral keratinocyte medium were purchased from ScienCell Research Laboratories (Carlsbad, CA). *Pseudomonas aeruginosa* (*P. aeruginosa*; ATCC #47085), *Escherichia coli* (*E. coli*; ATCC #43888), *Staphylococcus aureus* (*S. aureus*; ATCC #29213), *Enterococcus faecalis* (*E. faecalis*; ATCC #29212), multidrug-resistant *P. aeruginosa* (MDR-PA; ATCC #BAA-2110), and methicillin-resistant *S. aureus* (MRSA; ATCC #33591) were obtained from the American Type Tissue Culture Collection (Manassas, VA). Argon (Ar), carbon dioxide (CO_2), nitrogen (N_2), oxygen (O_2), nitric oxide (NO) calibration (25.87 ppm balance N_2), and pure NO (99.5%) gas cylinders were purchased from Airgas National Welders (Raleigh, NC). Distilled water was purified to a resistivity of 18.2 MΩ•cm and a total organic content of ≤6 ppb using a Millipore Milli-Q UV Gradient A10 system (Bedford, MA).

2.2.2. Synthesis of alkylamine-modified hyaluronic acid (HAMW-alkylamine)

Hyaluronic acid (HA6 and HA90) was modified with either PAPA, HEDA, DPTA, or DETA as adapted from previously published protocols.[31] Briefly, HA (1 g) was dissolved in 40 mL (HA6) or 100 mL (HA90) of distilled water with magnetic stirring. A 4:1 molar ratio of EDC and NHS, with respect to the carboxylic acid moieties on the HA scaffold, was added in addition to 1 mL of 0.5 M HCl. Following a 20 min activation period at room temperature, an 8:1 molar ratio of PAPA, DPTA, or DETA or a 4:1 molar ratio of HEDA was added dropwise to the reaction solution. The solution was stirred at room temperature for 48 h. Amine-modified HA was

precipitated in ethanol, collected via centrifugation, washed twice with ethanol, and dried in vacuo yielding a white solid for each modification.

2.2.3. Characterization of alkylamine-modified hyaluronic acid

The presence of unreacted starting materials (i.e., EDC, NHS) was assessed using high-performance liquid chromatography (HPLC; Agilent Technologies 1260 Infinity II LC System; Santa Clara, CA) equipped with an evaporative light scattering detector (ELSD). Aliquots (20 µL) of 0.1 mg mL^{-1} HA (unmodified and amine-modified), EDC, or NHS samples were analyzed using a Synergi 4 µm Hydro-RP column (250 x 4.6 mm; Phenomenex; Torrance, CA) and a mobile phase composed of 80:20 (v/v) acetonitrile:water at a flow rate of 1 mL min^{-1}. Elution was monitored via ELSD. Elemental (carbon, hydrogen, and nitrogen; CHN) analysis was conducted using a PerkinElmer Elemental Analyzer Series 2400 Instrument (Waltham, MA). Fourier transform infrared spectroscopy was performed using a PerkinElmer Spectrum 100 FTIR Spectrometer with universal ATR accessory (Waltham, MA). ^{1}H and ^{13}C nuclear magnetic resonance (NMR) spectra were recorded on a Bruker (600 MHz) spectrometer (Billerica, MA). Representative ^{1}H and ^{13}C NMR of HA and the alkylamine-modified HA derivatives included the following peaks (denoted by D-glucuronic acid (GlcA) and *N*-acetyl-D-glucosamine (GlcNAc) residues):

HA6 and HA90: ^{1}H NMR (600 MHz, D_2O, δ) 1.90 [GlcNAc: NHC(O)CH_3], 3.20-3.45 [GlcA C4: OCHCH(OH)CH(OH)C*H*(CHC(O)OH)O; GlcNAc C5, C6: C*H*CH_2OH, CHCH_2OH], 3.60-3.95 [GlcA C2, C3, C5: OCHC*H*(OH), OCHCH(OH)C*H*(OH), C*H*C(O)OH; GlcNAc C2, C3, C4: OCHC*H*(NHC(O)CH_3), OCHCH(NHC(O)CH_3)C*H*(CHOH)O, OCHCH(NHC(O)CH_3)CH(O)C*H*(OH)], 4.25-4.50 [GlcA C1: OC*H*(CHOH)O; GlcNAc C1:

OC*H*(CHNHC(O)CH_3)O]. ^{13}C NMR (600 MHz, D_2O, δ) 22.5 [GlcNAc: NHC(O)*C*H_3], 54.0 [GlcNAc C2: OCH*C*H(NHC(O)CH_3], 60.0 [GlcNAc C6: CH*C*H_2OH], 68.0 [GlcNAc C4: OCHCH(NHC(O)CH_3)CH(O)*C*H(OH)], 72.0 [GlcA C2: OCH*C*H(OH)], 73.5 [GlcA C3: OCHCH(OH)*C*H(OH)], 75.0 [GlcA C5: *C*HC(O)OH], 76.0 [GlcNAc C5: *C*HCH_2OH], 80.0 [GlcNAc C3: OCHCH(NHC(O)CH_3)*C*H(CHOH)O], 82.5 [GlcA C4: OCHCH(OH)CH(OH)*C*H(CHC(O)OH)O], 100.0-103.5 [GlcA C1: O*C*H(CHOH)O; GlcNAc C1: O*C*H(CHNHC(O)CH_3)O], 174.0-175.0 [GlcA C6: CH*C*(O)OH; GlcNAc: NH*C*(O)CH_3].

HA6-PAPA and HA90-PAPA: ^{1}H NMR (600 MHz, D_2O, δ) 0.80-0.90 [NHCH$_2$CH$_2$C*H$_3$*], 1.50 [NHCH$_2$C*H$_2$*CH$_3$], 1.75 [NHCH$_2$C*H$_2$*CH$_2$NHCH$_2$CH$_2$CH$_3$], 1.90 [GlcNAc: NHC(O)C*H$_3$*], 2.50-2.85 [NHCH$_2$CH$_2$C*H$_2$*NHC*H$_2$*CH$_2$CH$_3$], 3.20-3.45 [GlcA C4: OCHCH(OH)CH(OH)C*H*(CHC(O)OH)O; GlcNAc C5, C6: C*H*CH$_2$OH, CHC*H$_2$*OH], 3.50 [NHC*H$_2$*CH$_2$CH$_2$NHCH$_2$CH$_2$CH$_3$], 3.60-3.95 [GlcA C2, C3, C5: OCHC*H*(OH), OCHCH(OH)C*H*(OH), C*H*C(O)OH; GlcNAc C2, C3, C4: OCHC*H*(NHC(O)CH_3), OCHCH(NHC(O)CH_3)C*H*(CHOH)O, OCHCH(NHC(O)CH_3)CH(O)C*H*(OH)], 4.25-4.50 [GlcA C1: OC*H*(CHOH)O; GlcNAc C1: OC*H*(CHNHC(O)CH_3)O]. ^{13}C NMR (600 MHz, D_2O, δ) 10.0 [NHCH$_2$CH$_2$*C*H$_3$], 20.0 [NHCH$_2$*C*H$_2$CH$_3$], 22.5 [GlcNAc: NHC(O)*C*H$_3$], 25.5-27.0 [NHCH$_2$*C*H$_2$CH$_2$NHCH$_2$CH$_2$CH$_3$], 35.0-37.5 [NH*C*H$_2$CH$_2$CH$_2$NHCH$_2$CH$_2$CH$_3$], 43.0-45.0 [NHCH$_2$CH$_2$*C*H$_2$NHCH$_2$CH$_2$CH$_3$], 49.5 [NH*C*H$_2$CH$_2$CH$_3$], 54.0 [GlcNAc C2: OCH*C*H(NHC(O)CH_3], 60.0 [GlcNAc C6: CH*C*H_2OH], 68.0 [GlcNAc C4: OCHCH(NHC(O)CH_3)CH(O)*C*H(OH)], 72.0 [GlcA C2: OCH*C*H(OH)], 73.5 [GlcA C3: OCHCH(OH)*C*H(OH)], 75.0 [GlcA C5: *C*HC(O)OH], 76.0 [GlcNAc C5: *C*HCH_2OH], 80.0 [GlcNAc C3: OCHCH(NHC(O)CH_3)*C*H(CHOH)O], 82.5 [GlcA C4: OCHCH(OH)CH(OH)*C*H(CHC(O)OH)O], 100.0-103.5 [GlcA C1: O*C*H(CHOH)O; GlcNAc C1:

O*C*H(CHNHC(O)CH_3)O], 160.5 [GlcA C6: CH*C*(O)NH], 174.0-175.0 [GlcA C6: CH*C*(O)OH; GlcNAc: NH*C*(O)CH_3].

HA6-HEDA and HA90-HEDA: ^{1}H NMR (600 MHz, D_2O, δ) 1.90 [GlcNAc: NHC(O)C*H_3*], 2.70-3.00 [NHCH$_2$C*H_2*NHC*H_2*CH$_2$OH], 3.20-3.45 [GlcA C4: OCHCH(OH)CH(OH)C*H*(CHC(O)OH)O; GlcNAc C5, C6: C*H*CH$_2$OH, CHC*H_2*OH], 3.50 [NHC*H_2*CH$_2$NHCH$_2$CH$_2$OH], 3.55 [NHCH$_2$C*H_2*OH], 3.60-3.95 [GlcA C2, C3, C5: OCHC*H*(OH), OCHCH(OH)C*H*(OH), C*H*C(O)OH; GlcNAc C2, C3, C4: OCHC*H*(NHC(O)CH_3), OCHCH(NHC(O)CH_3)C*H*(CHOH)O, OCHCH(NHC(O)CH_3)CH(O)C*H*(OH)], 4.25-4.50 [GlcA C1: OC*H*(CHOH)O; GlcNAc C1: OC*H*(CHNHC(O)CH_3)O]. ^{13}C NMR (600 MHz, D_2O, δ) 22.5 [GlcNAc: NHC(O)*C*H_3], 34.0-38.5 [NH*C*H$_2$CH$_2$NHCH$_2$CH$_2$OH], 46.0 [NHCH$_2$*C*H$_2$NHCH$_2$CH$_2$OH], 49.5 [NH*C*H$_2$CH$_2$OH], 54.0 [GlcNAc C2: OCH*C*H(NHC(O)CH_3], 59.5 [NHCH$_2$*C*H$_2$OH], 60.0 [GlcNAc C6: CH*C*H$_2$OH], 68.0 [GlcNAc C4: OCHCH(NHC(O)CH_3)CH(O)*C*H(OH)], 72.0 [GlcA C2: OCH*C*H(OH)], 73.5 [GlcA C3: OCHCH(OH)*C*H(OH)], 75.0 [GlcA C5: *C*HC(O)OH], 76.0 [GlcNAc C5: *C*HCH$_2$OH], 80.0 [GlcNAc C3: OCHCH(NHC(O)CH_3)*C*H(CHOH)O], 82.5 [GlcA C4: OCHCH(OH)CH(OH)*C*H(CHC(O)OH)O], 100.0-103.5 [GlcA C1: O*C*H(CHOH)O; GlcNAc C1: O*C*H(CHNHC(O)CH_3)O], 160.5 [GlcA C6: CH*C*(O)NH], 174.0-175.0 [GlcA C6: CH*C*(O)OH; GlcNAc: NH*C*(O)CH_3].

HA6-DPTA and HA90-DPTA: ^{1}H NMR (600 MHz, D_2O, δ) 1.70-1.75 [NHCH$_2$C*H_2*CH$_2$NHCH$_2$C*H_2*CH$_2$NH$_2$], 1.90 [GlcNAc: NHC(O)C*H_3*], 2.55-2.60 [NHCH$_2$CH$_2$C*H_2*NHC*H_2*CH$_2$CH$_2$NH$_2$], 2.80-2.85 [NHCH$_2$CH$_2$C*H_2*NH$_2$], 3.20-3.45 [GlcA C4: OCHCH(OH)CH(OH)C*H*(CHC(O)OH)O; GlcNAc C5, C6: C*H*CH$_2$OH, CHC*H_2*OH], 3.50 [NHC*H_2*CH$_2$CH$_2$NHCH$_2$CH$_2$CH$_2$NH$_2$], 3.60-3.95 [GlcA C2, C3, C5: OCHC*H*(OH),

OCHCH(OH)C*H*(OH), C*HC*(O)OH; GlcNAc C2, C3, C4: OCHC*H*(NHC(O)CH_3), OCHCH(NHC(O)CH_3)C*H*(CHOH)O, OCHCH(NHC(O)CH_3)CH(O)C*H*(OH)], 4.25-4.50 [GlcA C1: OC*H*(CHOH)O; GlcNAc C1: OC*H*(CHNHC(O)CH_3)O]. ^{13}C NMR (600 MHz, D_2O, δ) 17.0 [NHCH$_2$CH$_2$*C*H$_2$NH$_2$], 22.5 [GlcNAc: NHC(O)*C*H$_3$], 24.5-27.5 [NHCH$_2$*C*H$_2$CH$_2$NHCH$_2$*C*H$_2$CH$_2$NH$_2$], 37.5 [NH*C*H$_2$CH$_2$CH$_2$NHCH$_2$CH$_2$CH$_2$NH$_2$], 45.5 [NHCH$_2$CH$_2$*C*H$_2$NHCH$_2$CH$_2$CH$_2$NH$_2$], 54.0 [GlcNAc C2: OCH*C*H(NHC(O)CH_3], 57.5 [NH*C*H$_2$CH$_2$CH$_2$NH$_2$], 60.0 [GlcNAc C6: CH*C*H$_2$OH], 68.0 [GlcNAc C4: OCHCH(NHC(O)CH_3)CH(O)*C*H(OH)], 72.0 [GlcA C2: OCH*C*H(OH)], 73.5 [GlcA C3: OCHCH(OH)*C*H(OH)], 75.0 [GlcA C5: *C*HC(O)OH], 76.0 [GlcNAc C5: *C*HCH$_2$OH], 80.0 [GlcNAc C3: OCHCH(NHC(O)CH_3)*C*H(CHOH)O], 82.5 [GlcA C4: OCHCH(OH)CH(OH)*C*H(CHC(O)OH)O], 100.0-103.5 [GlcA C1: O*C*H(CHOH)O; GlcNAc C1: O*C*H(CHNHC(O)CH_3)O], 160.5 [GlcA C6: CH*C*(O)NH], 174.0-175.0 [GlcA C6: CH*C*(O)OH; GlcNAc: NH*C*(O)CH_3].

HA6-DETA and HA90-DETA: ^{1}H NMR (600 MHz, D_2O, δ) 1.90 [GlcNAc: NHC(O)C*H$_3$*], 2.70-2.90 [NHCH$_2$C*H$_2$*NHC*H$_2$*C*H$_2$*NH$_2$], 3.20-3.45 [GlcA C4: OCHCH(OH)CH(OH)C*H*(CHC(O)OH)O; GlcNAc C5, C6: C*H*CH$_2$OH, CHC*H$_2$*OH], 3.50 [NHC*H$_2$*CH$_2$NHCH$_2$CH$_2$NH$_2$], 3.60-3.95 [GlcA C2, C3, C5: OCHC*H*(OH), OCHCH(OH)C*H*(OH), C*HC*(O)OH; GlcNAc C2, C3, C4: OCHC*H*(NHC(O)CH_3), OCHCH(NHC(O)CH_3)C*H*(CHOH)O, OCHCH(NHC(O)CH_3)CH(O)C*H*(OH)], 4.25-4.50 [GlcA C1: OC*H*(CHOH)O; GlcNAc C1: OC*H*(CHNHC(O)CH_3)O]. ^{13}C NMR (600 MHz, D_2O, δ) 22.5 [GlcNAc: NHC(O)*C*H$_3$], 37.5-39.5 [NH*C*H$_2$CH$_2$NHCH$_2$*C*H$_2$NH$_2$], 45.5-48.5 [NHCH$_2$*C*H$_2$NH*C*H$_2$CH$_2$NH$_2$], 54.0 [GlcNAc C2: OCH*C*H(NHC(O)CH_3], 60.0 [GlcNAc C6: CH*C*H$_2$OH], 68.0 [GlcNAc C4: OCHCH(NHC(O)CH_3)CH(O)*C*H(OH)], 72.0 [GlcA C2:

OCH*C*H(OH)], 73.5 [GlcA C3: OCHCH(OH)*C*H(OH)], 75.0 [GlcA C5: *C*HC(O)OH], 76.0 [GlcNAc C5: *C*HCH$_2$OH], 80.0 [GlcNAc C3: OCHCH(NHC(O)CH$_3$)*C*H(CHOH)O], 82.5 [GlcA C4: OCHCH(OH)CH(OH)*C*H(CHC(O)OH)O], 100.0-103.5 [GlcA C1: O*C*H(CHOH)O; GlcNAc C1: O*C*H(CHNHC(O)CH$_3$)O], 160.5 [GlcA C6: CH*C*(O)NH], 174.0-175.0 [GlcA C6: CH*C*(O)OH; GlcNAc: NH*C*(O)CH$_3$].

2.2.4. Synthesis of NO-releasing hyaluronic acid

Alkylamine-modified HA (45 mg) was dissolved in 7:3 methanol:water (3 mL) with sodium methoxide (NaOMe; 75 µL; 5.4 mM in methanol) in a 1-dram glass vial. The open vials were placed in a stainless-steel reaction vessel and stirred continuously via magnetic stirring. The vessel was purged with argon (10 s, 7 atm) three times followed by three additional long purges (10 min, 7 atm) to remove excess oxygen. The vessel was then pressurized to 20 atm with NO gas. After 3 d, the same argon purging protocol was followed to remove unreacted NO. The resulting NO-releasing HA was then precipitated in ethanol, collected by centrifugation, dried in vacuo, and stored in vacuum sealed bags at -20 °C as a white/yellow powder for each modification.

2.2.5. Characterization of NO storage and release

Absorbance measurements (200-450 nm) were made in 50 mM sodium hydroxide (NaOH) with a Molecular Devices SpectraMax M2 spectrophotometer (San Jose, CA) to confirm the presence of the *N*-diazeniumdiolate functional group. Real-time nitric oxide release was evaluated using a Sievers 280i Nitric Oxide Analyzer (NOA; Boulder, CO). Before use, samples were analyzed to characterize their NO release and ensure stability of the stored material. The NOA was calibrated with air passed through a NO zero filter (0 ppm NO) and 25.87 ppm of NO calibration

gas (balance N_2) prior to analysis. In a typical experiment, NO-releasing HA (~1 mg) was dissolved in 30 mL of deoxygenated PBS (10 mM, pH 7.4, 37 °C). The solution was purged with nitrogen gas at a flow rate of 200 mL min^{-1} to carry liberated NO to the instrument. Analysis was terminated when NO levels fell below the quantification limit of the instrument (10 ppb NO mg^{-1} HA).

2.2.6. Planktonic bactericidal assay

Bacterial cultures of *P. aeruginosa*, *E. coli*, *E. faecalis*, *S. aureus*, MDR-PA, and MRSA were grown from frozen (-80 °C) stocks overnight in TSB (3 mL) at 37 °C. An aliquot (1 mL) of the overnight solution was resuspended in fresh TSB (50 mL), grown to a concentration of 10^8 CFU mL^{-1}, and subsequently diluted to 10^6 CFU mL^{-1} in PBS (10 mM, pH 7.4). Weighed samples of control (amine-modified) HA, NO-releasing HA, or neomycin sulfate were dissolved in PBS and titrated with 1 M HCl to adjust the pH to 7.4. Samples were added to a 96-well polystyrene plate and serially diluted in PBS so that each well contained 100 μL of amine-modified HA, NO-releasing HA, or neomycin. Bacterial solution containing 10^6 CFU mL^{-1} (100 μL; 1 vol% TSB supplemented PBS) was added to each well, resulting in final HA concentrations from 0.25 to 32 mg mL^{-1} or neomycin concentrations from 0.5 to 1024 μg mL^{-1}. The 96-well plate was then incubated at 37 °C for 4 h with gentle shaking. Untreated bacterial solutions were included in each experiment to ensure bacteria viability over the 4-h duration. After the 4-h exposure, bacterial solutions were serially diluted (10-, 100-, and 1000-fold dilutions), spiral plated on TSA plates using an Eddy Jet spiral plater (IUL; Farmingdale, NY), and incubated overnight at 37 °C. Viability of bacteria following treatment with HA or neomycin was determined using a Flash & Go colony counter (IUL; Farmingdale, NY). The minimum bactericidal concentration after a 4-h

exposure period (MBC_{4h}) was defined as the minimum HA or neomycin concentration required to achieve a 3-log reduction (≥ 99.9% reduction) in bacterial viability relative to untreated bacteria (i.e., reduced bacterial counts from 10^6 to 10^3 CFU mL^{-1}). The limit of detection for this counting method is 2.5×10^3 CFU mL^{-1}.[62] The NO dose required for bactericidal action was calculated using both the MBC_{4h} of the NO-releasing HA samples (mg mL^{-1}) and the total NO released in pH 7.4 PBS (μmol NO mg^{-1}) at 4 h.

2.2.7. Time-based planktonic bactericidal assay

Bacteria solutions containing 10^6 CFU mL^{-1} of *P. aeruginosa* and *S. aureus* were prepared as described for the 4-h planktonic bactericidal assay. Weighed samples of NO-releasing HA6 were dissolved at 4 mg mL^{-1} or 32 mg mL^{-1} (for *P. aeruginosa* and *S. aureus* treatment, respectively) in PBS and titrated with 1 M HCl to adjust the pH to 7.4. An equivalent volume of 10^6 CFU mL^{-1} bacteria solution was added to each vial (3 mL total volume) to bring the final concentration of NO-releasing HA to 2 mg mL^{-1} or 16 mg mL^{-1}. Untreated bacteria solutions were included to ensure viability over the 4-h exposure period. The bacteria solutions were incubated at 37 °C with gentle shaking. At pre-determined time points (i.e., 0, 0.5, 1, 1.5, 2, 3, and 4 h), 100 μL aliquots of the bacteria solutions were removed and serially diluted (10- and 100-fold dilutions), plated on TSA plates using an Eddy Jet spiral plater, and incubated overnight at 37 °C. Bacteria viability was determined using a Flash & Go colony counter.

2.2.8. Biofilm eradication assay

Bacterial cultures of *P. aeruginosa* and MDR-*P. aeruginosa* were grown from frozen (-80 °C) stocks overnight in TSB (3 mL) at 37 °C and recultured in fresh TSB to a concentration of 10^8

CFU mL^{-1}. An aliquot of the 10^8 solution (18 μL) was added to 1800 μL of fresh TSB in a 24-well polystyrene plate and incubated at 37 °C with gentle shaking for 72 h, resulting in the formation of a viscous biofilm. Neomycin, HA6-DPTA/NO, or HA90-DPTA/NO was dissolved in PBS (750 μL, pH 7.4, 10 mM) in 1-dram vials and adjusted to pH 7.4 with 1 M HCl. Biofilms (250 μL) were rinsed with PBS (pH 7.4, 10 mM) and added to the 1-dram vials. Treatment with 4 to 32 mg mL^{-1} of HA6-DPTA/NO and HA90-DPTA/NO or 31.3-64,000 μg mL^{-1} neomycin sulfate occurred for 24 h at 37 °C with gentle shaking. Untreated biofilms were included in each experiment to ensure biofilm viability over the 24-h duration. Following treatment, biofilms (100 μL) were diluted 10-fold and dispersed via pipetting and vortexing. Biofilm solutions were further diluted (final dilutions of 1,000- and 100,000-fold), plated on TSA plates using an Eddy Jet spiral plater, and incubated overnight at 37 °C. Biofilm viability following treatment with HA or neomycin was determined using a Flash & Go colony counter. The minimum biofilm eradication concentration after a 24-h exposure period ($MBEC_{24h}$) was defined as the minimum concentration required to achieve a 5-log reduction (≥99.999% reduction) in bacterial viability relative to untreated bacteria (i.e., reduced bacterial counts from 10^8 to 10^3 CFU mL^{-1}). Non-NO-releasing HA6-DPTA and HA90-DPTA were evaluated using the same protocol at concentrations equivalent to the $MBEC_{24h}$ for their NO-releasing counterparts. The NO dose required for biofilm killing was calculated from the $MBEC_{24h}$ of the NO-releasing HA samples (mg mL^{-1}) and the total NO released in pH 7.4 PBS (μmol NO mg^{-1}).

2.2.9. In vitro cytotoxicity assay

L929 murine fibroblasts were grown in DMEM supplemented with 10 vol% FBS and 1 wt% penicillin streptomycin. Human gingival fibroblasts were grown in fibroblast medium

supplemented with 2 vol% FBS, 1 wt% penicillin streptomycin, and fibroblast growth supplement. Human oral keratinocytes were grown in serum-free oral keratinocyte medium supplemented with 1 wt% penicillin streptomycin and keratinocyte growth supplement. Cells were incubated in 5 vol% CO_2 under humidified conditions at 37 °C. After reaching 80% confluency, cells were seeded onto 96-well polystyrene plates at a density of 1×10^4 cells well^{-1}. After 24-h incubation at 37 °C, the supernatant was aspirated and replaced with 100 μL of either amine-modified or NO-releasing HA in fresh growth medium with HA concentrations ranging from 0.001 to 32 mg mL^{-1}. The cultures were then incubated for 24 h at 37 °C. Following exposure, the supernatant was aspirated, and the wells were washed twice with PBS. A 100 μL mixture of growth medium/MTS/PMS (105/20/1, v/v/v) was added to each well and incubated for 90 min at 37 °C. The absorbance of the solution in each well was measured at 490 nm using a Molecular Devices SpectraMax M2 Spectrophotometer (San Jose, CA). A blank mixture of growth medium/MTS/PMS and untreated cells were used as the blank and control, respectively. Cell viability for each sample was calculated as follows:

$$\%\ \text{cell viability} = \frac{(\text{Abs}_{490} - \text{Abs}_{\text{blank}})}{(\text{Abs}_{\text{control}} - \text{Abs}_{\text{blank}})} \times 100 \qquad \text{(Eq. 1)}$$

2.2.10. In vivo murine wound healing model

8-week old female C57B6/Ntac wild-type mice (body weight of ~20 g) were purchased from Taconic Farms (Rensselaer, NY). The animal studies were approved and carried out in compliance with the Institutional Animal Care and Use Committee standards. The mice were housed individually with 12 h light-dark cycles. For wounding, mice were anesthetized using gaseous isoflurane, hair was removed from the dorsal region of the mouse using clippers and a

depilatory cream, and the skin was prepared for surgery using Betadine and 70 vol% ethanol. A sterile 6-mm biopsy punch was used to outline a circular pattern between the shoulders. Forceps were used to lift the skin, and surgical scissors were used to create a full-thickness wound on each mouse. *Pseudomonas aeruginosa* (50 µL of 4 x 10^6 CFU mL^{-1}) was pipetted into the wound. Mice were randomly assigned into three treatment groups of 5 mice each and treated with 10 µL of either PEG 400 (Group A), 100 mg mL^{-1} HA6-DPTA in PEG 400 (Group B), or 100 mg mL^{-1} HA6-DPTA/NO in PEG 400 (Group C). Treatment began immediately following wounding and continued once daily for 7 d post-wounding. After the initial treatment, wounds were covered with Tegaderm to facilitate bacterial colonization. Throughout the experiment, mice were monitored and received acetaminophen in their drinking water (1.6 mg mL^{-1}) ad libitum. Each day, all wounds were measured in perpendicular directions using calipers for wound area calculations, and wounds were imaged.

On day 8 post-wounding, mice were sacrificed and residual wounds were harvested, stored at -80 °C, and processed for DNA extraction using a DNeasy Blood and Tissue Kit. To quantify levels of *P. aeruginosa* via quantitative PCR (qPCR), two primer sets were utilized to anneal and amplify the *P. aeruginosa oprL* gene: PA01 S[a] (5' ACCCGAACGCAGGCTATG 3'), PA01 A[a] (5' CAGGTCGGAGCTGTCGTACTC 3'), *oprL* F[a] (5' ATGGAAATGCTGAAATTCGGC 3'), *oprL* R[a] (5' CTTCTTCAGCTCGACGCGACG 3'). Each reaction was performed in triplicate and contained 1 µg purified DNA (6.5 µL), 12.5 µL iQ SYBR Green Supermix, 0.5 µL forward primer (100 µM), and 0.5 µL reverse primer (100 µM), and was analyzed using a CFX96 Real-Time PCR Detection System (Bio-Rad Laboratories, Inc.; Hercules, CA). The average cycle threshold (CT) value for each reaction was subtracted from 40. Technical triplicates were averaged to obtain relative expression of PA01 16s rRNA within the wound of each animal.

2.2.11. Enzymatic degradation of alkylamine-modified and NO-releasing HA

Degradation assays of hyaluronic acid were carried out using a procedure adapted from Turner *et al*.[63] Briefly, 50 mg of HA90, amine-modified HA90, or NO-releasing HA90 was dissolved in 5 mL of pH 5.0 buffer containing 0.15 M sodium chloride, 0.1 M sodium acetate, and 1 mM Na_2EDTA at 37 °C for 30 min with magnetic stirring. Hyaluronidase (2.5 mg) was dissolved in 1 mL of the same buffer and added directly to the HA solution. The mixture was incubated at 37 °C with vigorous stirring for 30 min. Following digestion, the reaction was terminated by placing the vial in a boiling water bath for 10 min. The solution was then cooled to room temperature. Insoluble enzyme fragments were removed via centrifugation (7500 rpm, 15 min). The supernatant was filtered using a 0.22-μM PTFE filter and analyzed using an aqueous gel permeation chromatography (GPC) system equipped with a Waters 2414 refractive index detector (Milford, MA) coupled to a Wyatt miniDawn TREOS multi-angle light scattering detector (MALS; Santa Barbara, CA). Measurements were conducted in 0.1 M phosphate buffer (pH 7.4) containing 0.1 M sodium nitrate and 0.02 wt% sodium azide. Nondegraded HA derivates were analyzed by GPC-MALS for molecular weight comparison.

2.2.12. Statistical analysis

Nitric oxide-release and elemental analysis measurements are presented as the average ± standard deviation from $n \geq 3$ separate synthesis batches. Weight-average molecular weight measurements (M_w) are provided as the average ± standard deviation from $n \geq 3$ separate degradation experiments. Bacteria viability, biofilm viability, and cytotoxicity results are depicted as the average ± standard deviation from $n \geq 3$ separate experiments with bacteria/mammalian cells grown on different days. Dose-response curves for mammalian cell viability were plotted

using GraphPad Prism 8 software (San Diego, CA). Non-linear regression (normalized response with variable slope) analysis was performed to determine IC_{50} values. *In vivo* wound healing data is presented as the average ± the standard deviation from n = 5 separate animals. Significance testing for NO-release properties, *in vitro* cytotoxicity studies, and enzymatic degradation was performed via a 2-tailed Student's *t*-test. Statistical analyses of wound closure and bacterial burden for the *in vivo* study were performed using a one-way ANOVA with Tukey's multiple comparison. Significance levels for both statistical methods are denoted as: * $p < 0.05$, ** $p < 0.01$, *** $p < 0.005$.

2.3. Results and discussion

2.3.1. Alkylamine modification of HA

Carbodiimide chemistry was utilized to graft a series of alkylamine NO donor precursors to the HA backbone and enable tunable NO storage and release (Figure 2.1A). The reaction was optimized for both HA6 and HA90 systems to maximize conversion of the carboxylic acid groups to amine-bearing moieties. A high molar excess of the functional group (8:1 molar ratio of amine to carboxylic acid) was used to minimize crosslinking between the diamine functional groups (DPTA and DETA) and the HA backbone.[31] Successful alkylamine modification was determined using ^{1}H and ^{13}C NMR, with the presence of a peak at ~160 ppm in the ^{13}C NMR spectra confirming amide bond formation (Figures 2.2 and 2.3). FTIR analysis also confirmed amide bond formation owing to the peak shape shift in the region of 1550-1650 cm^{-1} (Figure 2.4). Elemental (CHN) analysis revealed an increase in nitrogen content for HA from 3 to 6-10 wt% following amine modification, corresponding to a 60-85% carboxylic acid conversion efficiency (Table 2.1). Due to the high (4x) molar excess of EDC and NHS used for amine modification, sufficient

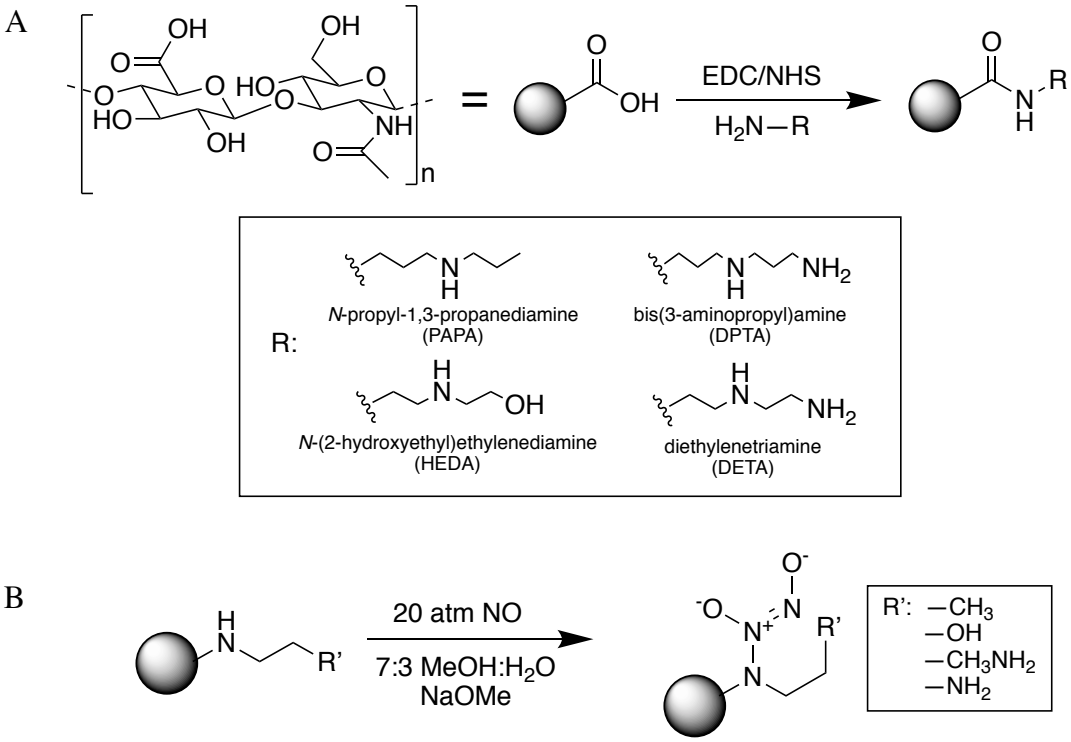

Figure 2.1 (A) Modification of hyaluronic acid with secondary amines. **(B)** Formation of *N*-diazeniumdiolates on secondary amine-modified hyaluronic acid.

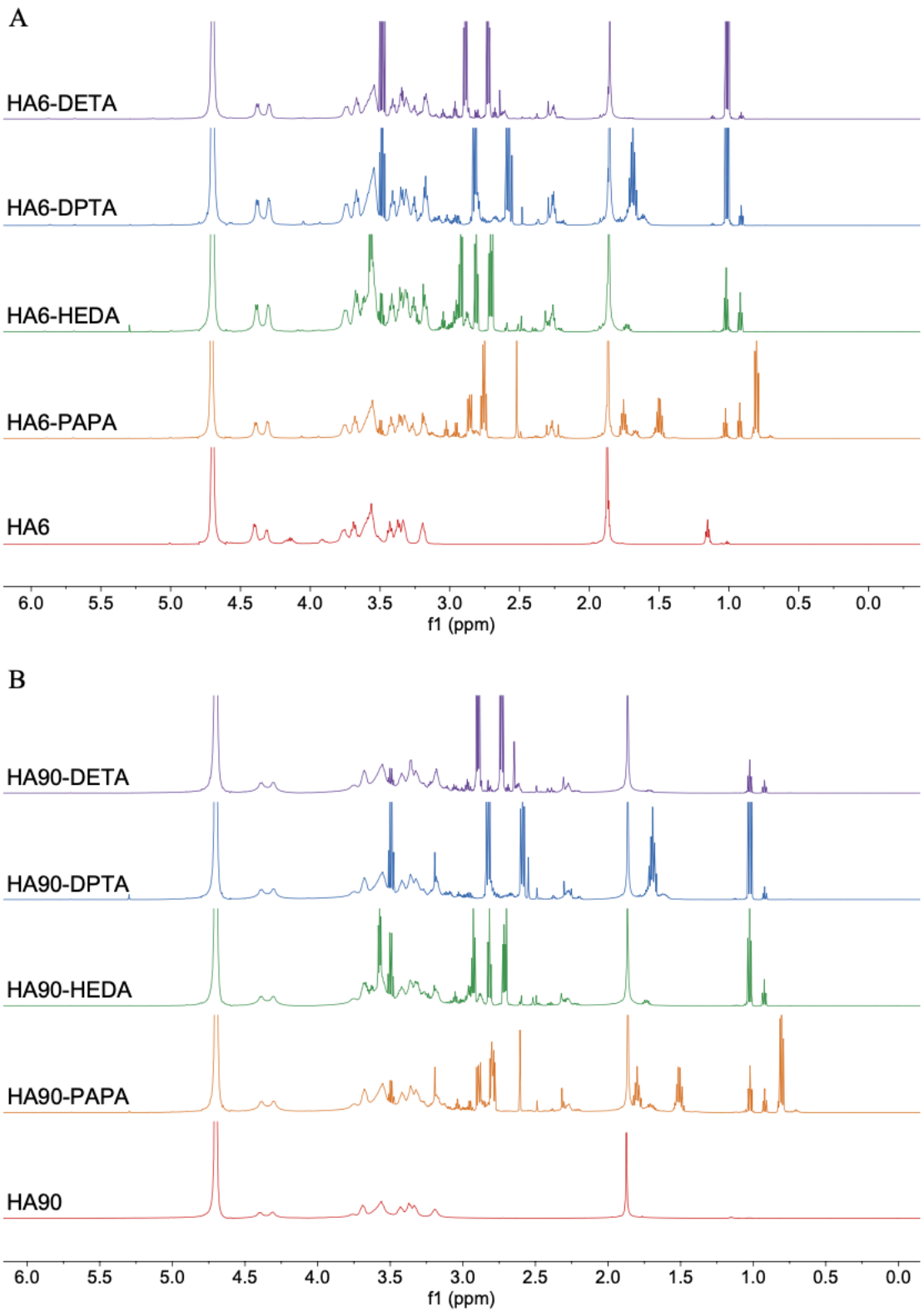

Figure 2.2 Representative ^{1}H NMR (600 MHz, D_2O) of **(A)** 6 and **(B)** 90 kDa unmodified and amine-modified HA derivatives.

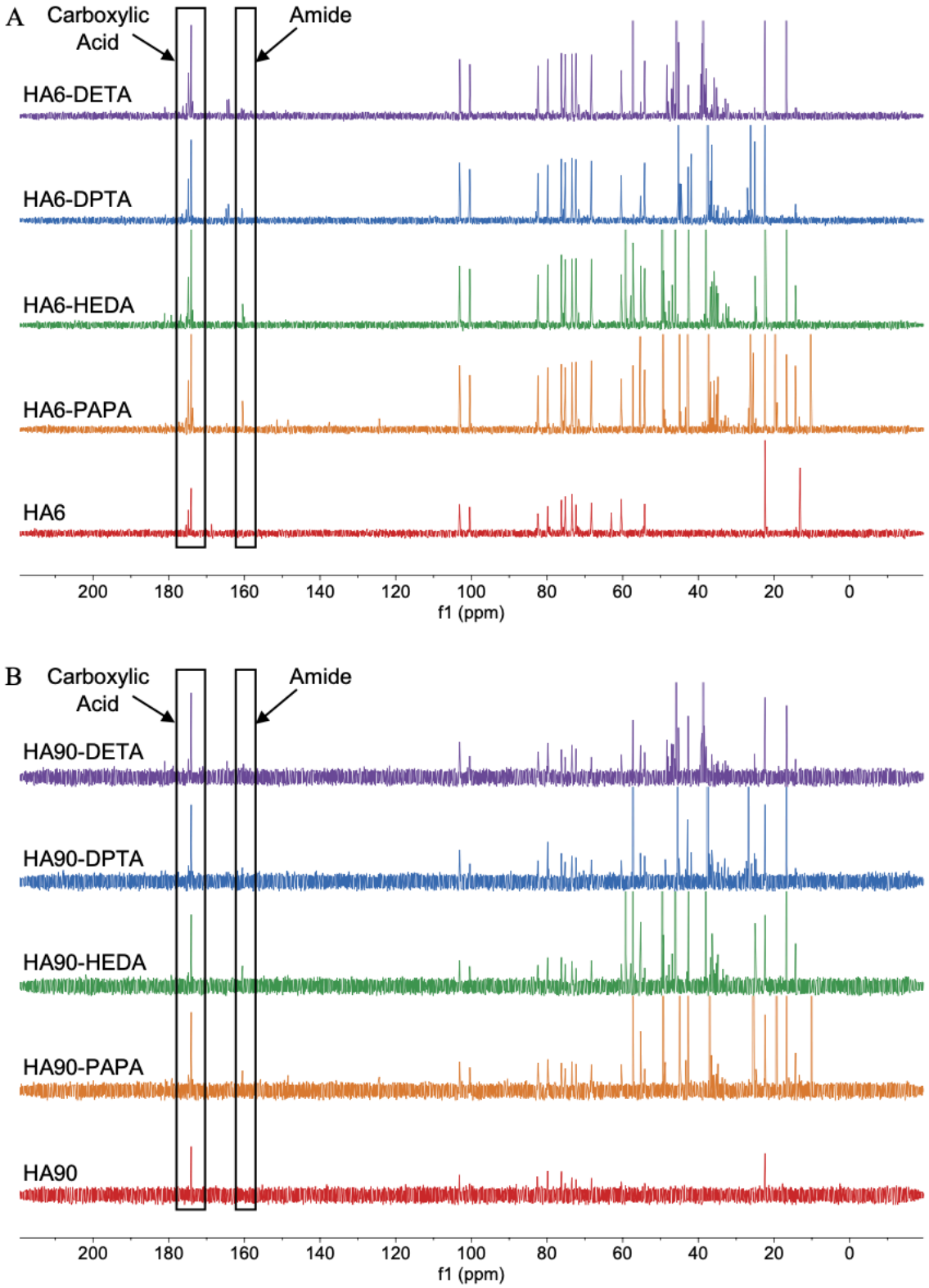

Figure 2.3 Representative ^{13}C NMR (600 MHz, D_2O) of **(A)** 6 and **(B)** 90 kDa unmodified and amine-modified HA derivatives.

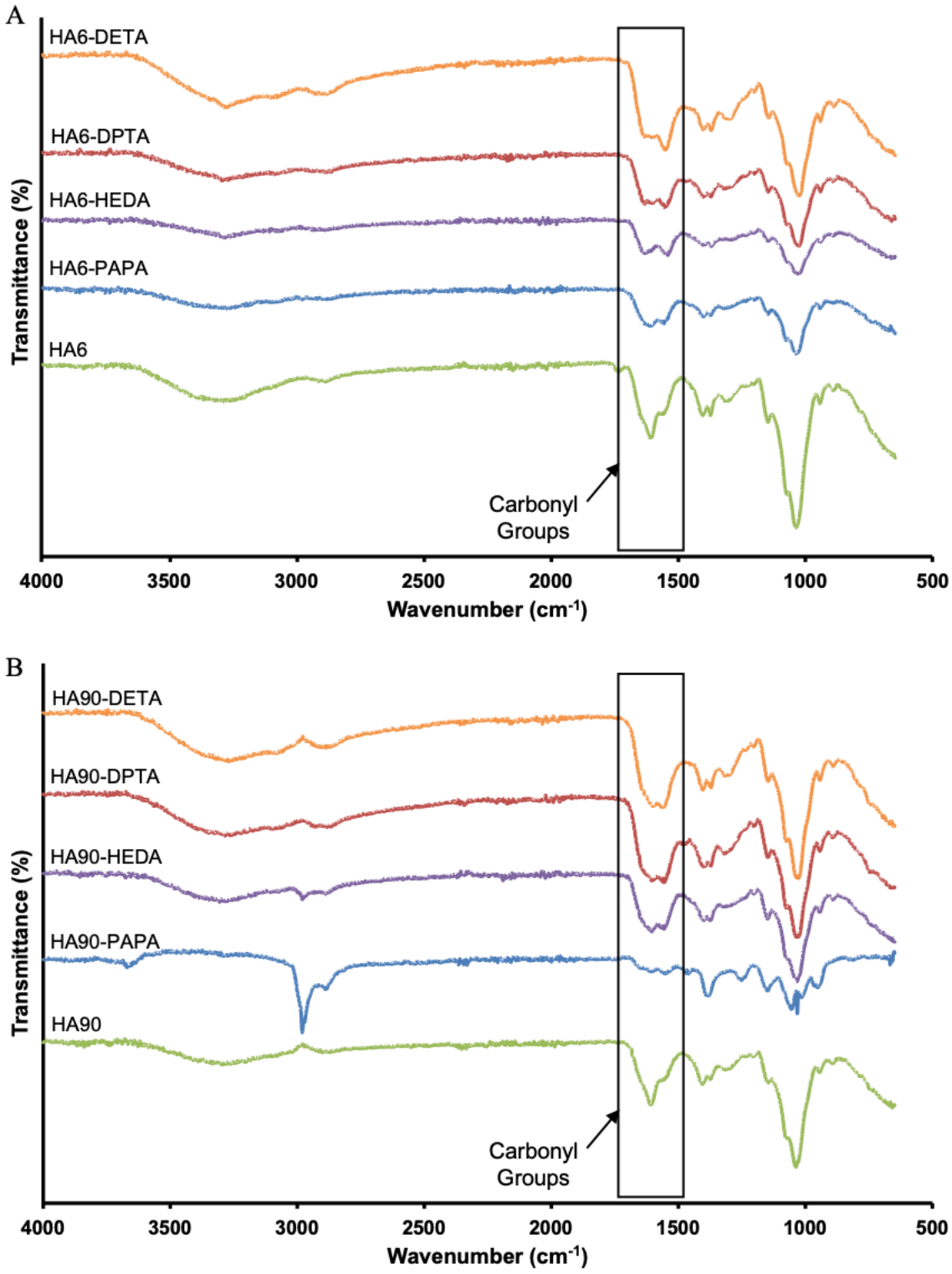

Figure 2.4 Representative FTIR analysis of **(A)** 6 and **(B)** 90 kDa unmodified and amine-modified HA derivatives.

Table 2.1 Elemental analysis of unmodified and amine-modified hyaluronic acid and reaction conversion of carboxylic acid moieties on hyaluronic acid to secondary amine-bearing amide groups.[a]

Modification	% C	% H	% N	Conversion Efficiency (%)
HA6	39.2 ± 0.8	6.2 ± 0.3	3.0 ± 0.1	—
HA6-PAPA	41.6 ± 0.7	7.7 ± 0.2	6.9 ± 0.2	67 ± 4
HA6-HEDA	40.6 ± 0.5	7.6 ± 0.2	8.2 ± 0.5	85 ± 9
HA6-DPTA	40.9 ± 0.9	7.6 ± 0.1	8.2 ± 0.8	62 ± 10
HA6-DETA	39.7 ± 0.2	6.9 ± 0.4	9.6 ± 0.4	73 ± 4
HA90	37.0 ± 0.2	6.1 ± 0.2	3.0 ± 0.0	—
HA90-PAPA	41.2 ± 1.2	7.6 ± 0.3	6.6 ± 0.4	63 ± 7
HA90-HEDA	40.2 ± 0.7	7.1 ± 0.3	7.4 ± 0.1	73 ± 2
HA90-DPTA	40.6 ± 1.5	7.4 ± 0.3	7.8 ± 0.5	57 ± 6
HA90-DETA	39.9 ± 1.0	7.3 ± 0.6	9.0 ± 0.1	66 ± 1

[a]Error represents standard deviation for $n \geq 3$ separate syntheses.

removal of reactants was measured using HPLC (Figure 2.5). The amine-modified HA derivatives did not contain detectable amounts of EDC or NHS, confirming that the ethanol washing procedure successfully removed these reactants.

2.3.2. Synthesis of N-diazeniumdiolate-functionalized HA

N-diazeniumdiolate NO donors were formed on secondary amines of modified HA via reaction with NO at high pressure (20 atm) in alkaline solution (Figure 2.1B). Formation of *N*-diazeniumdiolates was confirmed by the presence of a characteristic absorbance peak at 252-254 nm in the UV-Vis spectrum of the samples (Figure 2.6). Of note, HA derivatives both before and after NO payload liberation do not exhibit absorbance at 220-230 nm (UV-Vis) which would be indicative of nitrosamine formation.[64,65] The total NO payloads of the NO-releasing HA derivatives were found to be comparable to previously reported biopolymer systems (0.3-0.6 μmol NO mg^{-1} HA; Table 2.2).[31,32] The NO-release profiles of the *N*-diazeniumdiolate-functionalized HA derivatives (Table 2.2, Figure 2.7) demonstrate a broad range of NO-release kinetics dependent upon the precursor alkylamine structure. Both alkyl chain length and the terminal functional group of the alkylamine influence the stability of the *N*-diazeniumdiolate NO donor. The methyl- and hydroxyl-terminated PAPA and HEDA modifications lacked significant NO donor stabilization and led to fast NO donor breakdown (half-lives of 5-15 min). Electrostatic stabilization of the *N*-diazeniumdiolate by the positively charged primary amine terminal groups of DPTA and DETA extended their NO-release half-lives to 25-30 and 65-75 min, respectively. The difference in NO-release half-lives for the two primary amine-terminated modifications may be attributed to alkyl chain length, with the spacing between the primary and secondary amine on DETA offering enhanced stability compared to that of DPTA.[25]

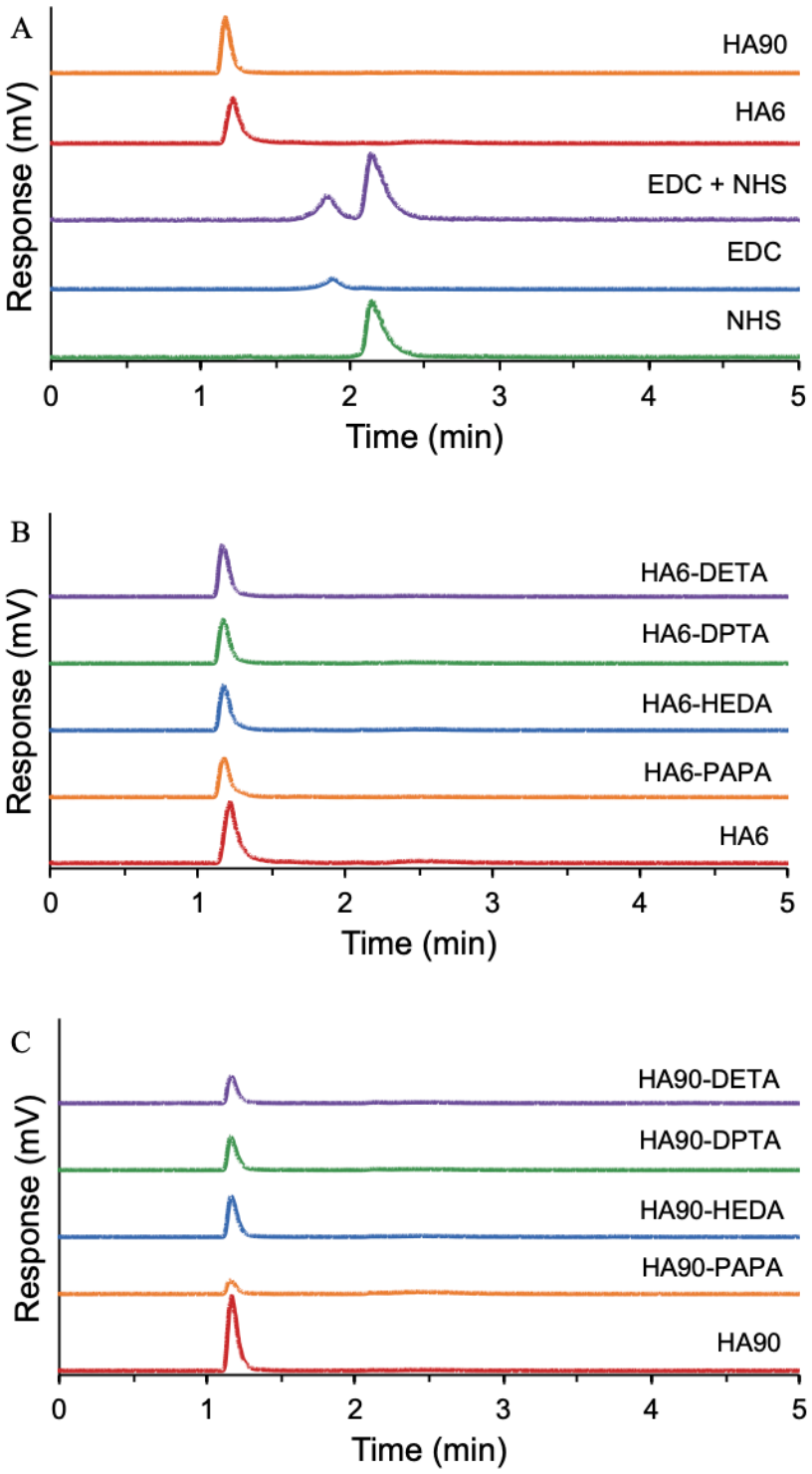

Figure 2.5 Analysis of **(A)** unreacted starting materials, **(B)** amine-modified HA6 derivatives, and **(C)** amine-modified HA90 derivatives via HPLC-ELSD. Amine-modified HA derivatives contain no detectable amounts of EDC and NHS reactants.

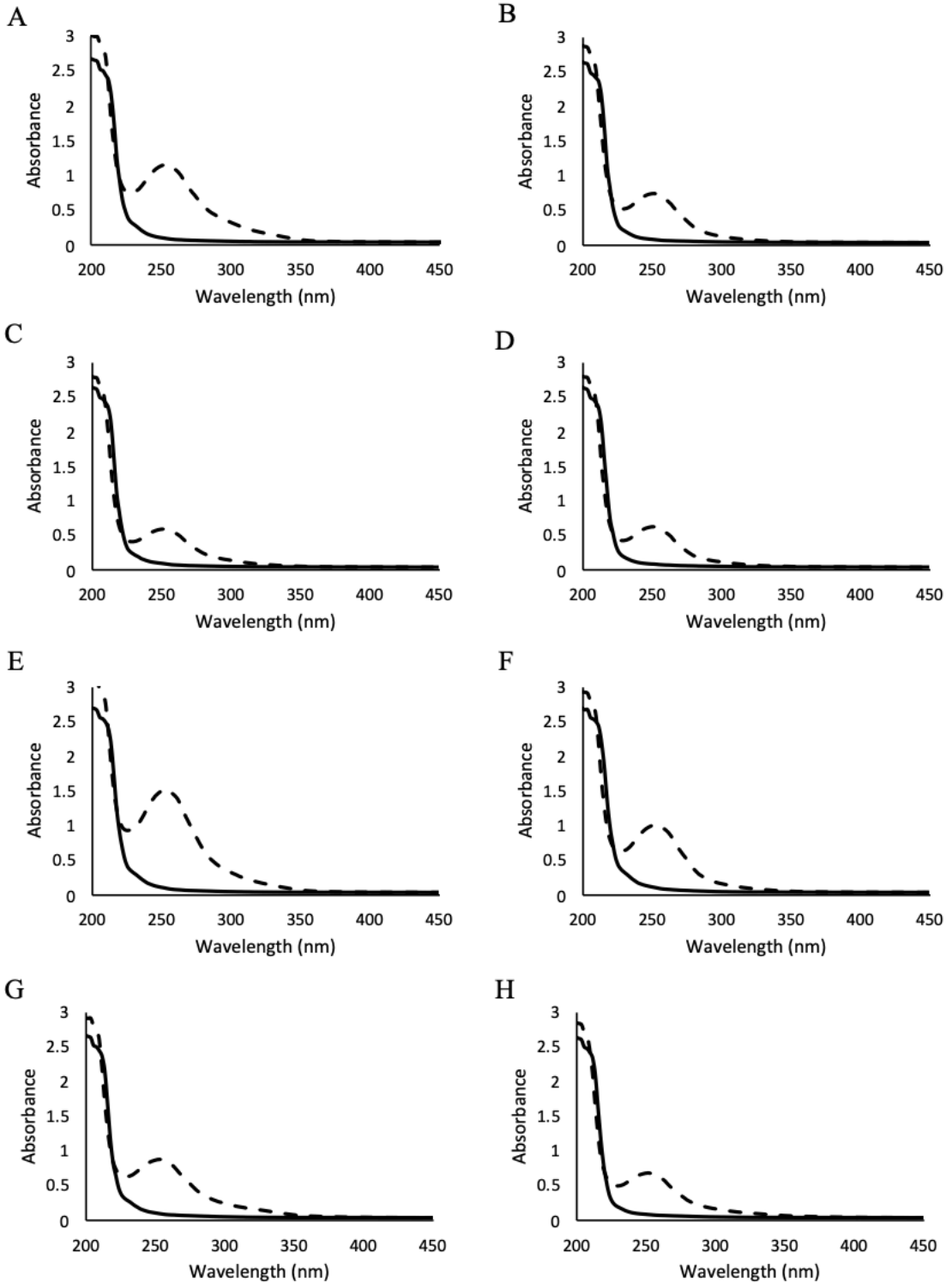

Figure 2.6 Representative UV-Vis spectra of control (—) and NO-releasing (- -) hyaluronic acid modifications. **(A)** HA6-PAPA, **(B)** HA90-PAPA, **(C)** HA6-HEDA, **(D)** HA90-HEDA, **(E)** HA6-DPTA, **(F)** HA90-DPTA, **(G)** HA6-DETA, and **(H)** HA90-DETA.

Table 2.2 Nitric oxide-release properties of NO-releasing hyaluronic acid in PBS (10 mM, pH 7.4, 37 °C).[a]

Biopolymer	$[NO]_t$ (μmol mg^{-1})[b]	$[NO]_{max}$ (ppb mg^{-1})[c]	$t_{1/2}$ (min)[d]	t_d (h)[e]	$[NO]_{t,4h}$ (μmol mg^{-1})[f]
HA6-PAPA/NO	0.46 ± 0.02	9440 ± 1450	5 ± 1	8.4 ± 0.7	0.43 ± 0.02
HA6-HEDA/NO	0.53 ± 0.08	7060 ± 1350	10 ± 3	7.4 ± 1.8	0.50 ± 0.06
HA6-DPTA/NO	0.56 ± 0.11	4280 ± 1570	24 ± 10	12.1 ± 3.1	0.50 ± 0.09
HA6-DETA/NO	0.45 ± 0.10	4080 ± 1680	63 ± 14	15.8 ± 3.0	0.33 ± 0.08
HA90-PAPA/NO	0.29 ± 0.04	4560 ± 2080	8 ± 2	3.5 ± 0.7	0.29 ± 0.04
HA90-HEDA/NO	0.48 ± 0.12	3130 ± 750	16 ± 4	6.3 ± 1.1	0.46 ± 0.12
HA90-DPTA/NO	0.41 ± 0.07	1690 ± 340	31 ± 9	9.1 ± 2.3	0.37 ± 0.05
HA90-DETA/NO	0.33 ± 0.06	1830 ± 430	74 ± 25	14.1 ± 3.0	0.23 ± 0.03

[a]Error represents the standard deviation for $n \geq 3$ separate syntheses. [b]Total NO released over full duration. [c]Maximum instantaneous NO concentration. [d]Half-life of NO release. [e]Duration of NO release. [f]Total NO released over 4 h.

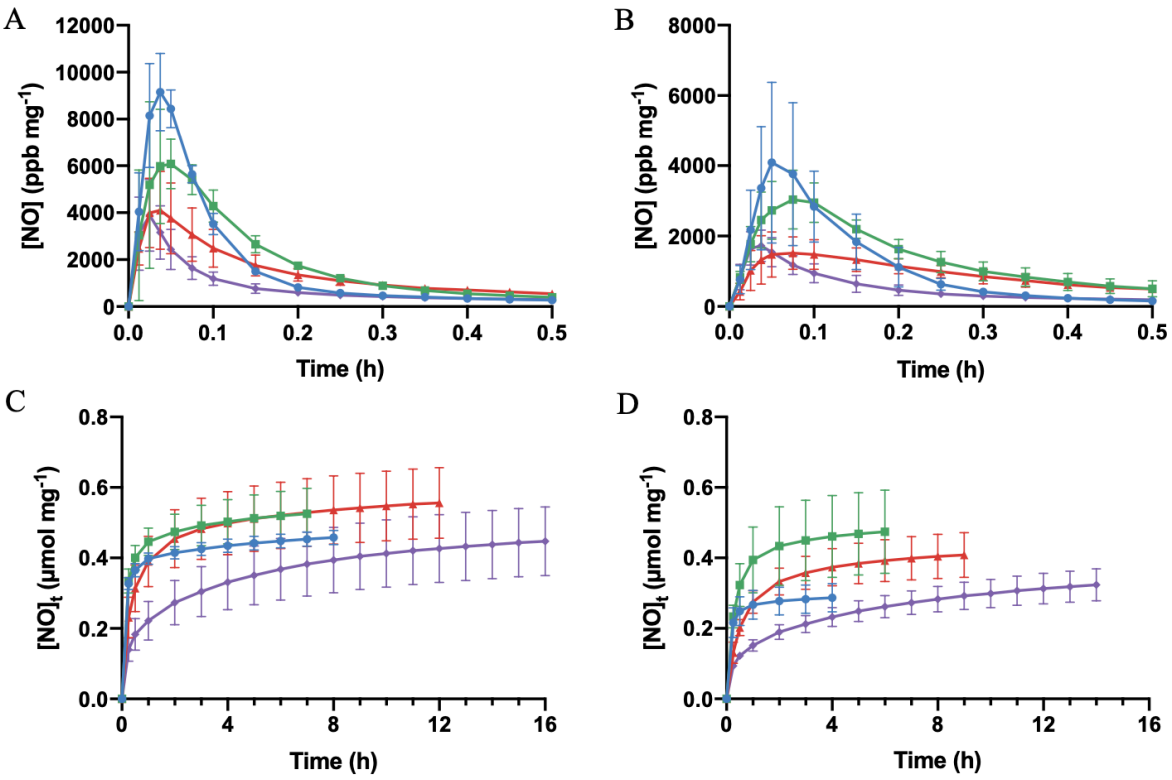

Figure 2.7 (A-B) Real-time NO-release profiles for the initial 30 minutes of release and **(C-D)** cumulative NO-release totals for **(A, C)** 6 kDa and **(B, D)** 90 kDa NO-releasing hyaluronic acid in PBS (10 mM, pH 7.4, 37 °C). Modifications include PAPA (blue circle), HEDA (green square), DPTA (red triangle), and DETA (purple diamond). Each data point represents the average ± standard deviation from n ≥ 3 separate synthesis batches.

With the exception of HEDA-modified HA, the HA6 derivatives stored significantly ($p < 0.05$) more NO with respect to HA mass than the HA90 derivatives. In addition to the lower amine functionalization observed with HA90 than HA6 (Table 2.1), it is hypothesized that the greater viscosity of the HA90 derivatives may hinder NO diffusion during the *N*-diazeniumdiolate formation process, resulting in a lower NO-loading efficiency. In contrast, the NO-release kinetics of the HA derivatives were not as strongly affected by HA molecular weight. The NO-release half-lives of the derivatives were not significantly different ($p > 0.05$) when comparing the HA6 and HA90 modifications. With the exception of PAPA-modified HA, NO-release durations were not significantly different ($p > 0.05$) between the two molecular weights. Nitric oxide-releasing HA prepared at both molecular weights exhibited tunable NO-release kinetics predominantly controlled by the precursor alkylamine structure rather than the properties of the HA backbone.

After storage at -20 °C for at least 1 y, NO-release properties were re-evaluated to assess the long-term stability of the NO-releasing materials. Importantly, the NO payloads were not significantly decreased following storage, with all modifications retaining at least 85% of their initial NO loading (Figure 2.8A). While the $[NO]_{max}$ levels were attenuated (Figure 2.8B), NO-release half-lives and durations were not significantly altered, with the exception of HA6-PAPA/NO (Figure 2.8C-D), demonstrating a general stability of the NO-releasing HA derivatives under cold temperature. Further, derivatives that were stored at room temperature (23 °C) for 7 d retained ≥ 95% of their initial NO payloads, indicating that short-term storage under ambient conditions does not substantially alter NO-release properties. Storage at room temperature for 8 weeks resulted in the materials retaining 70-85% of their initial NO payloads. To improve stability, HA powder should be stored at -20 °C (data not shown). However, storage at room temperatures proved adequate for near-term applications (≥ 95% retention for 7 d). Future work will focus on

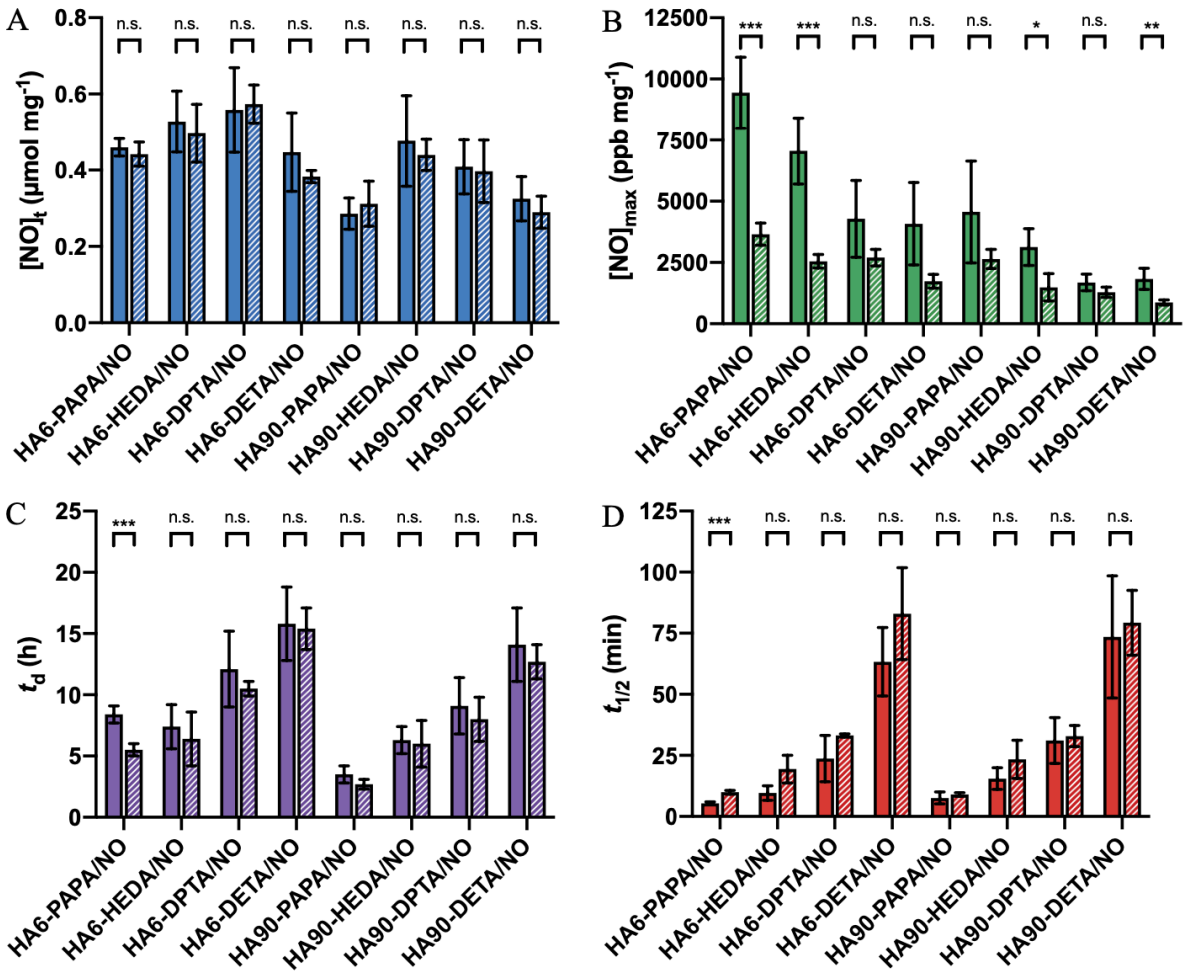

Figure 2.8 Stability of NO-releasing HA derivatives after ≥ 1 y of storage at -20 °C. Measurement of freshly prepared material (solid) and measurements after ≥ 1 y storage (striped) demonstrate the changes in **(A)** total NO payload, **(B)** maximum instantaneous NO concentration, **(C)** release duration, and **(D)** NO-release half-life. Error bars represent the standard deviation for measurements of n ≥ 3 separate synthesis batches. *p < 0.05, ** p < 0.01, *** p < 0.005, n.s. not statistically significant.

incorporating NO-releasing HA into wound dressings, hydrogels, and ointments, with the potential for further room temperature stability enhancement.

2.3.3. Antibacterial activity against antibiotic-susceptible bacteria strains

The antibacterial activity of NO-releasing HA was first evaluated against *E. coli*, *P. aeruginosa*, *S. aureus*, and *E. faecalis*, four common wound pathogens.[66,67] Bacteria were treated with a range of NO-releasing HA concentrations under static conditions to determine the minimum bactericidal concentration, or MBC_{4h}, defined as the concentration of HA required to reduce bacteria viability by 3-log (i.e., >99.9%) over 4 h. The MBC_{4h} was determined to be equivalent for *P. aeruginosa* following a 24- or 48-h incubation of agar plates prior to colony counting, demonstrating that there is not a significant contribution from the slower growth of damaged bacteria (Figure 2.9). All four NO-releasing HA derivatives at both molecular weights were able to kill Gram-negative pathogens *E. coli* and *P. aeruginosa* at concentrations at or below 8 mg mL^{-1}, with the HA6 derivatives exhibiting MBC_{4h} at or below 2 mg mL^{-1} (Table 2.3, Figure 2.10). Due to differences in NO loading, greater concentrations (i.e., 10-60% greater dose) of the HA90 derivatives were necessary to match the NO doses released from the HA6 derivatives. In addition, previous reports have shown that low molecular weight NO-releasing biopolymers exhibit greater antibacterial efficacy than their higher molecular weight counterparts, corroborating the results reported herein.[31,68]

The effect of HA molecular weight was more considerable when examining *S. aureus* and *E. faecalis*, both Gram-positive pathogens. Gram-positive bacteria are surrounded by a thicker peptidoglycan layer that may hinder NO diffusion into the bacterium.[69] As expected, greater concentrations of all NO-releasing HA derivatives, except HA6-DPTA/NO and HA90-DPTA/NO,

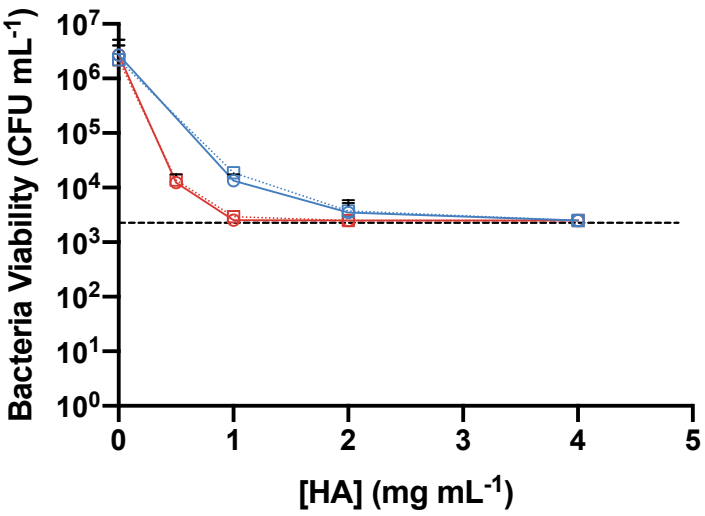

Figure 2.9 Viability of *P. aeruginosa* following 4-h treatment with HA6-HEDA/NO (blue) or HA6-DPTA/NO (red). Agar plates were incubated for 24 h (circle, solid line) or 48 h (square, dotted line) prior to colony counting. The dashed line indicates the limit of detection for the plate counting method. Error bars represent the standard deviation for n ≥ 3 separate experiments.

Table 2.3 Minimum bactericidal concentrations (MBC_{4h}) and bactericidal NO doses of NO-releasing hyaluronic acid against Gram-negative (*E. coli* and *P. aeruginosa*) and Gram-positive (*S. aureus* and *E. faecalis*) bacteria following 4-h exposure.[a]

Modification	*E. coli*		*P. aeruginosa*		*S. aureus*		*E. faecalis*	
	MBC_{4h} (mg mL^{-1})	NO Dose (μg mL^{-1})[b]	MBC_{4h} (mg mL^{-1})	NO Dose (μg mL^{-1})[b]	MBC_{4h} (mg mL^{-1})	NO Dose (μg mL^{-1})[b]	MBC_{4h} (mg mL^{-1})	NO Dose (μg mL^{-1})[b]
HA6-PAPA/NO	0.5	7 ± 1	1	13 ± 1	4	52 ± 2	8	103 ± 5
HA6-HEDA/NO	2	30 ± 4	2	30 ± 4	8	150 ± 14	16	240 ± 29
HA6-DPTA/NO	1	15 ± 3	1	15 ± 3	2	30 ± 5	2	30 ±5
HA6-DETA/NO	2	20 ± 5	2	20 ± 5	16	158 ± 38	32	317 ± 77
HA90-PAPA/NO	1	9 ± 1	2	17 ± 2	8	70 ± 10	>32	N.D.[c]
HA90-HEDA/NO	4	55 ± 14	4	55 ± 14	>32	N.D.[c]	>32	N.D.[c]
HA90-DPTA/NO	1	11 ± 2	2	22 ± 3	2	22 ± 3	2	22 ± 3
HA90-DETA/NO	8	55 ± 7	4	28 ± 4	32	221 ± 29	>32	N.D.[c]

[a]MBC_{4h} determined from $n \geq 3$ experiments. [b]NO dose derived from the MBC_{4h} and the total NO released over the 4-h exposure time in PBS (10 mM, pH 7.4, 37 °C). [c]NO dose could not be determined, as the MBC_{4h} exceeded the highest HA concentration that could be evaluated.

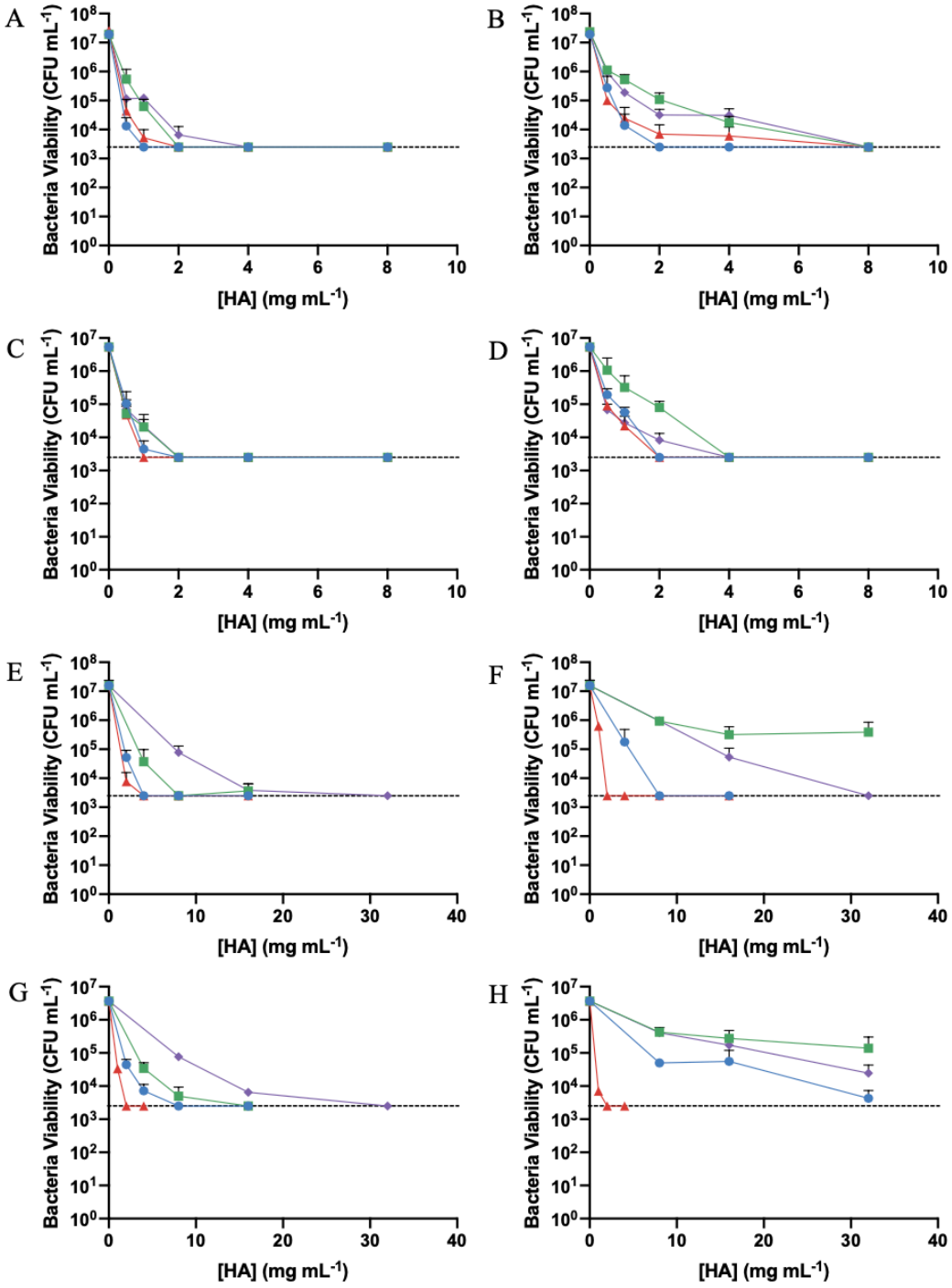

Figure 2.10 Antibacterial efficacy of **(A, C, E, G)** 6 kDa and **(B, D, F, H)** 90 kDa NO-releasing hyaluronic acid against **(A, B)** *E. coli*, **(C, D)** *P. aeruginosa*, **(E, F)** *S. aureus*, and **(G, H)** *E. faecalis*. Modifications include PAPA (blue circle), HEDA (green square), DPTA (red triangle), and DETA (purple diamond). The dashed line indicates the limit of detection for the plate counting method. Error bars represent the standard deviation for n ≥ 3 separate experiments.

were required for killing the Gram-positive strains relative to those which were required for the Gram-negative bacteria. All NO-releasing HA6 derivatives facilitated killing of both *S. aureus* and *E. faecalis* at concentrations at or below 32 mg mL^{-1}, but the PAPA, HEDA, and DETA-modified NO-releasing HA90 derivatives were unable to kill *E. faecalis* at 32 mg mL^{-1} (Table 2.3), supporting the notion that biopolymer size influences the effectiveness of NO delivery and bactericidal action. Of note, the high viscosity of HA90 prevented evaluation at HA concentrations greater than 32 mg mL^{-1}.

For all four bacteria strains, both HA6-DPTA/NO and HA90-DPTA/NO were able to elicit a 3-log reduction in bacteria viability at or below 2 mg mL^{-1}, regardless of bacteria identity (Table 2.3). The positively-charged primary amine terminal group may increase association with the negatively charged bacterial outer membrane, facilitating localized delivery of NO.[13] While both DPTA- and DETA-modified HA contain primary amines, only NO-releasing DPTA-modified HA exhibited enhanced bactericidal activity. The slower NO-release associated with DETA-modified HA, a result of increased *N*-diazeniumdiolate stabilization from the positively charged primary amine, leads to a net neutral charge of the functional group. Upon NO release, the primary amine again has a free positive charge. With DPTA-modified HA's weaker stabilization of the *N*-diazeniumdiolate and faster NO-release profile, the charge contribution from the primary amine is more pronounced, driving the polymer to the bacterial membrane. In addition, the slower release of NO from DETA-modified HA likely results in less NO accumulation over the 4-h exposure period. In this respect, larger HA doses are required to obtain the same NO payloads achieved with DPTA-modified HA.

The faster NO-releasing derivatives, PAPA and HEDA, have methyl and hydroxyl terminal groups, respectively. Without significant *N*-diazeniumdiolate stabilization from the terminal

functional group, NO may be prematurely released prior to HA localization at the bacteria surface. As the half-life of liberated NO is on the order of seconds[24], localized delivery is essential for effective killing. Additionally, the terminal hydroxyl moiety on HEDA has been reported to increase cellular compatibility due to its uncharged, hydrophilic nature.[60,70,71] This attribute would also likely decrease its antibacterial activity as a consequence. Of note, non-NO-releasing HA derivatives of both molecular weights were not bactericidal (i.e., < 3-log reduction) at the evaluated concentrations (Figure 2.11), indicating that NO is the predominant bactericidal agent even though structural properties of the HA biopolymer are influential in more effective killing.

The antibacterial activity of NO-releasing HA was also evaluated as a function of time (via time-kill assays) using *P. aeruginosa* and *S. aureus* as representative Gram-negative and Gram-positive strains. Only the HA6 derivatives were used to evaluate time-based efficacy given the high concentrations required of HA90-HEDA/NO and HA90-DETA/NO for *S. aureus* antibacterial action. Each bacteria strain was treated at a set dose of NO-releasing HA6 derivatives, with 2 mg mL^{-1} of each derivative used for *P. aeruginosa* and 16 mg mL^{-1} used for *S. aureus*. These doses were chosen to ensure bacteria killing by all derivatives within the 4-h exposure period. For both strains, HA6-DPTA/NO reached bactericidal levels the fastest, achieving a 3-log reduction in bacteria viability within 1 and 1.5 h for *P. aeruginosa* and *S. aureus*, respectively (Figure 2.12). In contrast, treatment with HA6-DETA/NO required the entire 4-h exposure period to reach the same degree of killing, highlighting the impact of DETA's slow release of NO into solution. Exposure to HA6-PAPA/NO or HA6-HEDA/NO required 2-4 h for a 3-log reduction in bacteria viability, indicating that more rapid NO release alone is not advantageous. The positive terminal functional group of DPTA facilitates bacterial localization, allowing for a faster delivery of NO into the bacteria compared to that achieved with PAPA and HEDA. These results suggest

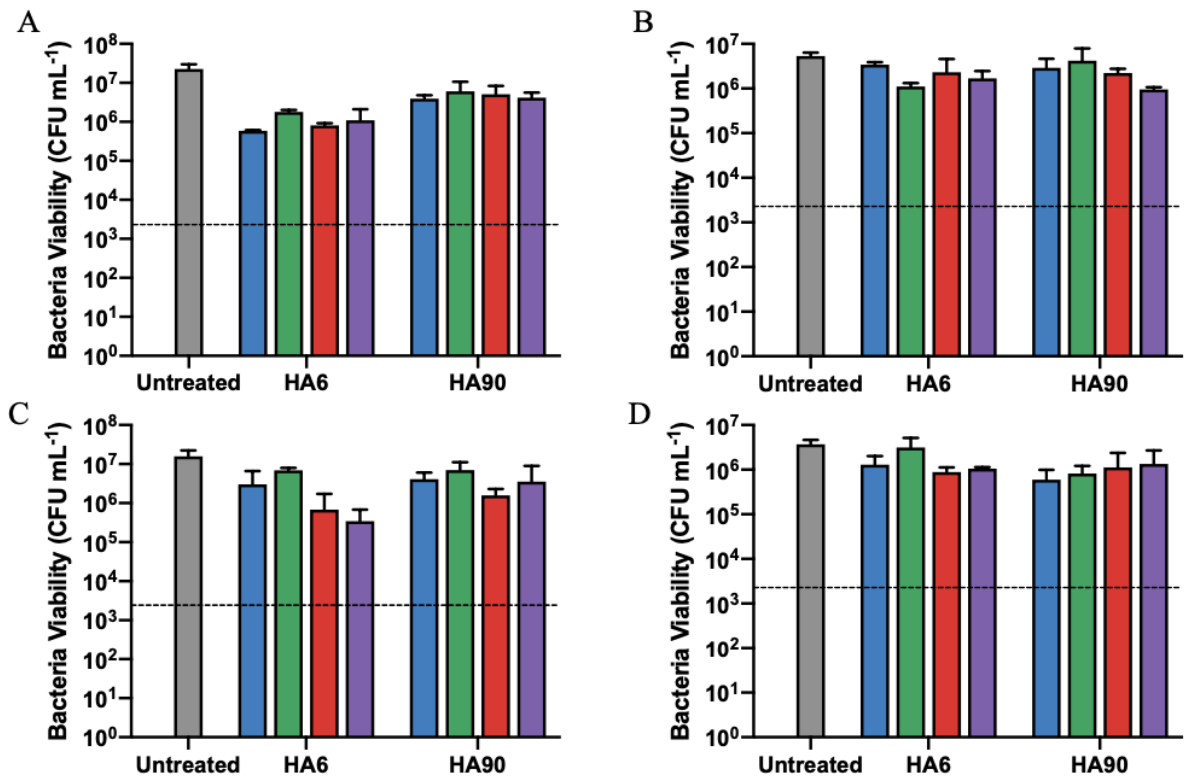

Figure 2.11 Colonies of **(A)** *E. coli*, **(B)** *P. aeruginosa*, **(C)** *S. aureus*, and **(D)** *E. faecalis* remaining after 4-h treatment with 6 kDa and 90 kDa amine-modified hyaluronic acid (without NO). Modifications include PAPA (blue), HEDA (green), DPTA (red), and DETA (purple). All modifications were evaluated at 8 mg mL^{-1} for **(A)** *E. coli* and **(B)** *P. aeruginosa*. Modifications were evaluated at 16 mg mL^{-1} for **(C)** *S. aureus* and **(D)** *E. faecalis* unless higher doses were necessary for eradication with the NO-releasing derivative. For both *S. aureus* and *E. faecalis*, HA6-DETA, HA90-HEDA, and HA90-DETA were evaluated at 32 mg mL^{-1}. For *E. faecalis*, HA90-PAPA was also evaluated at 32 mg mL^{-1}. The dashed line indicates the limit of detection for the plate counting method. Error bars represent the standard deviation for $n \geq 3$ separate experiments.

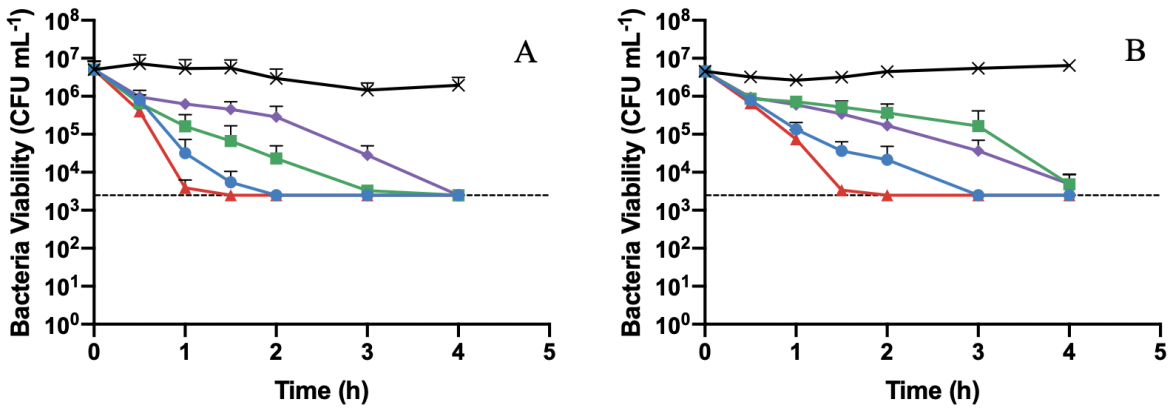

Figure 2.12 Time-based bactericidal assay of NO-releasing HA6 derivatives against **(A)** *P. aeruginosa* and **(B)** *S. aureus*. Treatments included HA6-PAPA/NO (blue circle), HA6-HEDA/NO (green square), HA6-DPTA/NO (red triangle), HA6-DETA/NO (purple diamond), and PBS (untreated; black cross). All HA derivatives were prepared at equivalent doses of 2 mg mL^{-1} for *P. aeruginosa* and 16 mg mL^{-1} for *S. aureus*. The dashed line indicates the limit of detection for the plate counting method. Error bars represent the standard deviation for $n \geq 3$ separate experiments.

that employing a positively charged terminal functional group and intermediate NO-release kinetics allows for both potent and rapid antibacterial action.

2.3.4. Antibacterial activity against antibiotic-resistant bacteria strains

Many chronic wounds become infected with antibiotic-resistant strains, making them more difficult to eradicate with conventional antibiotics. The two most bactericidal HA derivatives, HA6-DPTA/NO and HA90-DPTA/NO, were thus evaluated against Gram-negative multidrug-resistant *P. aeruginosa* (MDR-PA) and Gram-positive methicillin-resistant *S. aureus* (MRSA), as representative bacteria known to frequently infect wounds.[67,72,73] Both HA derivatives decreased bacteria viability by 3-log for MDR-PA and MRSA at 1 and 2 mg mL^{-1}, respectively (Figure 2.13, Table 2.4), demonstrating no loss of efficacy due to the antibiotic resistance mechanisms adopted by the bacteria. In contrast, these resistance mechanisms greatly decreased the therapeutic efficacy of neomycin sulfate, a conventional topical antibiotic. Susceptible *P. aeruginosa* and *S. aureus* strains required 32 and 2 μg mL^{-1} neomycin, respectively (Figure 2.14A-B). In evaluating resistant strains, MDR-PA required 128 μg mL^{-1} and MRSA saw no decrease in viability up to 1024 μg mL^{-1} neomycin (Figure 2.14C-D**)**. When comparing NO-releasing HA and neomycin, it is important to consider the active ingredient dose being administered. While the NO-releasing HA derivatives require a higher overall concentration, the corresponding mass is primarily comprised of the non-bactericidal HA backbone. For a more direct comparison, the NO dose released from the HA was determined over the 4-h assay (Figure 2.14, Tables 2.3 and 2.4). In treating *P. aeruginosa*, *S. aureus*, MDR-PA, and MRSA with HA6-DPTA/NO and HA90-DPTA/NO, 10-30 μg mL^{-1} NO was required for killing all strains (Figure 2.14). While neomycin decreased *S. aureus* viability at a lower dose, NO-releasing HA was more effective at killing the two antibiotic-resistant

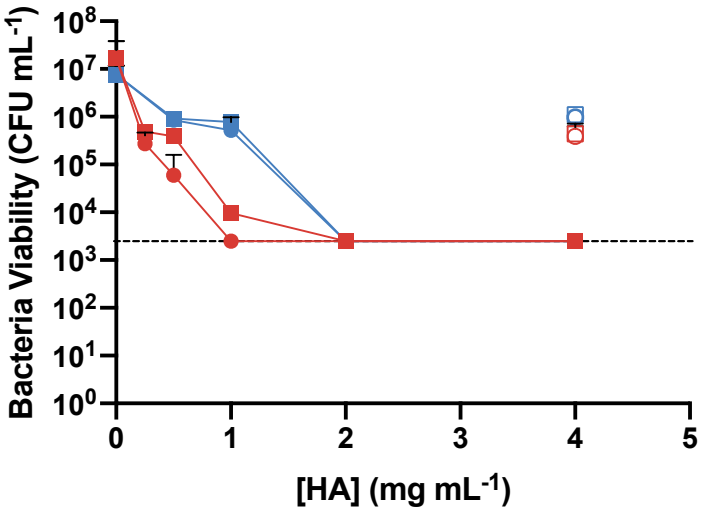

Figure 2.13 Antibacterial efficacy of HA6-DPTA/NO (solid circle) and HA90-DPTA/NO (solid square) against antibiotic-resistant bacteria strains, including multidrug-resistant *P. aeruginosa* (MDR-PA; red) and methicillin-resistant *S. aureus* (MRSA; blue). Of note, non-NO-releasing HA6-DPTA (hollow circle) and HA90-DPTA (hollow square) were not bactericidal at 4 mg mL^{-1}. The dashed line indicates the limit of detection for the plate counting method. Error bars represent the standard deviation for $n \geq 3$ separate experiments.

Table 2.4 Minimum bactericidal concentration (MBC_{4h}) and bactericidal NO dose of NO-releasing DPTA-modified hyaluronic acid against antibiotic-resistant bacteria.[a]

Modification	MDR-PA		MRSA	
	MBC_{4h} (mg mL^{-1})	NO Dose (μg mL^{-1})[b]	MBC_{4h} (mg mL^{-1})	NO Dose (μg mL^{-1})[b]
HA6-DPTA/NO	1	15 ± 3	2	30 ± 5
HA90-DPTA/NO	1	11 ± 2	2	22 ± 3

[a]MBC_{4h} determined from $n \geq 3$ experiments. [b]NO dose derived from the MBC_{4h} and the total NO released over the 4-h exposure time in PBS (10 mM, pH 7.4, 37 °C).

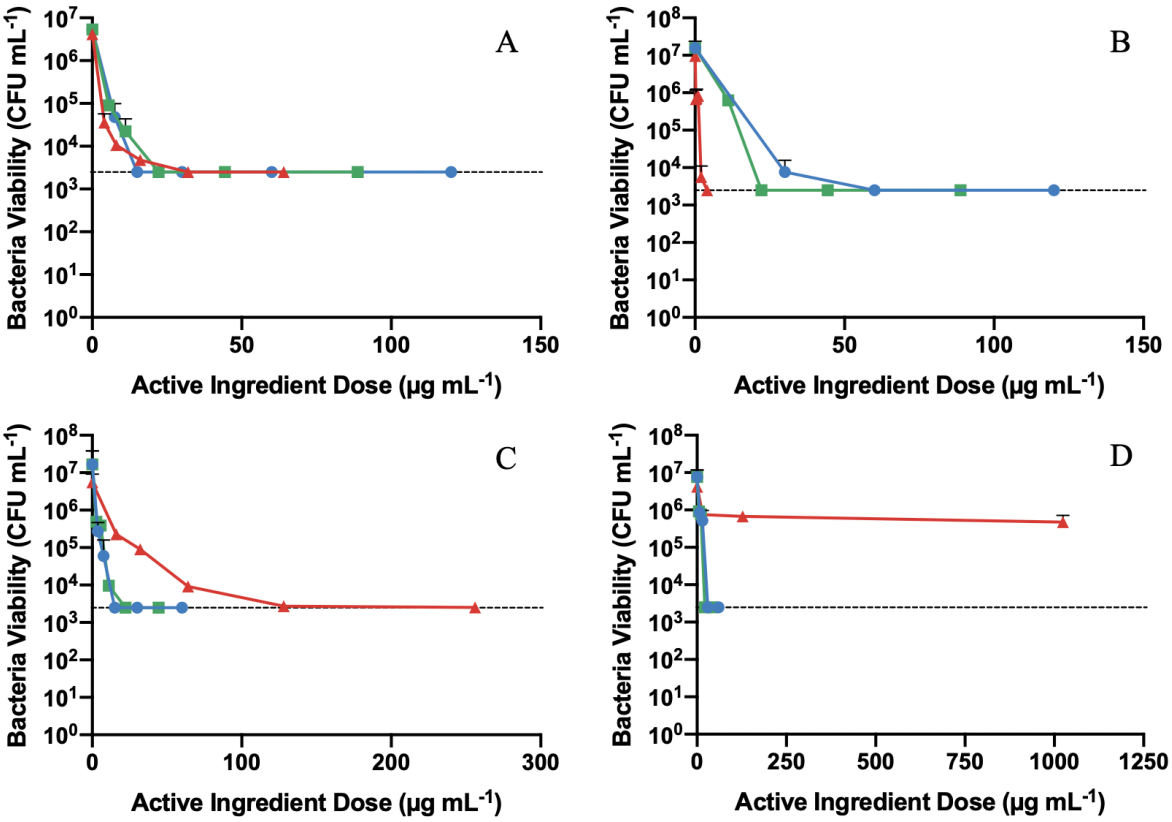

Figure 2.14 Antibacterial efficacy of active ingredient (neomycin or NO) against **(A)** *P. aeruginosa*, **(B)** *S. aureus*, **(C)** MDR-PA, and **(D)** MRSA following treatment with HA6-DPTA/NO (blue circle), HA90-DPTA/NO (green square), or neomycin sulfate (red triangle). The NO dose was calculated from the total NO released over the 4-h exposure time in PBS (10 mM, pH 7.4, 37 °C) for HA6-DPTA/NO and HA90-DPTA/NO. The dashed line indicates the limit of detection for the plate counting method. Error bars represent the standard deviation for $n \geq 3$ separate experiments.

strains, representing a major benefit of NO-releasing HA for treating wound infections over conventional antibiotics.

2.3.5. Antibiofilm action

As biofilms readily form in wounds, promoting antibiotic resistance and preventing wound closure, HA6-DPTA/NO and HA90-DPTA/NO were evaluated against *P. aeruginosa* and MDR-PA biofilms to determine the minimum biofilm eradication concentration ($MBEC_{24h}$). The $MBEC_{24h}$ represents the concentration of HA required to elicit a 5-log reduction in biofilm viability (Figure 2.15). *P. aeruginosa* biofilms were killed upon exposure to 8 mg mL^{-1} HA6-DPTA/NO and 16 mg mL^{-1} HA90-DPTA/NO, corresponding to NO doses of 134 ± 26 μg mL^{-1} and 197 ± 34 μg mL^{-1}, respectively (Figure 2.15A). In comparison, *P. aeruginosa* biofilms required 250 μg mL^{-1} neomycin for a 5-log reduction in biofilm viability. The differences were even more pronounced when treating MDR-PA biofilms. As shown in Figure 2.15B, 16 mg mL^{-1} HA6-DPTA/NO or 269 ± 53 μg mL^{-1} NO was required to kill the MDR-PA biofilms. The HA90-DPTA/NO was unable to kill MDR-PA biofilms at concentrations up to 32 mg mL^{-1}, suggesting that the lower molecular weight HA more easily associates with and/or penetrates through the biofilm matrix. Whereas 128 μg mL^{-1} neomycin was able to kill planktonic MDR-PA, the MDR-PA biofilm required a dose of 64,000 μg mL^{-1} neomycin (Figure 2.16), representing a 500-fold increase. In contrast, the $MBEC_{24h}$ of HA6-DPTA/NO was only 16-fold greater than the MBC_{4h} for planktonic MDR-PA. Similar to the planktonic studies, the non-NO-releasing counterparts, HA6-DPTA and HA90-DPTA, had no effect on biofilm viability at concentrations equivalent to the $MBEC_{24h}$ of the NO-releasing variants (Figure 2.17), implicating NO as the antibiofilm agent. In addition to its bactericidal mechanisms that are not reliant on specific metabolic processes, the

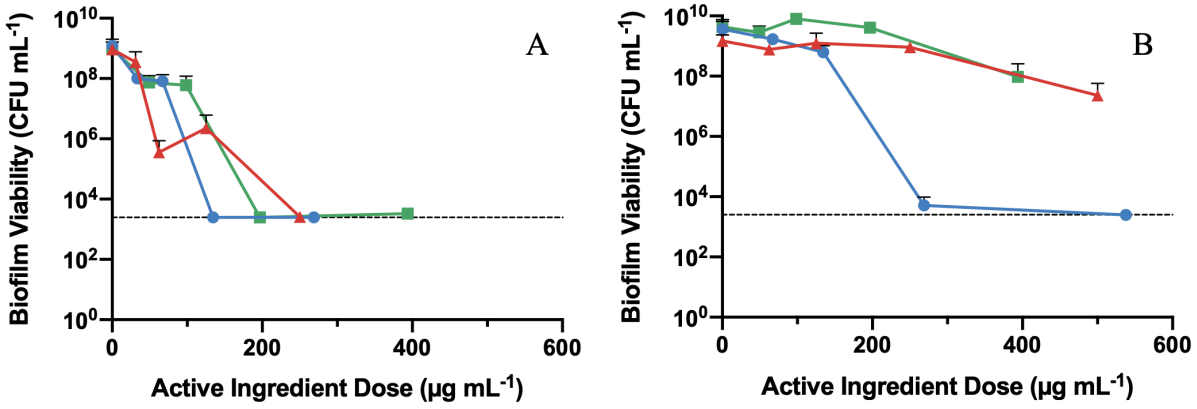

Figure 2.15 Biofilm viability following 24-h treatment of **(A)** *P. aeruginosa* and **(B)** MDR-PA biofilms with HA6-DPTA/NO (blue circle), HA90-DPTA/NO (green square), or neomycin (red triangle). Active ingredient dose is defined as the dose of either NO or neomycin. The dashed line indicates the limit of detection for the plate counting method. Error bars represent the standard deviation for $n \geq 3$ separate experiments.

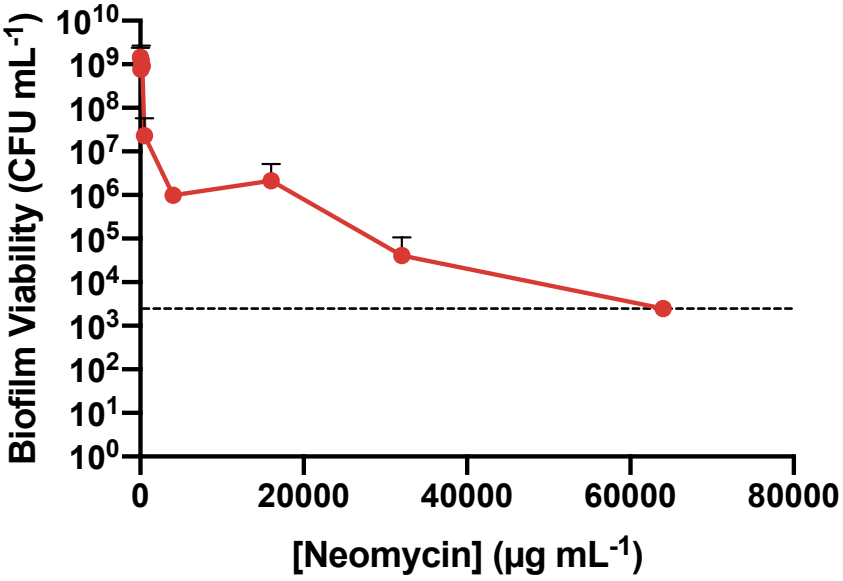

Figure 2.16 Biofilm viability following 24-h treatment of MDR-PA with neomycin sulfate. The dashed line indicates the limit of detection for the plate counting method. Error bars represent the standard deviation for $n \geq 3$ separate experiments.

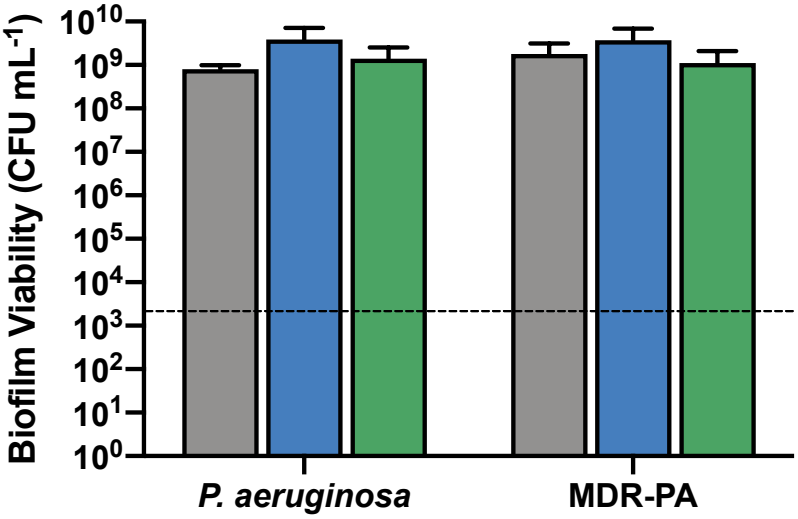

Figure 2.17 Biofilm viability following 24-h treatment of *P. aeruginosa* and MDR-PA with amine-modified (non-NO-releasing) HA-DPTA. Treatment with PBS (gray), HA6-DPTA (blue), and HA90-DPTA (green) was evaluated at the $MBEC_{24h}$ for the respective NO-releasing derivative. Of note, HA90-DPTA was prepared at 32 mg mL^{-1} for testing of MDR-PA biofilms due to the lack of determined $MBEC_{24h}$ for the NO-releasing counterpart. The dashed line indicates the limit of detection for the plate counting method. Error bars represent the standard deviation for $n \geq 3$ separate experiments.

small, uncharged nature of NO allows diffusion through the biofilm matrix to elicit killing, mitigating the need for considerably greater doses observed for conventional antibiotics.

2.3.6. In vitro cytotoxicity against murine fibroblasts

Hyaluronic acid acts as an endogenous signaling molecule for wound healing, with one of its many roles being to regulate fibroblast proliferation and migration.[54,74] L929 murine fibroblasts were chosen as a representative cell type for cytotoxicity evaluation. Hyaluronic acid on its own is regarded as nontoxic, but the chemical modification with amine ligands and subsequent *N*-diazeniumdiolates may alter its native biocompatibility. Murine fibroblasts were exposed to a range of concentrations of unmodified HA, amine-modified HA, or NO-releasing HA to determine the IC_{50} for each material, or the concentration of HA that reduces metabolic activity of the fibroblasts by 50% (Figure 2.18). As expected, unmodified HA6 and HA90 were not significantly toxic to cells (> 50% viability) at concentrations up to 32 mg mL^{-1} (Figure 2.19).

The cytotoxicity of amine-modified (i.e., non-NO-releasing) HA derivatives was highly influenced by the identity of the precursor amine (Figure 2.20A). The methyl-terminated derivatives (HA6-PAPA and HA90-PAPA) were the most cytotoxic, with IC_{50} values of 0.76 ± 0.07 and 1.94 ± 0.14 mg mL^{-1}, respectively. The presence of a terminal hydroxyl group, as is found in HEDA-modified HA, minimized this toxicity and allowed for retained metabolic activity (≥ 50%) up to 32 mg mL^{-1} (Figure 2.18). The primary amine-terminated derivatives (DPTA and DETA) exhibited differing degrees of cytotoxicity. The IC_{50} for HA6-DPTA and HA90-DPTA were 16.7 ± 1.9 and 21.8 ± 3.7 mg mL^{-1}, respectively, whereas both HA6-DETA and HA90-DETA had ≥ 100% metabolic activity up to 32 mg mL^{-1}, suggesting a proliferative effect. This discrepancy indicates that the length of the alkyl chain plays a role in cellular compatibility in

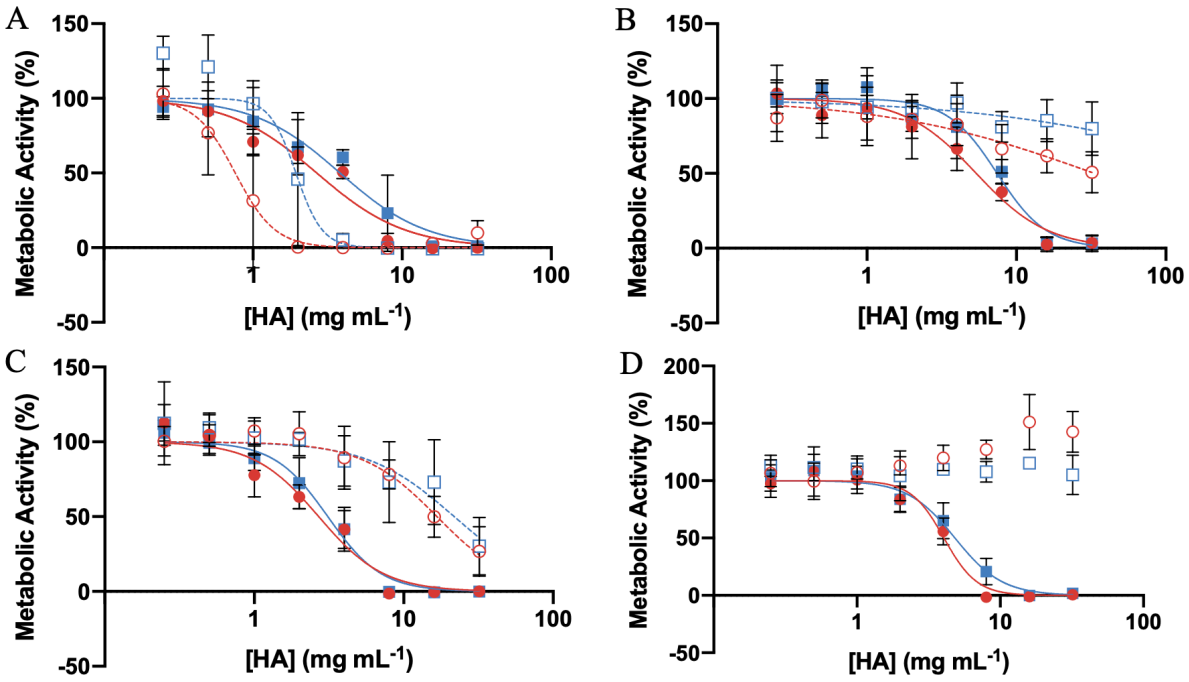

Figure 2.18 Dose-response curves after 24-h treatment of L929 murine fibroblasts with amine-modified (hollow) and NO-releasing (solid) HA derivatives. Modifications of 6 kDa (red circle) and 90 kDa (blue square) HA include **(A)** PAPA, **(B)** HEDA, **(C)** DPTA, and **(D)** DETA. Error bars represent the standard deviation for n ≥ 3 separate experiments.

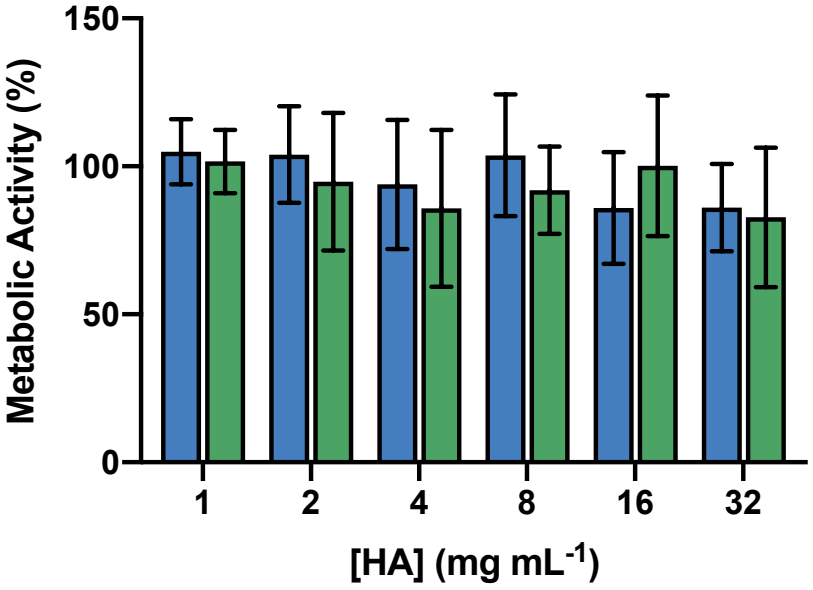

Figure 2.19 Viability of L929 murine fibroblasts following 24-h treatment with unmodified 6 kDa (blue) and 90 kDa (green) hyaluronic acid. Error bars represent the standard deviation for $n \geq 3$ separate experiments.

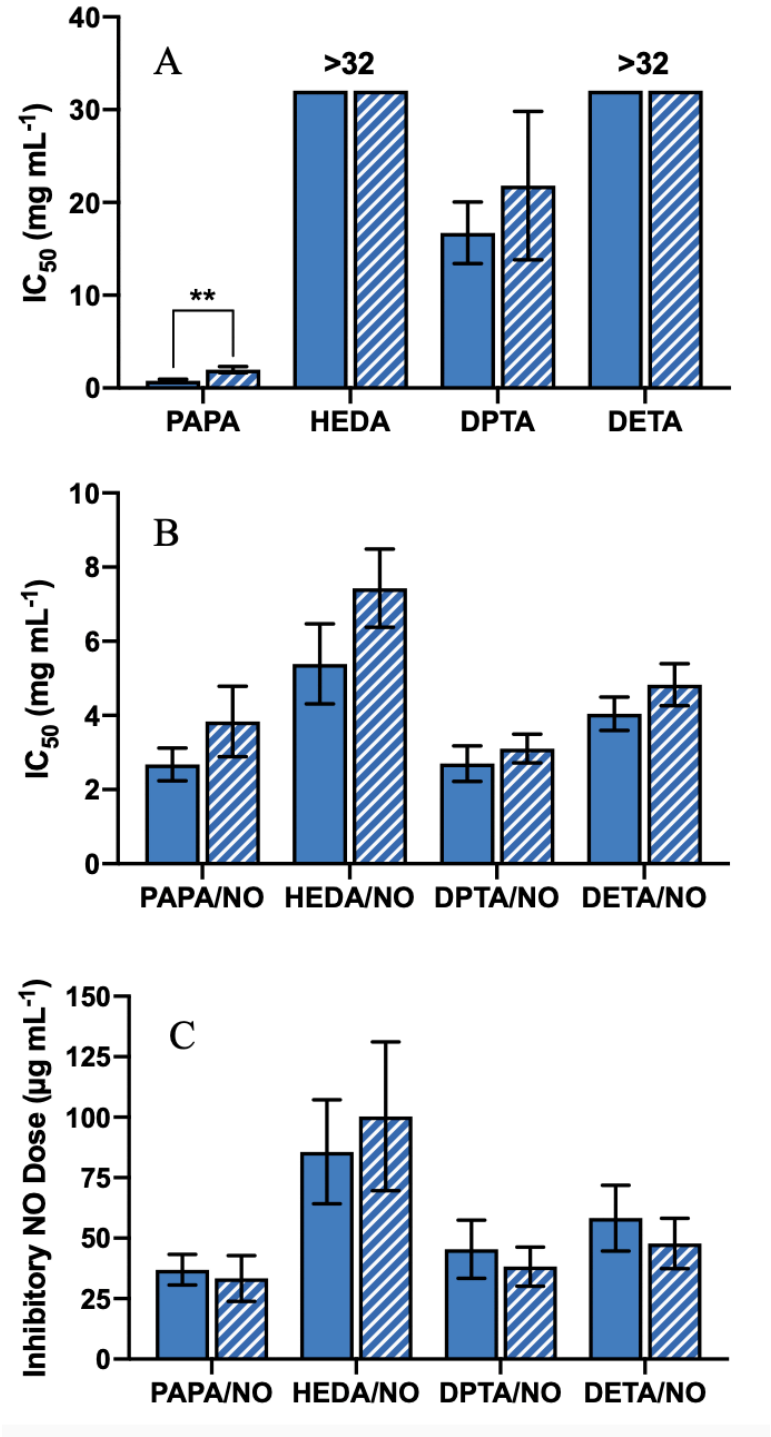

Figure 2.20 Concentration of **(A)** amine-modified and **(B)** NO-releasing HA6 (solid) and HA90 (striped) derivatives required to reduce enzymatic activity of L929 murine fibroblasts by 50% (IC_{50}). **(C)** Dose of NO released from HA6 (solid) and HA90 (striped) derivatives required to reduce enzymatic activity by 50%. Error bars represent the standard deviation for $n \geq 3$ separate experiments. *$p < 0.05$, **$p < 0.01$, ***$p < 0.005$.

addition to the identity of the terminal functional group, as was also observed in the antibacterial activity of the HA derivatives (Table 2.3).

Following *N*-diazeniumdiolation, the IC_{50} of the eight derivatives converged (Figure 2.20B). While PAPA-modified HA6 and HA90 prior to NO loading were the most toxic of the derivatives, low concentrations of NO were proliferative and increased the IC_{50} of HA6-PAPA and HA90-PAPA to 2.68 ± 0.23 and 3.84 ± 0.41 mg mL^{-1}, respectively. For HEDA, DPTA, and DETA modifications, the IC_{50} was decreased and appeared to coincide with the NO levels. The IC_{50} of each NO-releasing derivative fell to 2.7-7.4 mg mL^{-1}, a narrower range than was observed with the non-NO-releasing materials. While not statistically significant, the HA90 derivatives appeared to have slightly higher IC_{50} values for all modifications than the HA6 derivatives, suggesting that the higher molecular weight material may be more biocompatible. With respect to the NO-releasing polymers, however, the HA90 derivatives stored less NO compared to their HA6 counterparts. Upon calculating an inhibitory NO dose from the IC_{50} values, it can be seen that the difference between the two molecular weights was minimal (Figure 2.20C). Cytotoxic NO doses were achieved at 30-100 μg mL^{-1} (i.e., 1-3.3 mM), with the L929 fibroblasts withstanding the greatest doses of HA6-HEDA/NO and HA90-HEDA/NO compared to the other modifications before a significant reduction in metabolic activity.

To further evaluate the wound therapeutic potential of NO-releasing HAs, human gingival fibroblasts (HGF) and human oral keratinocytes (HOK) were treated with DPTA- and HEDA-modified HA derivatives due to their antibacterial potency and lesser cytotoxicity, respectively. As was observed with the L929 murine fibroblasts, both human-derived cell lines resulted in negligible toxicity for unmodified HA and HEDA-modified HA at concentrations up to 32 mg mL^{-1} (Figures 2.21 and 2.22). However, control (non-NO-releasing) DPTA-modified HA proved

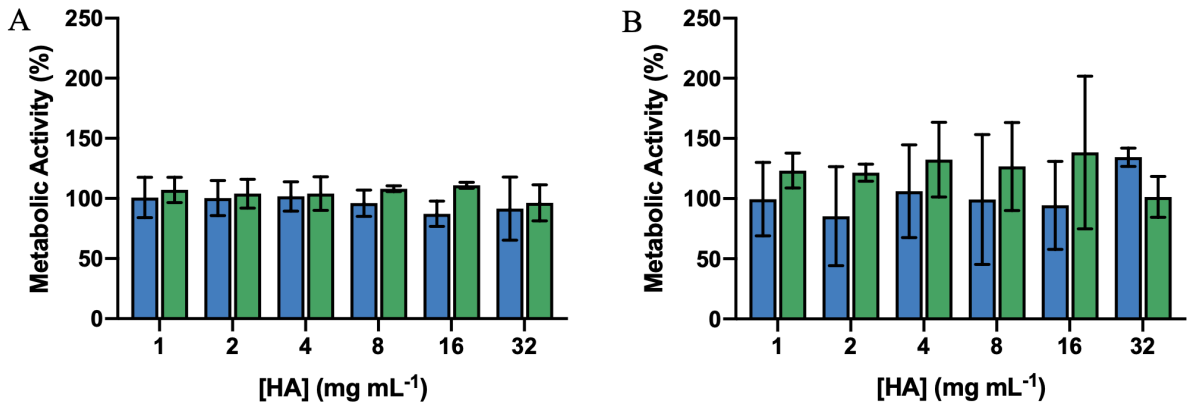

Figure 2.21 Viability of **(A)** human gingival fibroblasts and **(B)** human oral keratinocytes following 24-h treatment with unmodified 6 kDa (blue) and 90 kDa (green) hyaluronic acid. Error bars represent the standard deviation for $n \geq 3$ separate experiments.

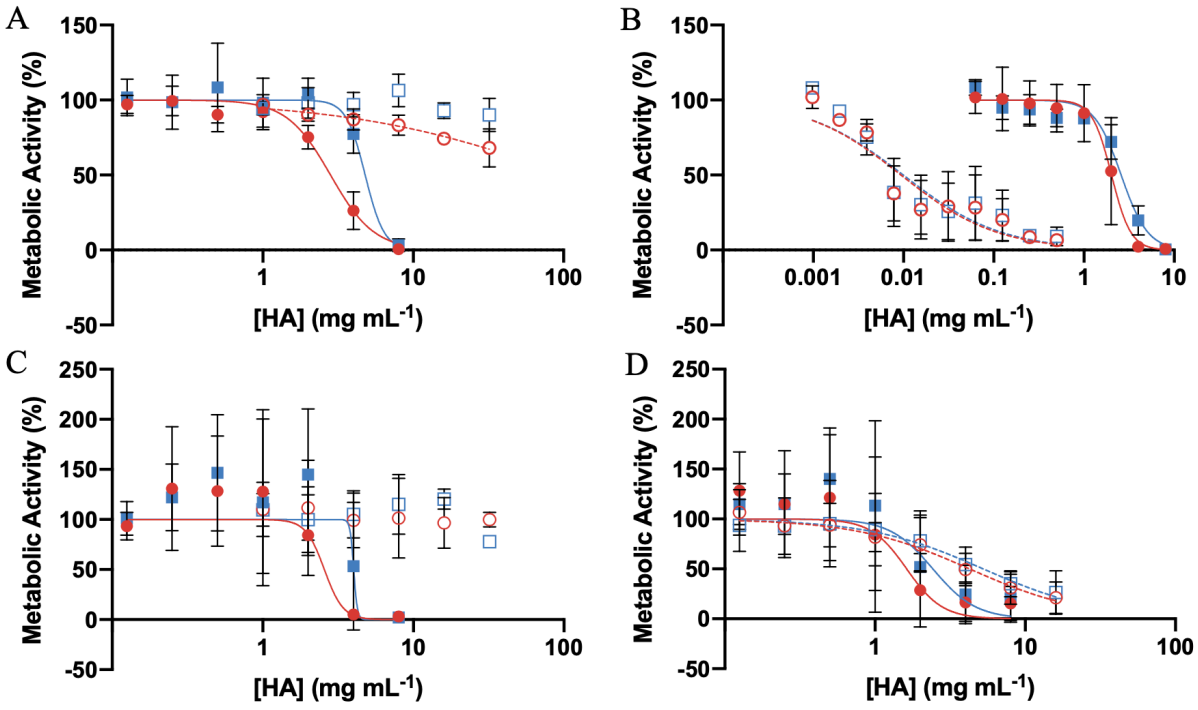

Figure 2.22 Dose-response curves after 24-h treatment of **(A-B)** human gingival fibroblasts and **(C-D)** human oral keratinocytes following treatment with amine-modified (hollow) and NO-releasing (solid) HA derivatives. Modifications of 6 kDa (red circle) and 90 kDa (blue square) HA include **(A, C)** HEDA and **(B, D)** DPTA. Error bars represent the standard deviation for n ≥ 3 separate experiments.

cytotoxic to HGF at low concentrations (~0.01 mg mL^{-1}; Figures 2.22 and 2.23). As observed for the L929 fibroblasts treated with PAPA-modified HA, *N*-diazeniumdiolate modification decreased the toxicity of DPTA-modified HA against HGF, providing further evidence that low levels of NO are proliferative. Upon treatment with the NO-releasing HA derivatives, the resulting IC_{50} values fell within 1.6-4.8 mg mL^{-1} for both human cell lines (Figure 2.23), corresponding to cytotoxic NO doses of 25-60 μg mL^{-1} and 30-70 μg mL^{-1} for HOK and HGF, respectively. Of importance, both NO-releasing HEDA- and DPTA-modified HA derivatives are able to eradicate planktonic Gram-negative pathogens at concentrations at or below their IC_{50} values. While the cytotoxicity to HA materials increased following amine modification and *N*-diazeniumdiolate formation, it is important to note that a monolayer of cells behaves differently than three-dimensional cell models or tissue and is often more susceptible to toxicity.[75,76] As such, studies using more complex tissue models are necessary to determine the therapeutic potential of the NO-releasing HA materials.

2.3.7. In vivo murine wound healing model

Mice were wounded using a standard biopsy punch procedure and infected with *P. aeruginosa*. Three treatment groups were composed of five mice each, with Group A receiving the vehicle (i.e., PEG) only, Group B receiving HA6-DPTA in PEG (50 mg kg^{-1} body weight), and Group C receiving HA6-DPTA/NO in PEG (50 mg kg^{-1} body weight). All mice were treated once daily beginning immediately following wounding and infection. Wounds were measured in perpendicular directions each day using calipers. The percentage of wound area remaining at each time point was calculated relative to the initial wound area to monitor wound closure. Of note, no adverse effects were observed in any mice following treatments with the three formulations.

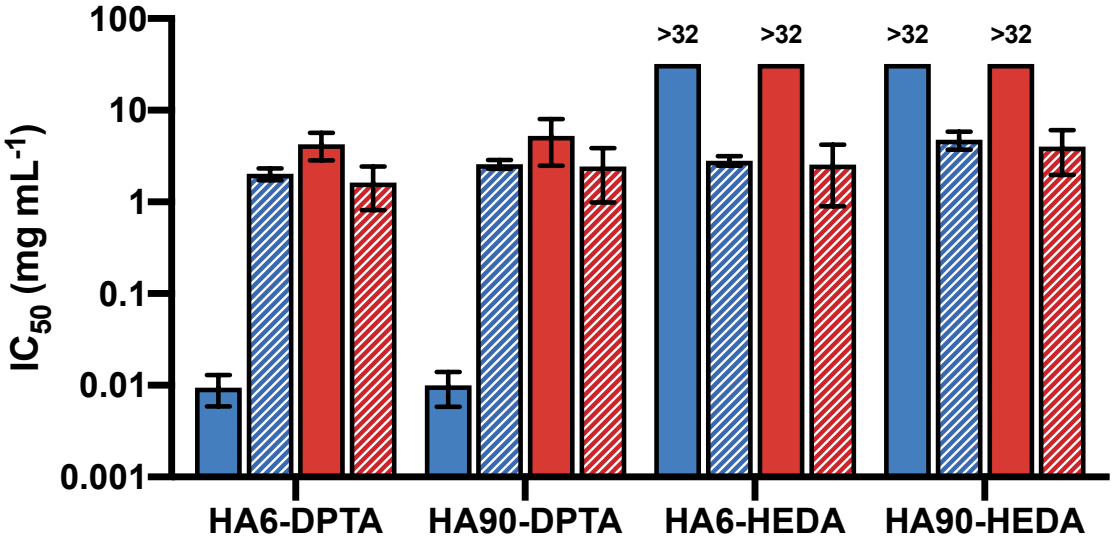

Figure 2.23 Concentration of amine-modified (solid) and NO-releasing (striped) HA derivatives required to reduce enzymatic activity of human gingival fibroblasts (blue) and human oral keratinocytes (red) by 50% (IC_{50}). Error bars represent the standard deviation for n ≥ 3 separate experiments.

While not statistically significant, the HA6-DPTA-treated wounds had less wound area remaining at all days than the PEG-treated wounds (Figure 2.24A). At days 2-8 post-wounding, wounds treated with HA6-DPTA/NO had the least wound area remaining of the three treatment groups, with significantly less wound area remaining than the wounds treated with the control vehicle (i.e., PEG) at days 4, 7, and 8. Further supporting NO's crucial role in the formulation, the NO-treated wounds led to significantly more wound healing than the HA6-DPTA-treated wounds on day 8 post-wounding. At the end of the study (i.e., on day 8 post-wounding), the PEG-treated wounds still exhibited ~15% of the initial wound area, whereas the NO-treated wounds retained less than 5% of the original wound, highlighting the wound healing potential of the combined therapeutic agent (Figure 2.24A-B). These results indicate that the amine-modified HA is capable of aiding wound healing, likely owing to low molecular weight HA's tissue remodeling properties. However, the combination of NO release and HA enhances the wound healing potential of the biopolymer.

The increased wound healing observed with HA6-DPTA and HA6-DPTA/NO treatment can also be partially attributed to the scaffolds' antibacterial properties. Excised wound tissue from mice treated with HA6-DPTA contained less *P. aeruginosa* genome than control-treated wounds (Figure 2.24C). This phenomenon is attributed to the antibacterial properties associated with primary amines (i.e., from the DPTA modification), as prior work has shown the benefits of terminal primary amines on bacterial killing, even in the absence of NO.[71] The high localized concentrations of primary amine-containing HA6-DPTA serve to decrease bacterial load. Wounds from mice treated with HA6-DPTA/NO also presented with decreased bacterial genome, with significantly lower PA01 16S rRNA expression than either the PEG- or HA6-DPTA-treated mice. These data highlight NO's superior antibacterial properties. From these results, it can be inferred

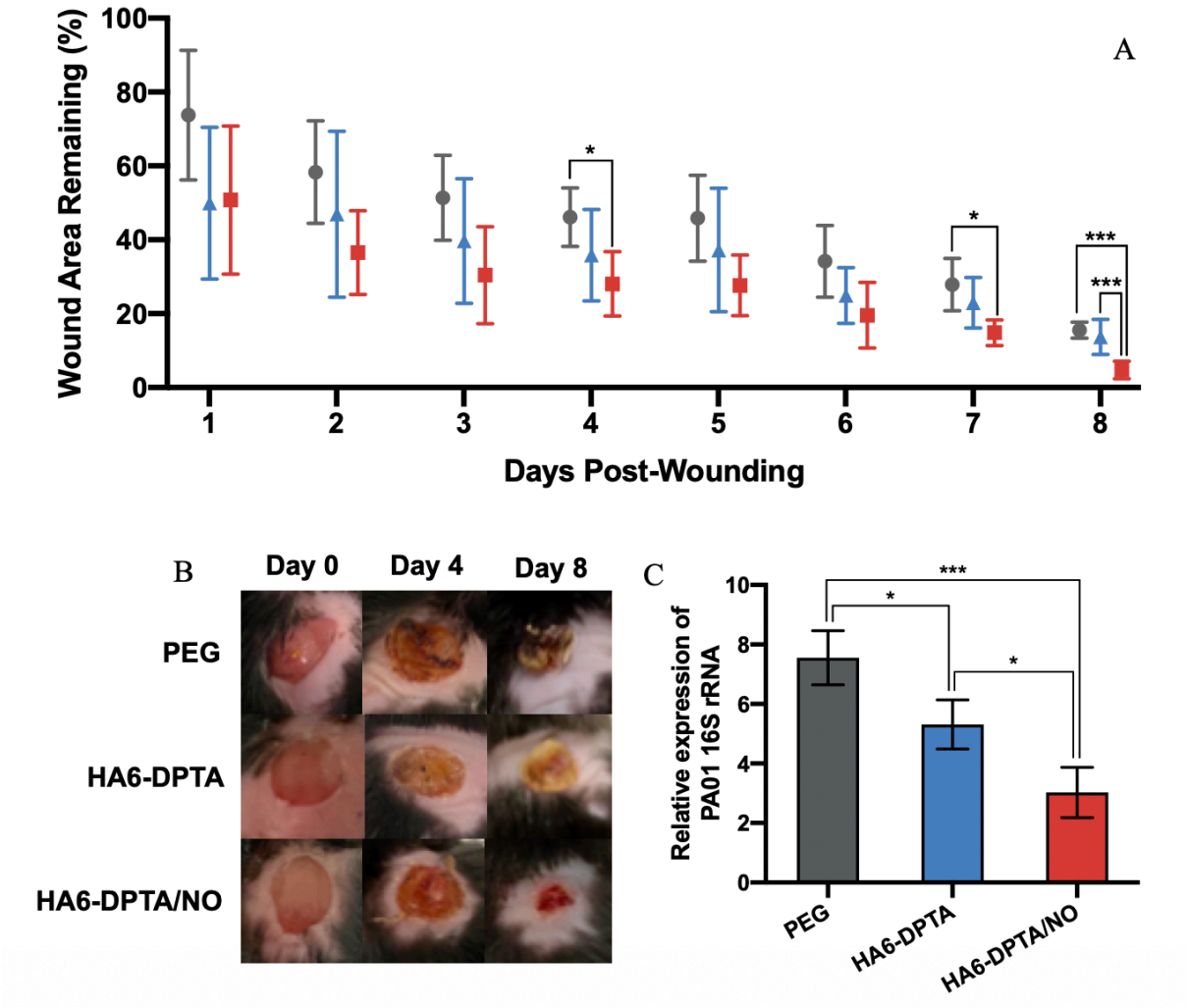

Figure 2.24 (A) Percentage of initial wound area remaining following daily treatment with PEG (gray circle), 50 mg kg^{-1} HA6-DPTA in PEG (blue triangle), or 50 mg kg^{-1} HA6-DPTA/NO (red square). **(B)** Representative images of wounds from each treatment group. **(C)** Relative quantity of *P. aeruginosa* genome remaining in wound tissue harvested 8 days post-wounding. Error bars represent the standard deviation for n = 5 mice. *p < 0.05, **p < 0.01, ***p < 0.005.

that treatment with the dual-action therapeutic led to improved and/or more rapid clearance of *P. aeruginosa*. While it is possible that similar wound healing benefits could be achieved by utilizing unmodified HA and a low molecular weight NO donor in combination, the developed therapeutic integrates the beneficial wound healing properties of both HA and NO into a single-agent therapy that can be easily integrated within current wound care practices (e.g., within ointments and wound dressings).

2.3.8. Enzymatic degradation of HA derivatives

Hyaluronic acid is degraded endogenously by hyaluronidases, a family of enzymes that cleave HA at the β-1,4 glycosidic bond.[77] In order to ascertain whether the amine-modified and NO-releasing HA derivatives function similarly to native HA, the HA90 derivatives were degraded using an excess of bovine testicular hyaluronidase (i.e., at a higher concentration than in the body, where concentrations are ~60 ng mL^{-1})[78] to allow for observations of degradation within a 30-min test period. The weight-average molecular weight (M_w) was quantified via GPC-MALS before and after the 30-min period to monitor HA degradation. Of note, the process of NO donor formation led to a decrease in HA molecular weight, suggesting oxidative degradation of the biopolymer, with the NO-releasing HA90 derivatives falling in the range of 40-55 kDa relative to the non-NO releasing derivatives (M_w = 75-90 kDa). Treatment with hyaluronidase led to a significant decrease in molecular weight for all HA90 modifications, regardless of alkylamine identity or NO storage (Figure 2.25, Table 2.5). After a 30 min period, the unmodified HA, amine-modified HA, and NO-releasing HA were degraded to 9.0 ± 0.1 kDa, 10-13 kDa, and 11.5-15 kDa, respectively. These minor differences may be attributed to slower enzyme kinetics as a result of HA modification or increased unit (i.e., disaccharide) molecular weight upon alkylamine incorporation.

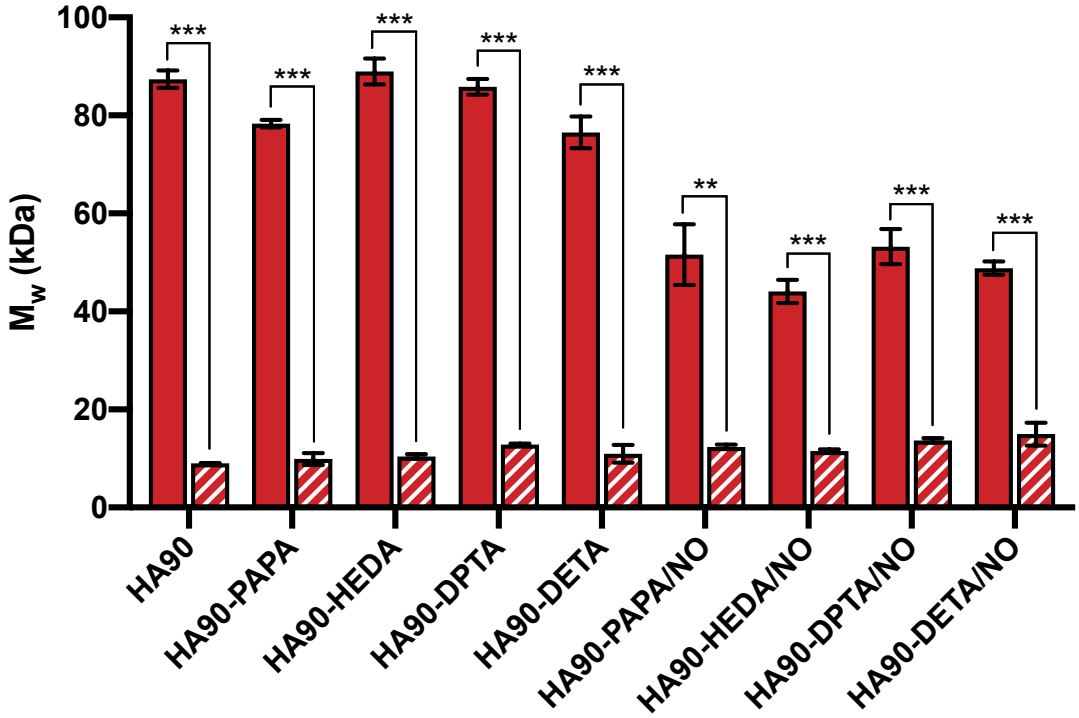

Figure 2.25 Molecular weight of unmodified, amine-modified, and NO-releasing HA90 derivatives before (solid) and after (striped) enzymatic degradation by hyaluronidase. Error bars represent the standard deviation for $n \geq 3$ separate experiments. *$p < 0.05$, **$p < 0.01$, ***$p < 0.005$.

Table 2.5 Molecular weight (M_w) and dispersity (Đ) of unmodified, amine-modified, and NO-releasing HA90 pre- and post-degradation by hyaluronidase.[a]

Modification	Trial	Nondegraded		Degraded	
		M_w (kDa)	Đ	M_w (kDa)	Đ
HA90	1	87.7	1.47	9.1	1.62
	2	85.4	1.43	8.9	1.58
	3	85.5	1.46	9.0	1.71
HA90-PAPA	1	79.2	1.46	10.6	1.47
	2	78.1	1.47	8.5	1.53
	3	77.7	1.45	10.6	1.50
HA90-PAPA/NO	1	46.7	1.57	12.1	1.34
	2	58.6	1.51	12.1	1.43
	3	49.5	1.63	12.9	1.34
HA90-HEDA	1	87.9	1.58	9.9	1.56
	2	87.0	1.66	10.8	1.67
	3	92.0	1.65	10.6	1.48
HA90-HEDA/NO	1	41.4	1.67	11.9	1.38
	2	45.2	1.68	11.2	1.42
	3	45.7	1.50	11.5	1.46
HA90-DPTA	1	76.1	1.92	12.9	1.60
	2	82.4	1.41	13.0	1.55
	3	86.6	1.68	12.6	1.61
HA90-DPTA/NO	1	50.1	1.81	14.2	1.54
	2	52.5	1.96	13.2	1.42
	3	57.0	1.70	13.3	1.54
HA90-DETA	1	78.7	1.50	11.8	1.33
	2	72.8	1.89	8.9	1.47
	3	78.1	1.46	12.2	1.39
HA90-DETA/NO	1	47.9	1.75	17.6	1.25
	2	50.4	1.61	13.1	1.39
	3	48.2	1.56	14.2	1.38

[a]Determined by GPC-MALS in 0.1 M phosphate buffer (pH 7.4) supplemented with 0.1 M $NaNO_3$ and 0.02 wt% NaN_3.

In either case, the HA90 derivatives retain the ability to be degraded by hyaluronidase, indicating the retention of properties common to unmodified HA. Unmodified HA6 was not able to be degraded by hyaluronidase, as the starting molecular weight of HA6 (~9 kDa) is a similar molecular weight to the degradation products of HA90. This suggests that degradation past this molecular weight range is not achievable by bovine testicular hyaluronidase within the given time frame and under the evaluated conditions. Although not investigated herein, it is likely that HA's other physiological properties (e.g., pro-wound healing activities) are also retained as the presence of NO does not appear to have a negative impact on hyaluronidase function for the degradation of HA90. Further *in vitro* and *in vivo* analyses are obviously necessary to fully elucidate the effects of altering HA structure and NO release on such biological processes.

2.4. Conclusions

Hyaluronic acid was modified to contain *N*-diazeniumdiolate donors to store and release NO with a degree of tunability. The role of the alkylamine substituent was evident in the antibacterial action of the HA derivatives, with DPTA-modified HA outperforming the other chemical modifications in decreasing bacteria viability of the common wound pathogens *E. coli*, *P. aeruginosa*, *S. aureus*, and *E. faecalis*. Both HA6-DPTA/NO and HA90-DPTA/NO demonstrated superior antibacterial activity against MDR-PA and MRSA compared to a conventional antibiotic, neomycin sulfate. Further, HA6-DPTA/NO was able to kill susceptible and multi-drug resistant *P. aeruginosa* biofilms at lower equivalent active ingredient doses than either HA90-DPTA/NO or neomycin, highlighting the benefit of a low molecular weight NO-releasing HA scaffold for biofilm treatment. Minimal cytotoxicity to L929 murine fibroblasts was found at doses equivalent to the MBC_{4h} for HA6-DPTA/NO and HA90-DPTA/NO, with NO levels

primarily dictating toxicity of the NO-releasing HA derivatives rather than properties of the HA backbone (i.e., molecular weight and functional moiety). Amine-modified and NO-releasing HA derivatives demonstrated similar biodegradability to unmodified HA, suggesting that altering the structure of HA does not significantly impact reactivity with endogenous enzymes. Based on the promising bactericidal activity of the NO-releasing HA derivatives in aqueous solution, work evaluating optimal formulations for topical delivery is currently underway, including the incorporation of the biopolymer within wound dressings, hydrogels, and ointments. Preliminary studies with HA6-DPTA/NO suspended within a PEG gel were shown to facilitate wound closure in a *P. aeruginosa*-infected murine wound model. Furthermore, the enhanced wound closure was correlated to lower levels of remaining bacterial genome in the wound tissue. The combination of HA's and NO's beneficial wound healing and antibacterial properties allowed for the development of a dual-action wound therapeutic that demonstrates promise in addressing complications associated with chronic wounds.

REFERENCES

(1) Velnar, T.; Bailey, T.; Smrkolj, V. The Wound Healing Process: An Overview of the Cellular and Molecular Mechanisms. *J. Int. Med. Res.* **2009**, *37*, 1528–1542.

(2) Guo, S.; DiPietro, L. A. Factors Affecting Wound Healing. *J. Dent. Res.* **2010**, *89*, 219–229.

(3) Bjarnsholt, T.; Kirketerp-Møller, K.; Jensen, P. Ø.; Madsen, K. G.; Phipps, R.; Krogfelt, K.; Høiby, N.; Givskov, M. Why Chronic Wounds Will Not Heal: A Novel Hypothesis. *Wound Repair Regen.* **2008**, *16*, 2–10.

(4) Malone-Povolny, M. J.; Maloney, S. E.; Schoenfisch, M. H. Nitric Oxide Therapy for Diabetic Wound Healing. *Adv. Healthc. Mater.* **2019**, *8*, 1801210.

(5) Richmond, N.; Maderal, A.; Vivas, A. Evidence-Based Management of Common Chronic Lower Extremity Ulcers. *Dermatol. Ther.* **2013**, *26*, 187–196.

(6) Singer, A. J.; Clark, R. A. F. Cutaneous Wound Healing. *N. Engl. J. Med.* **1999**, *341*, 738–746.

(7) Blakytny, R.; Jude, E. The Molecular Biology of Chronic Wounds and Delayed Healing in Diabetes. *Diabet. Med.* **2006**, *23*, 594–608.

(8) Reddy, M.; Gill, S. S.; Wu, W.; Kalkar, S. R.; Rochon, P. A. Does This Patient Have an Infection of a Chronic Wound? *J. Am. Med. Assoc.* **2012**, *307*, 605–611.

(9) Gjødsbøl, K.; Christensen, J. J.; Karlsmark, T.; Jørgensen, B.; Klein, B. M.; Krogfelt, K. A. Multiple Bacterial Species Reside in Chronic Wounds: A Longitudinal Study. *Int. Wound J.* **2006**, *3*, 225–231.

(10) Buch, P. J.; Chai, Y.; Goluch, E. D. Treating Polymicrobial Infections in Chronic Diabetic Wounds. *Clin. Microbiol. Rev.* **2019**, *32*, 1–17.

(11) Hall, C. W.; Mah, T. F. Molecular Mechanisms of Biofilm-Based Antibiotic Resistance and Tolerance in Pathogenic Bacteria. *FEMS Microbiol. Rev.* **2017**, *41*, 276–301.

(12) Ventola, C. L. The Antibiotic Resistance Crisis: Part 1: Causes and Threats. *Pharm. Ther.* **2015**, *40*, 277–283.

(13) Hetrick, E. M.; Shin, J. H.; Stasko, N. A.; Johnson, C. B.; Wespe, D. A.; Holmuhamedov, E.; Schoenfisch, M. H. Bactericidal Efficacy of Nitric Oxide-Releasing Silica Nanoparticles. *ACS Nano* **2008**, *2*, 235–246.

(14) Fang, F. C. Mechanisms of Nitric Oxide-Related Antimicrobial Activity. *J. Clin. Invest.* **1997**, *99*, 2818–2825.

(15) Yang, L.; Feura, E. S.; Ahonen, M. J. R.; Schoenfisch, M. H. Nitric Oxide–Releasing Macromolecular Scaffolds for Antibacterial Applications. *Adv. Healthc. Mater.* **2018**, *7*, 1–18.

(16) Privett, B. J.; Broadnax, A. D.; Bauman, S. J.; Riccio, D. A.; Schoenfisch, M. H. Examination of Bacterial Resistance to Exogenous Nitric Oxide. *Nitric Oxide* **2012**, *26*, 169–173.

(17) Carpenter, A. W.; Schoenfisch, M. H. Nitric Oxide Release: Part II. Therapeutic Applications. *Chem. Soc. Rev.* **2012**, *41*, 3742–3752.

(18) Nichols, S. P.; Storm, W. L.; Koh, A.; Schoenfisch, M. H. Local Delivery of Nitric Oxide: Targeted Delivery of Therapeutics to Bone and Connective Tissues. *Adv. Drug Deliv. Rev.* **2012**, *64*, 1177–1188.

(19) Witte, M. B.; Barbul, A. Role of Nitric Oxide in Wound Repair. *Am. J. Surg.* **2002**, *183*, 406–412.

(20) Smith, B. C.; Fernhoff, N. B.; Marletta, M. A. Mechanism and Kinetics of Inducible Nitric Oxide Synthase Auto- S -Nitrosation and Inactivation. *Biochemistry* **2012**, *51*, 1028–1040.

(21) Donnini, S.; Ziche, M. Constitutive and Inducible Nitric Oxide Synthase: Role in Angiogenesis. *Antioxidants Redox Signal.* **2002**, *4*, 817–823.

(22) Nathan, C. F.; Hibbs, J. B. Role of Nitric Oxide Synthesis in Macrophage Antimicrobial Activity. *Curr. Opin. Immunol.* **1991**, *3*, 65–70.

(23) Wo, Y.; Brisbois, E. J.; Bartlett, R. H.; Meyerhoff, M. E. Recent Advances in Thromboresistant and Antimicrobial Polymers for Biomedical Applications: Just Say Yes to Nitric Oxide (NO). *Biomater. Sci.* **2016**, *4*, 1161–1183.

(24) Hakim, T. S.; Sugimori, K.; Camporesi, E. M.; Andersen, G. Half-Life of Nitric Oxide in Aqueous Solutions with and without Haemoglobin. *Physiol. Meas.* **1996**, *17*, 267–277.

(25) Keefer, L. K. Fifty Years of Diazeniumdiolate Research: From Laboratory Curiosity to Broad-Spectrum Biomedical Advances. *ACS Chem. Biol.* **2011**, *6*, 1147–1155.

(26) Soto, R. J.; Yang, L.; Schoenfisch, M. H. Functionalized Mesoporous Silica via an Aminosilane Surfactant Ion Exchange Reaction: Controlled Scaffold Design and Nitric Oxide Release. *ACS Appl. Mater. Interfaces* **2016**, *8*, 2220–2231.

(27) Zhang, H.; Annich, G. M.; Miskulin, J.; Stankiewicz, K.; Osterholzer, K.; Merz, S. I.; Bartlett, R. H.; Meyerhoff, M. E. Nitric Oxide-Releasing Fumed Silica Particles: Synthesis, Characterization, and Biomedical Application. *J. Am. Chem. Soc.* **2003**, *125*, 5015–5024.

(28) Worley, B. V.; Soto, R. J.; Kinsley, P. C.; Schoenfisch, M. H. Active Release of Nitric

Oxide-Releasing Dendrimers from Electrospun Polyurethane Fibers. *ACS Biomater. Sci. Eng.* **2016**, *2*, 426–437.

(29) Stasko, N. A.; Schoenfisch, M. H. Dendrimers as a Scaffold for Nitric Oxide Release. *J. Am. Chem. Soc.* **2006**, *128*, 8265–8271.

(30) Ahonen, M. J. R.; Suchyta, D. J.; Zhu, H.; Schoenfisch, M. H. Nitric Oxide-Releasing Alginates. *Biomacromolecules* **2018**, *19*, 1189–1197.

(31) Lu, Y.; Slomberg, D. L.; Schoenfisch, M. H. Nitric Oxide-Releasing Chitosan Oligosaccharides as Antibacterial Agents. *Biomaterials* **2014**, *35*, 1716–1724.

(32) Riccio, D. A.; Schoenfisch, M. H. Nitric Oxide Release: Part I. Macromolecular Scaffolds. *Chem. Soc. Rev.* **2012**, *41*, 3731–3741.

(33) Seabra, A. B.; Justo, G. Z.; Haddad, P. S. State of the Art, Challenges and Perspectives in the Design of Nitric Oxide-Releasing Polymeric Nanomaterials for Biomedical Applications. *Biotechnol. Adv.* **2015**, *33*, 1370–1379.

(34) Schanuel, F. S.; Raggio Santos, K. S.; Monte-Alto-Costa, A.; de Oliveira, M. G. Combined Nitric Oxide-Releasing Poly(Vinyl Alcohol) Film/F127 Hydrogel for Accelerating Wound Healing. *Colloids Surfaces B Biointerfaces* **2015**, *130*, 182–191.

(35) Kang, Y.; Kim, J.; Lee, Y. M.; Im, S.; Park, H.; Kim, W. J. Nitric Oxide-Releasing Polymer Incorporated Ointment for Cutaneous Wound Healing. *J. Control. Release* **2015**, *220*, 624–630.

(36) Masters, K. S. B.; Leibovich, S. J.; Belem, P.; West, J. L.; Poole-Warren, L. A. Effects of Nitric Oxide Releasing Poly(Vinyl Alcohol) Hydrogel Dressings on Dermal Wound Healing in Diabetic Mice. *Wound Repair Regen.* **2002**, *10*, 286–295.

(37) Weller, R.; Finnen, M. J. The Effects of Topical Treatment with Acidified Nitrite on Wound Healing in Normal and Diabetic Mice. *Nitric Oxide* **2006**, *15*, 395–399.

(38) Phillips, R.; Adjei, O.; Lucas, S.; Benjamin, N. Pilot Randomized Double-Blind Trial of Treatment of Mycobacterium Ulcerans Disease (Buruli Ulcer) with Topical Nitrogen Oxides. *Society* **2004**, *48*, 2866–2870.

(39) Ormerod, A. D.; Shah, A. A. J.; Li, H.; Benjamin, N. B.; Ferguson, G. P.; Leifert, C. An Observational Prospective Study of Topical Acidified Nitrite for Killing Methicillin-Resistant Staphylococcus Aureus (MRSA) in Contaminated Wounds. *BMC Res. Notes* **2011**, *4*, 458.

(40) Kim, J. O.; Noh, J. K.; Thapa, R. K.; Hasan, N.; Choi, M.; Kim, J. H.; Lee, J. H.; Ku, S. K.; Yoo, J. W. Nitric Oxide-Releasing Chitosan Film for Enhanced Antibacterial and in Vivo Wound-Healing Efficacy. *Int. J. Biol. Macromol.* **2015**, *79*, 217–225.

(41) Brisbois, E. J.; Bayliss, J.; Wu, J.; Major, T. C.; Xi, C.; Wang, S. C.; Bartlett, R. H.; Handa, H.; Meyerhoff, M. E. Optimized Polymeric Film-Based Nitric Oxide Delivery Inhibits Bacterial Growth in a Mouse Burn Wound Model. *Acta Biomater.* **2014**, *10*, 4136–4142.

(42) Lowe, A.; Bills, J.; Verma, R.; Lavery, L.; Davis, K.; Balkus, K. J. Electrospun Nitric Oxide Releasing Bandage with Enhanced Wound Healing. *Acta Biomater.* **2015**, *13*, 121–130.

(43) Aya, K. L.; Stern, R. Hyaluronan in Wound Healing: Rediscovering a Major Player. *Wound Repair Regen.* **2014**, *22*, 579–593.

(44) Hussain, Z.; Thu, H. E.; Katas, H.; Bukhari, S. N. A. Hyaluronic Acid-Based Biomaterials: A Versatile and Smart Approach to Tissue Regeneration and Treating Traumatic, Surgical, and Chronic Wounds. *Polym. Rev.* **2017**, *57*, 594–630.

(45) Collins, M. N.; Birkinshaw, C. Hyaluronic Acid Based Scaffolds for Tissue Engineering - a Review. *Carbohydr. Polym.* **2013**, *92*, 1262–1279.

(46) Park, S. H.; Seo, J. Y.; Park, J. Y.; Ji, Y. B.; Kim, K.; Choi, H. S.; Choi, S.; Kim, J. H.; Min, B. H.; Kim, M. S. An Injectable, Click-Crosslinked, Cytomodulin-Modified Hyaluronic Acid Hydrogel for Cartilage Tissue Engineering. *NPG Asia Mater.* **2019**, *11*, 1–16.

(47) Xie, J.; Ji, Y.; Xue, W.; Ma, D.; Hu, Y. Hyaluronic Acid-Containing Ethosomes as a Potential Carrier for Transdermal Drug Delivery. *Colloids Surfaces B Biointerfaces* **2018**, *172*, 323–329.

(48) Wei, S.; Xie, J.; Luo, Y.; Ma, Y.; Tang, S.; Yue, P.; Yang, M. Hyaluronic Acid Based Nanocrystals Hydrogels for Enhanced Topical Delivery of Drug: A Case Study. *Carbohydr. Polym.* **2018**, *202*, 64–71.

(49) Dosio, F.; Arpicco, S.; Stella, B.; Fattal, E. Hyaluronic Acid for Anticancer Drug and Nucleic Acid Delivery. *Adv. Drug Deliv. Rev.* **2016**, *97*, 204–236.

(50) Suner, S. S.; Ari, B.; Onder, F. C.; Ozpolat, B.; Ay, M.; Sahiner, N. Hyaluronic Acid and Hyaluronic Acid:Sucrose Nanogels for Hydrophobic Cancer Drug Delivery. *Int. J. Biol. Macromol.* **2019**, *126*, 1150–1157.

(51) Galeano, M.; Polito, F.; Bitto, A.; Irrera, N.; Campo, G. M.; Avenoso, A.; Calò, M.; Cascio, P. Lo; Minutoli, L.; Barone, M.; Squadrito, F.; Altavilla, D. Systemic Administration of High-Molecular Weight Hyaluronan Stimulates Wound Healing in Genetically Diabetic Mice. *Biochim. Biophys. Acta* **2011**, *1812*, 752–759.

(52) Gao, F.; Liu, Y.; He, Y.; Yang, C.; Wang, Y.; Shi, X.; Wei, G. Hyaluronan Oligosaccharides Promote Excisional Wound Healing through Enhanced Angiogenesis. *Matrix Biol.* **2010**, *29*, 107–116.

(53) Tolg, C.; Telmer, P.; Turley, E. Specific Sizes of Hyaluronan Oligosaccharides Stimulate

Fibroblast Migration and Excisional Wound Repair. *PLoS One* **2014**, *9*, 1–10.

(54) Sattar, A.; Rooney, P.; Kumar, S.; Pye, D.; West, D. C.; Scott, I.; Ledger, P. Application of Angiogenic Oligosaccharides of Hyaluronan Increases Blood Vessel Numbers in Rat Skin. *J. Invest. Dermatol.* **1994**, *103*, 576–579.

(55) Vazquez, J. R.; Short, B.; Findlow, A. H.; Nixon, B. P.; Boulton, A. J. M.; Armstrong, D. G. Outcomes of Hyaluronan Therapy in Diabetic Foot Wounds. *Diabetes Res. Clin. Pract.* **2003**, *59*, 123–127.

(56) Hong, L.; Shen, M.; Fang, J.; Wang, Y.; Bao, Z.; Bu, S.; Zhu, Y. Hyaluronic Acid (HA)-Based Hydrogels for Full-Thickness Wound Repairing and Skin Regeneration. *J. Mater. Sci. Mater. Med.* **2018**, *29*, 150.

(57) Yapor, J. P.; Gordon, J. L.; Henderson, C. N.; Reynolds, M. M. Nitric Oxide-Releasing Emulsion with Hyaluronic Acid and Vitamin E. *RSC Adv.* **2019**, *9*, 21873–21880.

(58) Jin, H.; Yang, L.; Ahonen, M. J. R.; Schoenfisch, M. H. Nitric Oxide-Releasing Cyclodextrins. *J. Am. Chem. Soc.* **2018**, *140*, 14178-14184.

(59) Sutton, S. Accuracy of Plate Counts. *J. Valid. Technol.* **2011**, *17*, 42–46.

(60) Turner, R. E.; Lin, P.; Cowman, M. K. Self-Association of Hyaluronate Segments in Aqueous NaCl Solution. *Arch. Biochem. Biophys.* **1988**, *265*, 484–495.

(61) Sabaté, C. M.; Delalu, H. Synthesis and Characterization of Secondary Nitrosamines from Secondary Amines Using Sodium Nitrite and P-Toluenesulfonic Acid. *Chem. - An Asian J.* **2015**, *10*, 674–678.

(62) Plumlee, M. H.; Reinhard, M. Photochemical Attenuation of N-Nitrosodimethylamine (NDMA) and Other Nitrosamines in Surface Water. *Environ. Sci. Technol.* **2007**, *41*, 6170–6176.

(63) Gjødsbøl, K.; Christensen, J. J.; Karlsmark, T.; Jørgensen, B.; Klein, B. M.; Krogfelt, K. A. Multiple Bacterial Species Reside in Chronic Wounds: A Longitudinal Study. *Int. Wound J.* **2006**, *3*, 225–231.

(64) Chellan, G.; Shivaprakash, S.; Ramaiyar, S. K.; Varma, A. K.; Varma, N.; Sukumaran, M. T.; Vasukutty, J. R.; Bal, A.; Kumar, H. Spectrum and Prevalence of Fungi Infecting Deep Tissues of Lower-Limb Wounds in Patients with Type 2 Diabetes. *J. Clin. Microbiol.* **2010**, *48*, 2097–2102.

(65) Liu, N.; Chen, X. G.; Park, H. J.; Liu, C. G.; Liu, C. S.; Meng, X. H.; Yu, L. J. Effect of MW and Concentration of Chitosan on Antibacterial Activity of Escherichia Coli. *Carbohydr. Polym.* **2006**, *64*, 60–65.

(66) Silhavy, T. J.; Kahne, D.; Walker, S. The Bacterial Cell Envelope. *Cold Spring Harb. Perspect. Biol.* **2010**, *2*, 1–16.

(67) Thevenot, P.; Hu, W.; Tang, L. Surface Chemistry Influences Implant Biocompatibility. *Curr. Top. Med. Chem.* **2008**, *8*, 270–280.

(68) Yang, L.; Wang, X.; Suchyta, D. J.; Schoenfisch, M. H. Antibacterial Activity of Nitric Oxide-Releasing Hyperbranched Polyamidoamines. *Bioconjug. Chem.* **2018**, *29*, 35–43.

(69) De Oliveira, F. P.; Pires, B. M. F. B.; De Cássia Ferreira De Almeida Silva, K.; De Carvalho, B. T. F.; Teixeira, L. A.; De Paula, G. R.; De Oliveira, B. G. R. B. Prevalence, Antimicrobial Susceptibility, and Clonal Diversity of Pseudomonas Aeruginosa in Chronic Wounds. *J. Wound, Ostomy Cont. Nurs.* **2017**, *44*, 528–535.

(70) Pereira-Franchi, E. P. L.; Barreira, M. R. N.; Da Costa, N. de S. L. M.; Fortaleza, C. M. C. B.; Da Cunha, M. de L. R. de S. Prevalence of and Risk Factors Associated with the Presence of Staphylococcus Aureus in the Chronic Wounds of Patients Treated in Primary Health Care Settings in Brazil. *Rev. Soc. Bras. Med. Trop.* **2017**, *50*, 833–838.

(71) Yoneda, M.; Yamagata, M.; Suzuki, S.; Kimata, K. Hyaluronic Acid Modulates Proliferation of Mouse Dermal Fibroblasts in Culture. *J. Cell Sci.* **1988**, *90*, 265–273.

(72) Souza, A. G.; Silva, I. B. B.; Campos-Fernandez, E.; Barcelos, L. S.; Souza, J. B.; Marangoni, K.; Goulart, L. R.; Alonso-Goulart, V. Comparative Assay of 2D and 3D Cell Culture Models: Proliferation, Gene Expression and Anticancer Drug Response. *Curr. Pharm. Des.* **2018**, *24*, 1689–1694.

(73) Joseph, J. S.; Malindisa, S. T.; Ntwasa, M. Two-Dimensional (2D) and Three-Dimensional (3D) Cell Culturing in Drug Discovery. In *Cell Culture*; 2019; pp 21–42.

(74) Stern, R.; Jedrzejas, M. J. Hyaluronidases: Their Genomics, Structures, and Mechanisms of Action. *Chem. Rev.* **2006**, *106*, 818–839.

(75) Frost, G. I.; Csóka, T. B.; Wong, T.; Stern, R. Purification, Cloning, and Expression of Human Plasma Hyaluronidase. *Biochem. Biophys. Res. Commun.* **1997**, *236*, 10–15.

CHAPTER 3: ROLE OF NITRIC OXIDE-RELEASING GLYCOSAMINOGLYCANS ON WOUND HEALING

3.1. Introduction

Approximately 2% of the total population in the United States is living with a chronic wound, loosely defined as a skin trauma that fails to heal in a normal timeframe (i.e., 1-3 months).[1–4] These wounds often stall in a state of inflammation as a result of persistent stimuli, including prolonged pressure or repetitive tissue trauma, or due to underlying conditions, such as those that impair the host immune response (e.g., diabetes, cancer).[5–7] The delayed healing observed for chronic wounds is often potentiated by wound infection, especially in the case of biofilm formation. Biofilms, or cooperative communities of bacteria that self-secrete an exopolysaccharide (EPS) matrix, are difficult to eradicate with conventional antibiotics due to changes in bacterial metabolism and the presence of a viscous matrix that prevents antibiotic diffusion.[8–13] Further, bacteria are able to develop resistance to conventional antibiotics, rendering many current antibacterial therapies ineffective.[14,15] Due to the devastating ramifications of nonhealing wounds, including pain, amputation, and even death, new wound treatments that address both infection and impairment of the host immune response, without the potential for garnering resistant, are greatly needed.

Nitric oxide, an endogenous signaling molecule, represents an alternative therapeutic for treating chronic wounds due to its innate roles in mitigating both inflammation and infection.[16–19] Nitric oxide possesses broad-spectrum antibacterial action through multiple

mechanisms (i.e., nitrosative and oxidative stresses), in which reactive byproducts of NO cause thiol nitrosation, DNA deamination, and destruction of cell membranes through lipid peroxidation.[16,20,21] With NO's ability to penetrate through the EPS matrix, significantly lower concentrations of NO are required relative to traditional antibiotics to disrupt and eradicate biofilm-based bacteria.[22–24] Bacterial resistance to NO is also unlikely due to these multiple mechanisms of antibacterial action.[25,26] In addition to its bactericidal abilities, endogenous NO is directly involved in the wound healing pathway.[7,27] Nitric oxide is produced in large quantities (nM-μM) by immune cells (e.g., macrophages, neutrophils) as part of the immune response to eradicate bacteria in the wound environment.[24,28,29] Lesser concentrations of NO (pM-nM) are constitutively produced by endothelial cells and facilitate angiogenesis, collagen synthesis, and inflammatory cell proliferation and function.[30–33] These endogenous mechanisms have motivated the use of exogenous NO as a strategy for eradicating bacterial infections and assisting wound healing.

Treatment with gaseous NO has been demonstrated to reduce bacterial loads and accelerate wound closure.[34,35] However, such treatment is limited to use in hospital settings where continuous oversight is available due to systemic toxicity concerns.[28,36,37] *N*-diazeniumdiolate NO donors provide an alternative method to exogenous NO due to their spontaneous degradation to NO in physiological milieu.[38,39] Low molecular weight *N*-diazeniumdiolate NO donors have been utilized as wound therapeutics and shown to accelerate wound closure and decrease bacterial burden in rodent models.[40,41] While representing an efficacious system, the untargeted delivery of these donors and cytotoxicity of regenerated donor amines make small molecule donor systems difficult to use as therapeutics. The covalent attachment of NO donor functional groups to macromolecules mitigates these concerns.[20,42] Macromolecular NO-release vehicles are easily incorporated within

conventional wound therapies and dressings (e.g., fibrous bandages, hydrogels) in order to facilitate topical NO delivery.[43,44] For example, Lowe et al. covalently bound NO donors to acrylonitrile-based terpolymers, which were then electrospun to form non-woven fibrous wound dressings.[43] Alternatively, Masters et al. reported on the covalent attachment of NO donors to poly(vinyl alcohol) hydrogels.[44] Treatment of wounds with NO derived from macromolecular scaffolds, such as those reported by Lowe et al. and Masters et al., has accelerated wound closure, eradicated wound pathogens, increased collagen deposition, and promoted angiogenesis.[7,22,43,44]

Hyaluronic acid (HA) and chondroitin sulfate (CS), two biopolymers within the glycosaminoglycan (GAG) family, represent promising NO delivery scaffolds due to their endogenous production and roles in inflammation and tissue repair.[45–49] As additional benefits, both biopolymers exhibit high water solubility, low toxicity, and biodegradability.[47,49] Hyaluronic acid is composed of alternating D-glucuronic acid and *N*-acetyl-D-glucosamine residues and acts as a signaling molecule for wound healing with resulting actions dependent on HA molecular weight.[46,47,50,51] High molecular weight HA (≥ 1 MDa) is found in healthy tissue and signals for tissue maintenance.[46,52] Under stress, endogenous HA is enzymatically degraded by hyaluronidases to lower molecular weights (1-800 kDa), which signals for tissue repair actions, such as angiogenesis, the release of pro-inflammatory cytokines, and collagen deposition.[46,47,50,52]

As a result of HA's involvement in the wound healing pathway, several studies have investigated the supplementation of exogenous HA as a potential therapy. Both high molecular weight and low molecular weight HA wound therapies have demonstrated enhanced wound healing through a number of outcomes, including improving skin mechanical properties, alleviating inflammation, and increasing wound closure rates, angiogenesis, collagen deposition, and wound moisture.[47,53–57] Chondroitin sulfate possesses a similar structure to HA, consisting of

alternating D-glucuronic acid and *N*-acetyl-D-galactosamine residues, with the addition of a sulfate group.[58,59] In animal tissue, this sulfate group is predominantly found at either the 4 (chondroitin sulfate A; CSA) or 6 position (chondroitin sulfate C; CSC) of the N-acetyl-D-galactosamine residue.[48,58,60] The specific interactions of CS with bioactive molecules are a function of the sulfation degree and profile of the CS backbone.[49,58] Previous literature has reported that CS isomers can decrease inflammation, alter fibroblast/keratinocyte adhesion, proliferation, and migration, and modulate angiogenesis and collagen deposition, all of which are potentially beneficial for a wound therapeutic.[58,61–66] The structures of both HA and CS allow for facile chemical modification of the carboxylic acid groups, allowing for the covalent attachment of NO donors.[49,67] Through the combination of the beneficial wound healing properties of HA and CS with the multifaceted roles of NO, we sought to develop a multimodal macromolecular NO delivery system.

Herein, we describe the modification of HA (6, 50, and 90 kDa) and CS (30 kDa CSA and 20 kDa CSC) with alkylamine groups for subsequent *N*-diazeniumdiolate NO donor formation. These HA molecular weights were specifically chosen to interact with one or more of the main receptors for HA's wound healing pathways (TLR, RHAMM, and CD44 receptors).[47,50,51,68] The two CS isomers, CSA and CSC, were selected as they represent the two most abundant forms of CS isolated from animal tissue and may differ in wound healing properties as a result of their sulfation pattern.[49,58,59] The alkylamine groups used for modification have been described previously to confer a range of NO-release kinetics.[22,69,70] Glycosaminoglycan derivatives varying in biopolymer physical properties (i.e., GAG identity, HA molecular weight, CS sulfation pattern, alkylamine identity) and NO-release properties (i.e., NO payloads and kinetics) were screened for antibacterial and pro-wound healing properties using an arsenal of in vitro assays. Antibacterial

properties, including bacterial inhibition and eradication, were tested against prevalent wound pathogens, including clinical multidrug-resistant *P. aeruginosa* and *S. aureus* isolates. Aspects of wound healing, including cell proliferation and adhesion, were evaluated in vitro with human dermal fibroblasts and human epidermal keratinocytes as representative cell types in the wound environment. The role of biopolymer physical properties and NO-release properties on inflammation were further investigated using an in vitro assay via activation of the murine TLR4 receptor. Lastly, the most promising candidates from the in vitro antibacterial, wound healing, and inflammation studies were evaluated in a *P. aeruginosa*-infected murine wound model and via an in vitro migration assay to assess their potential as wound therapeutics.

3.2. Materials and methods

3.2.1. Materials

Ultra-low (< 6 kDa; HA6), super-low (< 50 kDa; HA50), and extra-low (80-110 kDa; HA90) molecular weight hyaluronic acid were purchased from Lotioncrafter (Eastsound, WA). Chondroitin sulfate A sodium salt (average molecular weight 20-30 kDa) and chondroitin sulfate C sodium salt were purchased from Biosynth Carbosynth (Compton, United Kingdom). Bis(3-aminopropyl)amine (DPTA), diethylenetriamine (DETA), *N*-(2-hydroxyethyl)ethylenediamine (HEDA), 1-ethyl-3-(3-dimethylaminopropyl)carbodiimide hydrochloride (EDC), *N*-hydroxysuccinimide (NHS), phenazine methosulfate (PMS), bovine collagen solution (type I), lipopolysaccharides from *Escherichia coli* O111:B4 (LPS), and antifoam B emulsion were purchased from MilliporeSigma (St. Louis, MO). 3-(4,5-dimethylthizol-2-yl)-5-(3-carboxymethoxyphenyl)-2-(4-sulfophenyl)-2H-tetrazolium inner salt (MTS) was purchased from Biovision (Milpitas, CA). Trypsin, penicillin streptomycin (PS), fetal bovine serum (FBS),

Dulbecco's modified Eagle's medium (DMEM), keratinocyte serum-free medium (SFM; with human recombinant epidermal growth factor, rEGF), bovine serum albumin (BSA), tumor necrosis factor recombinant human protein (TNF-α), and common laboratory salts and solvents were purchased from Thermo Fisher Scientific (Fair Lawn, NJ). HEK-Blue™ mTLR4 cells, HEK-Blue™ Null1-v cells, HEK-Blue™ Selection, Normocin™, Zeocin™, and QUANTI-Blue™ solution were purchased from Invivogen (San Diego, CA). Tryptic soy broth (TSB), Mueller Hinton II broth (MHB), and tryptic soy agar (TSA) were obtained from Becton, Dickinson, and Company (Franklin Lakes, NJ). Human dermal fibroblasts (HDF) and human epidermal keratinocytes (HEK) were obtained from the UNC Tissue Culture Facility (Chapel Hill, NC). *Pseudomonas aeruginosa* (*P. aeruginosa*, PAO1; ATCC 47085), *Staphylococcus aureus* (*S. aureus*; ATCC 29213), multidrug-resistant *P. aeruginosa* (MDR-PA; ATCC BAA-2110), and methicillin-resistant *S. aureus* (MRSA; ATCC 33591) were obtained from the American Type Culture Collection (Manassas, VA). Clinical multidrug resistant strains of *P. aeruginosa* (AR Bank #0239) and *S. aureus* (AR Bank #0565) were obtained from the CDC and FDA Antibiotic Resistant Isolate Bank (Atlanta, GA). Argon (Ar), carbon dioxide (CO_2), nitrogen (N_2), oxygen (O_2), nitric oxide (NO) calibration (25.87 ppm balance N_2), and pure NO (99.5%) gas cylinders were purchased from Airgas National Welders (Raleigh, NC). Distilled water was purified to a resistivity of 18.2 MΩ•cm and a total organic content of ≤ 6 ppb using a Millipore Milli-Q UV Gradient A10 system (Bedford, MA).

3.2.2. Synthesis of alkylamine-modified glycosaminoglycans

Hyaluronic acid (HA6, HA50, and HA90) and chondroitin sulfate (CSA and CSC) were modified with either HEDA, DPTA, or DETA as adapted from previously published protocols.[22,69]

Briefly, HA or CS (1 g) was dissolved in 40 mL distilled water, or in the case of HA90, 100 mL distilled water, with magnetic stirring. A 4:1 molar ratio of EDC and NHS, with respect to the carboxylic acid moieties on the GAG scaffold, was added. In addition, 1 mL of 0.5 M HCl was added to the HA reactions. Following a 20 min activation period at room temperature, a 4:1 molar ratio of HEDA, DPTA, or DETA, with respect to the carboxylic acid moieties on the GAG scaffold, was added to the reaction solution. The solution was then stirred at room temperature for 48 h. Amine-modified GAGs were precipitated in ethanol, collected via centrifugation, washed twice with ethanol, and dried in vacuo yielding a white/yellow solid for each modification.

3.2.3. Characterization of alkylamine-modified glycosaminoglycans

^{1}H and ^{13}C nuclear magnetic resonance (NMR) spectra were recorded on a Bruker (600 MHz) spectrometer (Billerica, MA). Attenuated total reflection Fourier transform infrared spectroscopy (ATR-FTIR) was performed using a Nicolet iS50 FTIR Spectrometer (Thermo Fisher Scientific; Fair Lawn, NJ). Elemental (carbon, hydrogen, nitrogen, sulfur; CHNS) analysis was conducted using a PerkinElmer Elemental Analyzer Series 2400 Instrument (Waltham, MA). Molecular weight determination was performed by first dissolving the unmodified or amine-modified GAGs at 1 mg mL^{-1} in 0.1 M phosphate buffer (pH 7.4) containing 0.1 M sodium nitrate and 0.02 wt% sodium azide. Solutions were filtered using a 0.22 μM PTFE filter and analyzed using an aqueous gel permeation chromatography (GPC) system equipped with a Waters 2414 refractive index detector (Milford, MA) coupled to a Wyatt miniDawn TREOS multi-angle light scattering detector (MALS; Santa Barbara, CA) using the same mobile phase as was used for sample preparation.

Representative ^{1}H and ^{13}C NMR of unmodified and amine-modified GAGs included the following peaks (denoted by D-glucuronic acid (GlcA), *N*-acetyl-D-glucosamine (GlcNAc), and *N*-acetyl-D-galactosamine (GalNAc) residues):

HA6, HA50, and HA90: ^{1}H NMR (600 MHz, D_2O, δ) 2.01 [GlcNAc: NHC(O)CH_3], 3.33 [GlcA C4], 3.45-3.61 [GlcNAc C5, C6], 3.64-3.94 [GlcA C2, C3, C5; GlcNAc C2, C3, C4], 4.46 [GlcA C1], 4.53 [GlcNAc C1]. ^{13}C NMR (600 MHz, D_2O, δ) 22.7 [GlcNAc: NHC(O)CH$_3$], 54.5 [GlcNAc C2], 60.7 [GlcNAc C6], 68.7 [GlcNAc C4], 72.5 [GlcA C2], 73.7 [GlcA C3], 75.2 [GlcA C5], 76.4 [GlcNAc C5], 80.2 [GlcNAc C3], 82.5 [GlcA C4], 100.5 [GlcA C1], 103.2 [GlcNAc C1], 168.0-175.0 [GlcA C6; GlcNAc: NHC(O)CH$_3$].

HA6-HEDA, HA50-HEDA, and HA90-HEDA: ^{1}H NMR (600 MHz, D_2O, δ) 2.01 [GlcNAc: NHC(O)CH_3]; 2.42 [NHCH$_2$CH_2NHCH$_2$CH$_2$OH], 3.06 [NHCH$_2$CH$_2$NHCH_2CH$_2$OH], 3.22 [GlcA C4], 3.29-3.59 [GlcNAc C5, C6; NHCH_2CH$_2$NHCH$_2$CH_2OH], 3.65-3.96 [GlcA C2, C3, C5; GlcNAc C2, C3, C4], 4.45 [GlcA C1], 4.54 [GlcNAc C1]. ^{13}C NMR (600 MHz, D_2O, δ) 22.5 [GlcNAc: NHC(O)CH$_3$], 35.0-36.8 [NHCH$_2$CH$_2$NHCH$_2$CH$_2$OH], 45.3 [NHCH$_2$$CH_2$NHCH$_2CH_2$OH], 49.6 [NHCH$_2CH_2NHCH_2CH_2$OH], 54.4 [GlcNAc C2], 56.6 [NHCH$_2$CH$_2$NHCH$_2$$CH_2$OH], 60.7 [GlcNAc C6], 68.7 [GlcNAc C4], 72.5 [GlcA C2], 73.7 [GlcA C3], 75.2 [GlcA C5], 76.4 [GlcNAc C5], 80.2 [GlcNAc C3], 82.5 [GlcA C4], 100.5 [GlcA C1], 103.2 [GlcNAc C1], 160.5 [GlcA C6], 173.7-175.6 [GlcA C6; GlcNAc: NHC(O)CH$_3$].

HA6-DPTA, HA50-DPTA, and HA50-DPTA: ^{1}H NMR (600 MHz, D_2O, δ) 1.88 [NHCH$_2$CH_2CH$_2$NHCH$_2$CH_2CH$_2$NH$_2$], 2.01 [GlcNAc: NHC(O)CH_3]; 2.42 [NHCH$_2$CH$_2$CH_2NHCH_2CH$_2$CH$_2$NH$_2$], 2.80 [NHCH$_2$CH$_2$CH$_2$NHCH$_2$CH$_2$CH_2NH$_2$], 3.02 [NHCH_2CH$_2$CH$_2$NHCH$_2$CH$_2$CH$_2$NH$_2$], 3.20 [GlcA C4], 3.25-3.57 [GlcNAc C5, C6], 3.67-3.92 [GlcA C2, C3, C5; GlcNAc C2, C3, C4], 4.45 [GlcA C1], 4.54 [GlcNAc C1]. ^{13}C NMR (600 MHz,

D_2O, δ) 22.5 [GlcNAc: NHC(O)CH_3], 24.9-26.9 [$NHCH_2CH_2CH_2NHCH_2CH_2CH_2NH_2$], 35.5-37.5 [$NHCH_2CH_2CH_2NHCH_2CH_2CH_2NH_2$], 45.5 [$NHCH_2CH_2CH_2NHCH_2CH_2CH_2NH_2$], 54.4 [GlcNAc C2], 60.4 [GlcNAc C6], 68.6 [GlcNAc C4], 72.5 [GlcA C2], 73.7 [GlcA C3], 75.2 [GlcA C5], 76.4 [GlcNAc C5], 80.2 [GlcNAc C3], 82.7 [GlcA C4], 100.5 [GlcA C1], 103.2 [GlcNAc C1], 160.8 [GlcA C6], 173.7-175.6 [GlcA C6; GlcNAc: $NHC(O)CH_3$].

HA6-DETA, HA50-DETA, and HA90-DETA: ^{1}H NMR (600 MHz, D_2O, δ) 2.01 [GlcNAc: NHC(O)CH_3]; 2.42 [$NHCH_2CH_2NHCH_2CH_2NH_2$], 2.90 [$NHCH_2CH_2NHCH_2CH_2NH_2$], 3.06 [$NHCH_2CH_2NHCH_2CH_2NH_2$], 3.22 [GlcA C4], 3.29-3.59 [GlcNAc C5, C6], 3.65-3.93 [GlcA C2, C3, C5; GlcNAc C2, C3, C4], 4.45 [GlcA C1], 4.54 [GlcNAc C1]. ^{13}C NMR (600 MHz, D_2O, δ) 22.5 [GlcNAc: NHC(O)CH_3], 35.7 [$NHCH_2CH_2NHCH_2CH_2NH_2$], 39.0 [$NHCH_2CH_2NHCH_2CH_2NH_2$], 45.5 [$NHCH_2CH_2NHCH_2CH_2NH_2$], 54.4 [GlcNAc C2], 57,4 [$NHCH_2CH_2NHCH_2CH_2NH_2$], 60.7 [GlcNAc C6], 68.7 [GlcNAc C4], 72.5 [GlcA C2], 73.7 [GlcA C3], 75.2 [GlcA C5], 76.4 [GlcNAc C5], 80.2 [GlcNAc C3], 82.5 [GlcA C4], 100.5 [GlcA C1], 103.2 [GlcNAc C1], 160.5 [GlcA C6], 173.7-175.6 [GlcA C6; GlcNAc: $NHC(O)CH_3$].

CSA: ^{1}H NMR (600 MHz, D_2O, δ) 2.04 [GalNAc: NHC(O)CH_3], 3.36 [GalNAc C6], 3.57 [GlcA C3], 3.62-3.90 [GlcA C2, C4, C5; GalNAc C5], 4.01 [GalNAc C2, C3], 4.20 [GalNAc C4], 4.46-4.56 [GlcA C1, GalNAc C1]. ^{13}C NMR (600 MHz, D_2O, δ) 22.4 [GalNAc: NHC(O)CH_3], 51.3 [GalNAc C2], 60.9 [GalNAc C6], 69.5 [GalNAc C4], 71.3-80.7 [GlcA C2, C3, C5; GalNAc C3, C5], 96.0 [GlcA C4], 100.7 [GlcA C1], 103.6 [GalNAc C1], 174.3-175.4 [GlcA C6; GalNAc: $NHC(O)CH_3$].

CSA-HEDA: ^{1}H NMR (600 MHz, D_2O, δ) 2.02 [GalNAc: NHC(O)CH_3], 2.43 [$NHCH_2CH_2NHCH_2CH_2OH$], 2.64-3.24 [$NHCH_2CH_2NHCH_2CH_2OH$], 3.34-3.50 [GalNAc C6,

$NHCH_2CH_2NHCH_2C\mathit{H}_2OH$], 3.57 [GlcA C3], 3.67-3.88 [GlcA C2, C4, C5; GalNAc C5], 4.00 [GalNAc C2, C3], 4.19 [GalNAc C4], 4.44-4.57 [GlcA C1, GalNAc C1]. ^{13}C NMR (600 MHz, D_2O, δ) 22.7 [GalNAc: $NHC(O)\mathit{C}H_3$], 36.9 [$NH\mathit{C}H_2CH_2NHCH_2CH_2OH$], 45.7 [$NHCH_2\mathit{C}H_2NHCH_2CH_2OH$], 49.8 [$NHCH_2CH_2NH\mathit{C}H_2CH_2OH$], 51.3 [GalNAc C2], 58.1 [$NHCH_2CH_2NHCH_2\mathit{C}H_2OH$], 60.9 [GalNAc C6], 69.5 [GalNAc C4], 71.3-80.7 [GlcA C2, C3, C5; GalNAc C3, C5], 93.6 [GlcA C4], 100.6 [GlcA C1], 103.9 [GalNAc C1], 160.7 [GlcA C6], 174.3-175.4 [GlcA C6; GalNAc: $NH\mathit{C}(O)CH_3$].

CSA-DPTA: ^1H NMR (600 MHz, D_2O, δ) 1.93 [$NHCH_2C\mathit{H}_2CH_2NHCH_2C\mathit{H}_2CH_2NH_2$], 2.01 [GalNAc: $NHC(O)C\mathit{H}_3$], 2.41 [$NHCH_2CH_2C\mathit{H}_2NHC\mathit{H}_2CH_2CH_2NH_2$], 2.85 [$NHCH_2CH_2CH_2NHCH_2CH_2C\mathit{H}_2NH_2$], 3.04 [$NHC\mathit{H}_2CH_2CH_2NHCH_2CH_2CH_2NH_2$], 3.36 [GalNAc C6], 3.57 [GlcA C3], 3.67-3.88 [GlcA C2, C4, C5; GalNAc C5], 4.00 [GalNAc C2, C3], 4.19 [GalNAc C4], 4.43-4.55 [GlcA C1, GalNAc C1]. ^{13}C NMR (600 MHz, D_2O, δ) 22.7 [GalNAc: $NHC(O)\mathit{C}H_3$], 24.8-26.0 [$NHCH_2\mathit{C}H_2CH_2NHCH_2\mathit{C}H_2CH_2NH_2$], 35.1-37.4 [$NH\mathit{C}H_2CH_2CH_2NHCH_2CH_2\mathit{C}H_2NH_2$], 41.8-45.1 [$NHCH_2CH_2\mathit{C}H_2NH\mathit{C}H_2CH_2CH_2NH_2$], 51.3 [GalNAc C2], 60.9 [GalNAc C6], 69.5 [GalNAc C4], 71.3-80.7 [GlcA C2, C3, C5; GalNAc C3, C5], 96.0 [GlcA C4], 100.6 [GlcA C1], 103.9 [GalNAc C1], 160.4 [GlcA C6], 173.0-174.8 [GlcA C6; GalNAc: $NH\mathit{C}(O)CH_3$].

CSA-DETA: ^1H NMR (600 MHz, D_2O, δ) 2.02 [GalNAc: $NHC(O)C\mathit{H}_3$], 2.43 [$NHCH_2CH_2NHCH_2C\mathit{H}_2NH_2$], 2.76-3.07 [$NHCH_2C\mathit{H}_2NHC\mathit{H}_2CH_2NH_2$], 3.34-3.42 [GalNAc C6, $NHC\mathit{H}_2CH_2NHCH_2CH_2NH_2$], 3.57 [GlcA C3], 3.67-3.85 [GlcA C2, C4, C5; GalNAc C5], 4.00 [GalNAc C2, C3], 4.20 [GalNAc C4], 4.46-4.57 [GlcA C1, GalNAc C1]. ^{13}C NMR (600 MHz, D_2O, δ) 22.7 [GalNAc: $NHC(O)\mathit{C}H_3$], 38.9 [$NH\mathit{C}H_2CH_2NHCH_2CH_2NH_2$], 43.0 [$NHCH_2CH_2NHCH_2\mathit{C}H_2NH_2$], 45.4 [$NHCH_2\mathit{C}H_2NHCH_2CH_2NH_2$], 51.3 [GalNAc C2], 57.4

[$NHCH_2CH_2NHCH_2CH_2NH_2$], 60.9 [GalNAc C6], 69.5 [GalNAc C4], 71.3-80.7 [GlcA C2, C3, C5; GalNAc C3, C5], 96.0 [GlcA C4], 100.9 [GlcA C1], 104.1 [GalNAc C1], 160.6 [GlcA C6], 173.9-175.3 [GlcA C6; GalNAc: $NHC(O)CH_3$].

CSC: ^{1}H NMR (600 MHz, D_2O, δ) 2.03 [GalNAc: $NHC(O)CH_3$], 3.35 [GalNAc C4], 3.49-3.90 [GlcA C2, C3, C4, C5; GalNAc C5], 3.92-4.05 [GalNAc C2, C3], 4.26 [GalNAc C6], 4.47-4.67 [GlcA C1, GalNAc C1]. ^{13}C NMR (600 MHz, D_2O, δ) 22.4 [GalNAc: $NHC(O)CH_3$], 51.6 [GalNAc C2], 61.2 [GalNAc C4], 69.5 [GalNAc C6], 71.0-80.7 [GlcA C2, C3, C5; GalNAc C3, C5], 96.0 [GlcA C4], 100.7 [GlcA C1], 102.2 [GalNAc C1], 171.0-177.2 [GlcA C6; GalNAc: $NHC(O)CH_3$].

CSC-HEDA: ^{1}H NMR (600 MHz, D_2O, δ) 2.02 [GalNAc: $NHC(O)CH_3$], 2.38-2.49 [$NHCH_2CH_2NHCH_2CH_2OH$], 2.96 [$NHCH_2CH_2NHCH_2CH_2OH$], 3.10 [$NHCH_2CH_2NHCH_2CH_2OH$], 3.19 [$NHCH_2CH_2NHCH_2CH_2OH$], 3.35 [GalNAc C4], 3.49-3.90 [GlcA C2, C3, C4, C5; GalNAc C5], 3.92-4.05 [GalNAc C2, C3], 4.26 [GalNAc C6], 4.47-4.67 [GlcA C1, GalNAc C1]. ^{13}C NMR (600 MHz, D_2O, δ) 22.4 [GalNAc: $NHC(O)CH_3$], 34.8-38 [$NHCH_2CH_2NHCH_2CH_2OH$], 45.4 [$NHCH_2CH_2NHCH_2CH_2OH$], 49.5 [$NHCH_2CH_2NHCH_2CH_2OH$], 51.6 [GalNAc C2], 57.5 [$NHCH_2CH_2NHCH_2CH_2OH$], 61.2 [GalNAc C4], 69.5 [GalNAc C6], 71.3-80.7 [GlcA C2, C3, C5; GalNAc C3, C5], 96.0 [GlcA C4], 100.7 [GlcA C1], 102.2 [GalNAc C1], 160.7 [GlcA C6], 171.0-177.2 [GlcA C6; GalNAc: $NHC(O)CH_3$].

CSC-DPTA: ^{1}H NMR (600 MHz, D_2O, δ) 1.80-1.91 [$NHCH_2CH_2CH_2NHCH_2CH_2CH_2NH_2$], 2.02 [GalNAc: $NHC(O)CH_3$], 2.34-2.46 [$NHCH_2CH_2CH_2NHCH_2CH_2CH_2NH_2$], 2.82 [$NHCH_2CH_2CH_2NHCH_2CH_2CH_2NH_2$], 3.03 [$NHCH_2CH_2CH_2NHCH_2CH_2CH_2NH_2$], 3.35 [GalNAc C4], 3.49-3.90 [GlcA C2, C3, C4, C5;

GalNAc C5], 3.92-4.05 [GalNAc C2, C3], 4.26 [GalNAc C6], 4.43-4.60 [GlcA C1, GalNAc C1]. ^{13}C NMR (600 MHz, D_2O, δ) 22.4 [GalNAc: NHC(O)*C*H_3], 24.8-26.0 [NHCH$_2$*C*H$_2$CH$_2$NHCH$_2$*C*H$_2$CH$_2$NH$_2$], 35.0-37.4 [NH*C*H$_2$CH$_2$CH$_2$NHCH$_2$CH$_2$*C*H$_2$NH$_2$], 42.2-45.4 [NHCH$_2$CH$_2$*C*H$_2$NH*C*H$_2$CH$_2$CH$_2$NH$_2$], 51.6 [GalNAc C2], 61.2 [GalNAc C4], 69.5 [GalNAc C6], 71.3-80.7 [GlcA C2, C3, C5; GalNAc C3, C5], 96.0 [GlcA C4], 100.7 [GlcA C1], 102.2 [GalNAc C1], 160.4 [GlcA C6], 172.0-179.2 [GlcA C6; GalNAc: NH*C*(O)CH$_3$].

CSC-DETA: ^{1}H NMR (600 MHz, D_2O, δ) 2.02 [GalNAc: NHC(O)C*H$_3$*], 2.38-2.50 [NHCH$_2$CH$_2$NHCH$_2$C*H$_2$*NH$_2$], 2.89-3.07 [NHCH$_2$C*H$_2$*NHC*H$_2$*CH$_2$NH$_2$], 3.34-3.42 [GalNAc C4, NHC*H$_2$*CH$_2$NHCH$_2$CH$_2$NH$_2$], 3.49-3.90 [GlcA C2, C3, C4, C5; GalNAc C5], 3.92-4.05 [GalNAc C2, C3], 4.26 [GalNAc C6], 4.47-4.67 [GlcA C1, GalNAc C1]. ^{13}C NMR (600 MHz, D_2O, δ) 22.4 [GalNAc: NHC(O)*C*H$_3$], 36.0 [NH*C*H$_2$CH$_2$NHCH$_2$CH$_2$NH$_2$], 38.9 [NHCH$_2$CH$_2$NHCH$_2$*C*H$_2$NH$_2$], 45.7 [NHCH$_2$*C*H$_2$NHCH$_2$CH$_2$NH$_2$], 51.6 [GalNAc C2], 57.5 [NHCH$_2$CH$_2$NH*C*H$_2$CH$_2$NH$_2$], 61.2 [GalNAc C4], 69.5 [GalNAc C6], 71.0-80.7 [GlcA C2, C3, C5; GalNAc C3, C5], 96.0 [GlcA C4], 100.7 [GlcA C1], 102.2 [GalNAc C1], 160.4 [GlcA C6], 172.0-179.2 [GlcA C6; GalNAc: NH*C*(O)CH$_3$].

Representative FTIR spectra of unmodified and amine-modified GAGs included the following peaks:

HA derivatives: $\bar{\nu}_{max}$/cm^{-1} 3320 (O-H), 1650 (C=O, carboxylic acid), 1575 (C=O, amide), 1420 and 1400 (C-H), 1160 and 1050 (C-C).

CSA derivatives: $\bar{\nu}_{max}$/cm^{-1} 3340 (O-H), 1660 (C=O, carboxylic acid), 1580 (C=O, amide), 1430 and 1400 (C-H), 1260 (S=O), 1150 and 1070 (C-C), 860 (C-O-S).

CSC derivatives: $\bar{\nu}_{max}/cm^{-1}$ 3350 (O-H), 1665 (C=O, carboxylic acid), 1590 (C=O, amide), 1430 and 1405 (C-H), 1270 (S=O), 1130 and 1060 (C-C), 890 (C-O-S).

3.2.4. Synthesis of NO-releasing glycosaminoglycans

Alkylamine-modified HA (45 mg) was dissolved in 7:3 methanol:water (3 mL) with sodium methoxide (NaOMe; 75 μL; 5.4 mM in methanol) in a 1-dram glass vial. Alkylamine-modified CS (45 mg) was dissolved in 1:1 methanol:water (3 mL) with 75 μL NaOMe. The open vials were placed in a stainless-steel reaction vessel and stirred continuously via magnetic stirring. The vessel was purged with argon (10 s, 7 atm) three times followed by three longer argon purges (10 min, 7 atm) to remove excess oxygen in the vessel and in the solutions. The vessel was pressurized to 15 atm with NO gas. After 72 h, the same argon purging procedure was followed to remove unreacted NO. The resulting NO-releasing GAGs were precipitated in ethanol, collected by centrifugation, dried in vacuo, and stored in vacuum sealed bags at -20 °C as a white/yellow powder for each modification.

3.2.5. Characterization of NO-release properties

Absorbance measurements (200-450 nm) were made in 50 mM sodium hydroxide (NaOH) with a Molecular Devices SpectraMax M2 spectrophotometer (San Jose, CA) to confirm presence of the *N*-diazeniumdiolate functional group. Real-time nitric oxide release was evaluated using a Sievers 280i Nitric Oxide Analyzer (NOA; Boulder, CO). Before use, samples were analyzed to characterize their NO release and ensure stability of the stored material. The NOA was calibrated with air passed through a NO zero filter (0 ppm NO) and 25.87 ppm of NO calibration gas (balance N_2) prior to analysis. In a typical experiment, NO-releasing GAGs (~1 mg) were dissolved in either

30 mL of deoxygenated PBS (10 mM, pH 7.4, 37 °C) or 30 mL of deoxygenated simulated wound fluid (SWF; 10% FBS in 10 mM PBS, pH 7.4, 37 °C). For samples analyzed in SWF, 75 μL of antifoam B emulsion was added to the flask. The solution was purged with nitrogen gas at a flow rate of 200 mL min^{-1} to carry liberated NO to the instrument. Analysis was terminated when NO levels fell below the quantification limit of the instrument normalized to the mass of NO-releasing material (10 ppb NO mg^{-1} GAG).

3.2.6. In vitro bacterial inhibition assay

Bacteria cultures of PAO1, ATCC MDR-PA, AR-0239, ATCC *S. aureus*, ATCC MRSA, and AR-0565 were grown from frozen (-80 °C) stocks on TSA plates. Colonies were isolated from the TSA plate and resuspended in SWF (Gram-negative) or SWF supplemented with 10% MHB (Gram-positive) at a concentration of 1 x 10^8 CFU mL^{-1}. Bacteria solutions were subsequently diluted to 5 x 10^5 CFU mL^{-1} and exposed to serial dilutions of NO-releasing GAGs (pH adjusted to 7.4 using 1 M HCl), where the highest concentration tested was 16 mg mL^{-1}. The 96-well plate was then incubated at 37 °C for 24 h. Untreated bacteria solutions were included in each experiment to ensure bacteria growth over the 24-h duration. The minimum inhibitory concentration (MIC_{24h}) was defined as the lowest concentration of test agent that prevented visible bacterial growth.

3.2.7. In vitro bacterial eradication assay

Bacteria cultures of PAO1, ATCC MDR-PA, AR-0239, ATCC *S. aureus*, ATCC MRSA, and AR-0565 were grown from frozen (-80 °C) stocks on TSA plates. Colonies were isolated from the TSA plate, resuspended in TSB (5 mL), and incubated at 37 °C overnight with vigorous (250

rpm) shaking. An aliquot (1 mL) of the overnight bacteria solution was added to fresh TSB (30 mL), grown to an OD_{600} of 0.25 for *P. aeruginosa* or 1.25 for *S. aureus* (corresponding to a concentration of 10^8 CFU mL^{-1}), and subsequently diluted 1:100 to 10^6 CFU mL^{-1} in PBS (10 mM, pH 7.4). Weighed samples of NO-releasing GAGs were dissolved in PBS and titrated to pH 7.4 with 1 M HCl. Samples were added to a 96-well polystyrene plate and serially diluted 1:2 in PBS so that each well contained 100 µL of NO-releasing GAG. Bacterial solution containing 10^6 CFU mL^{-1} (100 µL; 1 v/v TSB in PBS) was added to each well, resulting in final GAG concentrations of 0.5-16 mg mL^{-1}. Amine-modified (i.e., non-NO-releasing) GAGs were evaluated at 16 mg mL^{-1} to ensure the GAG backbone was not responsible for bactericidal action. The 96-well plate was then incubated at 37 °C for 4 h with gentle (100 rpm) shaking. Untreated bacteria solutions were included in each experiment to ensure bacteria viability over the 4-h duration. After the 4-h exposure, bacterial solutions were serially diluted (10-, 100-, and 1000-fold dilutions), spiral plated on TSA plates using an Eddy Jet spiral plater (IUL; Farmingdale, NY), and incubated overnight at 37 °C. Viability of bacteria following treatment with amine-modified or NO-releasing GAGs was determined using a Flash & Go colony counter (IUL; Farmingdale, NY). The minimum bactericidal concentration after a 4-h exposure period (MBC_{4h}) was defined as the minimum GAG concentration required to achieve a 3-log reduction (≥ 99.9% reduction) in bacteria viability relative to untreated bacteria (i.e., reduced bacterial counts from 10^6 to 10^3 CFU mL^{-1}). The limit of detection for this counting method is 2.5 x 10^3 CFU mL^{-1}.[71,72]

3.2.8. In vitro cytotoxicity assay

Human dermal fibroblasts (HDF) were grown in DMEM supplemented with 10 vol% FBS and 1 wt% PS. Human epidermal keratinocytes (HEK) were grown in keratinocyte SFM with 1

wt% PS and 5 ng mL^{-1} human recombinant epidermal growth factor (rEGF). Cells were incubated in 5 vol% CO_2 under humidified conditions at 37 °C. After reaching 80% confluency, a cell suspension of 1 x 10^5 cells mL^{-1} was prepared, and 100 µL was added to each well of a 96-well plate. After 24-h incubation at 37 °C, the supernatant was aspirated and replaced with 100 µL of either unmodified, amine-modified, or NO-releasing GAG in fresh growth medium (pH adjusted to 7.4 with 1 M HCl) with GAG concentrations ranging from 0.25 to 32 mg mL^{-1}. The cultures were then incubated for 24 h at 37 °C. Following exposure, the supernatant was aspirated, and the wells were washed twice with PBS. A 100-µL mixture of growth medium/MTS/PMS (105/20/1, v/v/v) was added to each well and incubated for 90 min at 37 °C. The absorbance of the solution in each well was measured at 490 nm using a Molecular Devices SpectraMax M2 spectrophotometer (San Jose, CA). A blank mixture of growth medium/MTS/PMS and untreated cells were used as the blank and control, respectively. Cell viability for each sample was calculated using Eq. 1.

$$\%\ \text{cell viability} = \frac{(\text{Abs}_{490,\text{sample}} - \text{Abs}_{490,\text{blank}})}{(\text{Abs}_{490,\text{control}} - \text{Abs}_{490,\text{blank}})} \times 100 \qquad \text{(Eq. 1)}$$

3.2.9. In vitro adhesion assay

Adhesion assays were carried out using a procedure adapted from Kucik and Wu.[73] Briefly, 96-well plates were coated with 100 µL of 32 µg mL^{-1} bovine collagen type I (10 µg cm^{-1} growth area) in PBS and incubated for 1 h at 37 °C. After 1 h, collagen solution was aspirated from the wells and replaced with 100 µL of 10 mg mL^{-1} BSA in PBS for 1 h at 37 °C. In tandem, 1.5-mL microcentrifuge tubes were coated with BSA using the same procedure at a greater volume (1.5 mL BSA solution). Following incubation, each plate and microcentrifuge tube was rinsed once

with PBS and once with the respective growth medium. Fresh growth medium, either blank or containing unmodified, amine-modified, or NO-releasing GAG, was added to the well plate (100 μL). HDF and HEK were grown under described conditions until 80% confluent. A cell suspension of 1 x 10^5 or 1.5 x 10^5 cells mL^{-1} was prepared for HDF and HEK, respectively. An aliquot of the cell suspension (100 μL) was added to each well, with final GAG concentrations spanning the range of 100 ng mL^{-1} to 100 μg mL^{-1}, and the plate was incubated for 1 h at 37 °C. Simultaneously, a 1-mL aliquot of the cell suspension was transferred to a BSA-coated 1.5-mL microcentrifuge tube. Cells were immediately pelleted at 3800×*g* for 15 min, the supernatant was removed, and the pellet was stored at -20 °C until needed. After 1 h, the 96-well plate was rinsed thrice with PBS to remove non-adhered cells, and a 100 μL mixture of growth medium/MTS/PMS (105/20/1, v/v/v) was added to each well. Growth medium/MTS/PMS solution was added to the empty wells as a blank. Growth medium/MTS/PMS (1 mL) was added to the cell pellet, which was gently vortexed and added to the well plate (100 μL $well^{-1}$) as a measure of the total number of cells initially added to each well. The plate was incubated for 90 min at 37 °C, and the absorbance of the solution in each well was measured at 490 nm using a Molecular Devices SpectraMax M2 spectrophotometer (San Jose, CA). Cell adhesion for each sample was calculated using Eq. 2.

$$\% \text{ cell adhesion} = \frac{(\text{Abs}_{490,\text{adhered}} - \text{Abs}_{490,\text{blank}})}{(\text{Abs}_{490,\text{total}} - \text{Abs}_{490,\text{blank}})} \times 100 \quad \text{(Eq. 2)}$$

3.2.10. In vitro proliferation assay

HDF and HEK were grown under described conditions until 80% confluent. A cell suspension of 3 x 10^4 or 7.5 x 10^4 cells mL^{-1} was prepared for HDF and HEK, respectively. An aliquot of the cell suspension (100 μL) was added to each well of a 96-well plate, and plates were

incubated at 37 °C for 24 h to ensure adhesion. After 24 h, the supernatant was aspirated and replaced with 200 μL of fresh growth medium, either blank or containing unmodified, amine-modified, or NO-releasing GAGs spanning the range of 100 ng mL^{-1} to 100 μg mL^{-1}. Importantly, after the initial 24 h of cell adhesion, growth medium was prepared without either FBS (for HDF) or rEGF (for HEK) to prevent excess unstimulated proliferation. The plate was then incubated for 72 h at 37 °C. Following exposure, the supernatant was aspirated, and the wells were washed twice with PBS. A 100 μL mixture of growth medium/MTS/PMS (105/20/1, v/v/v) was added to each well and incubated for 90 min at 37 °C. The absorbance of the solution in each well was measured at 490 nm using a Molecular Devices SpectraMax M2 spectrophotometer (San Jose, CA). A mixture of growth medium/MTS/PMS without cells and untreated cells were used as the blank and control, respectively. Cell proliferation, relative to untreated cells, was calculated using Eq. 3.

$$\% \text{ relative proliferation} = \frac{(\text{Abs}_{490,\text{sample}} - \text{Abs}_{490,\text{blank}})}{(\text{Abs}_{490,\text{control}} - \text{Abs}_{490,\text{blank}})} \times 100 \quad \text{(Eq. 3)}$$

3.2.11. In vitro inflammation assay

HEK-Blue™ mTLR4 cells were grown in DMEM supplemented with 10 vol% FBS, 1 wt% PS, 100 μg mL^{-1} Normocin™, and 1x HEK-Blue™ Selection. Cells were incubated in 5 vol% CO_2 under humidified conditions at 37 °C. After reaching 80% confluency, a cell suspension of 1.4 x 10^5 cells mL^{-1} was prepared. Fresh media (20 μL), either blank or containing test agent at 10x concentration, was added to wells of a 96-well plate. The cell suspension (180 μL) was added to each well, with a final concentration of cells in each well of 2.5 x 10^4 cells $well^{-1}$. Unmodified, amine-modified, and NO-releasing GAG samples were evaluated at final well concentrations of 100 ng mL^{-1} to 100 μg mL^{-1}. Positive controls included 100 pg mL^{-1} to 100 ng mL^{-1} of LPS and

TNF-α to ensure NF-κB activation and validate the assay. After incubation for 24 h at 37 °C, 20 μL of the supernatant from each well was removed and added to 180 μL QUANTI-Blue™ solution, prepared according to the manufacturer instructions. Plates were incubated for 1 h, and the absorbance of the solution in each well was measured at 630 nm using a Molecular Devices SpectraMax M2 spectrophotometer (San Jose, CA). Blank media and untreated cells were used as the blank and negative control, respectively. The relative concentration of secreted embryonic alkaline phosphatase (SEAP), produced as a result of NF-κB activation, is presented as the OD_{630} corrected for the blank.

HEK-Blue™ Null1-v cells that express endogenous levels of TLR3, TLR5, NOD1, ALPK1, and TIFA but are not transfected with the murine TLR4 receptor gene were used as a control to ensure measured activity was due to interaction with the TLR4 receptor. HEK-Blue™ Null1-v cells were grown in DMEM supplemented with 10 vol% FBS, 1 wt% PS, and 100 μg mL^{-1} Zeocin™ and utilized in the same manner for NF- κB activation experiments as described above.

3.2.12. In vivo murine wound healing model

Female C57B6/Ntac wild-type mice (body weight of ~20 g; 8-weeks old) were purchased from Taconic Farms (Rensselaer, NY). The animal studies were approved and carried out in compliance with the Institutional Animal Care and Use Committee standards. The mice were housed individually with 12-h light-dark cycles. For wounding, mice were anesthetized using gaseous isoflurane, hair was removed from the dorsal region of the mouse using clippers and a depilatory cream, and the skin was prepared for surgery using betadine and 70 vol% ethanol. A sterile 6-mm biopsy punch was used to outline a circular pattern between the shoulders. Forceps

were used to lift the skin, and surgical scissors were used to create a full-thickness wound on each mouse. *P. aeruginosa* (PAO1, 25 μL of 8 x 10^6 CFU mL^{-1}) was pipetted into the wound. For the first study, mice were randomly assigned into 3 treatment groups of 5 mice each and treated with 10 μL of either PEG 400, 100 mg mL^{-1} HA6-HEDA/NO in PEG 400, or 100 mg mL^{-1} CSC-HEDA/NO in PEG 400. For the subsequent study, mice were randomly assigned into 5 treatment groups of 5 mice each and treated with 10 μL of either PEG 400, 100 mg mL^{-1} CSC-HEDA in PEG 400, 100 mg mL^{-1} CSC-HEDA/NO in PEG 400, 100 mg mL^{-1} CSC-DPTA in PEG 400, or 100 mg mL^{-1} CSC-DPTA/NO in PEG 400. Treatment began immediately following wounding and continued once daily for 7 d post-wounding. Throughout the experiment, mice were monitored and received acetaminophen in their drinking water (1.6 mg mL^{-1}) ad libitum. Each day, all wounds were measured in perpendicular directions using calipers for wound area calculations and photographed. Mice were sacrificed on day 8 post-wounding.

3.2.13. In vitro migration assay

HDF and HEK were grown under described conditions until 80% confluent. A cell suspension of 1 x 10^5 cells mL^{-1} was prepared for HDF and HEK. An aliquot of the cell suspension (1000 μL) was added to each well of a 24-well plate, and plates were incubated at 37 °C for 48-72 h or until ~95% confluent. Following the formation of a near-monolayer, cells were scratched in perpendicular directions with a 200-μL sterile pipette tip to simulate wounding, rinsed with PBS to remove detached cells, and treated with either blank media or unmodified, amine-modified, or NO-releasing GAGs (1000 μL of 100 ng mL^{-1} to 100 μg mL^{-1}). Importantly, after the initial 48-72 h of adhesion and growth, growth medium was prepared without either FBS (for HDF) or rEGF (for HEK) to minimize proliferation. Each scratch was imaged in two locations at 0, 4, 8, 12, 24,

and 48 h using an EVOS XL Core Imaging System (Thermo Fisher Scientific; Fair Lawn, NJ). Two technical replicates were averaged at each time point, and n ≥ 3 separate experiments were performed with different populations of cells. Wound area was calculated using ImageJ software (NIH; Bethesda, MD). Remaining wound area was calculated using Eq. 4, where A_{0h} is the initial wound area and A_n is the remaining wound area after *n* hours.

$$\%\ \text{wound remaining} = \frac{A_n}{A_{0h}} \times 100 \qquad \text{(Eq. 4)}$$

3.2.14. Statistical analysis

NO-release and elemental analysis measurements are presented as the average ± standard deviation from n ≥ 3 separate synthesis batches. Bacteria viability, cytotoxicity, cell proliferation, and cell adhesion results are depicted as the average ± standard deviation from n ≥ 3 separate experiments with bacteria/mammalian cells grown on different days. Dose-response curves for mammalian cell viability were plotted using GraphPad Prism 9 software (San Diego, CA). Nonlinear regression (normalized response with variable slope) analysis was performed to determine IC_{50} values. In vivo wound-healing data are presented as the average ± standard deviation from n = 5 separate animals. Significance testing for cell adhesion, proliferation, inflammation, and migration assays was performed via a 2-tailed Student's *t*-test. Significance levels are denoted: *p < 0.05. Statistical analysis of wound closure for the in vivo study was performed using a one-way ANOVA with Tukey's multiple comparisons. Significance levels are denoted: *p < 0.05, **p < 0.01, ***p<0.005.

3.3. Results and Discussion

3.3.1. Modification of glycosaminoglycans with alkylamines

Carbodiimide chemistry was used to graft a series of alkylamines, including *N*-(2-hydroxyethyl)ethylenediamine (HEDA), bis(3-aminopropyl)amine (DPTA), and diethylenetriamine (DETA), onto five GAG backbones (Figure 3.1). Three hyaluronic acid derivatives, HA6 (12.2 kDa, Đ=1.52), HA50 (52.0 kDa, Đ=2.47), and HA90 (95.1 kDa, Đ=1.39), and two chondroitin sulfate derivatives, CSA (29.2 kDa, Đ=1.53) and CSC (17.0 kDa, Đ=2.27), were included to understand the role of molecular weight and sulfation pattern, respectively, on antibacterial and wound healing properties (Table 3.1). Successful incorporation of the alkylamine functional groups was monitored using ^{1}H and ^{13}C NMR spectroscopy (Figures 3.2 and 3.3), FTIR spectroscopy (Figure 3.4), and CHNS elemental analysis (Table 3.2). The addition of a peak at 160 ppm in the ^{13}C NMR spectra indicates the formation of amide bonds, confirming success of the carbodiimide reaction (Figure 3.3). Further, the peak in the carbonyl region of the FTIR spectra (1550-1700 cm^{-1}) demonstrates a marked change in shape, supporting an increase in amide content (~1580 cm^{-1}) (Figure 3.4). Elemental analysis (CHNS) was implemented to assess the extent to which the GAGs were modified with alkylamines. Glycosaminoglycan derivatives increased from 2-4 wt% to 7-18 wt% nitrogen, with CSC derivatives showing the greatest increase in nitrogen content (Table 3.2). Lastly, the range of molecular weights was retained for all derivatives following modification with alkylamines, with each amine-modified derivative possessing similar to or greater than the molecular weight of the unmodified GAG (Table 3.1).

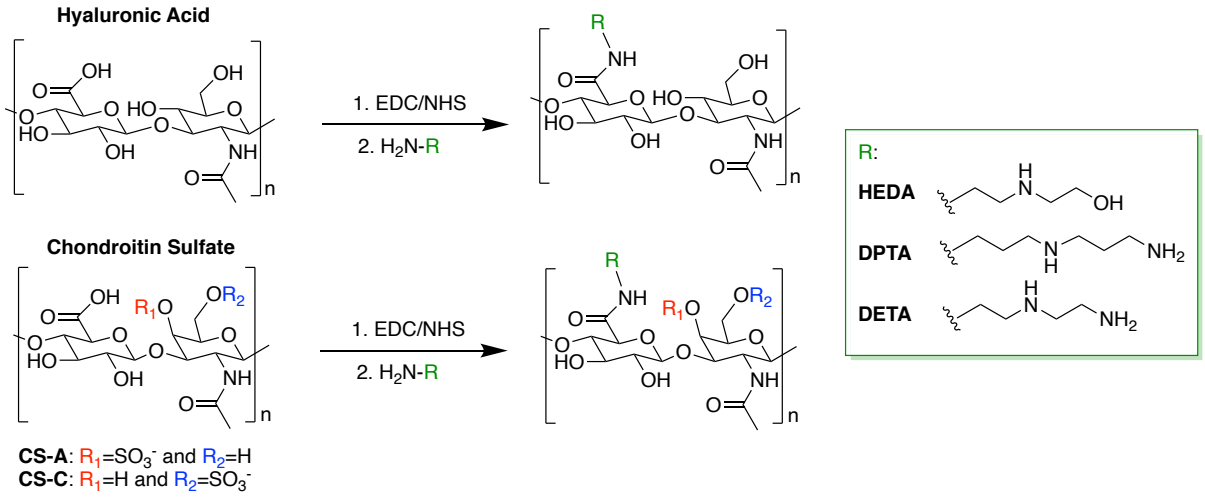

Figure 3.1 Modification of hyaluronic acid and chondroitin sulfate with alkylamines.

Table 3.1 Representative weight-average molecular weights (M_w) and dispersity (Đ) of unmodified and amine-modified hyaluronic acid and chondroitin sulfate.[a]

Modification	M_w (kDa)	Đ
HA6	12.2	1.52
HA50	52.0	2.47
HA90	95.1	1.39
CSA	29.2	1.53
CSC	17.0	1.97
HA6-HEDA	10.7	1.39
HA50-HEDA	59.3	2.55
HA90-HEDA	122.8	2.36
CSA-HEDA	45.7	1.52
CSC-HEDA	22.1	2.27
HA6-DPTA	13.9	1.18
HA50-DPTA	58.9	1.57
HA90-DPTA	95.8	1.62
CSA-DPTA	37.3	1.42
CSC-DPTA	37.5	1.35
HA6-DETA	11.6	1.47
HA50-DETA	47.3	2.16
HA90-DETA	89.7	1.90
CSA-DETA	34.7	1.71
CSC-DETA	50.8	1.21

[a]Determined by GPC-MALS in 0.1 M phosphate buffer (pH 7.4) supplemented with 0.1 M $NaNO_3$ and 0.02 wt% NaN_3.

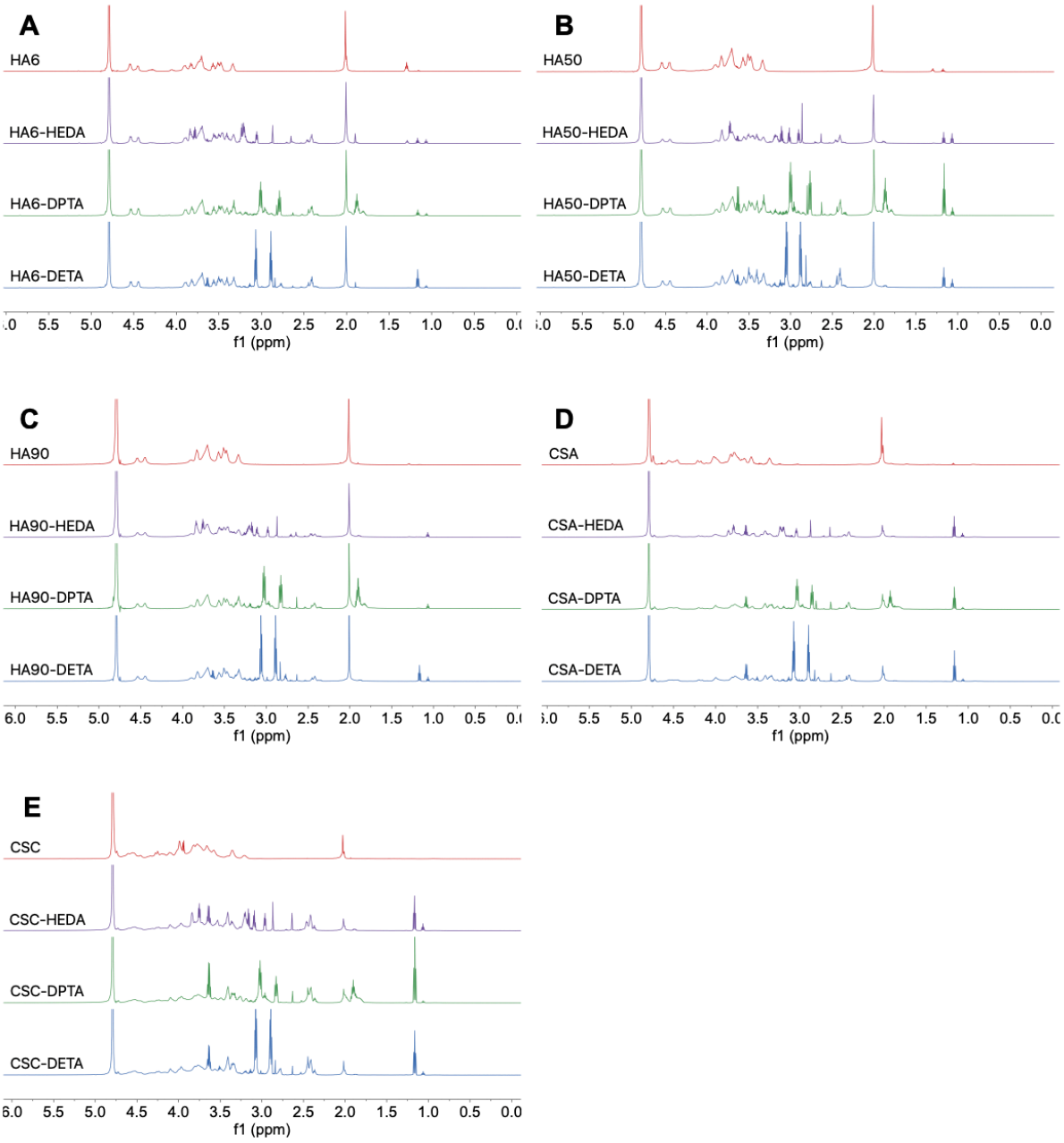

Figure 3.2 Representative ^{1}H NMR (600 MHz, D_2O) of unmodified and amine-modified **(A)** HA6, **(B)** HA50, **(C)** HA90, **(D)** CSA, and **(E)** CSC derivatives.

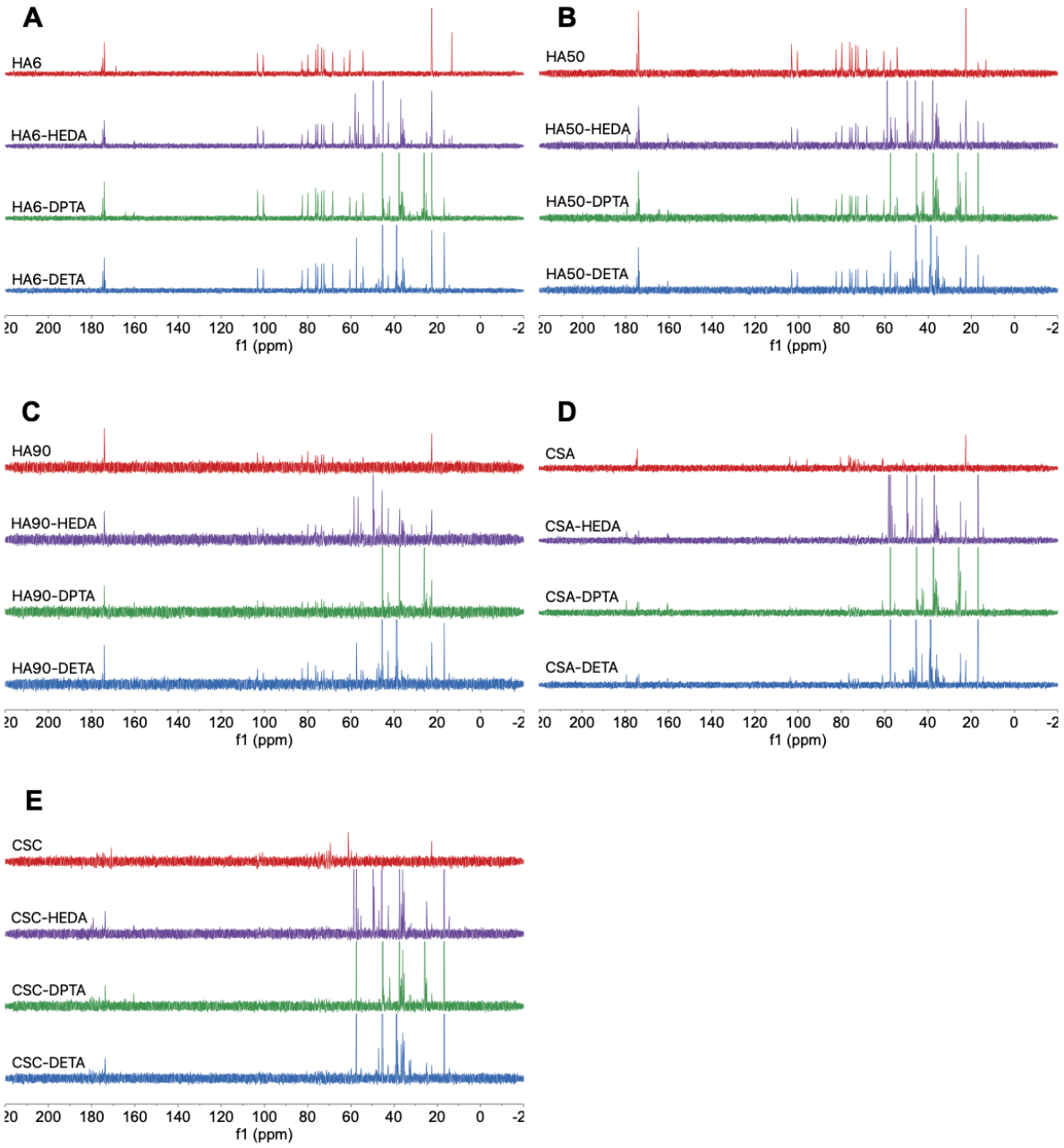

Figure 3.3 Representative ^{13}C NMR (600 MHz, D_2O) of unmodified and amine-modified **(A)** HA6, **(B)** HA50, **(C)** HA90, **(D)** CSA, and **(E)** CSC derivatives.

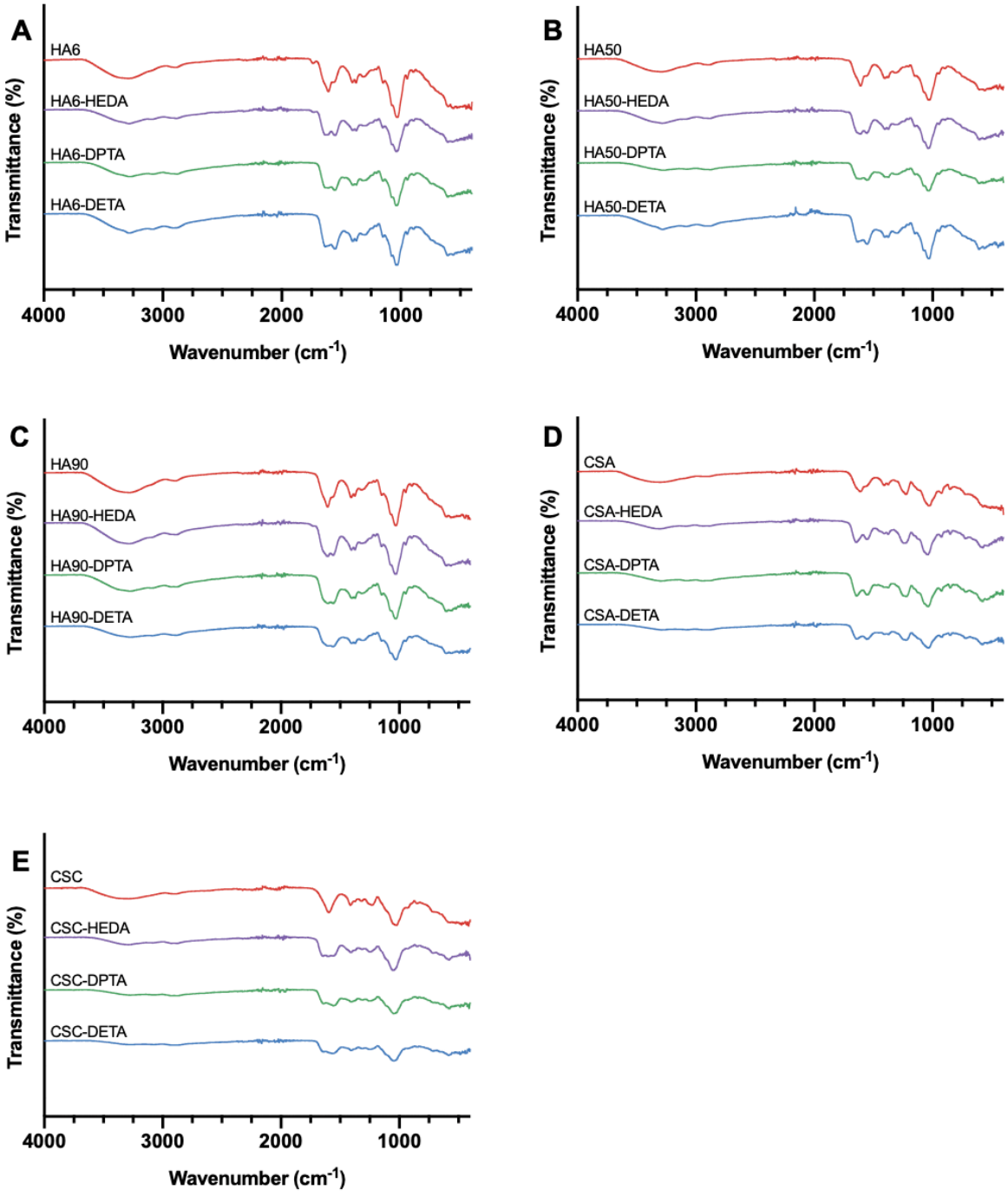

Figure 3.4 Representative FTIR analysis of unmodified and amine-modified **(A)** HA6, **(B)** HA50, **(C)** HA90, **(D)** CSA, and **(E)** CSC derivatives.

Table 3.2 Elemental analysis (CHNS) of unmodified and amine-modified hyaluronic acid and chondroitin sulfate.[a]

Modification	C (%)	H (%)	N (%)	S (%)
HA6	39.2 ± 0.8	6.2 ± 0.3	3.1 ± 0.1	N/A
HA50	37.2 ± 0.1	5.5 ± 0.2	3.0 ± 0.1	N/A
HA90	35.5 ± 1.7	5.9 ± 0.2	2.9 ± 0.1	N/A
CSA	29.0 ± 0.1	4.6 ± 0.1	4.0 ± 0.1	4.3 ± 0.5
CSC	32.9 ± 0.1	5.2 ± 0.1	1.7 ± 0.1	1.3 ± 0.4
HA6-HEDA	40.8 ± 0.9	6.9 ± 0.2	7.8 ± 0.1	N/A
HA50-HEDA	41.4 ± 0.5	6.6 ± 0.1	7.9 ± 0.3	N/A
HA90-HEDA	40.3 ± 0.6	6.7 ± 0.3	7.1 ± 0.1	N/A
CSA-HEDA	35.6 ± 0.4	5.7 ± 0.4	9.5 ± 0.1	3.5 ± 0.1
CSC-HEDA	39.3 ± 0.1	5.9 ± 0.1	12.8 ± 0.9	1.4 ± 0.1
HA6-DPTA	41.6 ± 0.8	7.4 ± 0.1	8.7 ± 0.1	N/A
HA50-DPTA	42.7 ± 1.3	7.6 ± 0.1	9.2 ± 0.1	N/A
HA90-DPTA	40.8 ± 0.3	6.8 ± 0.5	8.1 ± 0.2	N/A
CSA-DPTA	37.3 ± 0.3	6.6 ± 0.2	11.1 ± 0.9	3.4 ± 0.3
CSC-DPTA	40.8 ± 0.2	6.5 ± 0.2	16.3 ± 1.8	1.4 ± 0.2
HA6-DETA	41.4 ± 0.5	7.4 ± 0.2	10.2 ± 0.2	N/A
HA50-DETA	41.6 ± 0.7	7.0 ± 0.3	10.2 ± 0.3	N/A
HA90-DETA	40.5 ± 0.6	7.5 ± 0.2	9.1 ± 0.2	N/A
CSA-DETA	35.9 ± 0.9	6.2 ± 0.1	13.7 ± 2.7	3.3 ± 0.5
CSC-DETA	39.6 ± 0.3	6.5 ± 0.1	17.7 ± 2.2	1.3 ± 0.1

[a]Error represents standard deviation for $n \geq 3$ separate syntheses.

3.3.2. NO-release properties of glycosaminoglycans

The formation of *N*-diazeniumdiolate NO donors was carried out via exposure to high pressures of NO gas under basic conditions. *N*-diazeniumdiolate NO donor formation was confirmed using UV-Vis spectroscopy, with the appearance of a characteristic absorbance peak at 250-255 nm observed for each of the NO-releasing GAG derivatives (Figure 3.5). Of note, no peaks were observed for amine-modified (control) HA scaffolds in this region; however, amine-modified CS derivatives displayed a slight peak at 258-260 nm as a result of the sulfate groups on the backbone. The release of NO from the GAG scaffolds was directly monitored in real-time using a chemiluminescent nitric oxide analyzer (NOA), with each derivative evaluated in both PBS and simulated wound fluid (SWF; 10 vol% FBS in PBS). Nitric oxide payloads ranged from 0.2 to 0.8 μmol NO mg^{-1} GAG in PBS (pH 7.4) depending on the alkylamine modification, HA molecular weight, and CS sulfation pattern (Table 3.3). Glycosaminoglycans modified with DETA exhibit lower NO release payloads than HEDA- and DPTA-modified GAGs, which can be attributed to the stability of the NO donor. It is likely that more NO is released by these DETA-modified biopolymers at levels unmeasurable by the NOA after analysis is terminated. For DPTA- and DETA-modified HA, a slight decrease in NO payload is observed with increasing molecular weight. Greater chain entanglement and viscosity with increasing HA molecular weight may decrease accessibility of NO to the precursor NO donor moiety during the *N*-diazeniumdiolate formation process. Each of the CSC derivatives studied exhibited greater alkylamine functionalization (Table 3.2), and therefore greater NO payloads (Table 3.3), than all the CSA derivatives. This discrepancy between the CS isomers is likely a result of sulfation pattern.

The incorporation of three alkylamine substituents to the GAG backbones confers a range of NO-release kinetics in PBS. Nitric oxide-releasing GAGs modified with HEDA exhibited the

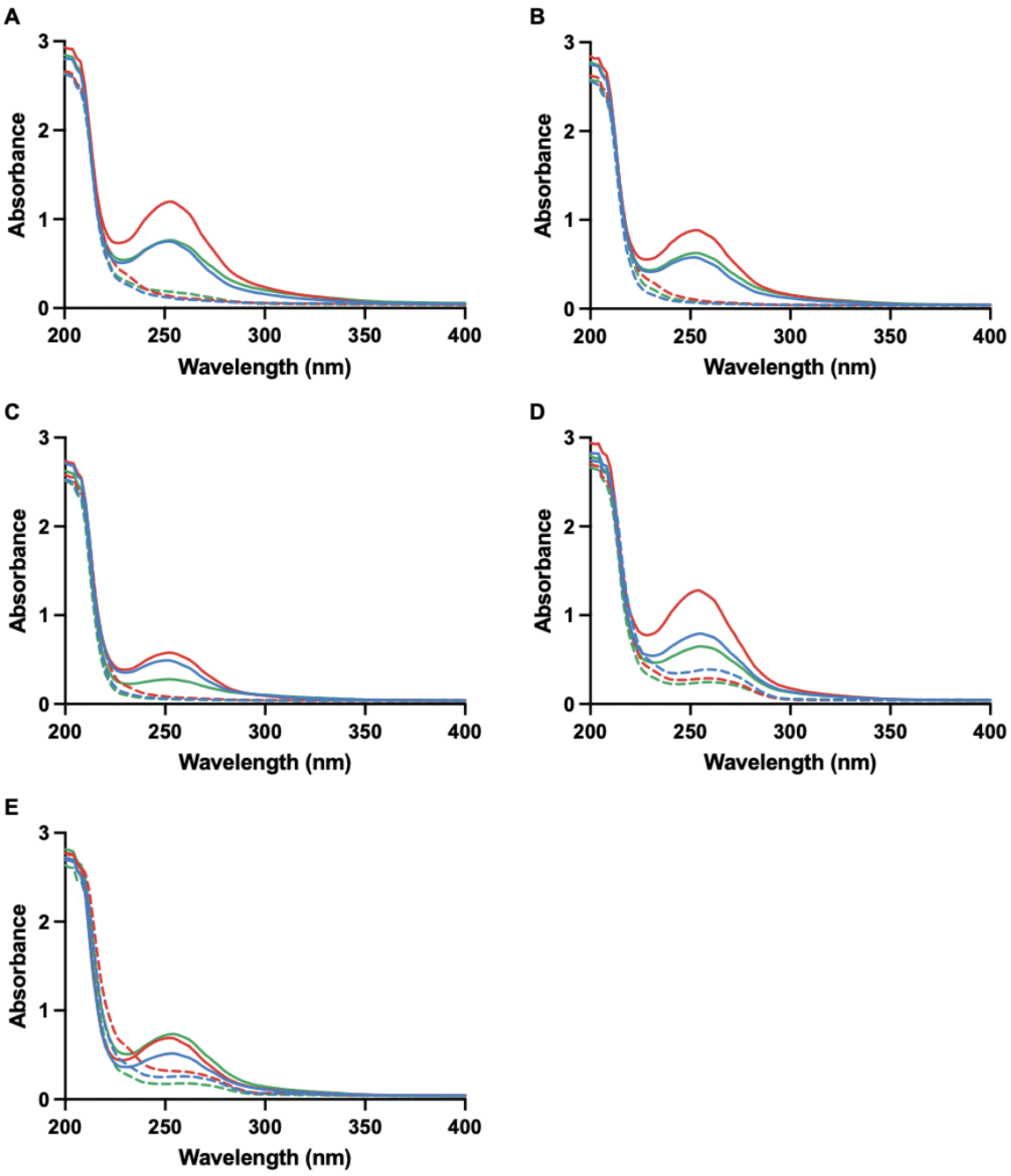

Figure 3.5 Representative UV-Vis spectra of control (- -) and NO-releasing (—) GAG derivatives modified with HEDA (blue), DPTA (red), or DETA (green). Spectra show **(A)** HA6, **(B)** HA50, **(C)** HA90, **(D)** CSA, and **(E)** CSC.

Table 3.3 Nitric oxide-release properties of GAG derivatives in PBS (10 mM, pH 7.4, 37 °C) and simulated wound fluid (10% v/v FBS in PBS, 37 °C).[a]

Modification	Phosphate Buffered Saline		Simulated Wound Fluid	
	$[NO]_t$ (μmol mg^{-1})[b]	$t_{1/2}$ (min)[c]	$[NO]_t$ (μmol mg^{-1})[b]	$t_{1/2}$ (min)[c]
HA6-HEDA/NO	0.45 ± 0.01	19 ± 2	0.40 ± 0.04	39 ± 17
HA50-HEDA/NO	0.34 ± 0.03	19 ± 1	0.34 ± 0.05	26 ± 6
HA90-HEDA/NO	0.42 ± 0.07	22 ± 3	0.39 ± 0.04	53 ± 13
CSA-HEDA/NO	0.31 ± 0.01	16 ± 1	0.22 ± 0.02	24 ± 3
CSC-HEDA/NO	0.46 ± 0.15	14 ± 1	0.38 ± 0.11	18 ± 4
HA6-DPTA/NO	0.51 ± 0.10	25 ± 2	0.51 ± 0.10	46 ± 11
HA50-DPTA/NO	0.46 ± 0.05	29 ± 6	0.43 ± 0.05	37 ± 6
HA90-DPTA/NO	0.35 ± 0.08	34 ± 5	0.34 ± 0.03	62 ± 16
CSA-DPTA/NO	0.48 ± 0.08	19 ± 1	0.42 ± 0.01	24 ± 6
CSC-DPTA/NO	0.78 ± 0.08	16 ± 3	0.91 ± 0.04	20 ± 4
HA6-DETA/NO	0.31 ± 0.01	60 ± 2	0.31 ± 0.05	84 ± 2
HA50-DETA/NO	0.28 ± 0.03	66 ± 20	0.27 ± 0.06	89 ± 3
HA90-DETA/NO	0.27 ± 0.03	75 ± 13	0.24 ± 0.02	76 ± 13
CSA-DETA/NO	0.26 ± 0.03	51 ± 6	0.22 ± 0.04	67 ± 13
CSC-DETA/NO	0.30 ± 0.07	88 ± 7	0.31 ± 0.11	108 ± 8

[a]Error represents the standard deviation of $n \geq 3$ separate syntheses. [b]Total NO released over release duration. [c]Half-life of NO release.

shortest half-lives and durations in PBS (Tables 3.3 and 3.4), owing to the reduced stabilization of the *N*-diazeniumdiolate moiety by the terminal hydroxyl group. Increased NO donor stabilization, and thus extended NO-release durations, were observed with the primary amine-terminated derivatives, DPTA and DETA. However, DETA resulted in even longer NO release as compared to DPTA (e.g., 8.1 ± 0.7 vs. 12.2 ± 0.4 h durations for HA6-DPTA/NO and HA6-DETA/NO, respectively), suggesting that the ethyl spacing between the NO donor-containing secondary amine and positively charged tertiary amine of DETA facilitates better stabilization than the propyl spacing of DPTA.

The kinetics of NO release changed when analyzed in SWF versus PBS. For all derivatives, the maximum instantaneous concentration of NO release was less in SWF compared to PBS (Table 3.4). As a result, the half-lives of NO release are extended for the majority of the GAG derivatives (Table 3.3). The components of FBS (e.g., glucose, proteins, enzymes, counterions) within SWF are expected to affect stabilization of the *N*-diazeniumdiolate NO donor, altering the kinetics of NO release. However, the majority of NO payloads were retained when evaluated in SWF as compared to PBS, indicating negligible scavenging from the protein components in FBS. As a result, NO totals should not be substantially altered when used in a wound environment even if there are 10-60% changes to the maximum flux and duration of NO release.

3.3.3. In vitro inhibitory and eradication activity against common wound pathogens

In developing a new chronic wound therapy, it is necessary to consider the antibacterial activity of the proposed material. Multiple isolates of *Pseudomonas aeruginosa* and *Staphylococcus aureus* were thus evaluated for both inhibition and eradication following treatment with NO-releasing GAGs. Three strains of each species were chosen to encompass a range of

Table 3.4 Nitric oxide-release properties of GAG derivatives in PBS (10 mM, pH 7.4, 37 °C) and simulated wound fluid (10% v/v FBS in PBS, 37 °C).[a]

Modification	Phosphate Buffered Saline		Simulated Wound Fluid	
	$[NO]_{max}$ (ppb mg^{-1})[b]	t_d (h)[c]	$[NO]_{max}$ (ppb mg^{-1})[b]	t_d (h)[c]
HA6-HEDA/NO	2270 ± 390	5.7 ± 1.4	1200 ± 360	7.6 ± 1.2
HA50-HEDA/NO	1460 ± 90	4.7 ± 0.3	940 ± 280	4.3 ± 0.4
HA90-HEDA/NO	1440 ± 310	5.5 ± 0.8	660 ± 170	7.5 ± 1.9
CSA-HEDA/NO	1600 ± 130	4.6 ± 0.3	610 ± 50	3.0 ± 0.5
CSC-HEDA/NO	2400 ± 980	3.5 ± 0.4	1600 ± 610	2.9 ± 0.8
HA6-DPTA/NO	2440 ± 580	8.1 ± 0.7	1290 ± 100	12.0 ± 1.6
HA50-DPTA/NO	1640 ± 480	7.2 ± 0.5	1120 ± 100	8.3 ± 1.3
HA90-DPTA/NO	1090 ± 240	6.9 ± 1.4	620 ± 40	10.7 ± 3.3
CSA-DPTA/NO	2560 ± 590	6.5 ± 0.6	1520 ± 310	5.4 ± 0.1
CSC-DPTA/NO	4450 ± 890	5.2 ± 0.6	3740 ± 590	6.0 ± 0.3
HA6-DETA/NO	1490 ± 340	12.2 ± 0.4	910 ± 190	13.3 ± 1.8
HA50-DETA/NO	1300 ± 330	11.6 ± 0.6	680 ± 210	12.2 ± 1.2
HA90-DETA/NO	1000 ± 360	12.3 ± 1.2	670 ± 30	11.5 ± 1.6
CSA-DETA/NO	1090 ± 270	9.8 ± 0.7	600 ± 100	9.5 ± 1.3
CSC-DETA/NO	670 ± 350	11.6 ± 0.9	510 ± 240	12.8 ± 2.6

[a]Error represents the standard deviation of $n \geq 3$ separate syntheses. [b]Maximum instantaneous NO concentration. [c]Duration of NO release.

antibiotic-resistance profiles, including two susceptible strains (PAO1 and ATCC *S. aureus*), two ATCC resistant strains (ATCC MDR-PA and ATCC MRSA), and two multidrug-resistant clinical isolates provided by the Centers for Disease Control (AR-0239 and AR-0565). Of note, *P. aeruginosa* strain AR-0239 and *S. aureus* strain AR-0565 are reported to be resistant to ≥ 15 and ≥10 common antibiotics, respectively. The use of these multidrug-resistant strains facilitates an evaluation of the NO-releasing GAGs on several acquired resistance mechanisms.

The inhibitory action of the NO-releasing GAG derivatives was first evaluated against the six wound pathogens. Bacteria were treated with NO-releasing GAGs in simulated wound fluid to determine the minimum inhibitory concentration, or MIC_{24h}, defined as the concentration of GAG required to prevent visible bacterial growth over 24 h. In evaluating the Gram-negative *P. aeruginosa* strains (i.e., PAO1, ATCC MDR-PA, and AR-0239), DETA-modified NO-releasing GAGs proved the most effective at preventing bacterial growth for each strain compared to the HEDA- and DPTA-modified derivatives (Table 3.5). The efficacy of this inhibition trended with NO-release duration. Derivatives with the shortest NO-releasing lifetime, HEDA-modified GAGs, required the largest concentrations of GAGs to inhibit *P. aeruginosa* growth. Derivatives with intermediate NO-release durations and half-lives (i.e., DPTA-modified GAGs) required intermediate GAG concentrations to inhibit bacterial growth (4-16 mg mL^{-1}). The sustained release of DETA-modified derivatives (9-13 h in SWF) was more effective in preventing bacterial growth over a 24-h experiment duration. Increased NO-releasing DETA-modified GAG concentrations were necessary to prevent bacterial growth in ATCC MDR-PA and AR-0239 in comparison to PAO1, suggesting that the resistance mechanisms adopted by the bacteria, such as the production of mucoid exopolysaccharide capsule,[74] may facilitate decreased permeability of NO through the bacterial cell membrane. However, these same strain differences were not observed for HEDA-

Table 3.5 Minimum inhibitory concentrations (MIC_{24h}) of NO-releasing glycosaminoglycan derivatives against antibiotic susceptible and drug-resistant strains of common wound pathogens in simulated wound fluid (10% v/v SWF in PBS)[a] following 24-h exposure.[b]

Modification	MIC_{24h} (mg mL^{-1})					
	PAO1	ATCC MDR-PA	AR-0239	ATCC *S. aureus*	ATCC MRSA	AR-0565
HA6-HEDA/NO	8	16	16	4	2	2
HA50-HEDA/NO	16	16	16	4	4	4
HA90-HEDA/NO	>16	16	4	2	2	2
CSA-HEDA/NO	16	>16	16	4	4	4
CSC-HEDA/NO	8	16	16	4	4	4
HA6-DPTA/NO	8	8	8	2	2	1
HA50-DPTA/NO	8	8	4	2	2	1
HA90-DPTA/NO	8	16	4	2	1	2
CSA-DPTA/NO	8	16	8	2	4	2
CSC-DPTA/NO	8	8	8	2	2	2
HA6-DETA/NO	1	4	4	2	2	2
HA50-DETA/NO	1	4	4	4	2	1
HA90-DETA/NO	2	8	2	2	1	2
CSA-DETA/NO	2	4	4	4	4	4
CSC-DETA/NO	1	4	8	2	2	1

[a]SWF was supplemented with 10% v/v Mueller-Hinton II broth for *S. aureus* strains. [b]MIC_{24h} values were determined from $n \geq 3$ separate experiments.

and DPTA-modified GAGs. Of note, NO-releasing DETA-modified GAGs were still able to inhibit all pathogens at concentrations ≤ 8 mg mL^{-1}. In contrast to the Gram-negative pathogens, Gram-positive *S. aureus* strains (i.e., ATCC *S. aureus*, ATCC MRSA, and AR-0565) were equally inhibited by all GAG derivatives, with each strain requiring 1-4 mg mL^{-1} of NO-releasing GAG to inhibit bacterial growth over 24 h (Table 3.5), indicating that even short-term NO release (3-8 h with HEDA-modified derivatives) is sufficient to inhibit the growth of *S. aureus* derivatives during the experimental timeframe. Negligible differences in MIC_{24h} were observed across the three *S. aureus* strains, which varied in resistance profile, indicating that the resistance mechanisms adopted by ATCC MRSA and AR-0565 do not affect the ability of NO to inhibit growth.

In addition to inhibition, bactericidal properties are expected for NO-based therapeutics owing to NO's antibacterial mechanisms (e.g., lipid peroxidation). Bacteria were treated with a range of NO-releasing GAG concentrations under static conditions to determine the minimum bactericidal concentration, or MBC_{4h}, defined as the concentration of GAG required to reduce bacterial viability by 3-log (i.e., >99.9%) over 4 h. While inhibition is beneficial over long-term exposures (i.e., 24 h), more rapid eradication is advantageous, as prior to eradication, bacteria will continue to replicate. As such, a 4-h exposure window was chosen to evaluate bactericidal properties. For all six bacteria strains, the NO-releasing DPTA-modified GAG derivatives were most effective at eradicating bacteria, requiring only 1-4 mg mL^{-1} of the NO-releasing GAG for a 3-log reduction (Figures 3.6-3.8, Table 3.6). Greater concentrations of the HEDA- and DETA-modified NO-releasing GAG derivatives were required for *P. aeruginosa* and *S. aureus*, with the exception of HA6-HEDA/NO (Table 3.6). In comparing the molecular weights of HA, the 6 kDa HA was more effective than the 50 or 90 kDa derivatives, especially for AR-0239 and AR-0565 (Figure 3.8), indicating that the lower molecular weight provides a beneficial property in faster

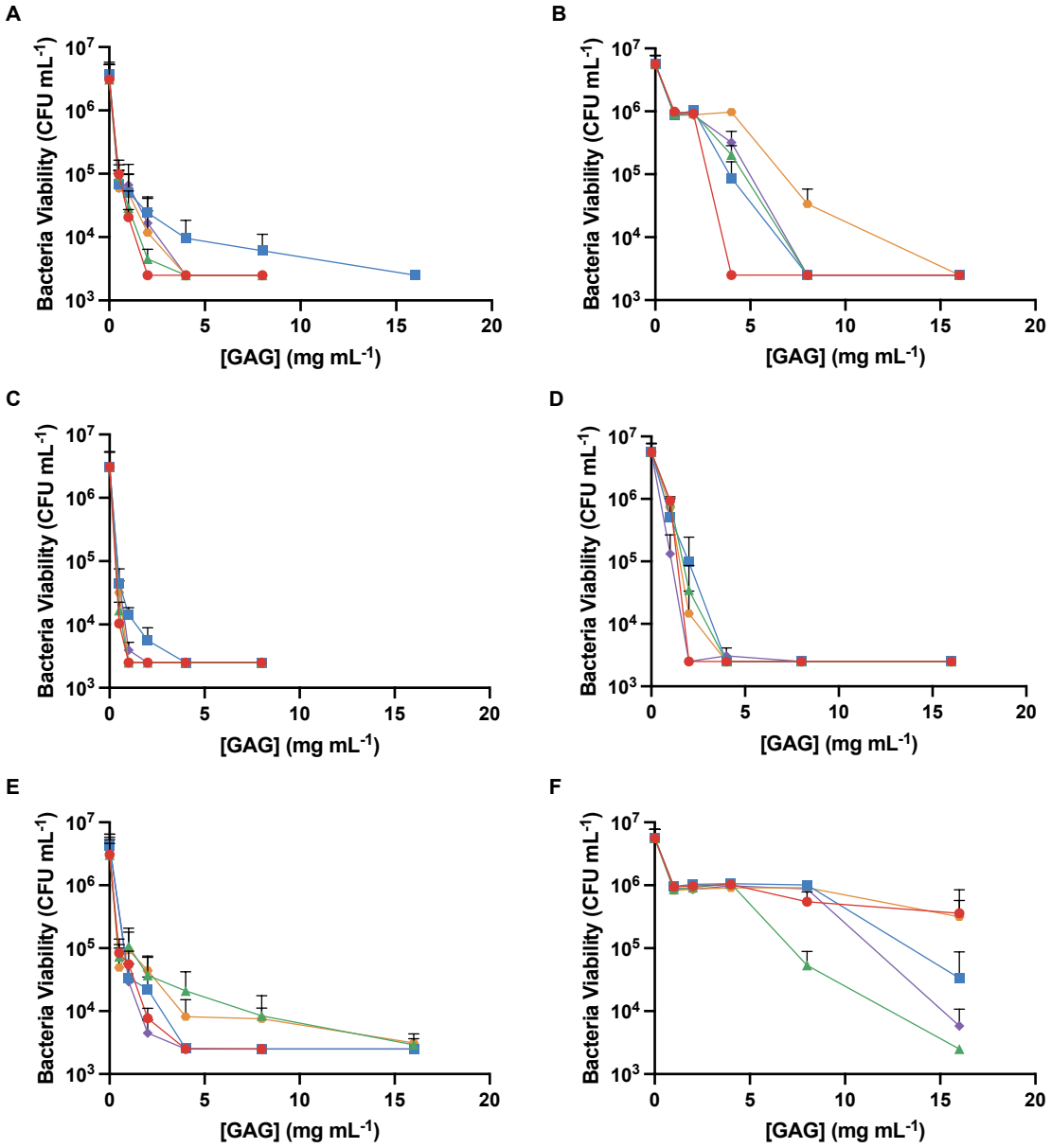

Figure 3.6 Antibacterial efficacy of NO-releasing GAG derivatives against **(A, C, E)** PAO1 and **(B, D, F)** ATCC *S. aureus*. Modifications of HA6 (red circle), HA50 (green triangle), HA90 (blue square), CSA (orange hexagon), and CSC (purple diamond) include **(A-B)** HEDA, **(C-D)** DPTA, and **(E-F)** DETA. Error bars represent the standard deviation for n ≥ 3 separate experiments.

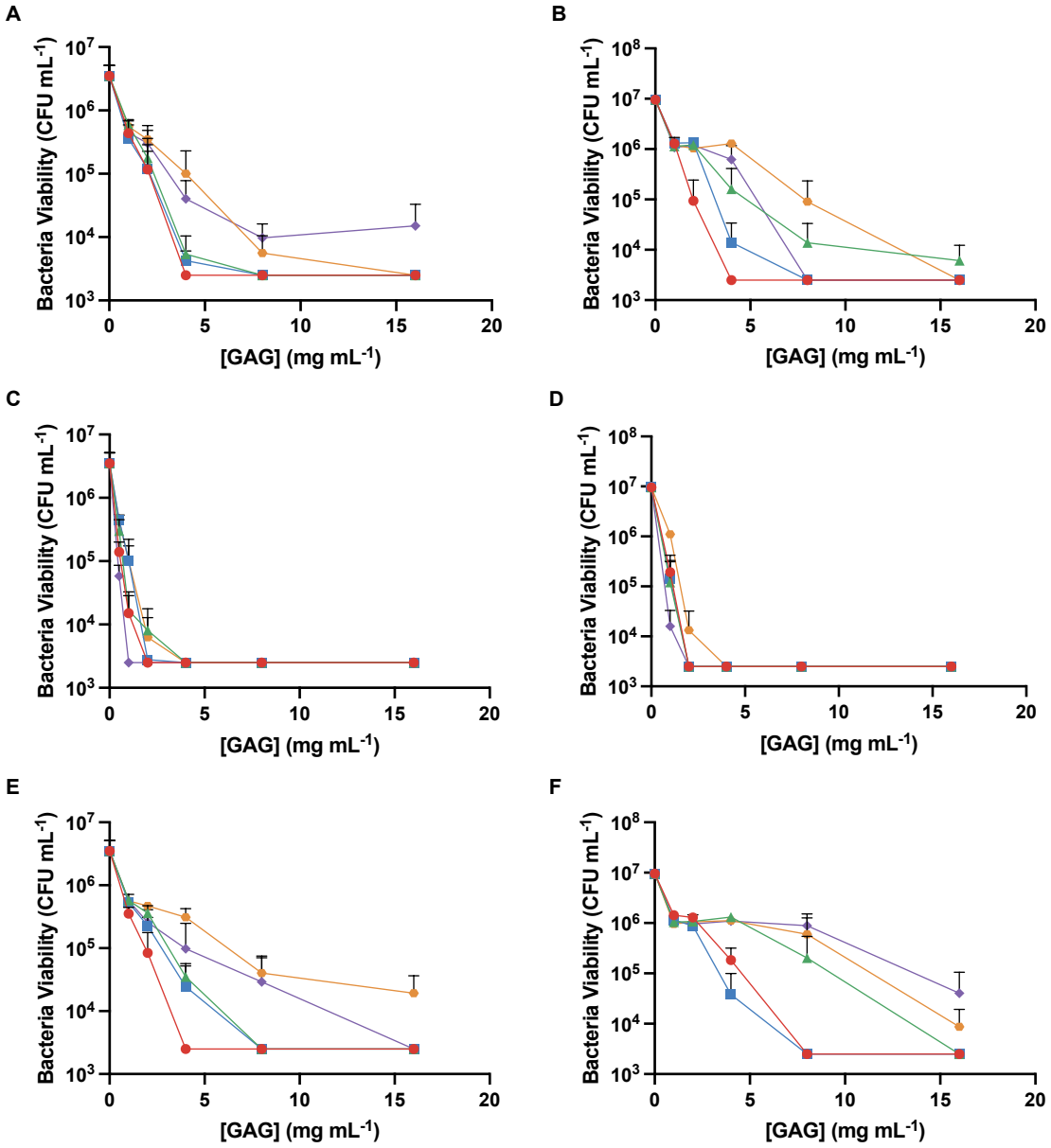

Figure 3.7 Antibacterial efficacy of NO-releasing GAG derivatives against **(A, C, E)** ATCC MDR-PA and **(B, D, F)** ATCC MRSA. Modifications of HA6 (red circle), HA50 (green triangle), HA90 (blue square), CSA (orange hexagon), and CSC (purple diamond) include **(A-B)** HEDA, **(C-D)** DPTA, and **(E-F)** DETA. Error bars represent the standard deviation for n ≥ 3 separate experiments.

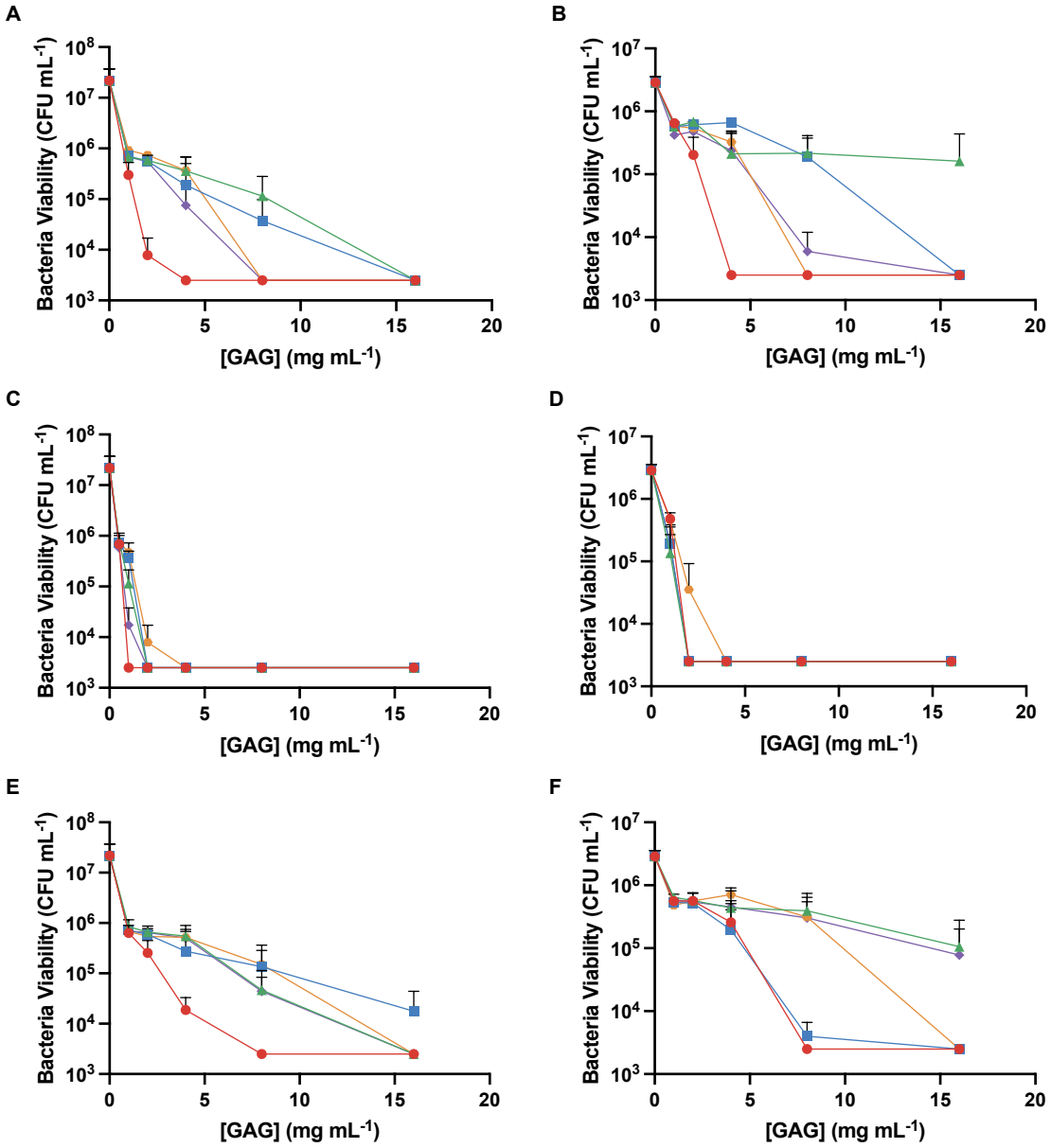

Figure 3.8 Antibacterial efficacy of NO-releasing GAG derivatives against CDC multidrug resistant isolates **(A, C, E)** AR-0239 and **(B, D, F)** AR-0565. Modifications of HA6 (red circle), HA50 (green triangle), HA90 (blue square), CSA (orange hexagon), and CSC (purple diamond) include **(A-B)** HEDA, **(C-D)** DPTA, and **(E-F)** DETA. Error bars represent the standard deviation for $n \geq 3$ separate experiments.

Table 3.6 Minimum bactericidal concentrations (MBC_{4h}) of NO-releasing glycosaminoglycan derivatives against antibiotic susceptible and drug-resistant strains of common wound pathogens in PBS following 4-h exposure.[a]

Modification	MBC_{4h} (mg mL^{-1})					
	PAO1	ATCC MDR-PA	AR-0239	ATCC *S. aureus*	ATCC MRSA	AR-0565
HA6-HEDA/NO	2	4	2	4	4	4
HA50-HEDA/NO	4	8	16	8	16	>16
HA90-HEDA/NO	16	8	16	8	8	16
CSA-HEDA/NO	4	16	8	16	16	8
CSC-HEDA/NO	4	>16	8	8	8	16
HA6-DPTA/NO	1	2	1	2	2	2
HA50-DPTA/NO	1	4	2	4	2	2
HA90-DPTA/NO	4	2	2	4	2	2
CSA-DPTA/NO	1	4	2	4	4	4
CSC-DPTA/NO	2	1	2	2	2	2
HA6-DETA/NO	4	4	4	>16	8	8
HA50-DETA/NO	16	8	16	16	16	>16
HA90-DETA/NO	4	8	16	>16	8	16
CSA-DETA/NO	16	>16	16	>16	16	16
CSC-DETA/NO	4	16	16	>16	>16	>16

[a]MBC_{4h} values were determined from $n \geq 3$ separate experiments.

diffusion to the bacteria and/or increased bacterial localization for NO delivery. We previously reported the benefits of 6 kDa NO-releasing HA for eradicating biofilm-based *P. aeruginosa* over 90 kDa NO-releasing HA as a result of more rapid diffusion through the EPS matrix.[22] This beneficial property may also translate to planktonic bacteria cultures. Significant differences in bactericidal activity were not observed between the two CS derivatives, which varied in sulfation pattern.

To confirm that NO was responsible for bactericidal activity rather than the biopolymer backbone, amine-modified GAGs (without NO) were evaluated against all six bacteria strains at 16 mg mL^{-1} (Figure 3.9). Negligible differences were observed for the three *S. aureus* strains (ATCC *S. aureus*, ATCC MRSA, and AR-0565), indicating that neither the GAG backbone nor amine modification were responsible for bactericidal activity (Figure 3.9B, D, and F). For the *P. aeruginosa* derivatives, negligible decreases in bacteria viability were observed for HEDA-modified GAGs. However, a subset of the DPTA- and DETA-modified derivatives resulted in slight decreases in bacteria viability. For example, treatment with CSC-DETA resulted in a 0.89-log reduction in PAO1 viability (Figure 3.9A). Treatment with HA50-DPTA resulted in 1.12- and 0.79-log reductions in ATCC MDR-PA and AR-0239 viabilities, respectively (Figures 3.9C and E). However, this activity was significantly lower than the 3-log reduction threshold considered to be bactericidal, implicating NO as the bactericidal agent.

3.3.4. In vitro cytotoxicity against human skin cells

While antibacterial activity is a primary goal, minimizing off-target toxicity to mammalian cells is equally important. In vitro cytotoxicity assays were performed using human dermal fibroblasts (HDFs) and human epidermal keratinocytes (HEKs) as representative cell types in the

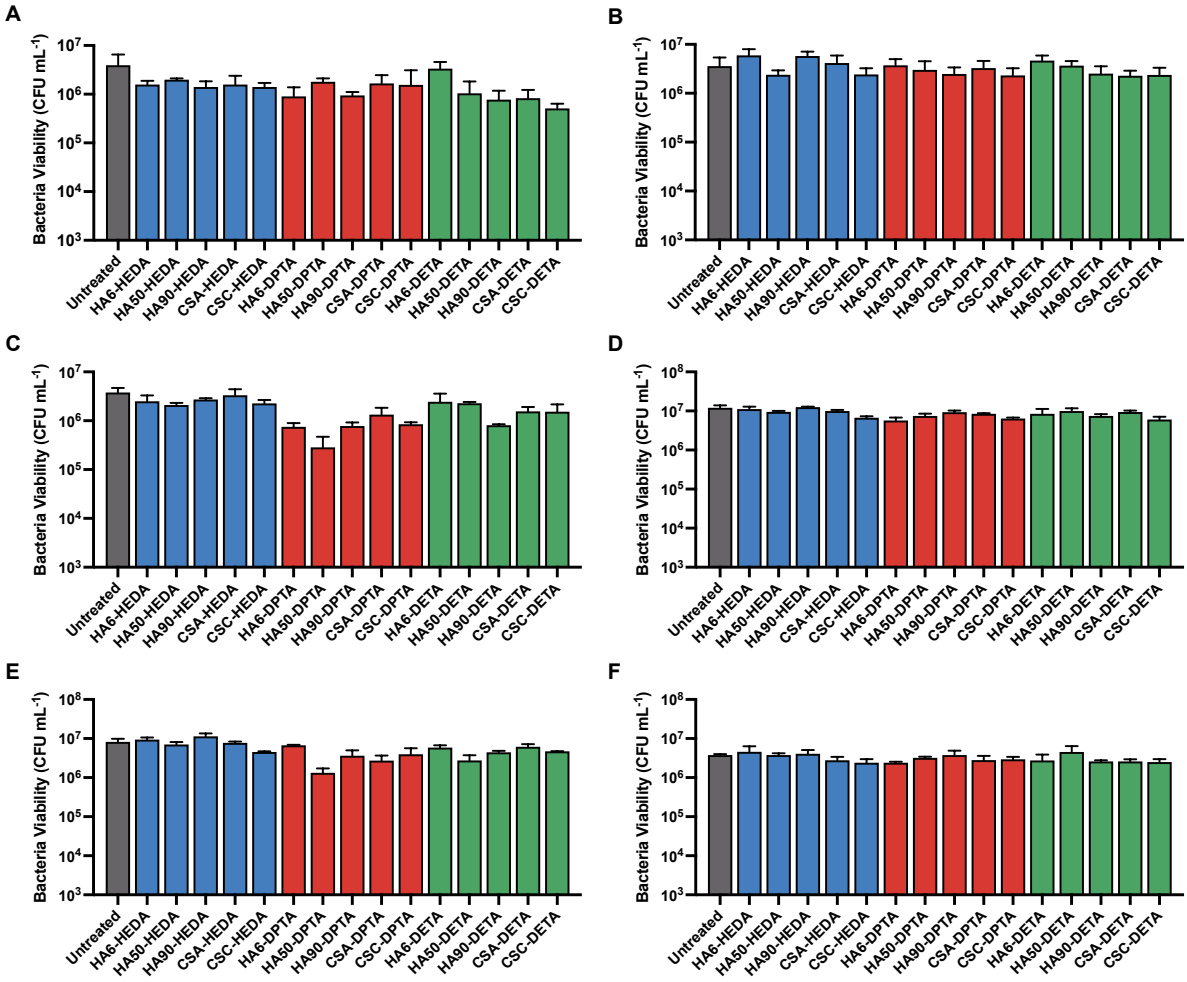

Figure 3.9 Colonies of **(A)** PAO1, **(B)** ATCC *S. aureus*, **(C)** ATCC MDR-PA, **(D)** ATCC MRSA, **(E)** AR-0239, and **(F)** AR-0565 remaining after 4-h treatment with amine-modified GAGs (without NO). All modifications were evaluated at 16 mg mL^{-1}. Error bars represent the standard deviation for $n \geq 3$ separate experiments.

wound environment. Glycosaminoglycans are endogenously found and thus expected to exhibit little-to-no toxicity; however, the effects of amine-modification and NO-loading on resulting toxicity to these cell types must still be considered. Fibroblasts and keratinocytes were dosed with a range of concentrations of unmodified GAGs, amine-modified GAGs, or NO-releasing GAGs to determine the IC_{50} for each material, which is defined as the concentration of GAG that reduces the metabolic activity of the cells by 50% (Figures 3.10-3.12). In addition to allowing for toxicity comparisons between the derivatives, the IC_{50} values help inform the upper limit for GAG concentrations utilized in further in vitro cell assays.

As expected, unmodified GAG derivatives did not impact HDF cell viability at concentrations up to 32 mg mL^{-1} (Figure 3.10A and B). However, a decrease in viability was found for HEKs upon treatment with 16-32 mg mL^{-1} of unmodified HA scaffolds (60-80% activity) or unmodified CS scaffolds (40-80% activity), indicating that the HEKs are more susceptible to these materials than HDFs (Figure 3.10C and D). The amine-modified and NO-releasing GAG derivatives would thus be expected to have greater toxicity to HEKs than HDFs. Indeed, this toxicity is reflected in the resulting IC_{50} values from the dose-response curves (Figures 3.11-3.13). When evaluating HDFs (Figure 3.11), both control HEDA- and DETA-modified GAGs (without NO) maintain ≥90% cell metabolic activity at concentrations up to 32 mg mL^{-1}, indicating that alkylamine modifications do not markedly change the toxicity profile at evaluated concentrations. A decrease in metabolic activity was observed for the same derivatives evaluated against HEKs at 16-32 mg mL^{-1} (Figure 3.12). For both cell types, DPTA modification led to greater cell toxicity, with IC_{50} values of 6-10 mg mL^{-1} and 2-5 mg mL^{-1} (excluding CSC-DPTA) for HDFs and HEKs, respectively (Figure 3.13). CSC-DPTA was the only DPTA-modified GAG derivative to exhibit an IC_{50} against HEK in line with the other alkylamine modifications (IC_{50} of 22 ± 8 mg mL^{-1}).

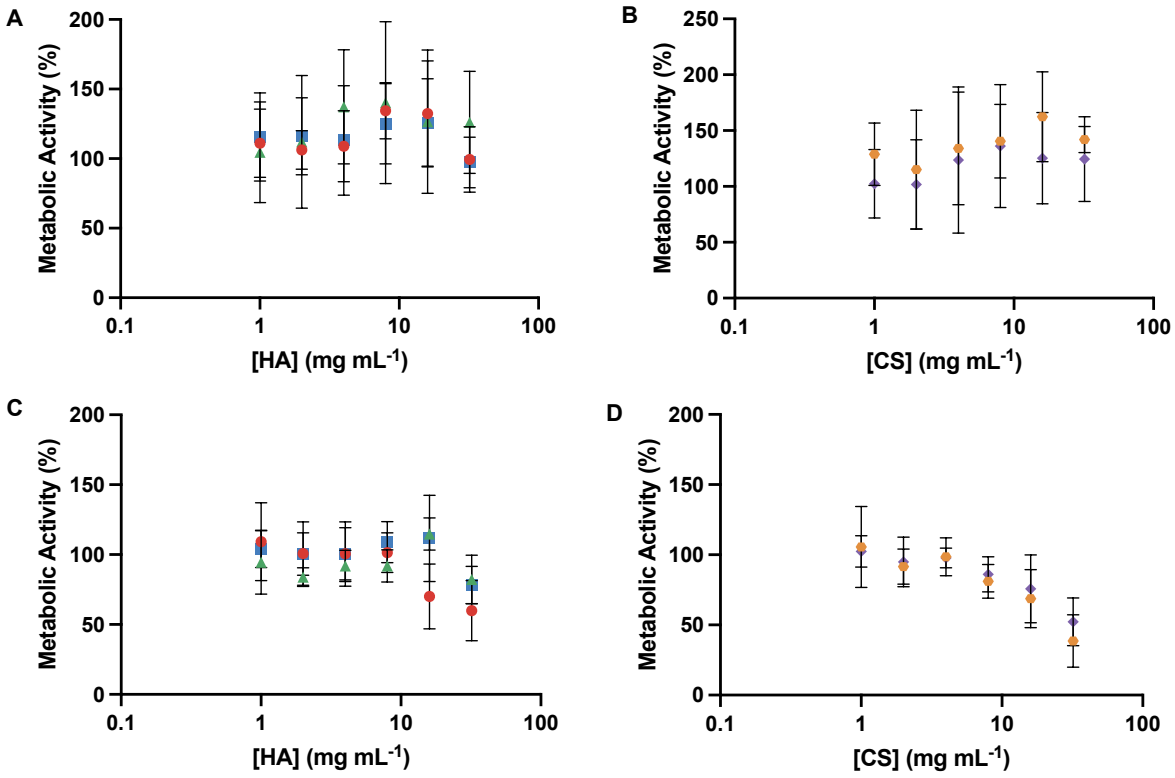

Figure 3.10 Dose-response curves for unmodified glycosaminoglycans against human dermal fibroblasts **(A-B)** and human epidermal keratinocytes **(C-D)**. Glycosaminoglycan derivatives include HA6 (red circle), HA50 (green triangle), HA90 (blue square), CSA (orange hexagon), and CSC (purple diamond). Error bars represent the standard deviation for $n \geq 3$ separate experiments.

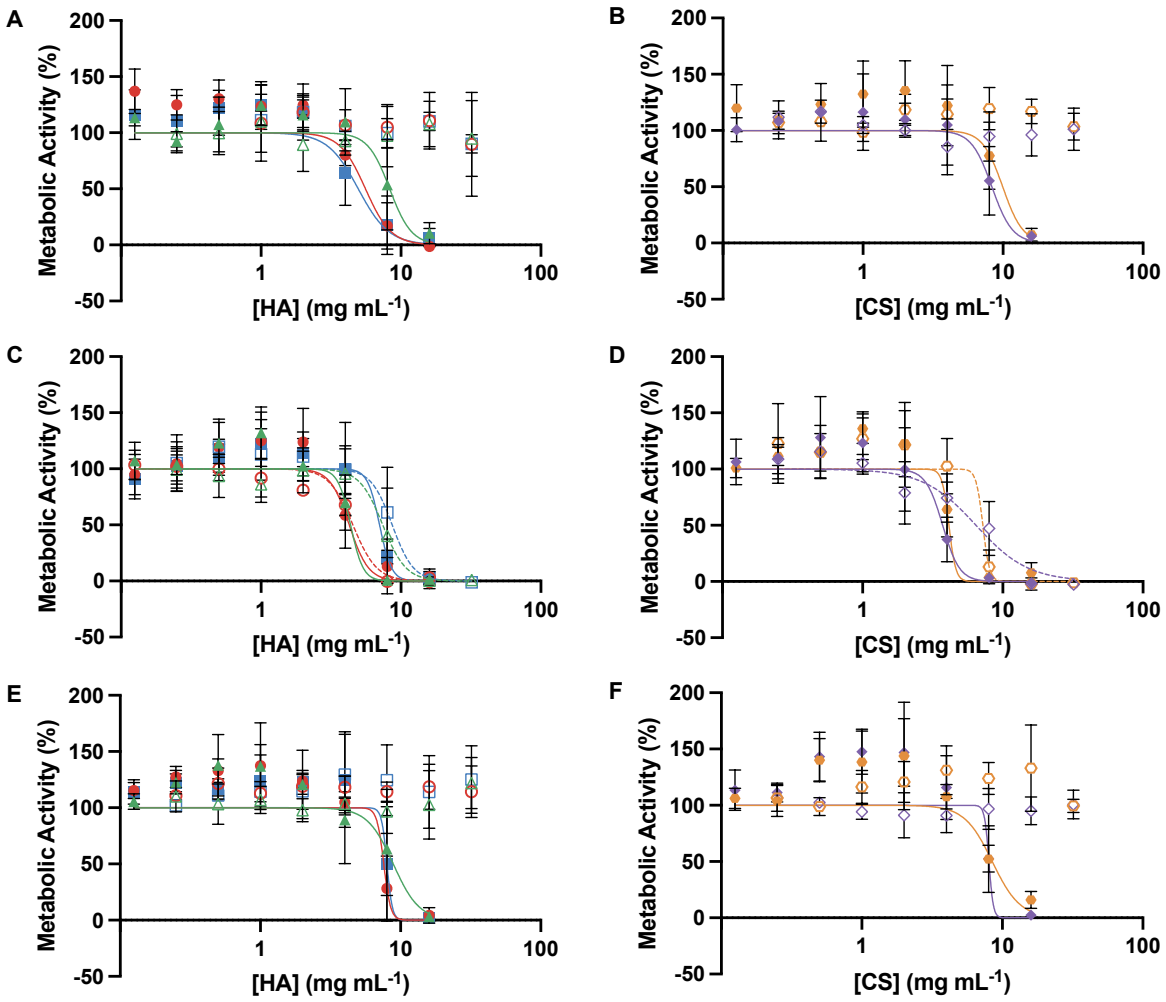

Figure 3.11 Dose-response curves after 24-h treatment of human dermal fibroblasts with amine-modified (hollow) and NO-releasing (solid) glycosaminoglycan derivatives. Modifications of HA6 (red circle), HA50 (green triangle), HA90 (blue square), CSA (orange hexagon), and CSC (purple diamond) include **(A-B)** HEDA, **(C-D)** DPTA, and **(E-F)** DETA. Error bars represent the standard deviation for $n \geq 3$ separate experiments.

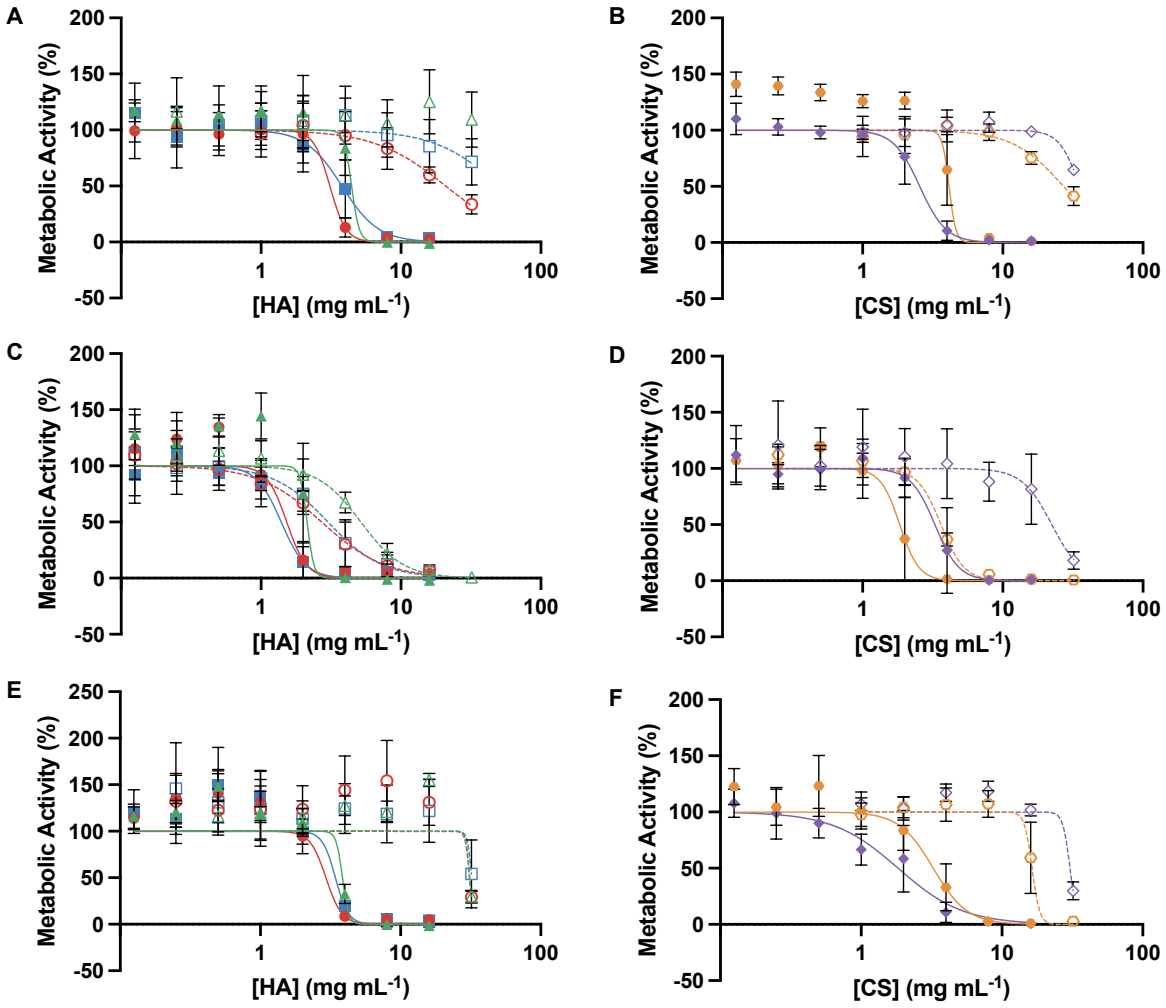

Figure 3.12 Dose-response curves after 24-h treatment of human epidermal keratinocytes with amine-modified (hollow) and NO-releasing (solid) glycosaminoglycan derivatives. Modifications of HA6 (red circle), HA50 (green triangle), HA90 (blue square), CSA (orange hexagon), and CSC (purple diamond) include **(A-B)** HEDA, **(C-D)** DPTA, and **(E-F)** DETA. Error bars represent the standard deviation for $n \geq 3$ separate experiments.

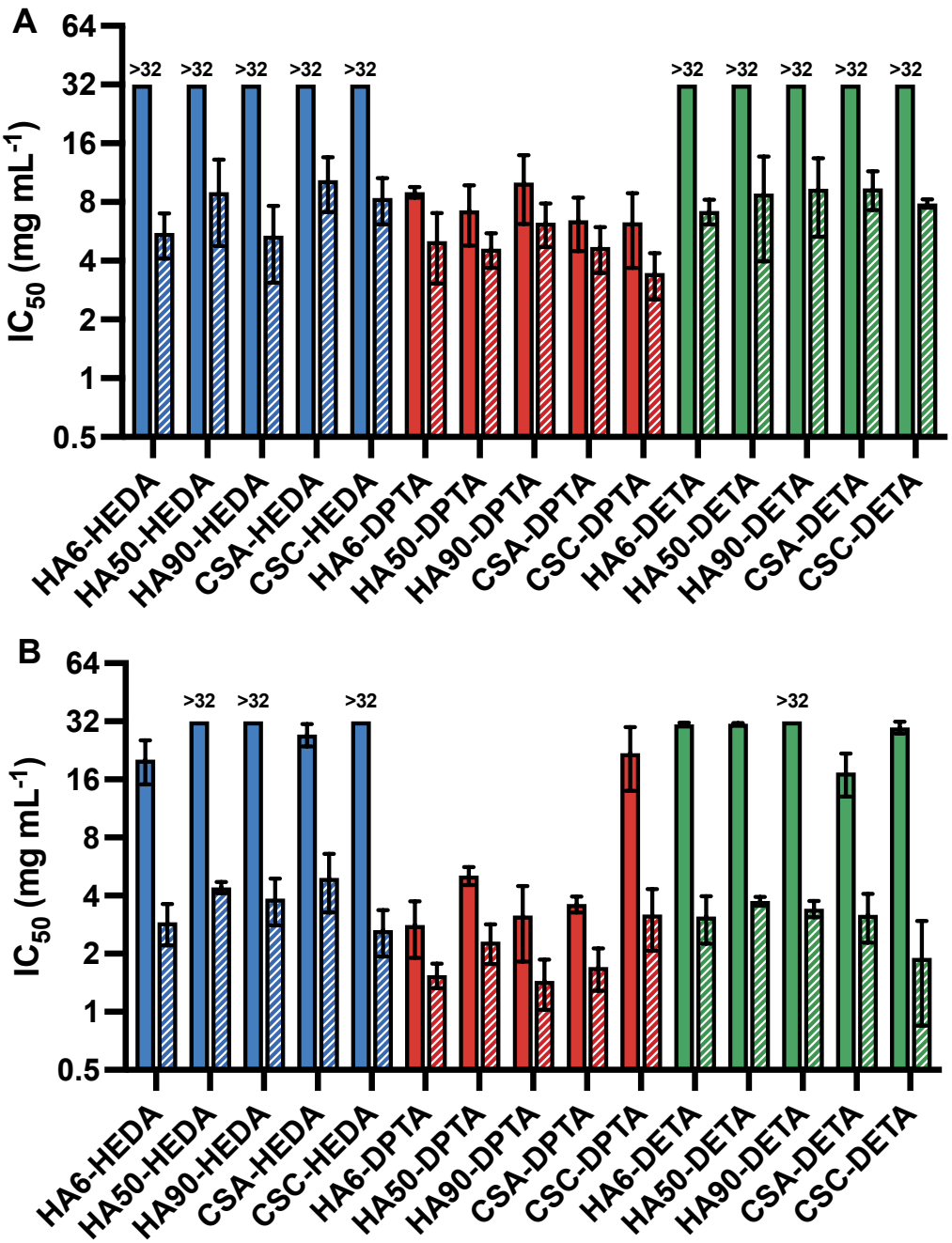

Figure 3.13 Concentration of amine-modified (solid) or NO-releasing (striped) glycosaminoglycan derivatives required to inhibit metabolic activity of **(A)** human dermal fibroblasts (HDFs) or **(B)** human epidermal keratinocytes (HEKs) by 50% (IC_{50}).

Upon *N*-diazeniumdiolate NO donor formation, the GAG derivatives exhibited similar IC_{50} values regardless of alkylamine, suggesting that the release of NO is strongly influential to the toxicity profile. For HDFs, NO-releasing DPTA-modified GAG biopolymers exhibited IC_{50} values of 3-6 mg mL^{-1}, whereas the NO-releasing HEDA- and DETA-modified systems exhibited IC_{50} values of 5-10 mg mL^{-1}. These overlapping ranges indicate that the NO loading on the material encompasses much of the toxicity profile, with lesser influence from the GAG backbone structure. For HEKs, the NO-releasing DPTA-modified GAG derivatives resulted in IC_{50} values of 1-3 mg mL^{-1} while the IC_{50} values for NO-releasing HEDA- and DETA-modified derivatives were 1-5 mg mL^{-1}. Although the cytotoxicity increased with NO donor formation, an in vitro monolayer of cells behaves differently than three-dimensional in vitro cell models or in vivo tissue. Indeed, monolayers of cells are often more susceptible to toxicity.[75,76] All further in vitro wound healing assays were performed using < 1 mg mL^{-1} GAG to ensure sufficient cell activity and survival. In vivo studies will be utilized to confirm the therapeutic utility of the NO-releasing GAG derivatives at greater concentrations.

3.3.5. In vitro adhesion of human skin cells to extracellular matrix components

The ability of mammalian cells to adhere to ECM components and/or other cells is important for successful wound healing.[73] The analysis of cell-ECM adhesion was evaluated using static adhesion assays by treating fibroblasts and keratinocytes with 100 ng mL^{-1} to 100 μg mL^{-1} of unmodified, amine-modified, or NO-releasing GAGs. Concurrent with treatment, the cells were seeded into collagen I-coated well plates, as collagen I is a major component of the ECM in the skin and facilitates adhesion. The effect of the GAGs on adhesion to collagen I was determined by monitoring the quantity of metabolically active cells adhered to the plate after multiple washes

(removal of non-adhered cells). Adhesion of HDFs and HEKs were first evaluated in response to treatment with unmodified GAGs. Treatment of HDFs with unmodified HA or CS resulted in a slight decrease in adhesion to the collagen I-coated surface relative to untreated cells but was within error (Figure 3.14). Treatment of the HEKs led to significantly less adhesion at one or more evaluated concentrations for all GAGs except for CSA (Figure 3.15), indicating that the sulfation pattern of CS may impact adhesion of cells to ECM components.

A decrease in HDF adhesion was only observed for DPTA-modified GAGs, both with and without NO, for treatments spanning 100 ng mL^{-1} to 100 μg mL^{-1} (Figure 3.16). HEDA- and DETA-modified GAGs were not significantly different than untreated cells. At three of the four evaluated concentrations, treatment with CSC-DPTA/NO significantly hindered cell adhesion. No major trends were observed regarding GAG identity, HA molecular weight, or CS sulfation pattern. The inhibition of adhesion was predominantly determined by alkylamine substituent. In contrast, treatment of HEKs with amine-modified and NO-releasing GAGs at the same concentrations demonstrated differences regarding GAG identity. The majority of the derivatives decreased HEK adhesion to ECM components at one or more of the evaluated concentrations (Figure 3.17). Treatment with each NO-releasing CSC derivative (CSC-HEDA/NO, CSC-DPTA/NO, and CSC-DETA/NO), however, did not influence cell adhesion to collagen I versus untreated cells. In terms of promoting or maintaining cell adhesion properties for both fibroblasts and keratinocytes, both CSC-HEDA and CSC-DETA were the only candidates exhibiting such behavior at all tested concentrations (with and without NO).

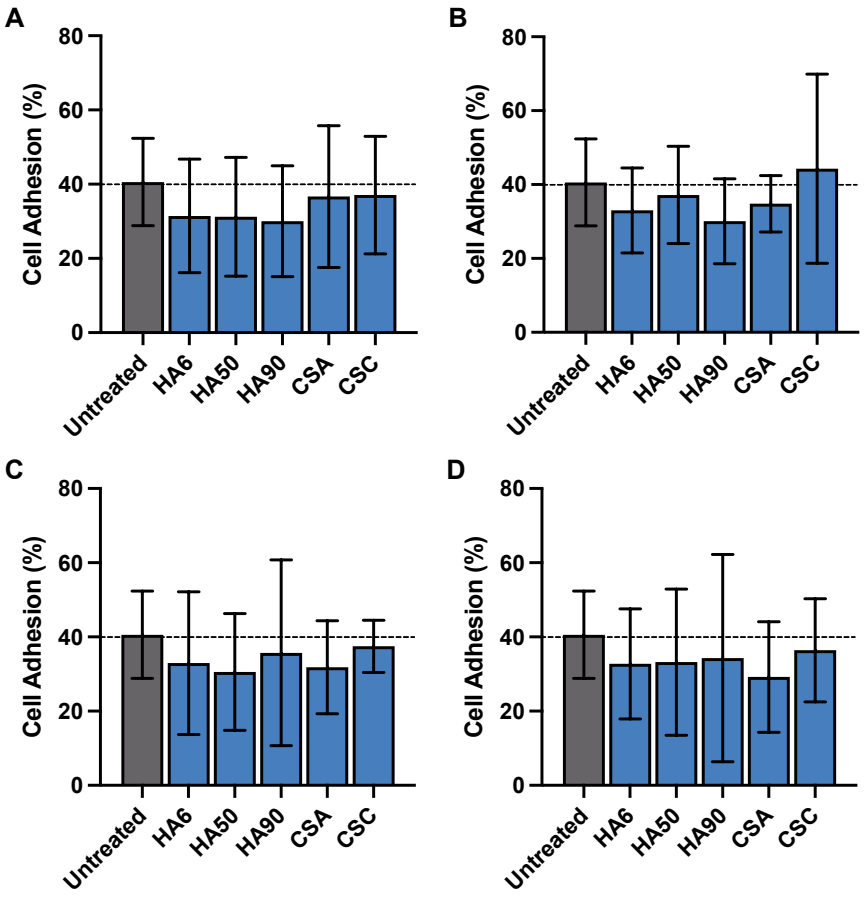

Figure 3.14 Adhesion of HDFs treated with unmodified GAGs at concentrations of **(A)** 100 ng mL^{-1}, **(B)** 1 µg mL^{-1}, **(C)** 10 µg mL^{-1}, and **(D)** 100 µg mL^{-1}. Adhesion of GAG derivatives is reported as a percentage of the total number of cells seeded in each well. Error bars represent the standard deviation of $n \geq 4$ separate experiments. * $p < 0.05$ compared to untreated cells.

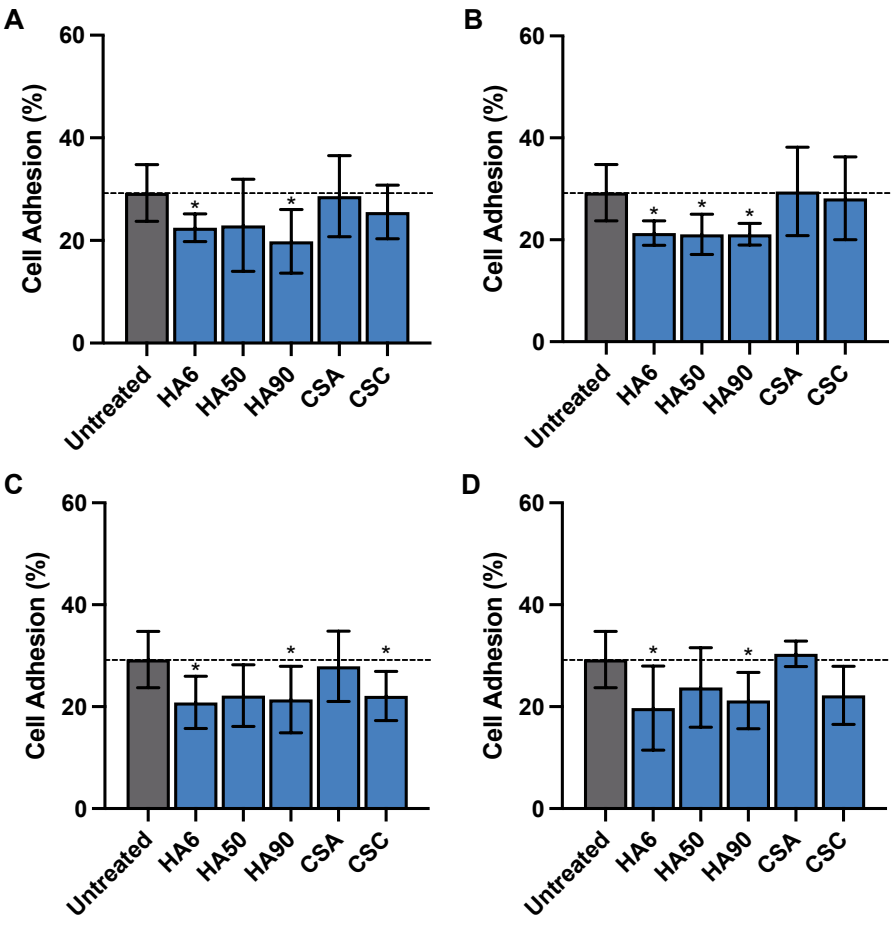

Figure 3.15 Adhesion of HEKs treated with unmodified GAGs at concentrations of **(A)** 100 ng mL^{-1}, **(B)** 1 µg mL^{-1}, **(C)** 10 µg mL^{-1}, and **(D)** 100 µg mL^{-1}. Adhesion of GAG derivatives is reported as a percentage of the total number of cells seeded in each well. Error bars represent the standard deviation of $n \geq 4$ separate experiments. * $p < 0.05$ compared to untreated cells.

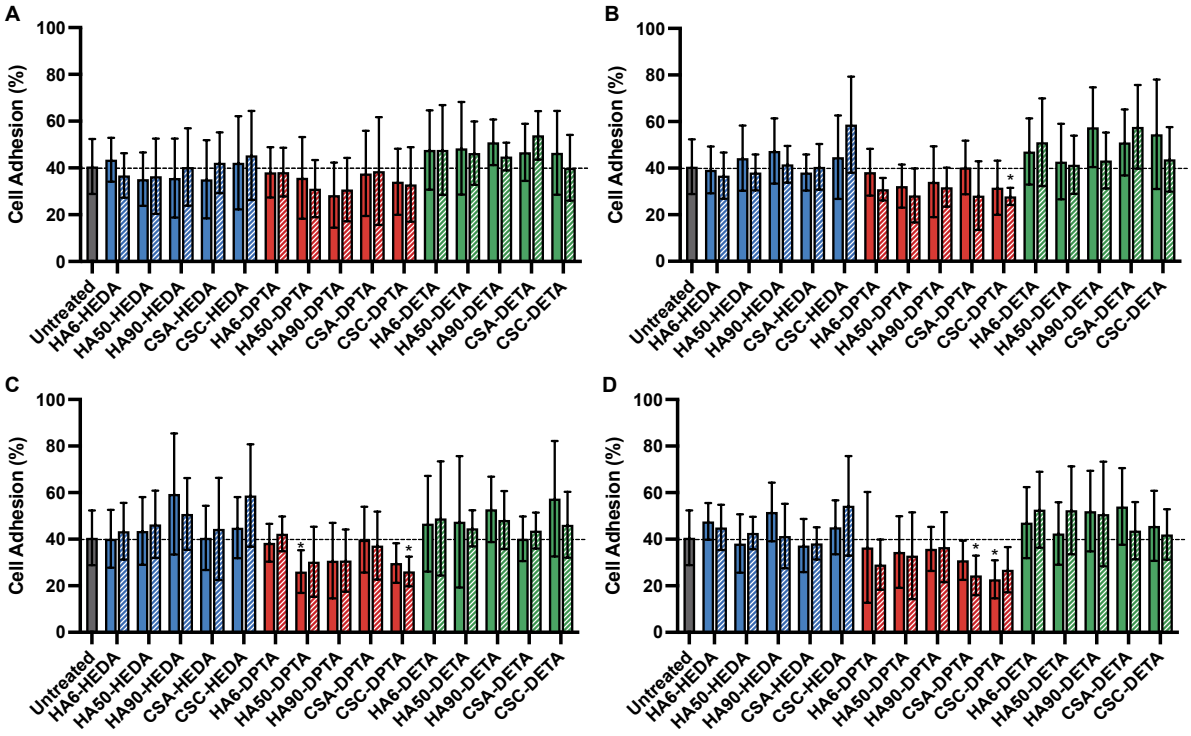

Figure 3.16 Adhesion of HDFs treated with amine-modified (solid) or NO-releasing (striped) GAG derivatives at concentrations of **(A)** 100 ng mL^{-1}, **(B)** 1 μg mL^{-1}, **(C)** 10 μg mL^{-1}, and **(D)** 100 μg mL^{-1}. Adhesion of GAG derivatives is reported as a percentage of the total number of cells seeded in each well. Error bars represent the standard deviation of $n \geq 5$ separate experiments. * $p < 0.05$ compared to untreated cells.

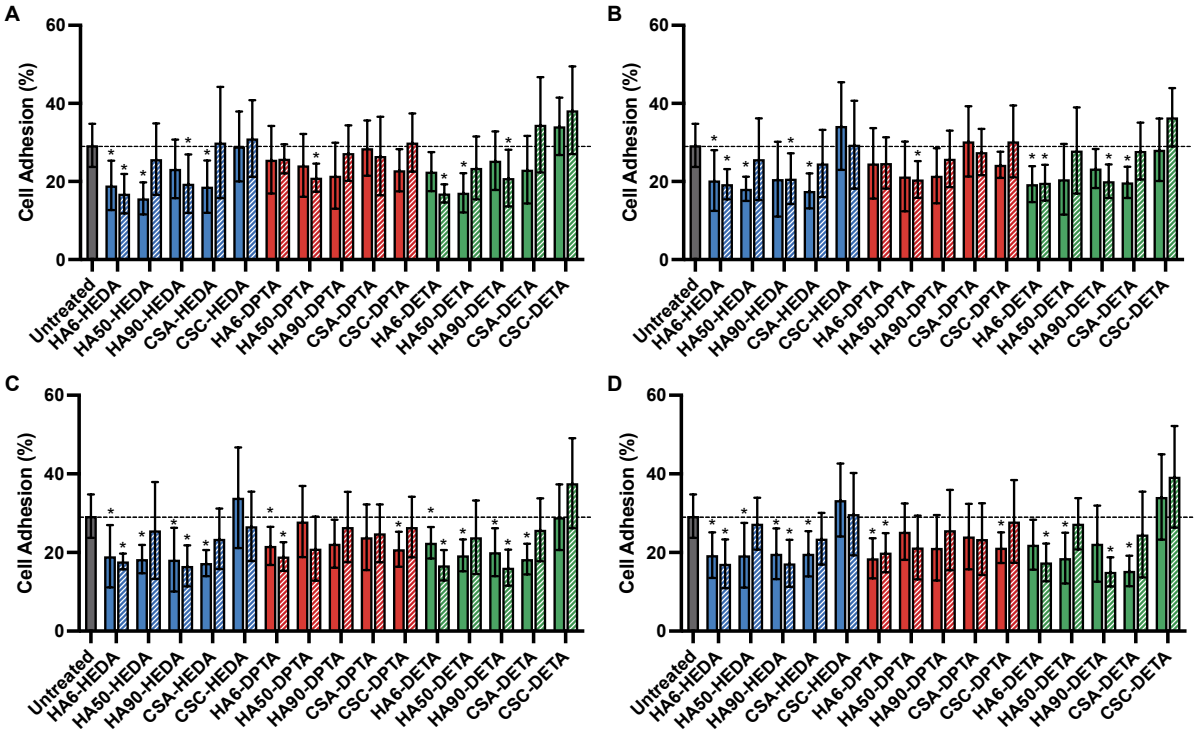

Figure 3.17 Adhesion of HEKs treated with amine-modified (solid) or NO-releasing (striped) GAG derivatives at concentrations of **(A)** 100 ng mL^{-1}, **(B)** 1 μg mL^{-1}, **(C)** 10 μg mL^{-1}, and **(D)** 100 μg mL^{-1}. Adhesion of GAG derivatives is reported as a percentage of the total number of cells seeded in each well. Error bars represent the standard deviation of $n \geq 5$ separate experiments. * $p < 0.05$ compared to untreated cells.

3.3.6. In vitro proliferation of human skin cells

Following adhesion, cells such as fibroblasts and keratinocytes must proliferate in the wound environment. The proliferation of dermal fibroblasts is essential to wound healing, as these cells play key roles in the deposition of new ECM as well as wound contraction.[77] Epidermal keratinocytes are involved in restoration of the epidermis; upon migration to the wound site, keratinocytes proliferate to begin filling the region of missing tissue.[78] Due to the importance of cell proliferation, the effect of unmodified, amine-modified, and NO-releasing GAGs was evaluated using in vitro proliferation assays. The impact of unmodified materials on HDF and HEK proliferation was first investigated by treating both HDFs and HEKs with unmodified HA and CS. Treatment with unmodified HA90 and CSC resulted in slightly lower proliferation of HDFs at all concentrations tested versus untreated cells (Figure 3.18). Each of the unmodified materials facilitated lower proliferation of HEKs at 10 or 100 μg mL^{-1} (Figure 3.19), indicating that the unmodified materials themselves do not facilitate significantly enhanced fibroblast and keratinocyte proliferation over 100 ng mL^{-1} to 100 μg mL^{-1}.

This effect was altered upon modification of the biopolymers with alkylamines and *N*-diazeniumdiolate NO donors. Treatment of the HDFs with HEDA- and DETA-modified GAGs with and without NO donors exhibited similar proliferation to untreated cells (Figure 3.20). However, the DPTA moiety, either alone or in addition to NO donor formation, facilitated similar or enhanced HDF proliferation compared to untreated cells. This enhancement is most clearly observed with HA6-DPTA and HA6-DPTA/NO, which significantly increase proliferation at 1-100 μg mL^{-1} treatment doses. A different trend was observed when the same derivatives were used to treat HEKs. Nearly all of the HEDA- and DETA-modified GAGs, with and without NO, decreased or retained proliferation properties compared to untreated cells (Figure 3.21). HA6-

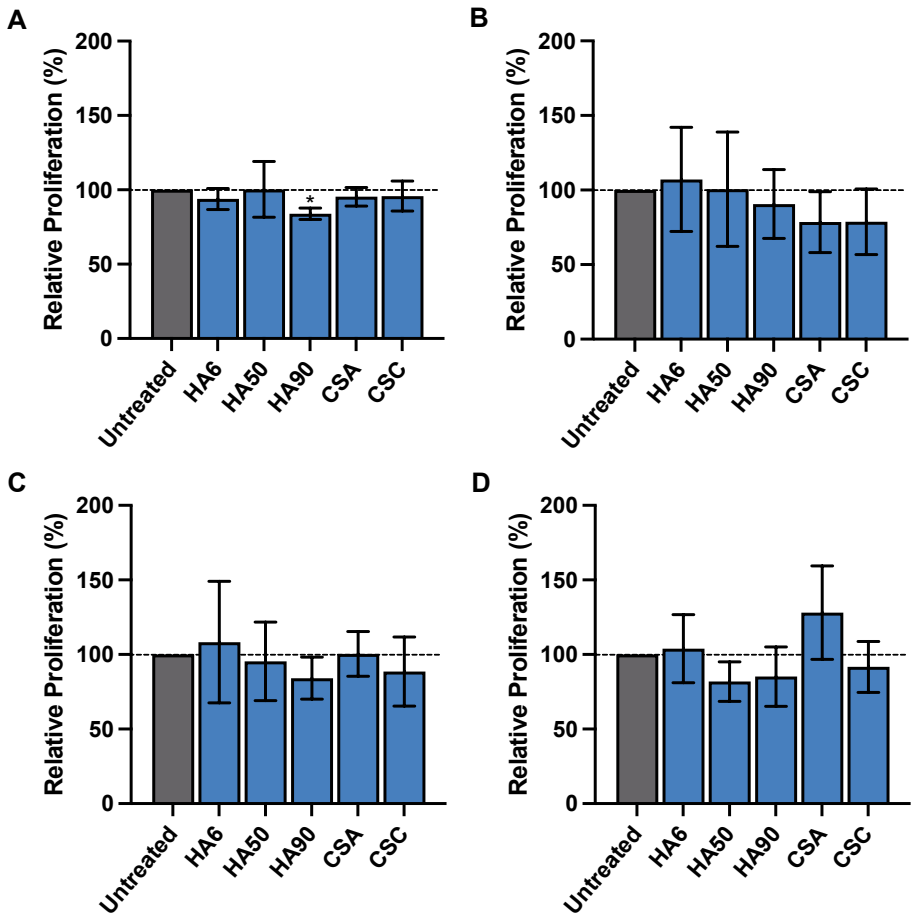

Figure 3.18 Proliferation of HDFs treated with unmodified GAGs at concentrations of **(A)** 100 ng mL^{-1}, **(B)** 1 µg mL^{-1}, **(C)** 10 µg mL^{-1}, and **(D)** 100 µg mL^{-1}. Proliferation of GAGs is reported relative to untreated cells (set to 100% proliferation). Error bars represent the standard deviation of $n \geq 4$ separate experiments. * $p < 0.05$ compared to untreated cells.

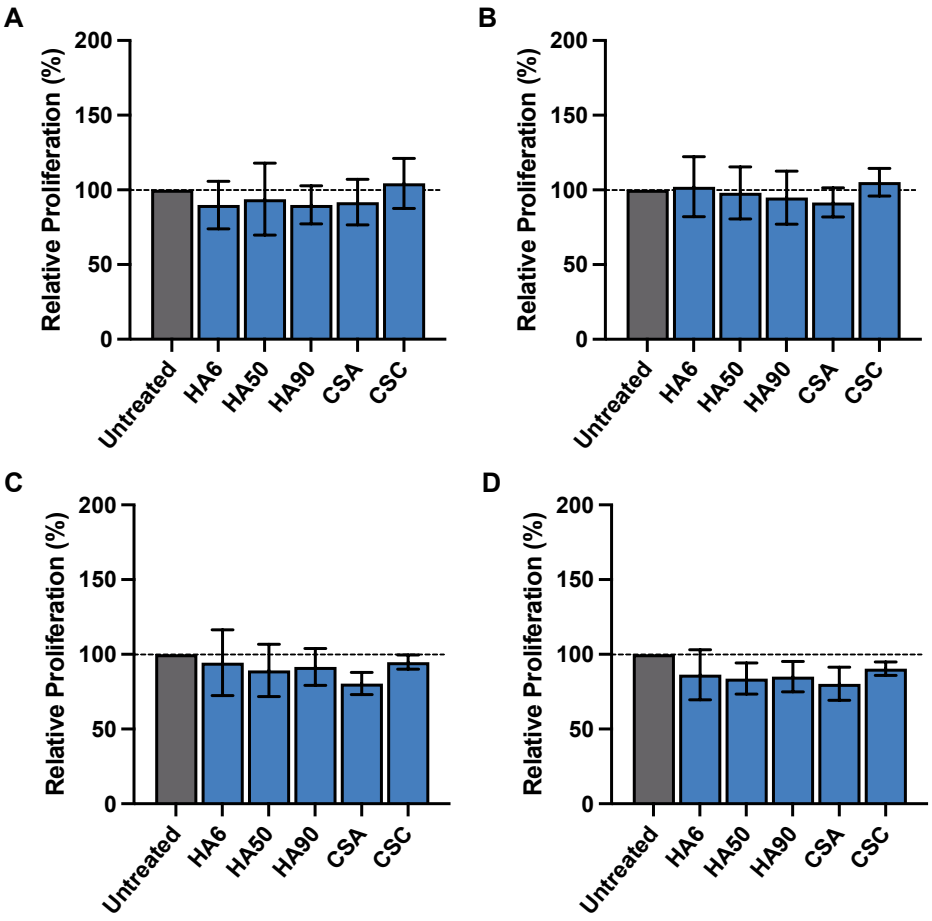

Figure 3.19 Proliferation of HEKs treated with unmodified GAGs at concentrations of **(A)** 100 ng mL^{-1}, **(B)** 1 µg mL^{-1}, **(C)** 10 µg mL^{-1}, and **(D)** 100 µg mL^{-1}. Proliferation of GAGs is reported relative to untreated cells (set to 100% proliferation). Error bars represent the standard deviation of $n \geq 3$ separate experiments. * $p < 0.05$ compared to untreated cells.

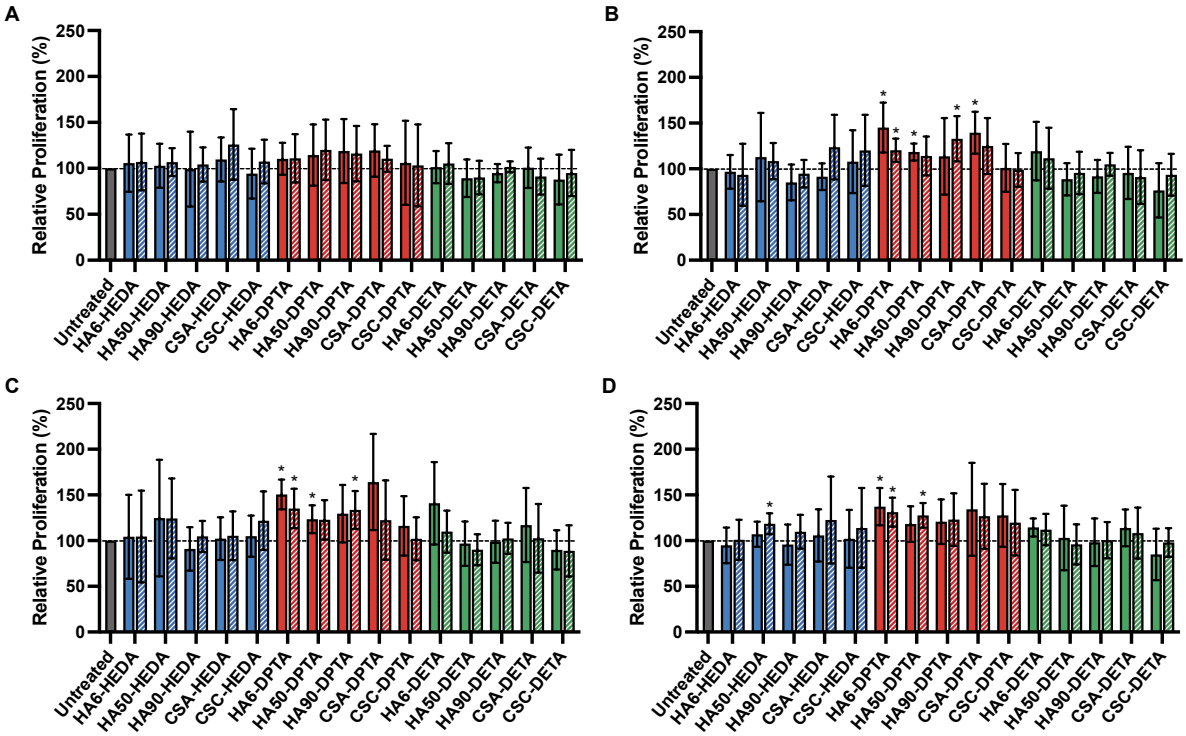

Figure 3.20 Proliferation of HDFs treated with amine-modified (solid) or NO-releasing (striped) GAG derivatives at concentrations of **(A)** 100 ng mL^{-1}, **(B)** 1 µg mL^{-1}, **(C)** 10 µg mL^{-1}, and **(D)** 100 µg mL^{-1}. Proliferation of GAG derivatives is reported relative to untreated cells (set to 100% proliferation). Error bars represent the standard deviation of $n \geq 4$ separate experiments. * $p < 0.05$ compared to untreated cells.

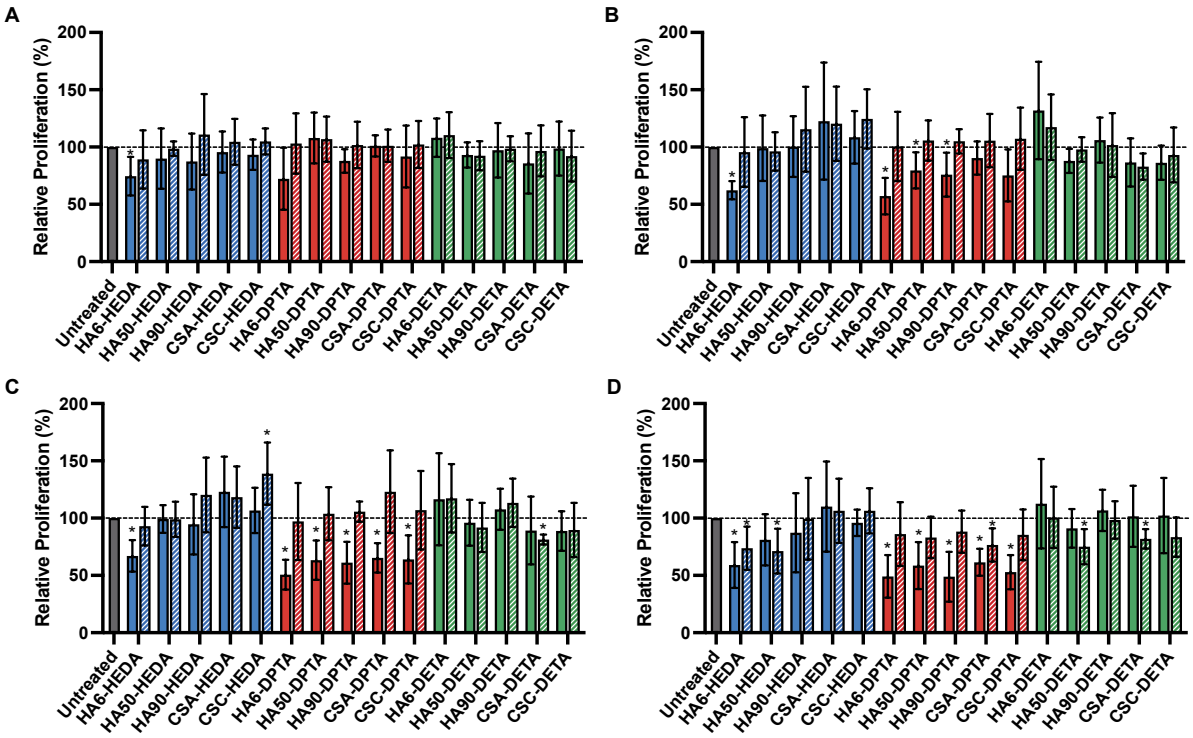

Figure 3.21 Proliferation of HEKs treated with amine-modified (solid) or NO-releasing (striped) GAG derivatives at concentrations of **(A)** 100 ng mL^{-1}, **(B)** 1 μg mL^{-1}, **(C)** 10 μg mL^{-1}, and **(D)** 100 μg mL^{-1}. Proliferation of GAG derivatives is reported relative to untreated cells (set to 100% proliferation). Error bars represent the standard deviation of $n \geq 4$ separate experiments. * $p < 0.05$ compared to untreated cells.

HEDA decreased HEK proliferation at all concentrations tested. The CSC-HEDA/NO enhanced cell proliferation at 10 μg mL^{-1}, making it the only GAG derivative to elevate proliferation at any of the evaluated concentrations. Contrary to the proliferative effects observed for DPTA-modified GAGs against HDFs, the proliferation of HEKs lessened substantially over 1-100 μg mL^{-1} for non-NO-releasing DPTA-modified GAGs. However, the modification of the DPTA-modified GAGs with NO was compensatory and allowed for proliferation to be restored to untreated levels when treated with 1-10 μg mL^{-1}. The contrasting effects of DPTA-modified GAGs motivated their further study in order to understand their impact on wound healing in a more complex model (i.e., containing both fibroblasts and keratinocytes). With respect to the materials that best promoted or maintained proliferation of HDFs and HEKs, only CSA-HEDA, CSC-HEDA, HA6-DETA, and HA90-DETA fulfilled this requirement for both amine-modified and NO-releasing forms.

3.3.7. In vitro TLR4 inflammation assay

Inflammation is a central component to wound healing. Toll-like receptors (TLRs) are expressed on many cells that facilitate wound healing processes, including macrophages, neutrophils, fibroblasts, and keratinocytes. Toll-like receptor 4 (TLR4) is expressed by these four cell types, among others, and is shown to be associated with wound healing.[79] Hyaluronic acid fragments with a molecular weight of 10-250 kDa have been shown to interact with TLR4 during the inflammatory phase of wound healing.[50,51] In contrast, Stabler et al. reported that CS decreases NF-κB activation via TLR4 inhibition, although how sulfation pattern affects this process remains unclear.[80] The interactions between amine-modified and NO-releasing GAGs with TLR4 were thus evaluated using an in vitro assay that measures NF-κB-induced SEAP activity resulting from TLR4 activation on HEK-Blue™ mTLR4 cells. Positive controls included TNF-α and LPS. TNF-

α is a cytokine that interacts with many receptors leading to NF-κB activation. LPS activates NF-κB via TLR4 (Figure 3.22).[81,82] Unmodified GAGs were first evaluated at 100 ng mL^{-1} to 100 μg mL^{-1} using this assay. Increasing SEAP activity was observed with increasing concentration of GAGs (Figure 3.23). At 100 μg mL^{-1}, both HA50 and HA90 exhibited significantly more NF-κB-induced SEAP production than untreated cells (Figure 3.23D). However, HA6 did not increase SEAP concentration, suggesting a molecular weight threshold for TLR4 activation. Both CSA and CSC interacted with TLR4, leading to activation at a greater level than that achieved with the HA derivatives. Of note, CSA exhibited greater activation of TLR4 than CSC, demonstrating the role that sulfation pattern plays in CS's inflammatory properties.

In evaluating amine-modified and NO-releasing GAGs, negligible increases in TLR4 activity were observed compared to untreated cells upon treatment of cells with 100 ng mL^{-1} to 10 μg mL^{-1}, with the exception of CSA-HEDA at 10 μg mL^{-1} (Figure 3.24A-C). At 100 μg mL^{-1} GAG treatment doses (Figure 3.24D), five of the fifteen amine-modified GAGs significantly increased SEAP concentrations compared to untreated cells, indicating that these biopolymers maintained some interaction with TLR4, albeit at lesser levels than the unmodified GAGs. Regardless of the alkylamine used to form the NO donor, each NO-releasing GAG derivative exhibited negligible TLR4 activation at concentrations up to 100 μg mL^{-1}. By minimizing TLR4 activity, downstream activation of NF-κB should be lessened. Activation of NF-κB is a key component in the inflammatory process and associated with many inflammatory diseases. Decreased TLR4 activity as a result of NO release clearly supports NO's roles as an anti-inflammatory agent.[17,18]

To ensure that the NF-κB activation resulted from TLR4 activity and not that of other receptors (e.g., TLR3, TLR5, NOD1, ALPK1, and TIFA receptors present at endogenous levels on the HEK-Blue™ mTLR4 cells), HEK-Blue™ Null1-v cells were evaluated in the same manner.

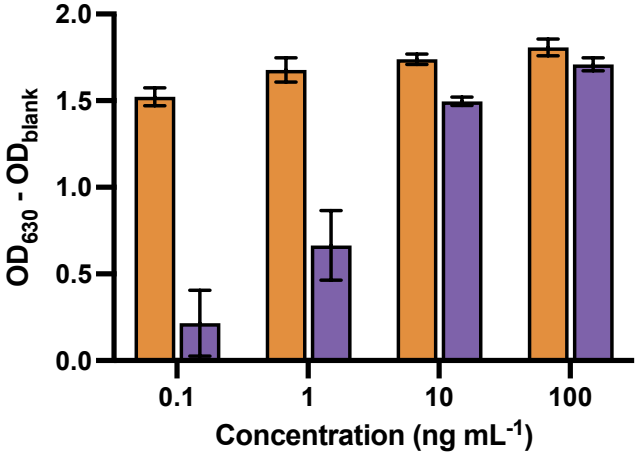

Figure 3.22 Activation of NF-κB in HEK-Blue™ mTLR4 cells upon treatment with LPS (orange) or TNF-α (purple) at concentrations of 0.1 to 100 ng mL^{-1}. NF-κB-induced SEAP activity is reported as the OD_{630} corrected for blank media. Error bars represent the standard deviation of $n \geq 3$ separate experiments.

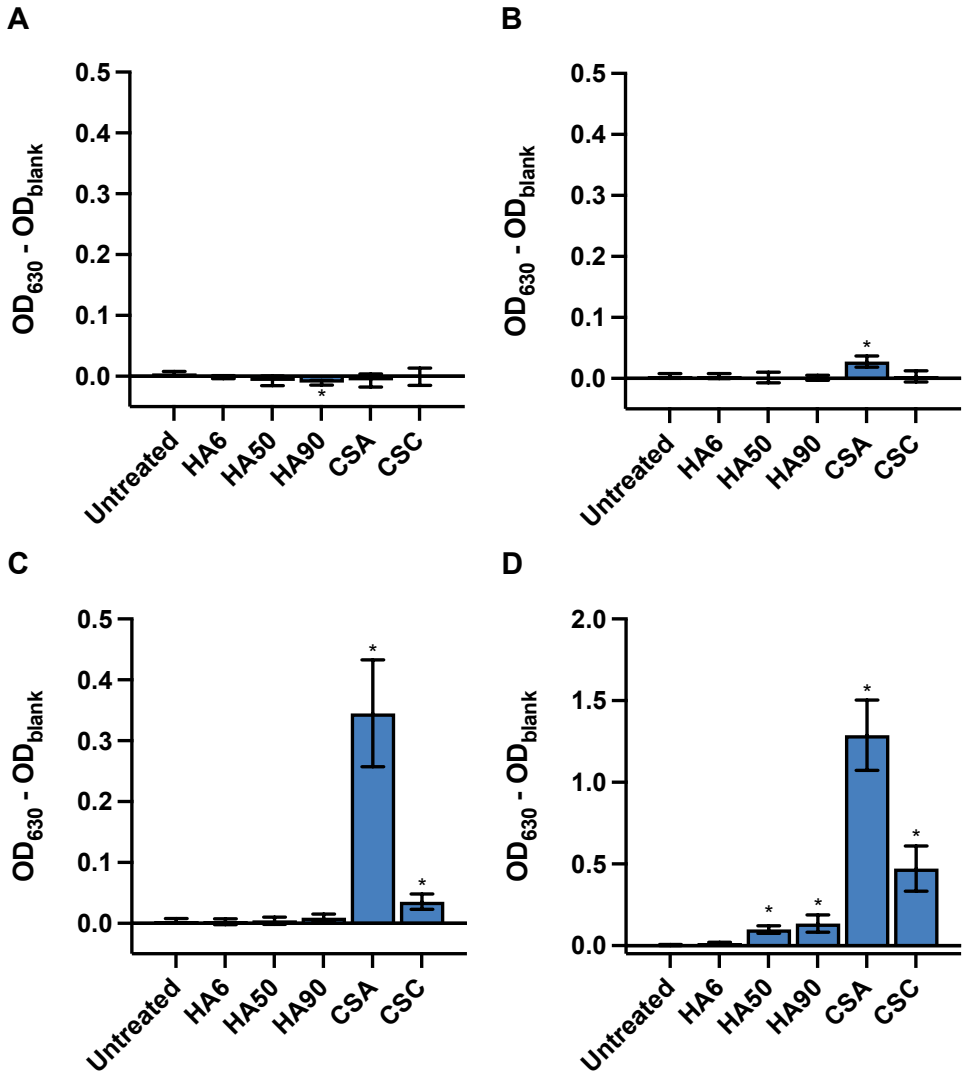

Figure 3.23 Activation of NF-κB via murine TLR4 receptor in HEK-Blue™ mTLR4 cells upon treatment with unmodified GAGs at concentrations of **(A)** 100 ng mL^{-1}, **(B)** 1 μg mL^{-1}, **(C)** 10 μg mL^{-1}, and **(D)** 100 μg mL^{-1}. NF-κB-induced SEAP activity is reported as the OD_{630} corrected for blank media. Error bars represent the standard deviation of $n \geq 3$ separate experiments. Of note, the y-axis of **(D)** uses a different range to present the data. * $p < 0.05$ compared to untreated cells.

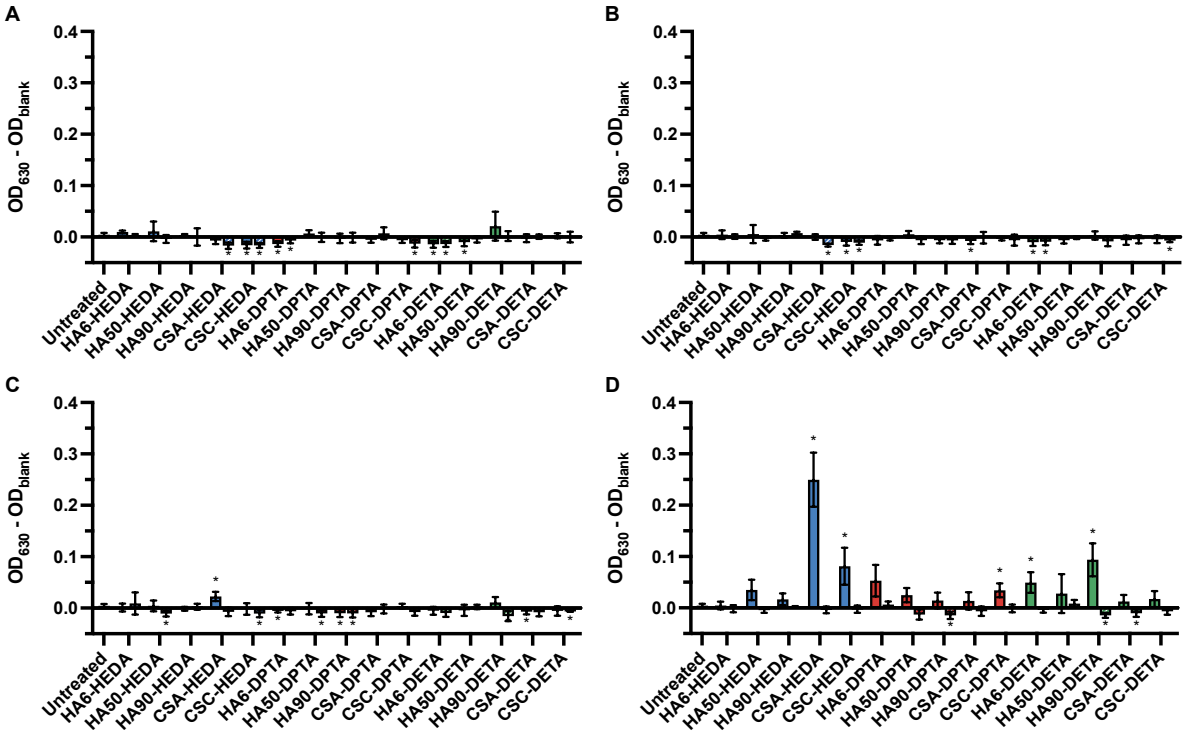

Figure 3.24 Activation of NF-κB via murine TLR4 receptor in HEK-Blue™ mTLR4 cells upon treatment with amine-modified (solid) or NO-releasing (striped) GAG derivatives at concentrations of **(A)** 100 ng mL^{-1}, **(B)** 1 μg mL^{-1}, **(C)** 10 μg mL^{-1}, and **(D)** 100 μg mL^{-1}. NF-κB-induced SEAP activity is reported as the OD_{630} corrected for blank media. Error bars represent the standard deviation of $n \geq 3$ separate experiments. * $p < 0.05$ compared to untreated cells.

These cells exhibit endogenous levels of TLR3, TLR5, NOD1, ALPK1, and TIFA receptors but are not transfected with the murine TLR4 receptor gene. TNF-α was included as a positive control to confirm NF-κB activation, and LPS served as a negative control, as without TLR4 present, it does not cause NF-κB activation (Figure 3.25). As expected, all GAG derivatives, whether unmodified, amine-modified, or NO-releasing, exhibited negligible NF-κB activation without TLR4 present (Figures 3.26 and 3.27), confirming that the activation or lack thereof of NF-κB by the GAG derivatives is the result of TLR4 activity. Unequivocally, NO release from NO donor-modified GAGs decreases TLR4 activity in vitro.

3.3.8. In vivo evaluation of NO-releasing glycosaminoglycans on infected murine wounds

The in vitro assays described heretofore were utilized to narrow the list of wound healing candidates for further in vivo evaluation. The antibacterial experiments pointed to HA6-HEDA/NO along with all NO-releasing DPTA-modified GAGs as the most effective for eradicating multiple strains/resistance profiles of *P. aeruginosa* and *S. aureus*. When summarizing the proliferation and adhesion assays for HDFs and HEKs, CSC-HEDA and CSC-HEDA/NO were revealed as the only derivatives with all neutral or positive influences on proliferation and adhesion regardless of concentration (Figure 3.28). HA6-HEDA/NO and CSC-HEDA/NO were thus selected as most suitable therapeutic candidates for the initial in vivo wound healing study.

Mice were wounded using a standard biopsy punch procedure with the wound inoculated with 2 x 10^5 CFU of PAO1. Initial in vivo experiments included three treatment groups, with one group receiving vehicle only (i.e., PEG), a second group receiving HA6-HEDA/NO in PEG (50 mg kg^{-1} body weight), and a third group receiving CSC-HEDA/NO in PEG (50 mg kg^{-1} body weight). Mice were treated once daily beginning immediately following the wounding and

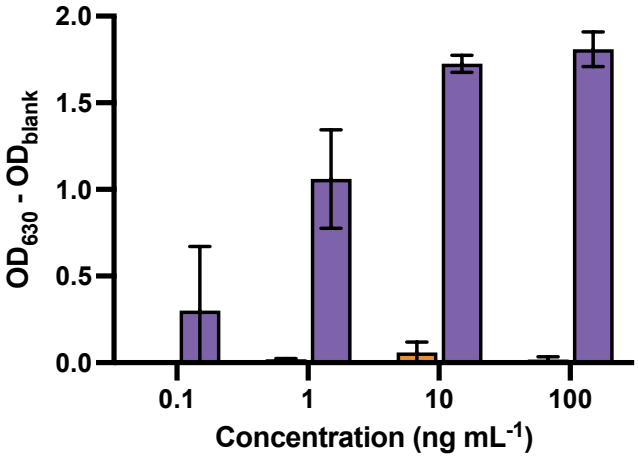

Figure 3.25 Activation of NF-κB in HEK-Blue™ Null1-v cells upon treatment with LPS (orange) or TNF-α (purple) at concentrations of 0.1 to 100 ng mL^{-1}. Cells express endogenous levels of TLR3, TLR5, NOD1, ALPK1, and TIFA but are not transfected with the murine TLR4 receptor gene. NF-κB-induced SEAP activity is reported as the OD_{630} corrected for blank media. Error bars represent the standard deviation of n = 3 separate experiments.

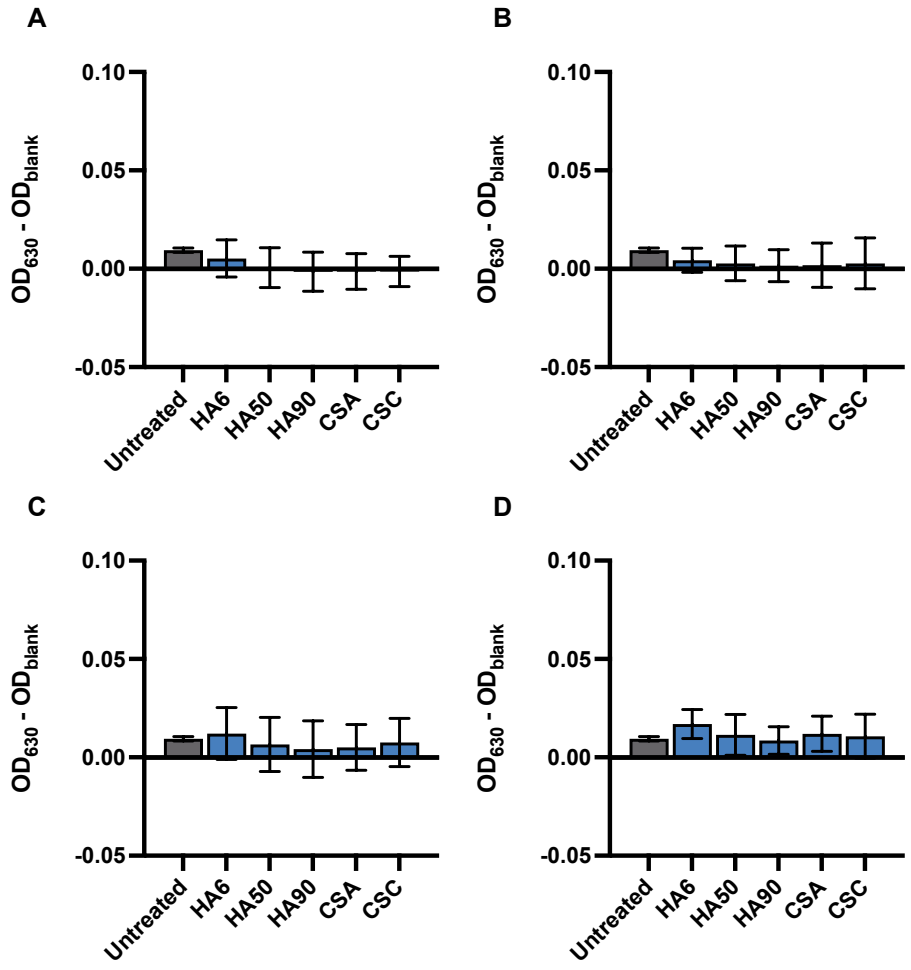

Figure 3.26 Activation of NF-κB in HEK-Blue™ Null1-v cells upon treatment with unmodified GAGs at concentrations of **(A)** 100 ng mL^{-1}, **(B)** 1 µg mL^{-1}, **(C)** 10 µg mL^{-1}, and **(D)** 100 µg mL^{-1}. Cells express endogenous levels of TLR3, TLR5, NOD1, ALPK1, and TIFA but are not transfected with the murine TLR4 receptor gene. NF-κB-induced SEAP activity is reported as the OD_{630} corrected for blank media. Error bars represent the standard deviation of n = 3 separate experiments.

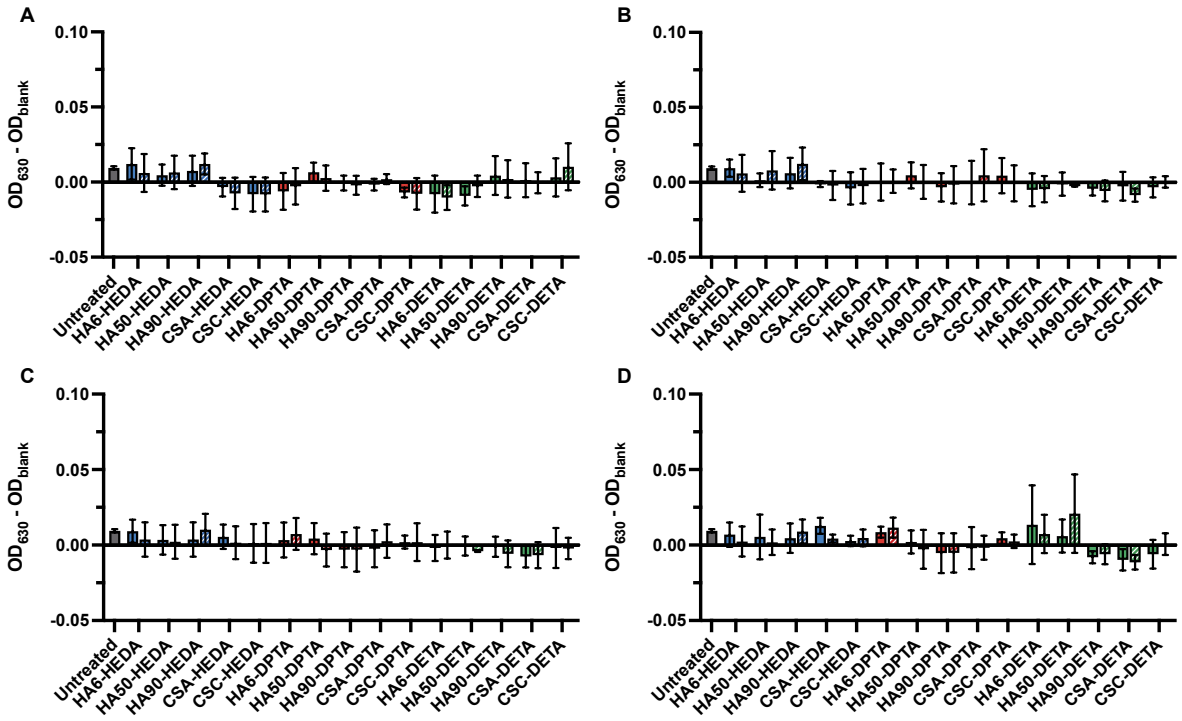

Figure 3.27 Activation of NF-κB in HEK-Blue™ Null1-v cells upon treatment with amine-modified (solid) or NO-releasing (striped) GAG derivatives at concentrations of **(A)** 100 ng mL^{-1}, **(B)** 1 μg mL^{-1}, **(C)** 10 μg mL^{-1}, and **(D)** 100 μg mL^{-1}. Cells express endogenous levels of TLR3, TLR5, NOD1, ALPK1, and TIFA but are not transfected with the murine TLR4 receptor gene. NF-κB-induced SEAP activity is reported as the OD_{630} corrected for blank media. Error bars represent the standard deviation of n = 3 separate experiments.

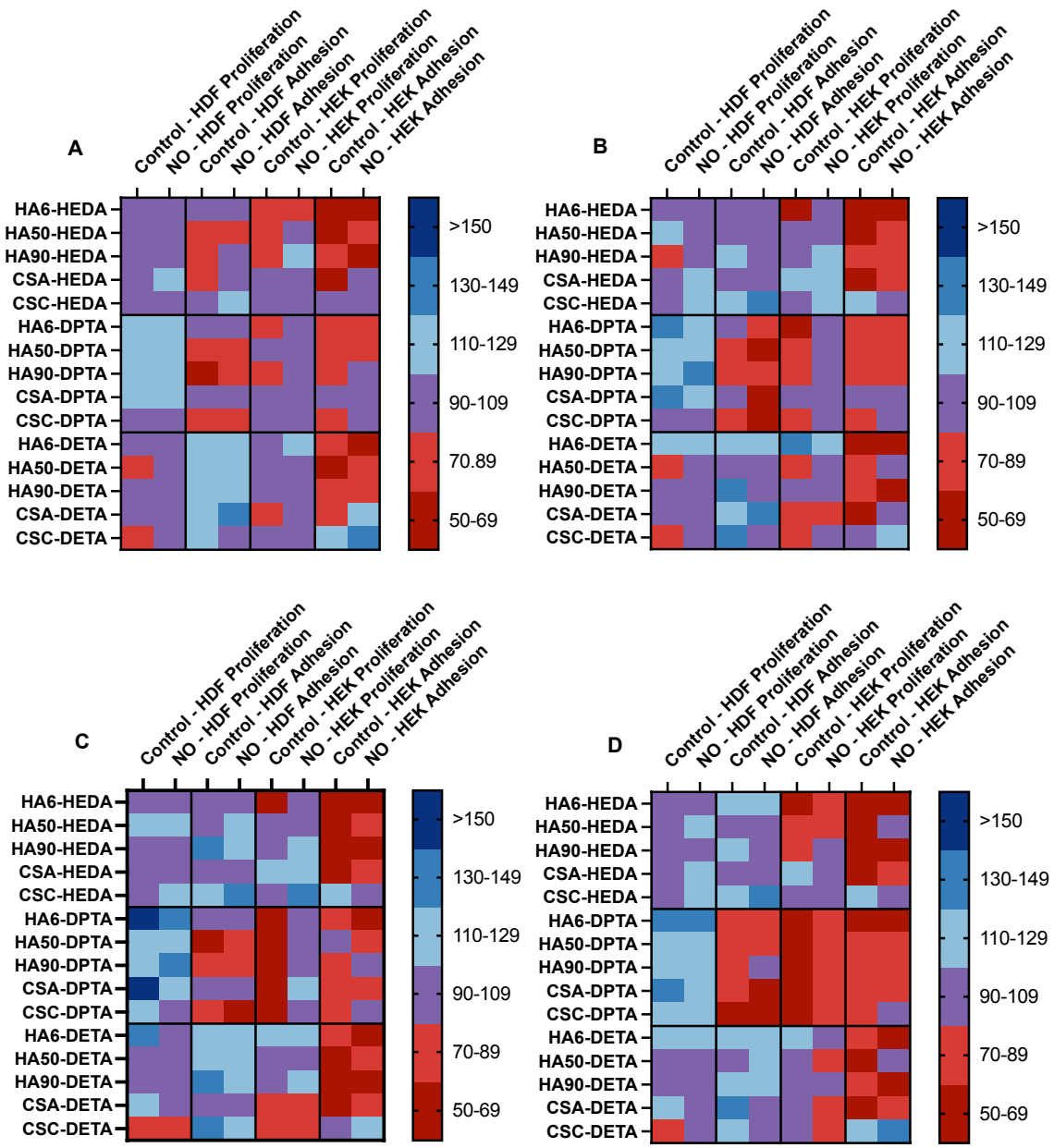

Figure 3.28 Heat maps displaying a positive (blue), negative (red), or neutral (purple) effect on HDF and HEK adhesion and proliferation following treatment with **(A)** 100 ng mL^{-1}, **(B)** 1 µg mL^{-1}, **(C)** 10 µg mL^{-1}, or **(D)** 100 µg mL^{-1} of amine-modified (control) or NO-releasing GAGs. Data represents the average of $n \geq 3$ separate experiments.

infection procedure. Wounds were imaged daily and measured in perpendicular directions with calipers. The percentage of wound area remaining at each time point was calculated relative to the initial wound area to monitor wound closure. Wounds treated with HA6-HEDA/NO increased in size over the initial 24 h following wounding but then began to decrease in size (Figure 3.29A). Treatment with HA6-HEDA/NO did not significantly decrease remaining wound area compared to the PEG controls at any time point. In contrast, treatment of mice with CSC-HEDA/NO decreased remaining wound area compared to the PEG control on days 3 through 7 post-wounding. For example, CSC-HEDA/NO treated wounds retained ~60% and ~15% of their wound areas at day 3 and 7 post-wounding, respectively, whereas PEG-treated wounds exhibited ~105% and ~45% at the same timepoints. The CSC-HEDA/NO treatment also proved better (i.e., greater wound closure) than HA6-HEDA/NO on days 2 through 4 post-wounding. The discrepancy between the two treatments cannot be attributed to NO payloads as HA6-HEDA/NO and CSC-HEDA/NO released similar amounts of NO, 0.40 ± 0.04 and 0.38 ± 0.11 μmol NO mg^{-1}, respectively, in SWF. Further, CSC-HEDA/NO only releases NO for 2.9 ± 0.8 h in SWF compared to 7.6 ± 1.2 h for HA6-HEDA/NO, suggesting NO-release duration is also not a major factor. We thus set out to evaluate the therapeutic activity of the CSC-HEDA backbone (without NO) to determine how the biopolymer alone may influence wound healing.

While CSC-HEDA/NO promoted faster wound healing, it did not exhibit the strongest antibacterial properties in vitro. In the second study, CSC-DPTA/NO was included to determine the effect of greater antibacterial properties on wound healing. The inclusion of non-NO-releasing CSC-HEDA and CSC-DPTA controls were necessary to determine the role of the biopolymer scaffold alone. The following five treatment groups were used: (1) vehicle only (i.e., PEG); (2) CSC-HEDA in PEG (50 mg kg^{-1} body weight); (3) CSC-HEDA/NO in PEG (50 mg kg^{-1} body

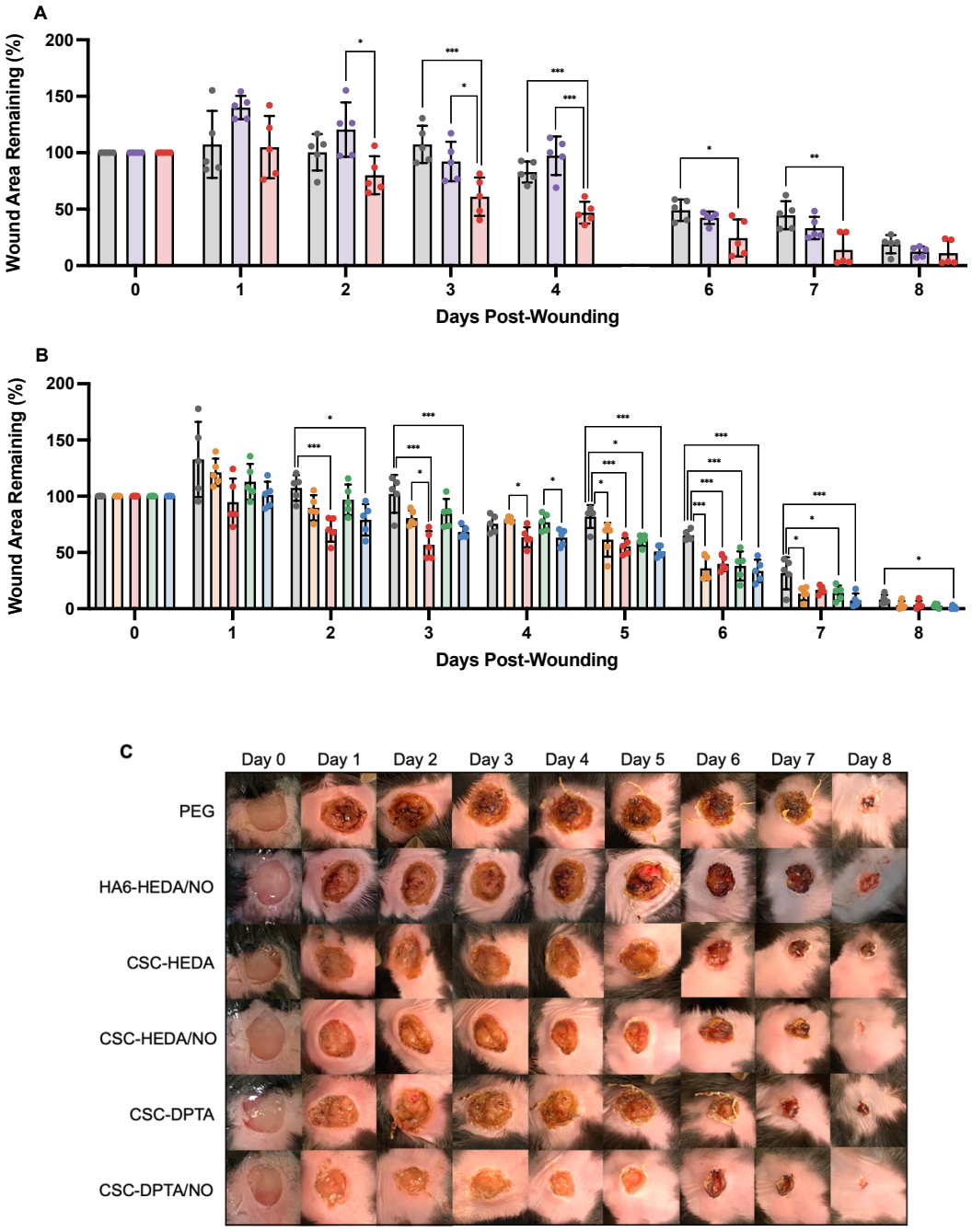

Figure 3.29 (A) Percentage of initial wound area remaining following daily treatment with PEG (gray), 50 mg kg^{-1} of HA6-HEDA/NO in PEG (purple), or 50 mg kg^{-1} of CSC-HEDA/NO in PEG (red). Of note, mice were treated and imaged on day 5 post-wounding but not measured. **(B)** Percentage of initial wound area remaining following daily treatment with PEG (gray), 50 mg kg^{-1} of CSC-HEDA in PEG (orange), 50 mg kg^{-1} of CSC-HEDA/NO in PEG (red), 50 mg kg^{-1} of CSC-DPTA in PEG (green), or 50 mg kg^{-1} of CSC-DPTA/NO in PEG (blue). **(C)** Representative images of wounds from each treatment group. Error bars represent the standard deviation for n = 5 mice. *$p < 0.05$, **$p < 0.01$, ***$p < 0.005$.

weight); (4) CSC-DPTA in PEG (50 mg kg^{-1} body weight); and, (5) CSC-DPTA/NO in PEG (50 mg kg^{-1} body weight). As was described above, the wounds were treated immediately following wounding/infection and once daily thereafter.

Beginning on day 2 post-wounding, both NO-releasing derivatives (i.e., CSC-HEDA/NO and CSC-DPTA/NO) were providing a substantial benefit to wound healing compared to PEG-treated (control) wounds (Figure 3.29B). On days 2 and 3 post-wounding, wound closure for the NO-releasing CSC biopolymers was significantly more advanced than the PEG-treated wounds. By day 4, the CSC-HEDA/NO and CSC-DPTA/NO demonstrated significantly greater wound closure than the CSC-HEDA and CSC-DPTA controls, highlighting the benefit to NO release, especially during the early wound healing phases, due to NO's ability to clear infection. This effect corroborates what is seen endogenously, where greater concentrations of NO are present at the initial stages of wound healing to assist in the inflammatory stage.[27] On day 5-7 post-wounding, treatments with NO-releasing and control GAGs were characterized by smaller wound areas relative to PEG controls, with no significant differences observed between the controls (i.e., amine-modified) and NO-releasing GAGs. On day 6 post-wounding, PEG-treated mice still exhibited 61-72% of their initial wounding area, whereas all mice treated with the GAGs had only 21-55% of their wound areas remaining. While NO was most essential at the early stages for infection clearance, it is clear that the amine-modified GAG backbone also acts as a pro-wound healing agent itself. A portion of the early-stage success for the NO-releasing GAGs must be attributed to the bioactive biopolymer backbone. However, the role of NO is still apparent at later time points, as mice in the CSC-HEDA/NO and CSC-DPTA/NO treatment groups exhibited the most visually healed wounds at day 8 post-wounding (Figure 3.29C). At all time points, there were no significant differences between CSC-HEDA/NO and CSC-DPTA/NO, suggesting that the identity of the

GAG is more influential than the alkylamine substituent for murine wound healing. Of note, no adverse effects were observed in mice following treatment with any of the developed formulations. In all, these in vivo studies indicate that the NO-releasing GAGs exhibit pro-wound healing benefit contributions from both NO and the CS backbone.

3.3.9. In vitro migration of human skin cells

An in vitro cell migration assay was employed to evaluate potential mechanisms for the enhanced in vivo wound healing. A standard scratch assay was used to "wound" a near-monolayer of HDF or HEK prior to treatment with HA6 or CSC (unmodified, with HEDA- or DPTA-modification, or NO-releasing). The unmodified HA6 dosing of the HDF resulted in similar migration patterns as untreated cells (Figure 3.30A). While not significant, treatment of HDF with HA6-HEDA or HA6-HEDA/NO yielded migration similar to or slower than untreated cells (Figure 3.30B and C). Treatment of HDF with CSC was similar to or slightly slower than untreated cells, whereas treatment with CSC-HEDA, CSC-HEDA/NO, or CSC-DPTA/NO slowed migration further (Figure 3.30D, E, F, and H). These results suggest that the enhanced in vivo wound healing in the murine model is not the result of enhanced fibroblast migration.

Similarly, treatment of HEK scratches with GAGs also did not yield any significant changes in cell migration (Figure 3.31). The use of HA6 and HA6-HEDA/NO resulted in similar migration patterns as untreated cells, with some concentrations leading to slightly enhanced migration while others decreased migration (Figure 3.31A and C). Furthermore, treatment of HEK with CSC yielded an increase in the migration rate when treated at 100 ng mL^{-1}, 1 µg mL^{-1}, or 100 µg mL^{-1}, albeit not statistically significant (Figure 3.31D). Contrasting one another, treatment with CSC-HEDA resulted in similar or increased migration rates to untreated cells whereas treatment

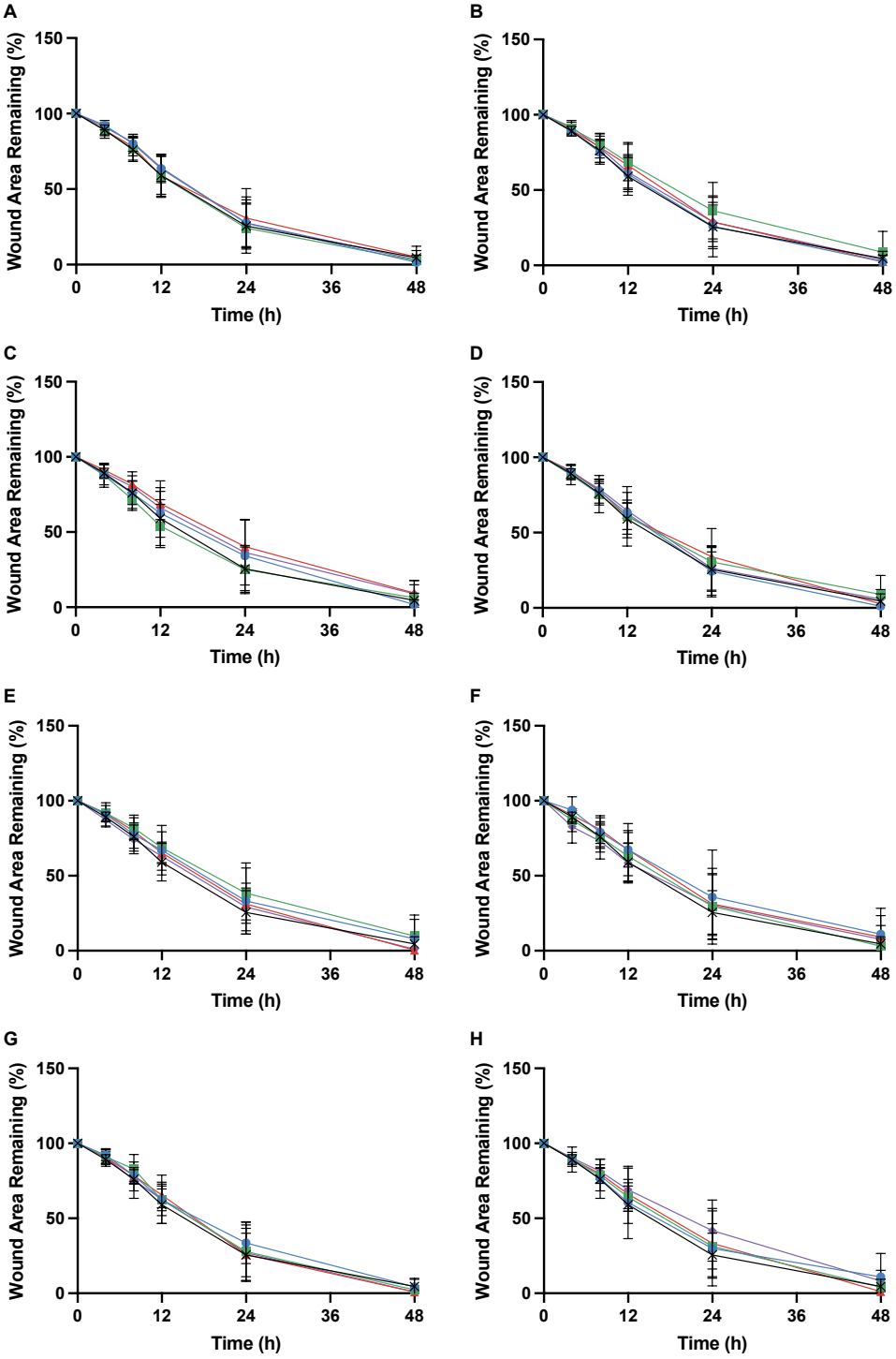

Figure 3.30 Percentage of initial in vitro wounding area remaining following treatment of human dermal fibroblasts with **(A)** HA6, **(B)** HA6-HEDA, **(C)** HA6-HEDA/NO, **(D)** CSC, **(E)** CSC-HEDA, **(F)** CSC-HEDA/NO, **(G)** CSC-DPTA, or **(H)** CSC-DPTA/NO at concentrations of 100 ng mL^{-1} (purple diamond), 1 µg mL^{-1} (red triangle), 10 µg mL^{-1} (green square), or 100 µg mL^{-1} (blue circle). All treatments are compared to untreated cells (black cross).

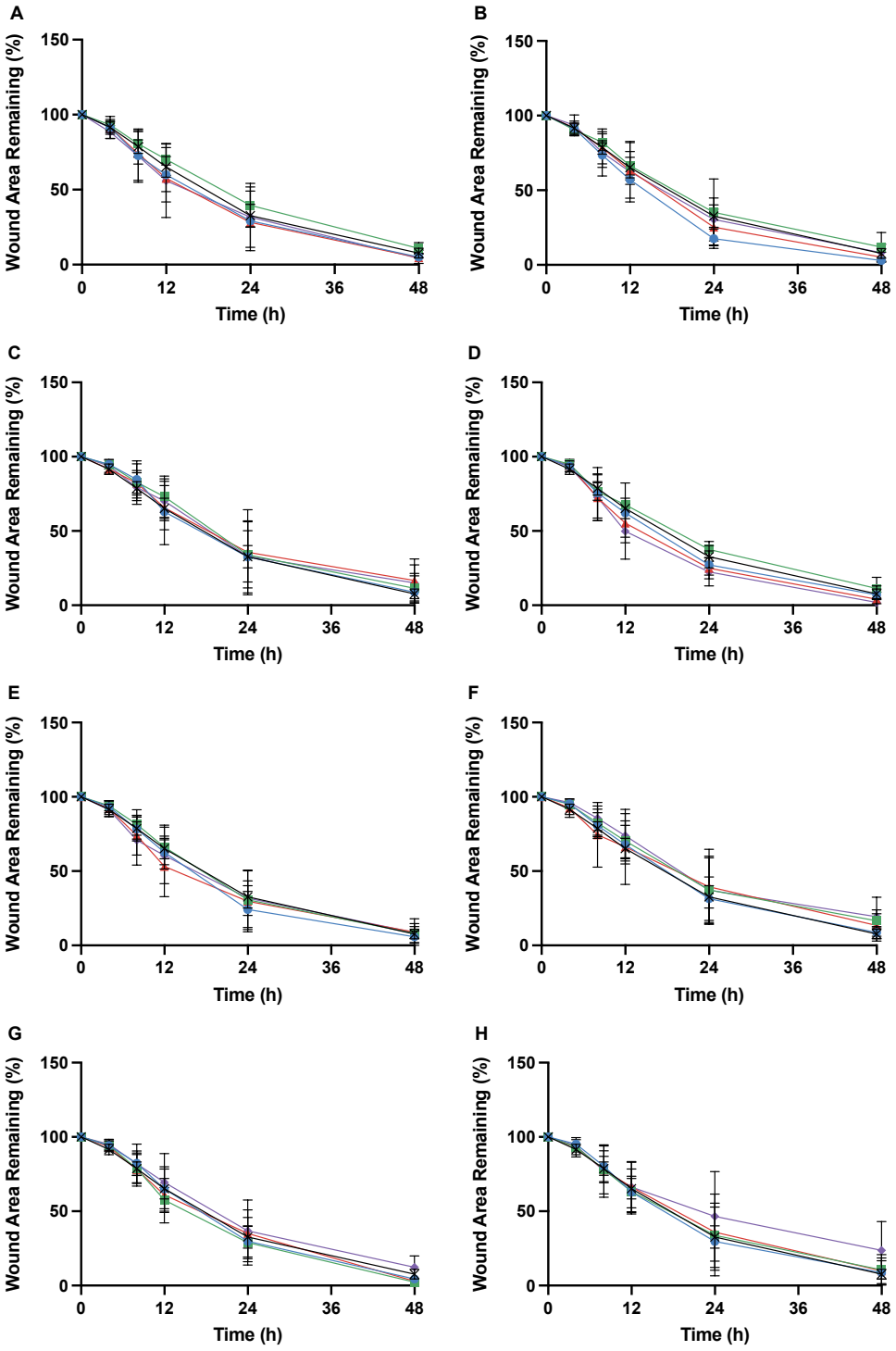

Figure 3.31 Percentage of initial in vitro wounding area remaining following treatment of human epidermal keratinocytes with **(A)** HA6, **(B)** HA6-HEDA, **(C)** HA6-HEDA/NO, **(D)** CSC, **(E)** CSC-HEDA, **(F)** CSC-HEDA/NO, **(G)** CSC-DPTA, or **(H)** CSC-DPTA/NO at concentrations of 100 ng mL^{-1} (purple diamond), 1 µg mL^{-1} (red triangle), 10 µg mL^{-1} (green square), or 100 µg mL^{-1} (blue circle). All treatments are compared to untreated cells (black cross).

with CSC-HEDA/NO facilitated similar or decreased migration rates to untreated cells (Figure 3.31E and F). Lastly, treatment of HEK with 100 ng mL^{-1} CSC-DPTA/NO seemingly slowed migration (Figure 3.31H). However, no significant trends were observed upon treatment of HEK with any GAGs. As stated for HDF migration, it is unlikely that the enhancement of wound healing observed in mice was due to increased keratinocyte migration.

3.4. Conclusions

A series of glycosaminoglycans were modified with *N*-diazeniumdiolate NO donors to store and tunably release NO in the wound environment. The role of native GAG properties (i.e., identity, molecular weight, sulfation pattern) and NO donor properties (i.e., alkylamine substituent, NO-release kinetics) were evaluated using in vitro antibacterial and wound healing assays. The results of these studies determined that DETA-modified GAG derivatives were most effective at inhibiting bacterial growth. However, DPTA-modified GAG derivatives outperformed the other two amine modifications in facilitating bacterial eradication. Bacterial eradication with NO released from these DPTA-modified compounds was not dependent on resistance mechanisms adopted by the bacteria. These materials therefore represent a promising alternative to conventional antibiotics in treating antibiotic-resistant bacterial infections. Investigation of fibroblast and keratinocyte adhesion and proliferation as a result of GAG treatment revealed trends based on the alkylamine modification, NO-release capacity, and GAG identity. These in vitro assays highlighted CSC-HEDA/NO as being the best pro-wound healing agent of the GAG derivatives. The addition of NO release to GAG scaffolds decreased their activation profiles of TLR4, a receptor found on many wound-related cells that signals for pro-inflammatory activity, suggesting that these NO-releasing GAGs may exhibit anti-inflammatory properties. An in vivo

infected murine wound model analysis of one NO-releasing HA6 and one NO-releasing CSC derivative presented CSC as a more beneficial backbone for the development of a wound healing agent. Further analysis comparing CSC-HEDA/NO, which demonstrated beneficial wound healing properties in vitro, and CSC-DPTA/NO, which was a stronger antibacterial agent, demonstrated that both significantly increased the rate at which infected murine wounds heal. Active NO release was determined to be most impactful during the initial days following wounding, whereas the CSC-HEDA and CSC-DPTA backbones were equally as effective as their NO counterparts at increasing healing rates by day 5 post-wounding, supporting the idea that wound healing benefits are coming from both active NO release and a bioactive GAG backbone. These benefits are likely not due to increased fibroblast or keratinocyte migration but are instead related to antibacterial efficacy, cell proliferation and adhesion, and anti-inflammatory activity. The combination of these beneficial properties has allowed for the development of a multi-functional antibacterial wound healing agent that demonstrates promise in addressing complications related to chronic wounds.

REFERENCES

(1) Sen, C. K.; Gordillo, G. M.; Roy, S.; Kirsner, R.; Lambert, L.; Hunt, T. K.; Gottrup, F.; Gurtner, G. C.; Longaker, M. T. Human Skin Wounds: A Major and Snowballing Threat to Public Health and the Economy. *Wound Repair Regen.* **2009**, *17*, 763–771.

(2) Sen, C. K. Human Wounds and Its Burden: An Updated Compendium of Estimates. *Adv. Wound Care* **2019**, *8*, 39–48.

(3) Järbrink, K.; Ni, G.; Sönnergren, H.; Schmidtchen, A.; Pang, C.; Bajpai, R.; Car, J. The Humanistic and Economic Burden of Chronic Wounds: A Protocol for a Systematic Review. *Syst. Rev.* **2017**, *6*, 1–7.

(4) Han, G.; Ceilley, R. Chronic Wound Healing: A Review of Current Management and Treatments. *Adv. Ther.* **2017**, *34*, 599–610.

(5) Stechmiller, J. K.; Childress, B.; Cowan, L. Arginine Supplementation and Wound Healing. **2005**, No. February 2005, 52–61.

(6) Guo, S.; DiPietro, L. A. Factors Affecting Wound Healing. *J. Dent. Res.* **2010**, *89*, 219–229.

(7) Malone-Povolny, M. J.; Maloney, S. E.; Schoenfisch, M. H. Nitric Oxide Therapy for Diabetic Wound Healing. *Adv. Healthc. Mater.* **2019**, *8*, 1801210.

(8) Gjødsbøl, K.; Christensen, J. J.; Karlsmark, T.; Jørgensen, B.; Klein, B. M.; Krogfelt, K. A. Multiple Bacterial Species Reside in Chronic Wounds: A Longitudinal Study. *Int. Wound J.* **2006**, *3*, 225–231.

(9) Bjarnsholt, T.; Kirketerp-Møller, K.; Jensen, P. Ø.; Madsen, K. G.; Phipps, R.; Krogfelt, K.; Høiby, N.; Givskov, M. Why Chronic Wounds Will Not Heal: A Novel Hypothesis. *Wound Repair Regen.* **2008**, *16*, 2–10.

(10) Percival, S. L.; Hill, K. E.; Williams, D. W.; Hooper, S. J.; Thomas, D. W.; Costerton, J. W. A Review of the Scientific Evidence for Biofilms in Wounds. *Wound Repair Regen.* **2012**, *20*, 647–657.

(11) Donlan, R. M.; Costerton, J. W. Biofilms: Survival Mechanisms of Clinically Relevant Microorganisms. *Clin. Microbiol. Rev.* **2002**, *15*, 167–193.

(12) Buch, P. J.; Chai, Y.; Goluch, E. D. Treating Polymicrobial Infections in Chronic Diabetic Wounds. *Clin. Microbiol. Rev.* **2019**, *32*, e0009.

(13) Ceri, H.; Olson, M. E.; Turner, R. J. Needed, New Paradigms in Antibiotic Development. *Expert Opin. Pharmacother.* **2010**, *11*, 1233–1237.

(14) Ventola, C. L. The Antibiotic Resistance Crisis: Part 1: Causes and Threats. *Pharm. Ther.* **2015**, *40*, 277–283.

(15) Tenover, F. C. Mechanisms of Antimicrobial Resistance in Bacteria. *Am. J. Med.* **2006**, *119*, S3-S10.

(16) Carpenter, A. W.; Schoenfisch, M. H. Nitric Oxide Release: Part II. Therapeutic Applications. *Chem. Soc. Rev.* **2012**, *41*, 3742–3752.

(17) Donnini, S.; Ziche, M. Constitutive and Inducible Nitric Oxide Synthase: Role in Angiogenesis. *Antioxidants Redox Signal.* **2002**, *4*, 817–823.

(18) Nathan, C. F.; Hibbs, J. B. Role of Nitric Oxide Synthesis in Macrophage Antimicrobial Activity. *Curr. Opin. Immunol.* **1991**, *3*, 65–70.

(19) Cirino, G.; Distrutti, E.; Wallace, J. L. Nitric Oxide and Inflammation. *Inflamm. Allergy - Drug Targets* **2006**, *5*, 115–119.

(20) Hetrick, E. M.; Shin, J. H.; Stasko, N. A.; Johnson, C. B.; Wespe, D. A.; Holmuhamedov, E.; Schoenfisch, M. H. Bactericidal Efficacy of Nitric Oxide-Releasing Silica Nanoparticles. *ACS Nano* **2008**, *2*, 235–246.

(21) Fang, F. C. Antimicrobial Reactive Oxygen and Nitrogen Species: Concepts and Controversies. *Nat. Rev. Microbiol.* **2004**, *2*, 820–832.

(22) Maloney, S. E.; McGrath, K. V.; Ahonen, M. J. R.; Soliman, D. S.; Feura, E. S.; Hall, H. R.; Wallet, S. M.; Maile, R.; Schoenfisch, M. H. Nitric Oxide-Releasing Hyaluronic Acid as an Antibacterial Agent for Wound Therapy. *Biomacromolecules* **2021**, *22*, 867–879.

(23) Ahonen, M. J. R.; Dorrier, J. M.; Schoenfisch, M. H. Antibiofilm Efficacy of Nitric Oxide-Releasing Alginates against Cystic Fibrosis Bacterial Pathogens. *ACS Infect. Dis.* **2019**, *5*, 1327–1335.

(24) Barraud, N.; Kelso, M.; Rice, S.; Kjelleberg, S. Nitric Oxide: A Key Mediator of Biofilm Dispersal with Applications in Infectious Diseases. *Curr. Pharm. Des.* **2014**, *21*, 31–42.

(25) Privett, B. J.; Broadnax, A. D.; Bauman, S. J.; Riccio, D. A.; Schoenfisch, M. H. Examination of Bacterial Resistance to Exogenous Nitric Oxide. *Nitric Oxide* **2012**, *26*, 169–173.

(26) Rouillard, K. R.; Novak, O. P.; Pistiolis, A. M.; Yang, L.; Ahonen, M. J. R.; McDonald, R. A.; Schoenfisch, M. H. Exogenous Nitric Oxide Improves Antibiotic Susceptibility in Resistant Bacteria. *ACS Infect. Dis.* **2021**, *7*, 23–33.

(27) Efron, D. T.; Most, D.; Barbul, A. Role of Nitric Oxide in Wound Healing. *Curr. Opin. Clin. Nutr. Metab. Care* **2000**, *3*, 197–204.

(28) Schairer, D. O.; Chouake, J. S.; Nosanchuk, J. D.; Friedman, A. J. The Potential of Nitric Oxide Releasing Therapies as Antimicrobial Agents. *Virulence* **2012**, *3*, 271–279.

(29) Neufeld, B. H.; Reynolds, M. M. Critical Nitric Oxide Concentration for Pseudomonas Aeruginosa Biofilm Reduction on Polyurethane Substrates. *Biointerphases* **2016**, *11*, 1–8.

(30) Cooke, J. P. NO and Angiogenesis. *Atheroscler. Suppl.* **2003**, *4*, 53–60.

(31) Morbidelli, L.; Donnini, S.; Ziche, M. Role of Nitric Oxide in the Modulation of Angiogenesis. *Curr. Pharm. Des.* **2005**, *9*, 521–530.

(32) Coleman, J. W. Nitric Oxide in Immunity and Inflammation. *Int. Immunopharmacol.* **2001**, *1*, 1397–1406.

(33) Witte, M. B.; Thornton, F. J.; Efron, D. T.; Barbul, A. Enhancement of Fibroblast Collagen Synthesis by Nitric Oxide. *Nitric Oxide - Biol. Chem.* **2000**, *4*, 572–582.

(34) Miller, C. C.; Miller, M. K.; Ghaffari, A.; Kunimoto, B. Treatment of Chronic Nonhealing Leg Ulceration with Gaseous Nitric Oxide: A Case Study. *J. Cutan. Med. Surg.* **2004**, *8*, 233–238.

(35) Ghaffari, A.; Jalili, R.; Ghaffari, M.; Miller, C.; Ghahary, A. Efficacy of Gaseous Nitric Oxide in the Treatment of Skin and Soft Tissue Infections. *Wound Repair Regen.* **2007**, *15*, 368–377.

(36) Yang, Y.; Qi, P. K.; Yang, Z. L.; Huang, N. Nitric Oxide Based Strategies for Applications of Biomedical Devices. *Biosurface and Biotribology* **2015**, *1*, 177–201.

(37) Weinberger, B.; Laskin, D. L.; Heck, D. E.; Laskin, J. D. The Toxicology of Inhaled Nitric Oxide. *Toxilogical Sci.* **2001**, *59*, 5–16.

(38) Hrabie, J. A.; Keefer, L. K. Chemistry of the Nitric Oxide-Releasing Diazeniumdiolate ("nitrosohydroxylamine") Functional Group and Its Oxygen-Substituted Derivatives. *Chem. Rev.* **2002**, *102*, 1135–1154.

(39) Keefer, L. K. Fifty Years of Diazeniumdiolate Research: From Laboratory Curiosity to Broad-Spectrum Biomedical Advances. *ACS Chem. Biol.* **2011**, *6*, 1147–1155.

(40) Dashti, N.; Ansari, M.; Shabani, M.; Vardasti, S.; Mirsalehian, A. The Effect of Nitric Oxide Donor in Diabetic Wound Healing. *Iran. J. Public Health* **2003**, *32*, 59–63.

(41) Brisbois, E. J.; Bayliss, J.; Wu, J.; Major, T. C.; Xi, C.; Wang, S. C.; Bartlett, R. H.; Handa, H.; Meyerhoff, M. E. Optimized Polymeric Film-Based Nitric Oxide Delivery Inhibits Bacterial Growth in a Mouse Burn Wound Model. *Acta Biomater.* **2014**, *10*, 4136–4142.

(42) Riccio, D. A.; Schoenfisch, M. H. Nitric Oxide Release: Part I. Macromolecular Scaffolds.

Chem. Soc. Rev. **2012**, *41*, 3731–3741.

(43) Lowe, A.; Bills, J.; Verma, R.; Lavery, L.; Davis, K.; Balkus, K. J. Electrospun Nitric Oxide Releasing Bandage with Enhanced Wound Healing. *Acta Biomater.* **2015**, *13*, 121–130.

(44) Masters, K. S. B.; Leibovich, S. J.; Belem, P.; West, J. L.; Poole-Warren, L. A. Effects of Nitric Oxide Releasing Poly(Vinyl Alcohol) Hydrogel Dressings on Dermal Wound Healing in Diabetic Mice. *Wound Repair Regen.* **2002**, *10*, 286–295.

(45) Melrose, J. Glycosaminoglycans in Wound Healing. *Bone Tissue Regen. Insights* **2016**, *7*, 29–50.

(46) Aya, K. L.; Stern, R. Hyaluronan in Wound Healing: Rediscovering a Major Player. *Wound Repair Regen.* **2014**, *22*, 579–593.

(47) Fallacara, A.; Baldini, E.; Manfredini, S.; Vertuani, S. Hyaluronic Acid in the Third Millennium. *Polymers* **2018**, *10*, 701.

(48) Zhao, L.; Liu, M.; Wang, J.; Zhai, G. Chondroitin Sulfate-Based Nanocarriers for Drug / Gene Delivery. *Carbohydr. Polym.* **2015**, *133*, 391–399.

(49) Schiraldi, C.; Cimini, D.; De Rosa, M. Production of Chondroitin Sulfate and Chondroitin. *Appl. Microbiol. Biotechnol.* **2010**, *87*, 1209–1220.

(50) Graça, M. F. P.; Miguel, S. P.; Cabral, C. S. D.; Correia, I. J. Hyaluronic Acid — Based Wound Dressings : A Review. *Carbohydr. Polym.* **2020**, *241*, 116364.

(51) Yang, H.; Song, L.; Zou, Y.; Sun, D.; Wang, L.; Yu, Z.; Guo, J. Role of Hyaluronic Acids and Potential as Regenerative Biomaterials in Wound Healing. *ACS Appl. Bio Mater.* **2020**, *4*, 311–324.

(52) Hussain, Z.; Thu, H. E.; Katas, H.; Nasir, S.; Bukhari, A.; Bukhari, S. N. A. Hyaluronic Acid-Based Biomaterials: A Versatile and Smart Approach to Tissue Regeneration and Treating Traumatic, Surgical, and Chronic Wounds. *Polym. Rev.* **2017**, *57*, 594–630.

(53) Gao, F.; Liu, Y.; He, Y.; Yang, C.; Wang, Y.; Shi, X.; Wei, G. Hyaluronan Oligosaccharides Promote Excisional Wound Healing through Enhanced Angiogenesis. *Matrix Biol.* **2010**, *29*, 107–116.

(54) Tolg, C.; Telmer, P.; Turley, E. Specific Sizes of Hyaluronan Oligosaccharides Stimulate Fibroblast Migration and Excisional Wound Repair. *PLoS One* **2014**, *9*, 1–10.

(55) Sattar, A.; Rooney, P.; Kumar, S.; Pye, D.; West, D. C.; Scott, I.; Ledger, P. Application of Angiogenic Oligosaccharides of Hyaluronan Increases Blood Vessel Numbers in Rat Skin. *J. Invest. Dermatol.* **1994**, *103*, 576–579.

(56) Vazquez, J. R.; Short, B.; Findlow, A. H.; Nixon, B. P.; Boulton, A. J. M.; Armstrong, D. G. Outcomes of Hyaluronan Therapy in Diabetic Foot Wounds. *Diabetes Res. Clin. Pract.* **2003**, *59*, 123–127.

(57) Hong, L.; Shen, M.; Fang, J.; Wang, Y.; Bao, Z.; Bu, S.; Zhu, Y. Hyaluronic Acid (HA)-Based Hydrogels for Full-Thickness Wound Repairing and Skin Regeneration. *J. Mater. Sci. Mater. Med.* **2018**, *29*, 1–11.

(58) Corsuto, L.; Rother, S.; Koehler, L.; Bedini, E.; Moeller, S.; Schnabelrauch, M.; Hintze, V.; Schiraldi, C.; Scharnweber, D. Sulfation Degree Not Origin of Chondroitin Sulfate Derivatives Modulates Keratinocyte Response. *Carbohydr. Polym.* **2018**, *191*, 53–64.

(59) Mikami, T.; Kitagawa, H. Biosynthesis and Function of Chondroitin Sulfate. *Biochim. Biophys. Acta - Gen. Subj.* **2013**, *1830*, 4719–4733.

(60) Lamari, F. N. The Potential of Chondroitin Sulfate as a Therapeutic Agent. *Connect. Tissue Res.* **2008**, *49*, 289–292.

(61) Kirker, K. R.; Luo, Y.; Nielson, J. H.; Shelby, J.; Prestwich, G. D. Glycosaminoglycan Hydrogel Films as Bio-Interactive Dressings for Wound Healing. *Biomaterials* **2002**, *23*, 3661–3671.

(62) Gilbert, M. E.; Kirker, K. R.; Gray, S. D.; Ward, P. D.; Szakacs, J. G.; Prestwich, G. D.; Orlandi, R. R. Chondroitin Sulfate Hydrogel and Wound Healing in Rabbit Maxillary Sinus Mucosa. *Laryngoscope* **2004**, *114*, 1406–1409.

(63) Pal, D.; Saha, S. Chondroitin: A Natural Biomarker with Immense Biomedical Applications. *RSC Adv.* **2019**, *9*, 28061–28077.

(64) Zou, X. H.; Foong, W. C.; Cao, T.; Bay, B. H.; Ouyang, H. W.; Yip, G. W. Chondroitin Sulfate in Palatal Wound Healing. *J. Dent. Res.* **2004**, *83*, 880–885.

(65) Zou, X. H.; Jiang, Y. Z.; Zhang, G. R.; Jin, H. M.; Hieu, N. T. M.; Ouyang, H. W. Specific Interactions between Human Fibroblasts and Particular Chondroitin Sulfate Molecules for Wound Healing. *Acta Biomater.* **2009**, *5*, 1588–1595.

(66) Kwon, H. J.; Han, Y. Chondroitin Sulfate-Based Biomaterials for Tissue Engineering. *Turkish J. Biol.* **2016**, *40*, 290–299.

(67) Scharnweber, D.; Hübner, L.; Rother, S.; Hempel, U.; Anderegg, U.; Samsonov, S. A.; Pisabarro, M. T.; Hofbauer, L.; Schnabelrauch, M.; Franz, S.; Simon, J.; Hintze, V. Glycosaminoglycan Derivatives: Promising Candidates for the Design of Functional Biomaterials. *J. Mater. Sci. Mater. Med.* **2015**, *26*, 232.

(68) Vigani, B.; Rossi, S.; Sandri, G.; Bonferoni, M. C.; Caramella, C. M.; Ferrari, F. Hyaluronic Acid and Chitosan-Based Nanosystems: A New Dressing Generation for Wound Care.

Expert Opin. Drug Deliv. **2019**, *16*, 715–740.

(69) Ahonen, M. J. R.; Suchyta, D. J.; Zhu, H.; Schoenfisch, M. H. Nitric Oxide-Releasing Alginates. *Biomacromolecules* **2018**, *19*, 1189–1197.

(70) Jin, H.; Yang, L.; Ahonen, M. J. R.; Schoenfisch, M. H. Nitric Oxide-Releasing Cyclodextrins. *J. Am. Chem. Soc.* **2018**, *140*, 14178–14184.

(71) Sutton, S. Accuracy of Plate Counts. *J. Valid. Technol.* **2011**, *17*, 42–46.

(72) IUL. Eddy Jet 2 User's Guide. 2012, pp 1–50.

(73) Kucik, D. F.; Wu, C. Cell-Adhesion Assays. In *Cell Migration: Developmental Methods and Protocols*; Humana Press Inc.: Totowa, New Jersey, 2005; pp 43–54.

(74) Jain, S.; Ohman, D. E. Role of an Alginate Lyase for Alginate Transport in Mucoid Pseudomonas Aeruginosa. *Infect. Immun.* **2005**, *73*, 6429–6436.

(75) Souza, A. G.; Silva, I. B. B.; Campos-Fernandez, E.; Barcelos, L. S.; Souza, J. B.; Marangoni, K.; Goulart, L. R.; Alonso-Goulart, V. Comparative Assay of 2D and 3D Cell Culture Models: Proliferation, Gene Expression and Anticancer Drug Response. *Curr. Pharm. Des.* **2018**, *24*, 1689–1694.

(76) Joseph, J. S.; Malindisa, S. T.; Ntwasa, M. Two-Dimensional (2D) and Three-Dimensional (3D) Cell Culturing in Drug Discovery. In *Cell Culture*; 2019; pp 21–42.

(77) Desjardins-Park, H. E.; Foster, D. S.; Longaker, M. T. Fibroblasts and Wound Healing: An Update. *Regen. Med.* **2018**, *13*, 491–495.

(78) Pastar, I.; Stojadinovic, O.; Yin, N. C.; Ramirez, H.; Nusbaum, A. G.; Sawaya, A.; Patel, S. B.; Khalid, L.; Isseroff, R. R.; Tomic-Canic, M. Epithelialization in Wound Healing: A Comprehensive Review. *Adv. Wound Care* **2014**, *3*, 445–464.

(79) Chen, L.; Dipietro, L. A. Toll-like Receptor Function in Acute Wounds. *Adv. Wound Care* **2017**, *6*, 344–355.

(80) Stabler, T. V.; Huang, Z.; Montell, E.; Vergés, J.; Kraus, V. B. Chondroitin Sulphate Inhibits NF-KB Activity Induced by Interaction of Pathogenic and Damage Associated Molecules. *Osteoarthr. Cartil.* **2017**, *25*, 166–174.

(81) Park, B. S.; Lee, J. O. Recognition of Lipopolysaccharide Pattern by TLR4 Complexes. *Exp. Mol. Med.* **2013**, *45*, e66.

(82) Moresco, E. M. Y.; LaVine, D.; Beutler, B. Toll-like Receptors. *Curr. Biol.* **2011**, *21*, R488–R493.

CHAPTER 4: NITRIC OXIDE-RELEASING HEMODIALYSIS CATHETER LOCK SOLUTIONS

4.1. Introduction

Tunneled dialysis catheters (TDCs) are frequently employed for hemodialysis access as they can be utilized immediately upon placement. Most often, TDCs are utilized for temporary access in patients waiting for arteriovenous fistulas and grafts to mature. However, TDCs may be necessary for long-term use in patients without a suitable vein for a fistula or graft.[1,2] Roughly 80% of dialysis patients begin with a TDC, making them an essential part of dialysis access despite many associated shortcomings.[1,3] Tunneled dialysis catheters are more prone to infection, thrombosis, and stenosis than other access types (e.g., fistulas and grafts),[1,2] necessitating the development of prevention and treatment strategies targeted at these major complications.

Upon TDC placement, the catheter surface is rapidly coated with extracellular matrix proteins and immune proteins.[4,5] This protein coating facilitates the adhesion of bacteria and also triggers a coagulation cascade, resulting in the formation of a thrombus.[4,6] Both infection and thrombosis can result in catheter failure. Infection is the second leading cause of mortality in dialysis patients, accounting for 15-20% of deaths.[1,7] Biofilms, or cooperative communities of bacteria encased in a self-secreted exopolysaccharide (EPS) matrix, can form on the catheter surface in as few as 3 d after implantation.[5] Biofilms are responsible for the persistence of catheter-related infections and are a source of bacterial dissemination to other sites in the body, with both Gram-positive (e.g., *Staphylococcus epidermidis*, *Staphylococcus aureus*, and *Enterococcus faecalis*) and Gram-negative (e.g., *Pseudomonas aeruginosa*, *Escherichia coli*, and *Klebsiella*

spp.) bacteria associated with catheter-related bloodstream infections.[4,8–10] Not only can biofilm formation lead to systemic infections, the presence of bacteria are associated with an increased risk of heart failure, stroke, and peripheral vascular disease.[10] Thrombosis presents an equally significant challenge in maintaining hemodialysis access through a TDC. Thrombosis occurs frequently in patients with a TDC, either within the catheter (e.g., intraluminally) or within the vein in which the catheter is placed.[11,12] Depending on the location of the thrombus, dialysis access may be hindered due to occlusion.[11,13]

Current strategies for mitigating catheter-related complications are insufficient and nearly always target only a single problem (i.e., thrombosis or infection). Thrombosis is most frequently prevented with local administration of anticoagulants (e.g., heparin lock solutions), but treatment strategies for removing existing thrombi are limited and usually necessitate catheter removal.[1,6,12,14] Infection is typically addressed by catheter removal and/or with antimicrobials or antiseptics administered topically, systemically, or within/on the surface of the catheter itself, through the surface immobilization of antimicrobials, the incorporation of antimicrobials within the catheter material, or as intraluminal lock solutions.[1,5,10,11,15] The use of antibiotic/antiseptic lock solutions has garnered much interest due to the potential for incorporation within current clinical practices. Lock solutions for infection control have been reported using gentamicin,[16–19] vancomycin,[20,21] cefotaxime,[22] cefazolin,[19,20] ceftazidime,[20] minocycline,[18] citrate,[23–25] taurolidine,[23,26] and ethanol.[27,28] While a reduction in catheter-related infections has been demonstrated with many such antimicrobial lock systems, concerns surrounding these strategies include the potential to promote bacterial resistance as well as leakage of cytotoxic antibiotics/antiseptics from the catheter tip.[10] In order to maintain efficacy while minimizing potential complications, the use of more biocompatible antimicrobial agents that are unlikely to

promote bacterial resistance are necessary. In addition to possessing antimicrobial action, the use of a lock solution that also prevents thrombosis would allow for both major complications to be addressed with a single agent.

Nitric oxide (NO), an endogenous signaling molecule, possesses these attributes, and NO-release lock solutions may represent a potential new strategy for improving the performance of TDCs. Nitric oxide exerts broad-spectrum antimicrobial action through oxidative and nitrosative stresses.[29] Reaction with oxygen and superoxide (byproducts of bacterial metabolism) lead to the production of dinitrogen trioxide and peroxynitrite, respectively, initiating DNA damage, thiol nitrosation, and destruction of the bacterial membrane.[29,30] Most importantly, bacterial resistance to NO has not been observed and is unlikely to due to the above multiple mechanisms of action.[31,32] As an additional benefit, NO can prevent thrombosis.[6] Endothelial cells that line the inner wall of blood vessels produce NO at a surface flux of 0.8-6.8 pmol cm^{-2} s^{-1} to facilitate blood vessel dilation and prevent platelet activation/thrombosis.[33,34] The formation of thrombi on medical surfaces may be prevented by mimicking such surface NO flux.

Due to NO's roles in mitigating infection and thrombosis, researchers have sought to develop NO-releasing biomedical devices.[6,35,36] Related to catheters, multiple studies have incorporated NO donors within or attached to the catheter surface with promising trends in decreasing infection and thrombosis.[34,37–42] However, these strategies are only effective so long as NO release is maintained. Replenishable NO sources, such as nitric oxide-releasing lock solutions, are therefore advantageous. To date, only one NO-based lock solution study has been reported, where antibacterial NO levels and performance were maintained for at least 18 h. However, the prevention of bacterial adhesion was only reported for up to 18 h, and longer prevention time frames (48-72 h) would be more desirable.[43]

Herein, we describe the preparation of NO-releasing lock solutions with tunable NO-release profiles and active NO-release durations of at least 72 h. In order to maximize efficacy and clinical translatability, physiologically relevant nitric oxide concentrations (i.e., >0.8-6.8 pmol cm^{-2} s^{-1} as produced by eNOS), to prevent thrombosis,[33,34] or greater, to promote antibacterial action, must be maintained for 72 h, as lock solutions are changed every 48-72 h between dialysis sessions. By varying the concentration and release profile of NO from the catheter surface, we evaluated the role of NO-release properties on bacterial adhesion, mammalian cell toxicity, and protein adsorption using in vitro methods. A porcine hemodialysis catheter model is underway to determine in vivo efficacy in preventing infection, thrombosis, and stenosis.

4.2. Materials and methods

4.2.1. Materials

Diethylenetriamine (DETA), bis(3-aminopropyl)amine (DPTA), and phenazine methosulfate (PMS) were purchased from MilliporeSigma (Burlington, MA). Dulbecco's modified Eagle's medium (DMEM), trypsin, penicillin streptomycin (PS), fetal bovine serum (FBS), sodium dodecyl sulfate (SDS), Pierce™ BCA protein assay kit, LC/MS grade formic acid, LC/MS grade acetonitrile, LC/MS grade water, and common laboratory salts and solvents were purchased from Fisher Scientific (Fair Lawn, NJ). 3-(4,5-dimethylthizol-2-yl)-5-(3-carboxymethoxyphenyl)-2-(4-sulfophenyl)-2H-tetrazolium inner salt (MTS) was purchased from Biovision (Milpitas, CA). Tryptic soy broth (TSB), tryptic soy agar (TSA), and Hickman® 13.5 F dual-lumen long-term hemodialysis catheters were obtained from Becton, Dickinson, and Company (Franklin Lakes, NJ). *Staphylococcus epidermidis* (*S. epidermidis*, ATCC 12228), *Pseudomonas aeruginosa* (*P. aeruginosa*, ATCC 47085), and Vero C1008 cells (ATCC CRL-

1586™) were purchased from the American Type Culture Collection (Manassas, VA). Nitrogen (N_2), oxygen (O_2), carbon dioxide (CO_2), pure nitric oxide (NO; 99.5%), and NO calibration gas (25.87 ppm balance N_2) were obtained from Airgas National Welders (Raleigh, NC). Distilled water was purified to a resistivity of 18.2 MΩ·cm and a total organic content of ≤6 ppb using a Millipore Milli-Q UV Gradient A10 system (Bedford, MA).

4.2.2. Synthesis of NO donors (DETA/NO and DPTA/NO)

Diethylenetriamine and bis(3-aminopropyl)amine were dissolved in anhydrous acetonitrile at 50 mg mL^{-1}. Each solution (50 mL) was placed into Teflon cups within Parr hydrogenation reaction vessels with magnetic stirring. Vessels were purged with argon a total of six times (three 10-s purges followed by three 10-min purges) to remove dissolved oxygen prior to being pressurized with 15 bar NO for 72 h. Following the reaction, the same argon purging procedure was utilized to remove unreacted NO. The *N*-diazeniumdiolate-functionalized amines (i.e., DETA/NO and DPTA/NO), which precipitated as a white solid, were collected via centrifugation and washed with cold diethyl ether to remove acetonitrile and unreacted amines. The powders were dried in vacuo to remove residual solvent and stored in sealed vials at -20 °C. Attenuated total reflection Fourier transform infrared spectroscopy (ATR-FTIR) was performed using a Nicolet iS50 FTIR Spectrometer (Thermo Fisher Scientific; Fair Lawn, NJ). ^{1}H and ^{13}C nuclear magnetic resonance (NMR) spectra were recorded on a Bruker (600 MHz) spectrometer (Billerica, MA). Representative ^{1}H and ^{13}C NMR of the NO donors included the following peaks: DETA/NO: ^{1}H NMR (D_2O, 600 MHz, δ) 2.62 (t, 4H), 3.03 (t, 4H). ^{13}C NMR (D_2O, 600 MHz, δ) 37.3, 55.2. DPTA/NO: ^{1}H NMR (D_2O, 600 MHz, δ) 1.45 (quint, 4H), 2.62 (t, 4H), 2.92 (t, 4H). ^{13}C NMR (D_2O, 600 MHz, δ) 29.0, 38.4, 51.8.

4.2.3. Preparation of NO-releasing lock solutions

Nitric oxide donors (DETA/NO or DPTA/NO) were dissolved in sterile pH 7.4 phosphate buffered saline (PBS; 10 mM) at 25-75 mg mL^{-1} of total NO donor content. The pH of the solution was corrected to pH 7.4 using 5 M HCl. To ensure sterility, solutions were filtered through 0.22-μm syringe filters into sterile 10 mL vials. For each experiment, 3.9 mL of a control (PBS) lock solution or an NO-releasing lock solution was added to Hickman® dual-lumen hemodialysis catheter, with 1.9 mL added to the red lumen and 2.0 mL added to the blue lumen.

4.2.4. Analysis of NO-release properties

Nitric oxide release was monitored in real time using a Sievers 280i Nitric Oxide Analyzer (NOA; Boulder, CO). The NOA was calibrated with air passed through a NO zero filter (0 ppm NO) and 25.87 ppm NO calibration gas (balance N_2) prior to analysis. In a typical experiment for analyzing the native NO-releasing materials, 1-2 mg of NO donor was introduced into a round-bottom flask containing 30 mL deoxygenated PBS (10 mM, pH 7.4, 37 °C). The solution was purged with nitrogen gas at a flow rate of 200 mL min^{-1} to carry liberated NO into the instrument. The analysis was terminated when NO levels fell below the quantification limit of the instrument normalized to the mass of NO donor (10 ppb NO mg^{-1} NO donor).

To monitor NO released from the catheter surface (via NO diffusion through the catheter), the middle portion (excluding both the tip and hub ends of the catheter) of the Hickman® dual-lumen hemodialysis catheter was placed in a 100-mL three-neck flask containing 60 mL of deoxygenated PBS (10 mM, pH 7.4, 37 °C) (Figure 4.1). Catheters were filled with the NO-releasing catheter lock solutions at NO donor concentrations of 25 or 50 mg mL^{-1}. Analysis of NO

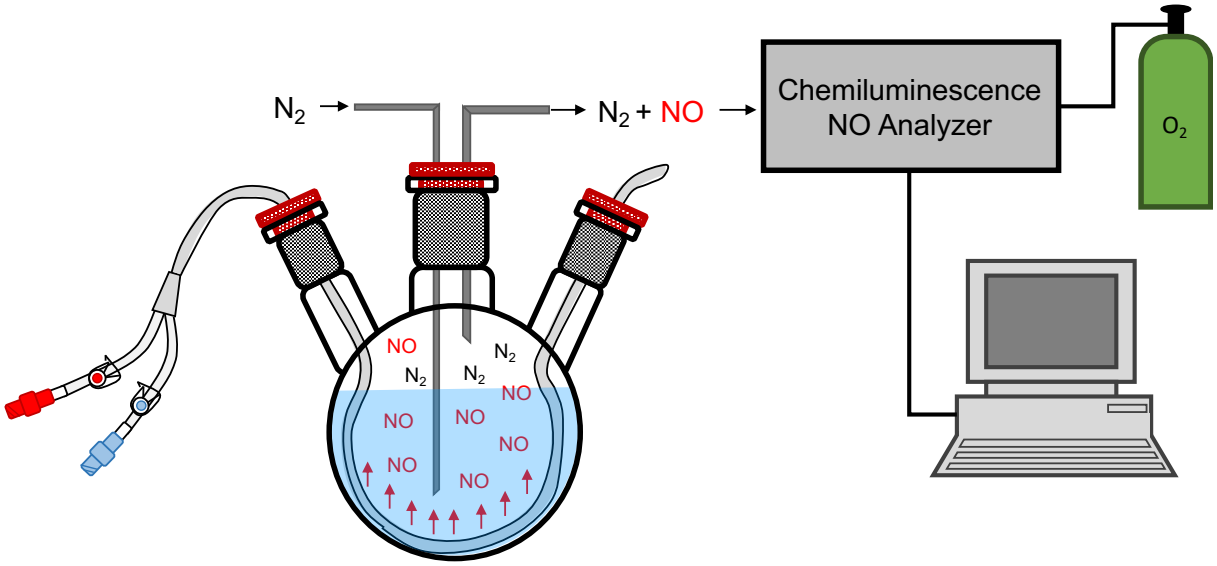

Figure 4.1 Analysis of surface NO flux using a chemiluminescent nitric oxide analyzer. Catheters are partially submerged in pH 7.4 PBS (10 mM, 37 °C).

release was terminated at 72 h to simulate the use of the catheter lock solutions between hemodialysis events. Of note, the NO flux did not reach levels below the quantification limit of the instrument (10 ppb NO) during the 72-h experiment duration.

4.2.5. Analysis of NO donor diffusion through catheter surface

Hickman® dual-lumen catheters were filled with either a control solution (PBS only) or an NO-releasing catheter lock solution (25 or 50 mg mL^{-1}) with the middle portion of the catheter (excluding both the tip and hub ends of the catheter) placed into a 50-mL conical tube containing 30 mL LC/MS grade water. An aliquot of the catheter extract solution (1.5 mL) was removed after 24, 48, and 72 h to monitor for leaching of the NO donors from the catheter. Extract samples were collected from n=3 separate catheters/experiments. The presence of DETA or DPTA in the aliquots was assessed using HPLC (Agilent Technologies 1260 Infinity II LC System; Santa Clara, CA) and a single quadrupole mass spectrometer detector (MSD; Agilent Technologies Infinity Lab 6125 MSD, Santa Clara, CA). Standards of DETA and DPTA ranging from 0.8-100 μg mL^{-1} were prepared in LC/MS grade water to create a calibration curve. The aliquots and standards were analyzed using a Synergi 4 μm Hydro-RP column (250 x 4.6 mm; Phenomenex; Torrance, CA) and a mobile phase composed of 95:5 (v/v) water:acetonitrile with 0.1 vol% formic acid at a flow rate of 1 mL min^{-1}. Elution was monitored via MSD. The optimized electrospray ionization parameters included: a fragmentor voltage of 80 V for DETA and 110 V for DPTA; a capillary voltage of 2,500 V; a drying gas temperature of 350°C; a drying gas flow rate of 12.0 L/min; and, a nebulizer pressure of 35 psig. Selected ion monitoring was used for the quantification of each analyte. Using these parameters, the limits of quantification for DETA and DPTA were found to be 1.6 μg mL^{-1} and 0.8 μg mL^{-1}, respectively.

4.2.6. Bacterial adhesion inhibition assay

Prior to each experiment, catheters were washed copiously with 70 vol% ethanol (both inside the lumens and on the surface), soaked in 70% ethanol for a minimum of 18 h, and exposed to UV radiation for a minimum of 30 min to ensure sterilization. Bacteria cultures of *P. aeruginosa* and *S. epidermidis* were grown from frozen (-80 °C) stock solutions on TSA plates. Colonies were isolated from the TSA plate, resuspended in TSB (5 mL), and incubated at 37 °C overnight with vigorous (250 rpm) shaking. An aliquot (1 mL) of the overnight solution was resuspended in fresh TSB (30 mL), grown to a concentration of 10^8 CFU mL^{-1}, and subsequently diluted to 10^6 CFU mL^{-1} in 30 mL PBS (10 mM, pH 7.4) in a 50-mL conical tube. Hickman® dual-lumen hemodialysis catheters were filled with either a control solution (PBS only) or an NO-releasing solution (25-75 mg mL^{-1} NO donor in 10 mM PBS). The middle portion of the catheters (excluding both the tip and hub ends) were placed into the 50-mL conical tube containing 10^6 CFU mL^{-1} bacteria. Catheters were soaked in the bacteria solution for 1, 4, or 48 h with gentle shaking (100 rpm) at 37 °C. Following incubation, catheters were removed from the bacteria solution, rinsed twice in conical tubes containing PBS to remove non-adhered bacteria, and placed in a conical tube containing 30 mL of fresh PBS. The catheter-containing tube was gently sonicated for 10 min and vortexed to liberate adhered bacteria into the solution. The PBS solution containing collected bacteria and its 10- and 100-fold dilutions were spiral plated on TSA plates using an Eddy Jet spiral plater (IUL; Farmingdale, NY) and incubated overnight at 37 °C. The concentration of bacteria adhered to the catheter was quantified using a Flash & Go colony counter (IUL; Farmingdale, NY) relative to the surface area of the catheter exposed to the bacteria solution. The limit of detection for this counting method is 4×10^2 CFU cm^{-2} (based on the surface area of the catheter in the soak solution).[44,45] Percent reduction in bacterial adhesion upon NO treatment

compared to catheters without the NO lock solution was calculated using Eq. 1, where A_{PBS} represents bacteria adhered to the PBS-filled catheters and A_{NO} represents bacteria adhered to the NO-releasing catheters.

$$\text{Percent reduction} = \frac{(A_{PBS} - A_{NO})}{A_{PBS}} \times 100\% \quad \text{(Eq. 1)}$$

4.2.7. Removal of pre-adhered bacteria

Prior to each experiment, catheters were sterilized as described above. Overnight bacteria cultures of *P. aeruginosa* and *S. epidermidis* were grown as described above for the adhesion inhibition assay. An aliquot (1 mL) of the overnight solution was resuspended in fresh TSB (30 mL), grown to a concentration of 10^8 CFU mL^{-1}, and subsequently diluted to 10^6 CFU mL^{-1} in 30 mL TSB in a 50-mL conical tube. Hickman® dual-lumen hemodialysis catheters were filled with PBS. The middle portion of the catheters (excluding both the tip and hub ends) were placed into the 50-mL conical tube containing 10^6 CFU mL^{-1} bacteria in TSB. After 24-h incubation with gentle shaking (100 rpm) to facilitate bacterial adhesion, catheters were removed from the bacteria growth solution, gently rinsed twice in PBS to remove non-adhered bacteria, and placed in a 50-mL conical tube containing 30 mL of PBS. Nitric oxide-releasing lock solutions were prepared as described above. The PBS within the catheters was replaced with either a fresh control solution (PBS only) or a NO-releasing catheter lock solution (25 or 50 mg mL^{-1} NO donor). Catheters were incubated for 48 h with gentle shaking (100 rpm) at 37 °C. Following treatment, catheters were removed from the solution, rinsed twice in conical tubes containing PBS to remove non-adhered bacteria, and placed in a conical tube containing 30 mL of fresh PBS. The catheter-containing tube was gently sonicated for 10 min and vortexed to liberate adhered bacteria into the solution. The

PBS solution containing collected bacteria and its 10- and 100-fold dilutions were spiral plated on TSA plates using an Eddy Jet spiral plater (IUL; Farmingdale, NY) and incubated overnight at 37 °C. The concentrations of bacteria remaining adhered to the catheter were determined using a Flash & Go colony counter (IUL; Farmingdale, NY) and normalized to the surface area of the catheter that was soaked in the bacteria solution. The limit of detection for this counting method is 4 x 10^2 CFU cm^{-2}.[44,45] Percent reduction in catheter surface bacterial adhesion was calculated using Eq. 1.

4.2.8. Surface antifouling test

Prior to each experiment, catheters were sterilized as described for the adhesion inhibition assay (see above). Hickman® dual-lumen hemodialysis catheters were filled with either a control solution (PBS only) or an NO-releasing catheter lock solution (25 or 50 mg mL^{-1} NO donor). The middle portion of the catheter (excluding both the tip and hub ends) was placed into a 50-mL conical tube containing 30 mL of 50 vol% fetal bovine serum (in PBS). The catheters were incubated at 37 °C with gentle shaking (100 rpm) for 24 h. Following incubation, the catheters were rinsed twice with PBS and placed in a conical tube containing 30 mL of 10 mg mL^{-1} SDS in PBS. The catheters in SDS were gently shaken (100 rpm) at 37 °C for 2 h and then sonicated briefly (10 min). An aliquot of the SDS solution containing detached protein (0.1 mL) was mixed with BCA protein assay kit reagent (2 mL) and incubated for 30 min at 60 °C. Protein concentrations were calculated using the absorbance measured at 562 nm and a standard calibration curve as specified in the kit. The limit of quantification for this method was 4.5 ± 2.4 μg protein cm^{-2}.

4.2.9. Elution cytotoxicity assay

Prior to each experiment, catheters were sterilized as described for the adhesion inhibition assay (see above). Hickman® dual-lumen hemodialysis catheters were filled with either a control solution (PBS only) or an NO-releasing catheter lock solution (25 or 50 mg mL^{-1} NO donor). The middle portion of the catheter (excluding both the tip and hub ends) was placed into a 50-mL conical tube containing 30 mL DMEM supplemented with 10 vol% FBS and 1 wt% PS. The catheter-containing solutions were incubated at 37 °C with gentle shaking (100 rpm) for 72 h. An aliquot of the catheter extract solution (500 μL) was removed after 24, 48, and 72 h and immediately frozen at -20 °C. Extract samples were collected from n = 3 separate experiments. Vero cells were grown in DMEM supplemented with 10 vol% FBS and 1 wt% PS in 5 vol% CO_2 under humidified conditions at 37 °C. After reaching 80% confluency, a cell suspension of 1 x 10^5 cells mL^{-1} was prepared, and 100 μL was added to each well of a 96-well plate. After 24-h incubation at 37 °C, the supernatant was aspirated and replaced with 100 μL of fresh media or catheter extract. The cultures were then incubated for 24 h at 37 °C. Following exposure, the supernatant was aspirated, and the cells were washed with PBS. A 100-μL mixture of DMEM/MTS/PMS (105/20/1, v/v/v) was added to each well and incubated for 90 min at 37 °C. The absorbance of the solution in each well was measured at 490 nm using a Molecular Devices SpectraMax M2 spectrophotometer (San Jose, CA). A blank mixture of growth medium/MTS/PMS and cells cultured with fresh media (no extract) were used as the blank and control, respectively. Cell viability for each sample was calculated using Eq. 2.

$$\%\ \text{cell viability} = \frac{(Abs_{490,sample} - Abs_{490,blank})}{(Abs_{490,control} - Abs_{490,blank})} \times 100\% \qquad \text{(Eq. 2)}$$

4.2.10. Statistical analysis

Nitric oxide-release measurements on NO donors prior to use in lock solutions are presented as the average ± standard deviation for $n \geq 3$ separate synthesis batches. Nitric oxide-release measurements from the catheter surface are presented as the average ± standard deviation for $n \geq 3$ individually prepared lock solutions. For catheter surface NO measurements, the half-life of NO release was estimated based on first-order kinetics using a Michaelis-Menten fit in GraphPad Prism 9. Bacterial/biofilm adhesion results are depicted as the average ± standard deviation for $n \geq 3$ separate experiments with bacteria grown on different days. Cell elusion toxicity, protein adhesion, and NO donor diffusion studies are presented as the average ± standard deviation for $n \geq 3$ separate experiments. Significance testing for protein adhesion was performed via a two-tailed Student's *t*-test, with $p < 0.05$ used as the threshold for statistical significance.

4.3. Results and discussion

4.3.1. Preparation and NO release characterization of lock solutions

N-diazeniumdiolate NO donors, DPTA/NO and DETA/NO, were synthesized via exposure to high pressure gaseous NO under alkaline conditions. Successful formation of the NO donor moiety was confirmed using FTIR, ^{1}H NMR, and ^{13}C NMR (Figures 4.2, 4.3, and 4.4). Peaks were observed in the FTIR spectra (Figure 4.2) of DPTA/NO and DETA/NO consistent with *N*-diazeniumdiolate formation, including N-O stretching (1230 cm^{-1} and 1185-1195 cm^{-1}), N-N stretching (1100 cm^{-1}), and in-plane N2 symmetric stretching (1150 cm^{-1} and 975-980 cm^{-1}).[46–48] Integration of peaks in the ^{1}H NMR spectra suggested a >94% conversion from small molecule amines DETA and DPTA to NO-releasing DETA/NO and DPTA/NO, respectively (Figure 4.3). Indeed, this conversion efficiency is supported by the near-theoretical NO payloads achieved from

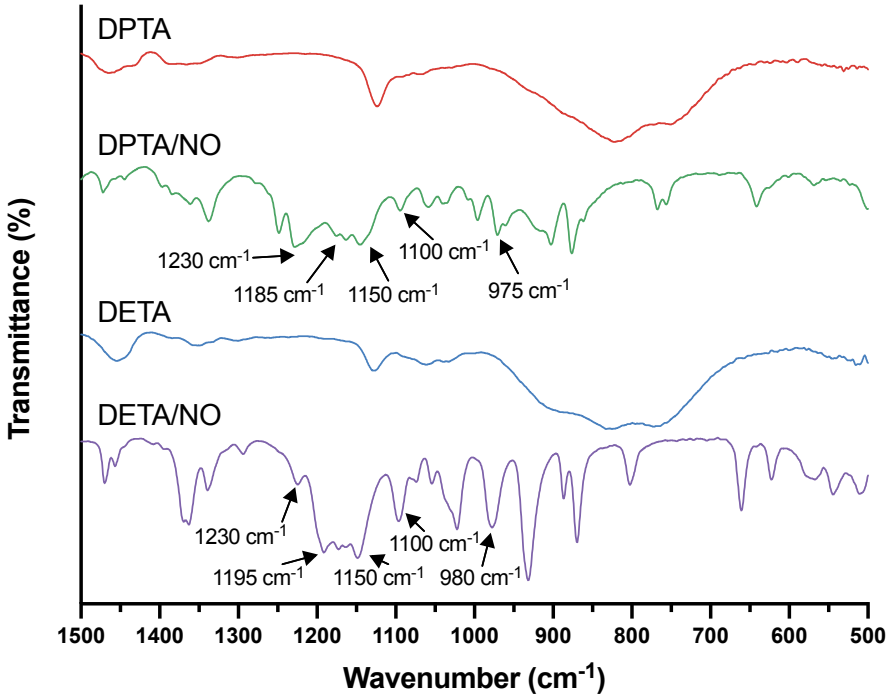

Figure 4.2 Representative FTIR analysis of DPTA and DETA before and after *N*-diazeniumdiolate NO donor formation. N-O stretches (1230 cm^{-1} and 1185-1195 cm^{-1}), N-N stretches (1100 cm^{-1}), and in-plane N2 symmetric stretches (1150 cm^{-1} and 975-980 cm^{-1}) are observed due to the presence of the *N*-diazeniumdiolate group.

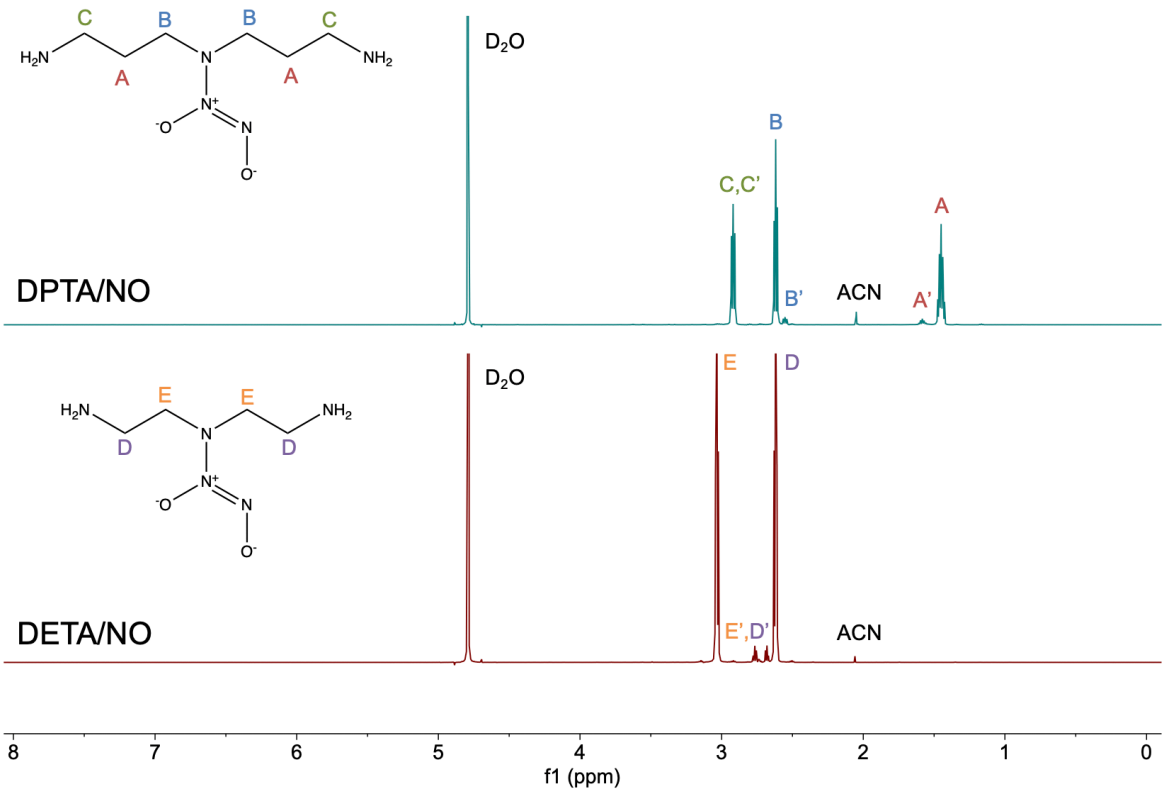

Figure 4.3 Representative ^{1}H NMR (600 MHz, D_2O) of DPTA/NO and DETA/NO. Peaks labeled A through E represent DPTA/NO and DETA/NO, and peaks labeled A' through E' represent DPTA and DETA without an *N*-diazeniumdiolate NO donor.

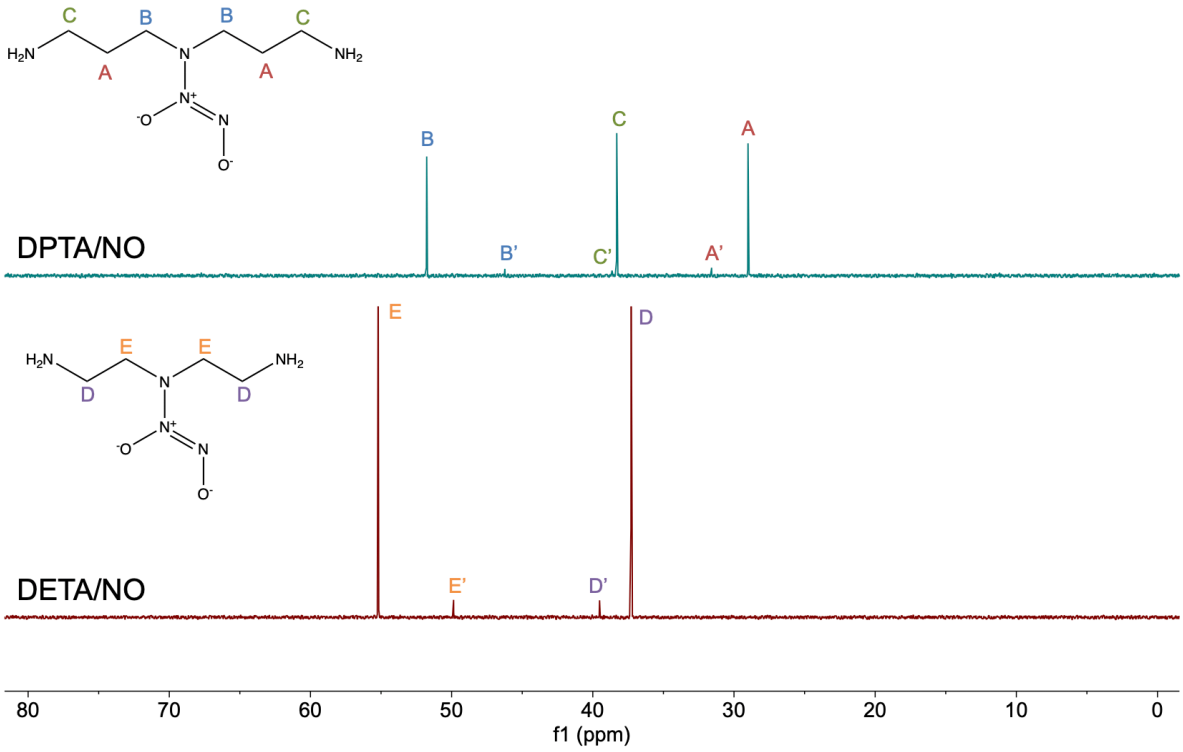

Figure 4.4 Representative ^{13}C NMR (600 MHz, D_2O) of DPTA/NO and DETA/NO. Peaks labeled A through E represent DPTA/NO and DETA/NO, and peaks labeled A' through E' represent DPTA and DETA without an *N*-diazeniumdiolate NO donor.

the NO donors (Table 4.1). These NO donors were selected for lock solution preparation due to their high NO payloads per unit mass and range of kinetics. Whereas DETA/NO produces a stable, low flux of NO over ~7 d, DPTA/NO releases NO with a higher maximum flux and shorter release duration (~2 d).

Lock solutions were prepared to contain 25 or 50 mg mL^{-1} of DPTA/NO or DETA/NO in pH 7.4 PBS (10 mM) as a means to evaluate the role of NO surface flux and total NO released on bacterial and protein adhesion properties. Nitric oxide release from the catheter surface was monitored using a chemiluminescent nitric oxide analyzer as displayed in Figure 4.1. The initial flux of NO was proved to be dependent upon both the identity and concentration of the NO donor (Figure 4.5A). As expected from the NO-release profiles of the donors themselves (Table 4.1), lock solutions containing DPTA/NO exhibited a higher initial flux and faster NO release (half-lives of 10-17 h) whereas DETA/NO-based solutions exhibited slow, sustained NO release (half-lives of 62-68 h) (Table 4.2). Of note, the NO-release half-lives were extended within the lock solutions compared to those of the free donor. The added catheter diffusion barrier, wherein NO has to first diffuse into the external solution from within the catheter to then be carried to the NO detector, is likely to delay NO measurements. The extended half-lives are also hypothesized to be due in part to the high localized concentrations of the NO donor, slightly increasing the pH upon NO release, which in turn slows subsequent NO release. The effect of the slight increase in pH (up to pH ~8) was most evident for the 50 mg mL^{-1} DPTA/NO lock solution, as this solution initially displayed a surface flux that was approximately double that of the 25 mg mL^{-1} DPTA/NO (~430 vs. ~260 pmol NO cm^{-2} s^{-1}). The NO-release payload though was similar between the 25 mg mL^{-1} and 50 mg mL^{-1} DPTA/NO lock solutions (~5.2 and ~6.0 μmol NO cm^{-2}, respectively), indicating that the larger concentration of NO donor leads to premature self-termination of NO

Table 4.1 Nitric oxide-release properties from DPTA/NO and DETA/NO.[a]

NO Donor	t[NO] (μmol mg^{-1})[b]	t[NO]$_{theor}$ (μmol mg^{-1})[c]	[NO]$_{max}$ (ppb mg^{-1})[d]	t_d (h)[e]	$t_{1/2}$ (h)[f]
DPTA/NO	10.1 ± 0.9	10.5	2590 ± 100	44 ± 2	5.2 ± 0.3
DETA/NO	12.1 ± 1.4	12.3	500 ± 50	178 ± 14	35.6 ± 3.9

[a]Error represents the standard deviation for n ≥ 3 separate syntheses. [b]Total NO released over full duration. [c]Theoretical total NO payload. [d]Maximum instantaneous NO concentration. [e]Duration of NO release. [f]Half-life of NO release.

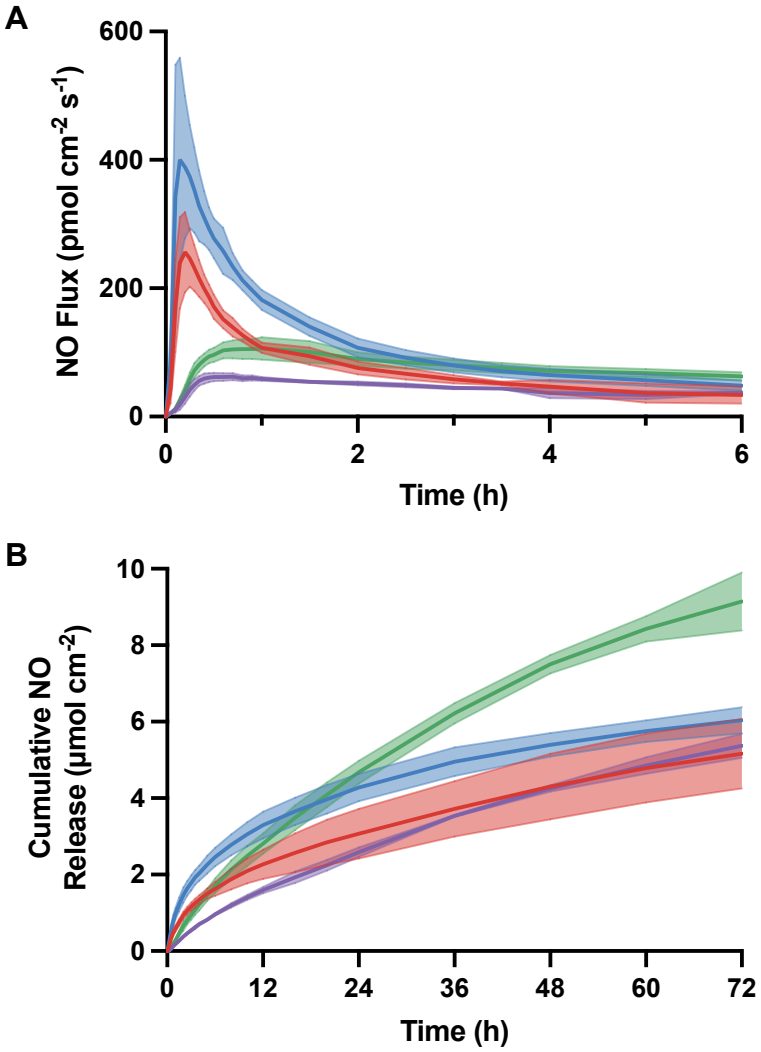

Figure 4.5 (A) Real-time NO-release profiles for the initial 6 h of release and **(B)** cumulative NO-release totals for 25 mg mL^{-1} DETA/NO (purple), 50 mg mL^{-1} DETA/NO (green), 25 mg mL^{-1} DPTA/NO (red), and 50 mg mL^{-1} DPTA/NO (blue) lock solutions. Each curve represents the average ± standard deviation from $n \geq 3$ separate analyses.

Table 4.2 Nitric oxide-release properties from DPTA/NO and DETA/NO lock solutions from within silicone catheters.[a]

NO Donor	Concentration (mg mL^{-1})	$t[NO]_{72h}$ (μmol cm^{-2})[b]	$[NO]_{max}$ (pmol cm^{-2} s^{-1})[c]	$t_{1/2}$ (h)[d]
DPTA/NO	25	5.16 ± 0.91	263 ± 61	17 ± 5
	50	6.04 ± 0.34	432 ± 140	10 ± 3
DETA/NO	25	5.37 ± 0.32	64 ± 7	68 ± 22
	50	9.15 ± 0.76	110 ± 16	62 ± 25

[a]Error represents the standard deviation for $n \geq 3$ analyses of individually prepared lock solutions. [b]Total NO released over 72 h. [c]Maximum instantaneous NO flux. [d]Half-life of NO release based on total NO payload as modeled using Michaelis-Menten kinetics.

release (Figure 4.5B, Table 4.2). This phenomenon was not as prevalent for the DETA/NO lock solutions, potentially due to the less rapid initial release of NO, with 25 mg mL^{-1} DETA/NO releasing ~5.4 μmol NO cm^{-2} and 50 mg mL^{-1} DETA/NO releasing ~9.2 μmol NO cm^{-2}. Importantly, NO release was maintained above physiological levels for at least 72 h for all four lock solutions, with each system releasing NO at concentrations above 6 pmol cm^{-2} s^{-1} at the 72-h timepoint, meeting the ideal threshold for mitigating thrombosis.

To ensure that NO was the primary molecule diffusing through the catheter surface and not the entire NO donor, samples of an external soak solution were collected at 24, 48, and 72 h to determine DPTA and DETA content released from DPTA/NO- and DETA/NO-loaded catheters, respectively. External soak solutions were analyzed in an acidic environment to promote breakdown of any remaining NO donor molecules. Soak solutions for catheters containing four different lock solutions (25 and 50 mg mL^{-1} of DPTA/NO or DETA/NO) as well as DPTA and DETA calibration standards were analyzed via LC/MS (Figure 4.6A). Calibration standards were plotted using a quadratic fit to allow for the determination of NO donor precursor concentrations in the catheter soak solutions (Figure 4.6B). The percent of NO donor that leached through the catheter surface was calculated relative to the total NO donor in each catheter. On average, all catheters leached < 0.2% of the NO donor content into the surrounding environment, with 25 mg mL^{-1} DPTA/NO- and 50 mg mL^{-1} DETA/NO-filled catheters leaching < 0.02% (Figure 4.6C). In evaluating the 50 mg mL^{-1} DPTA/NO-filled catheters, one catheter leached substantially more than the other two replicates, suggesting that the catheter surface may have been compromised. This outlier led to a large error associated with the measurement (Figure 4.6C). Overall, these results clearly indicate that NO diffuses through the catheter surface as a dissolved gas rather than attached to the NO donor to generate the observed surface flux of NO.

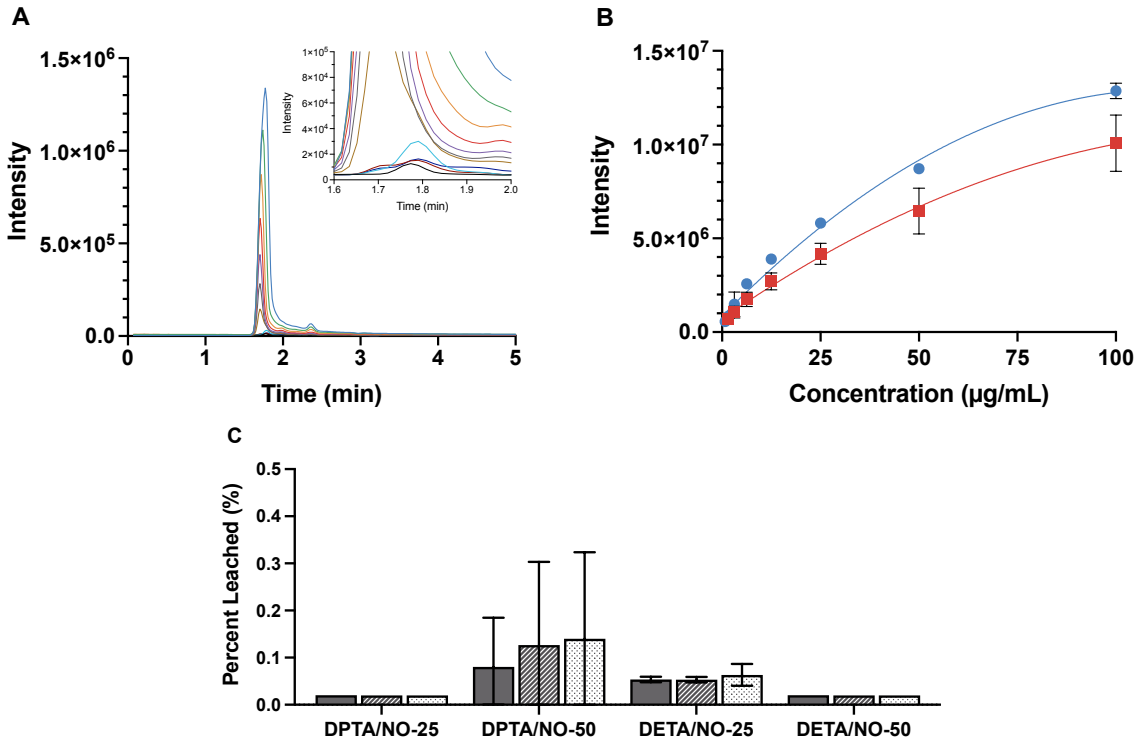

Figure 4.6 (A) Analysis via LC/MS of DETA/NO standards and catheter leachate solutions. Curves represent DETA/NO standards, including 100 (blue), 50 (green), 25 (orange), 12.5 (red), 6.25 (purple), 3.13 (gray), 1.56 (brown), and 0 (black) µg mL^{-1} DETA/NO, as well as catheter leachate solutions from catheters filled with 50 mg mL^{-1} DETA/NO lock solutions after 24 h (cyan), 48 h (maroon), and 72 h (indigo). Inset is an enlarged section of the chromatogram including the DETA/NO peak to visualize small peaks from catheter leachate solutions. **(B)** Calibration curves using a quadratic fit for LC/MS analysis of DPTA/NO (blue) and DETA/NO (red). **(C)** Quantity of NO donor (DPTA/NO or DETA/NO) leached from the catheter surface over 24 (solid), 48 (striped), and 72 h (dotted) as quantified by LC/MS. The amount of leached NO donor is reported relative to the total concentration of NO donor within the catheter. The limit of detection for this method is 0.02% leached. For samples where all measurements fell below this threshold, no error bars are presented.

4.3.2. Inhibition of bacterial adhesion to catheter surface

The first stage of biofilm formation is adhesion of planktonic bacteria to the catheter surface.[49,50] By inhibiting this adhesion step, the formation of biofilms are hindered, ideally leading to decreased incidences of catheter-related infections. Due to their high prevalence and clinical significance in catheter-related infections, *P. aeruginosa* and *S. epidermidis* were selected for evaluation of the prepared NO-releasing lock solutions.[8–10] Catheters were soaked in 1 vol% growth medium in PBS, initially containing 10^6 CFU mL^{-1} bacteria, for short (1- or 4-h) or extended (48-h) adhesion periods. The concentration of bacteria in the external soak solution increased over the 48-h experiment (data not shown), indicating that sufficient nutrient conditions were present to facilitate bacterial viability and moderate growth over the course of the experiment.

Following short-term or extended exposure to the bacteria soak solution, non-adhered bacteria were rinsed from the catheter. The adhered bacteria were then collected from the catheter surface into fresh PBS. For both *P. aeruginosa* and *S. epidermidis* adhesion studies, an increased number of bacteria was found adhered to the catheter with increasing exposure time (Figure 4.7). Furthermore, *P. aeruginosa* adhered to the catheter in greater quantities than *S. epidermidis*, consistent with previous reports in which *P. aeruginosa* achieved larger densities of surface coverage than *S. aureus* or *S. epidermidis*.[39,41,42] In evaluating Gram-negative *P. aeruginosa*, the DPTA/NO lock solutions better prevented bacterial adhesion at 1-h exposures (Figure 4.7A), likely owing to their more rapid release of NO during this period. By 4 h, the DPTA/NO and DETA/NO lock solutions were similarly effective at preventing *P. aeruginosa* adhesion, with increased inhibition found for the 50 mg mL^{-1} versus the 25 mg mL^{-1} lock solutions (Figure 4.7C). Over 48-h exposure, only the 50 mg mL^{-1} DETA/NO solution maintained substantial inhibitory action, reducing adhesion by 88.9% compared to the control PBS catheters (Figure 4.7E, Table 4.3). The

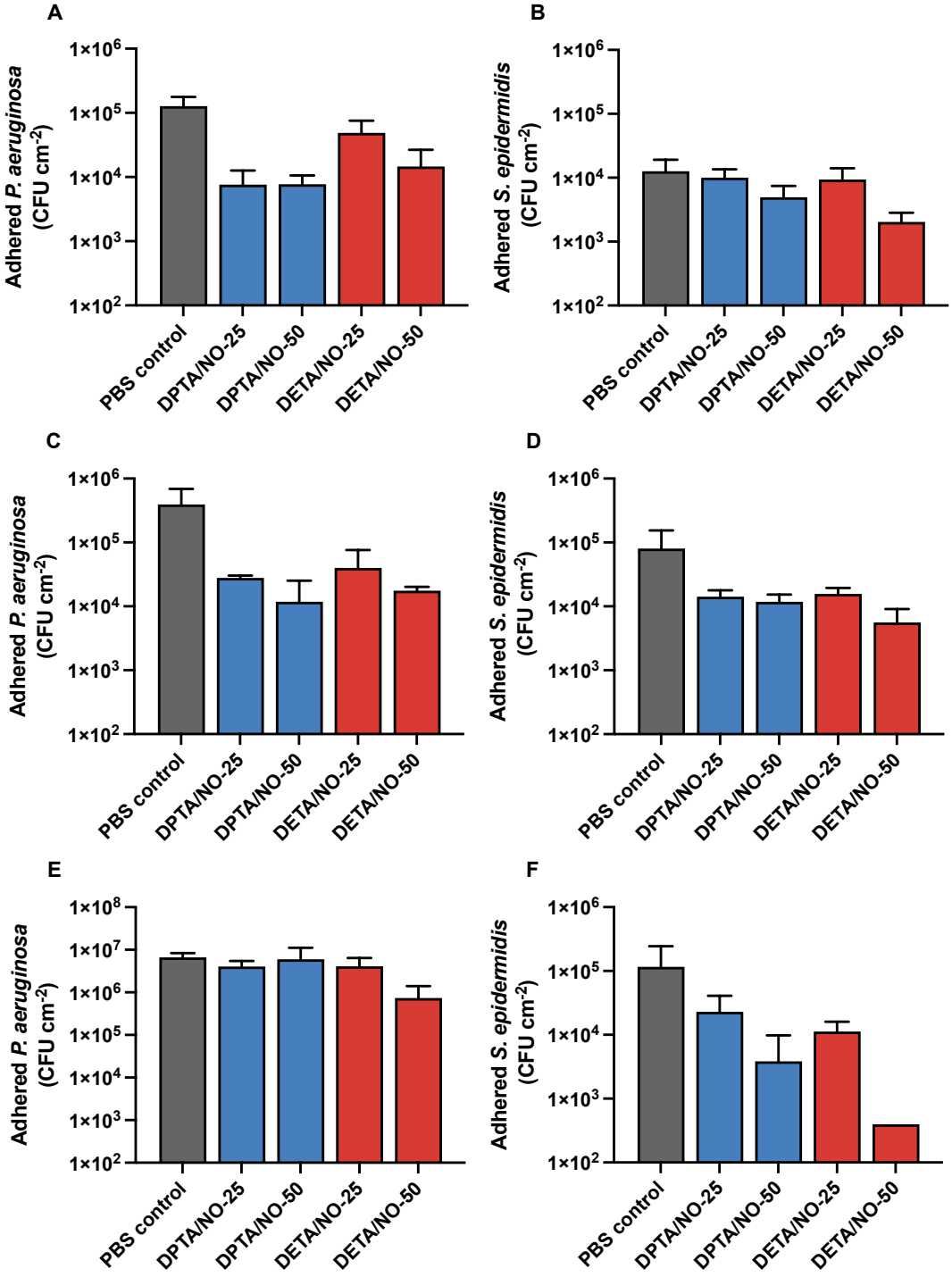

Figure 4.7 Quantity of **(A, C, E)** *P. aeruginosa* or **(B, D, F)** *S. epidermidis* adhered to catheters following **(A-B)** 1-, **(C-D)** 4-, or **(E-F)** 48-h exposure to bacteria solution in 1 vol% TSB-supplemented PBS. Evaluated lock solutions included a PBS control and 25 mg mL^{-1} or 50 mg mL^{-1} of DPTA/NO or DETA/NO in PBS. Of note, the y-axis of **(E)** is extended to fit the data. Each bar represents the average ± standard deviation from $n \geq 3$ separate experiments. Error bars are not presented if all replicates fell below the LOD of the plate counting method.

Table 4.3 Reduction in bacterial adhesion to the catheter surface following exposure to bacteria solution (*P. aeruginosa* or *S. epidermidis*) for 1, 4, or 48 h. Percent reduction is calculated relative to catheters containing a PBS control lock solution.[a]

Lock Solution	Percent Reduction (%)					
	P. aeruginosa			*S. epidermidis*		
	1 h	4 h	48 h	1 h	4 h	48 h
25 mg mL^{-1} DPTA/NO	94.0	92.9	39.4	20.3	82.3	80.2
50 mg mL^{-1} DPTA/NO	93.9	97.0	9.5	60.8	85.2	96.7
25 mg mL^{-1} DETA/NO	61.6	89.9	38.1	25.9	80.4	90.3
50 mg mL^{-1} DETA/NO	88.6	95.6	88.9	83.8	93.0	99.7

[a]Percent reduction calculated using the average of $n \geq 3$ trials for both control and treated lock solutions.

NO flux of the other three lock solutions is likely insufficient over this later timeframe to prevent adhesion of *P. aeruginosa*, suggesting a threshold for NO flux to inhibit bacterial adhesion. These results also support that a sustained NO flux, rather than an initial burst, is more effective at preventing bacterial adhesion of *P. aeruginosa* over longer periods.

As a representative Gram-positive bacterial species, adhesion of *S. epidermidis* was evaluated in the same manner. In contrast to the studies performed with *P. aeruginosa*, the 50 mg mL^{-1} DETA/NO lock solution was the most effective over both short-term and extended exposures with an 83.8, 93.0, and 99.7% reduction in bacterial adhesion over 1, 4, and 48 h, respectively (Table 4.3, Figure 4.7B, D, and F). In general, a greater reduction in *S. epidermidis* adhesion over time was observed without a decrease in viability in the external soak solution (data not shown), demonstrating that active NO release prevents the adhesion of bacteria through a mechanism that does not rely on bacterial eradication. Further, the NO fluxes at later time points (between 4 and 48 h) proved sufficient in continuing to prevent *S. epidermidis* adhesion. The NO threshold for preventing *S. epidermidis* adhesion may thus be lower than that required to inhibit *P. aeruginosa* adhesion.

While 50 mg mL^{-1} DETA/NO lock solutions were determined to be the most effective at preventing bacterial adhesion for both *P. aeruginosa* and *S. epidermidis*, the influence of a DPTA/NO and DETA/NO mixture and/or greater concentration of DETA/NO on further reduction was evaluated next. As DETA/NO was more effective than DPTA/NO, a mixture of 10 mg mL^{-1} DPTA/NO and 40 mg mL^{-1} DETA/NO was evaluated against *S. epidermidis* relative to 50 mg mL^{-1} of either NO donor alone (Figure 4.8). At all time points (i.e., 1, 4, and 48 h), the mixture behaved more similarly to 50 mg mL^{-1} DPTA/NO than DETA/NO, even though it was predominantly composed of DETA/NO. The addition of DPTA/NO was thus not found to be

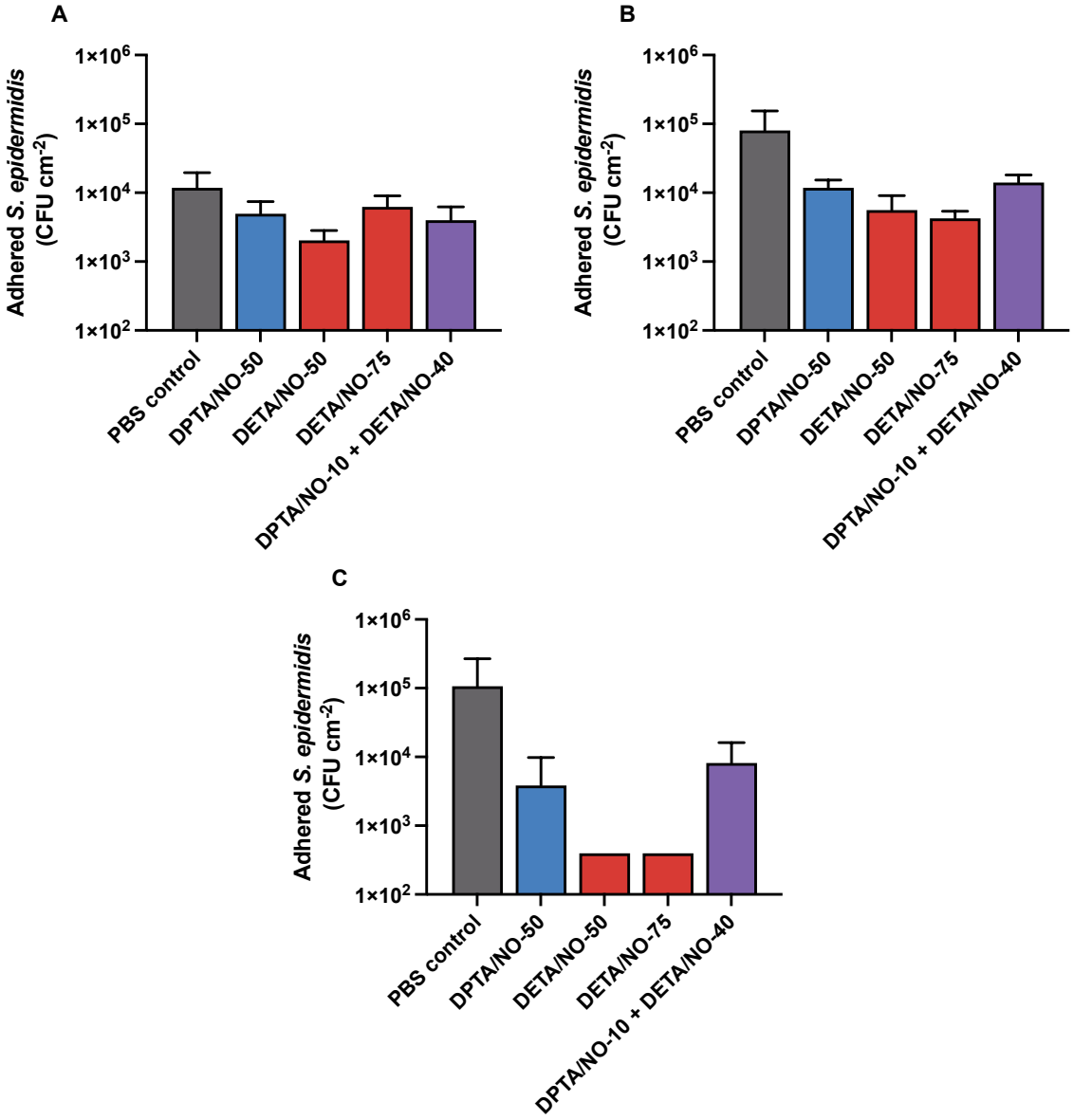

Figure 4.8 Quantity of *S. epidermidis* adhered to catheters following **(A)** 1-, **(B)** 4-, or **(C)** 48-h exposure to bacteria solution in 1 vol% TSB-supplemented PBS. Evaluated lock solutions included a PBS control, 50 mg mL^{-1} DPTA/NO in PBS, 50 or 75 mg mL^{-1} DETA/NO in PBS, and a hybrid 10 mg mL^{-1} DPTA/NO and 40 mg mL^{-1} DETA/NO in PBS. Each bar represents the average ± standard deviation from $n \geq 3$ separate experiments. Error bars are not presented if all replicates fell below the LOD of the plate counting method.

beneficial in further preventing bacterial adhesion. Greater concentrations (75 mg mL^{-1}) of DETA/NO as lock solutions were also evaluated against *S. epidermidis* (Figure 4.8). After 1 h, the 50 mg mL^{-1} solution proved more effective than 75 mg mL^{-1}. At 4 and 48 h, 50 and 75 mg mL^{-1} were similarly effective, suggesting no additional benefit to utilizing a larger concentration of DETA/NO. The equivalence in efficacy between the 50 and 75 mg mL^{-1} lock solutions suggests that a critical threshold for the prevention of bacterial adhesion is met with either solution and that increasing the NO flux past that threshold does not provide further benefit.

4.3.3. Removal of pre-adhered bacteria on the catheter surface

In addition to preventing bacterial adhesion, it was essential to understand whether the NO-releasing lock solutions can decrease the magnitude/viability of bacteria adhered to the catheter prior to treatment. By removing adhered bacteria from the catheter, the catheter lock solution can be used to treat patients with established catheter infections rather than only prevent them from occurring. Bacteria were thus adhered to the catheter surface under 100% growth conditions for 24 h prior to treatment with an NO-releasing lock solution. Control (PBS) or NO-releasing lock solutions were then introduced to the catheters for 48 h under static conditions. For *P. aeruginosa*, large quantities of bacteria adhered to the surface, consistent with biofilm formation (Figure 4.9A). Robust levels of bacteria were maintained at $>10^7$ CFU cm^{-2} after 48-h treatment with a PBS lock solution. Similar to the bacterial adhesion results, DETA/NO lock solutions were the most effective at removing pre-adhered bacteria over the 48-h exposure time. The sustained flux of NO from these lock solutions outperformed the NO burst from DPTA/NO solutions. As anticipated, the 50 mg mL^{-1} DETA/NO lock solution was more effective at pre-adhered bacteria removal than the 25 mg mL^{-1} solution, facilitating a 98.7% decrease in bacterial adhesion (Table 4.4).

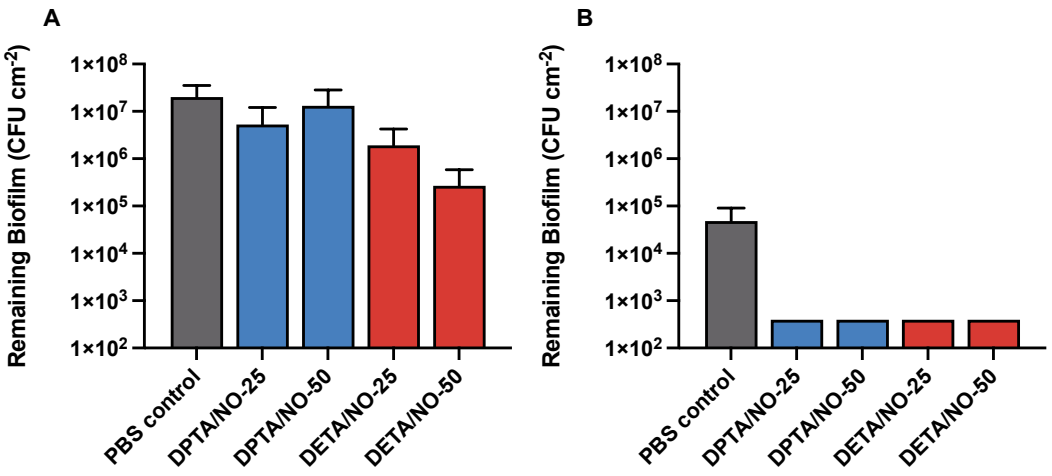

Figure 4.9 Quantity of **(A)** *P. aeruginosa* or **(B)** *S. epidermis* biofilm remaining following a 48-h treatment with lock solutions. Evaluated lock solutions included a PBS control and 25 mg mL^{-1} or 50 mg mL^{-1} of DPTA/NO or DETA/NO in PBS. Each bar represents the average ± standard deviation from $n \geq 3$ separate experiments. Error bars are not presented if all replicates fell below the LOD of the plate counting method.

Table 4.4 Reduction in pre-adhered bacteria (*P. aeruginosa* or *S. epidermidis*) remaining on the catheter surface following exposure to lock solutions for 48 h. Percent reduction is calculated relative to catheters containing a PBS control lock solution.[a]

Lock Solution	Percent Reduction (%)	
	P. aeruginosa	*S. epidermidis*
25 mg mL^{-1} DPTA/NO	73.9	99.2
50 mg mL^{-1} DPTA/NO	35.0	99.2
25 mg mL^{-1} DETA/NO	90.6	99.2
50 mg mL^{-1} DETA/NO	98.7	99.2

[a]Percent reduction calculated using the average of $n \geq 3$ trials for both control and treated lock solutions.

The coverage of pre-adhered bacteria with *S. epidermidis* (~5 x 10^4 CFU cm^{-2}) was less than that for *P. aeruginosa* following 24-h adhesion/growth and 48-h treatment with a PBS control lock solution (Figure 4.9B). However, this result is in agreement with the earlier bacterial adhesion studies (Figure 4.7) and previously published work.[39] *S. epidermidis* simply does not adhere to the silicone catheter as readily as *P. aeruginosa*. Upon treatment with the NO-releasing lock solutions, all four solutions decreased bacterial adhesion by 99.2% (the detection limit of the plate counting method utilized). As shown in Table 4.4, the 50 mg mL^{-1} DETA/NO lock solutions proved most effective at both removing pre-adhered bacteria and preventing the adhesion of new bacteria to the surface.

4.3.4. Prevention of protein adhesion to catheter surface

Upon catheter insertion, proteins rapidly coat the surface, serving as a nidus for biofilm formation and thrombosis.[1,6] By preventing the initial adhesion of proteins to the surface, it is likely that the downstream formation of biofilms and thrombi will be attenuated. Prior research suggests that active NO release reduces the adhesion of thrombus-related proteins.[51] The influence of the NO-releasing lock solutions on protein adhesion was thus also investigated through an in vitro assay. Catheters were filled with either a control or NO-releasing lock solution and soaked in proteinaceous solution (50 vol% FBS in PBS, containing approximately 0.5-1 g total protein)[52,53] for 24 h. Control catheters, filled with a PBS lock solution, were coated with 30 ± 8 μg protein cm^{-2} following exposure (Figure 4.10). Lock solutions prepared with DPTA/NO demonstrated 25-40% reductions in protein adhesion, with 22 ± 7 and 19 ± 2 μg protein cm^{-2} for 25 and 50 mg mL^{-1} lock solutions, respectively. DETA/NO-based lock solutions exhibited an even more significant decrease in protein adhesion (i.e., 60-65% reduction), with only 10 ± 5 and 11 ±

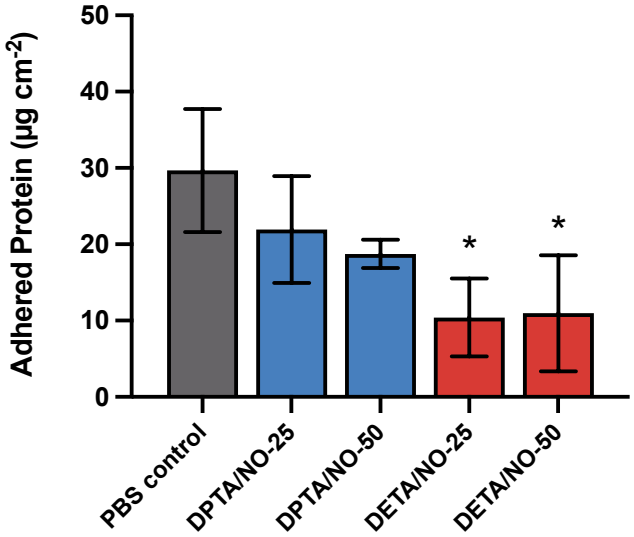

Figure 4.10 Quantity of protein adhered to catheters following 24-h exposure to 50 vol% fetal bovine serum. Evaluated lock solutions included a PBS control and 25 mg mL^{-1} or 50 mg mL^{-1} of DPTA/NO or DETA/NO in PBS. Each bar represents the average ± standard deviation from $n \geq 3$ separate experiments. *$p < 0.05$.

8 μg protein cm^{-2} for the 25 and 50 mg mL^{-1} lock solutions, respectively. Of note, the different DETA/NO-based lock solutions did not show a concentration dependence in preventing protein adhesion. The lack of concentration dependence conveys that the NO flux from both solutions is above the critical level needed to prevent protein adhesion. Overall, the results suggest that the low, sustained flux of DETA/NO is most beneficial in preventing protein adhesion.

4.3.5. In vitro cytotoxicity of catheter extract solutions

To determine the effects of NO release on cell toxicity and any influence of NO flux on healthy cells, catheters containing control PBS or NO-releasing lock solutions were soaked in cell media with the extract solution collected at 24, 48, and 72 h. As a representative cell type, Vero cells were then exposed to the extract solutions for 24 h and their viability quantified using the MTS assay. Treatment with all extract solutions maintained >80% cell viability following 24-h exposure, indicating minimal toxicity as might be expected for low NO flux solutions (Figure 4.11). The lowest viability (~84% viable) was found for the 50 mg mL^{-1} DETA/NO lock solution after a 72-h extraction protocol. This solution likely contains the highest concentration of NO byproducts given the greater NO payloads achieved with the 50 mg mL^{-1} DETA/NO solutions compared to the other lock solutions. The slight decrease in viability seen with this solution provides further rationale to utilize the lowest effective NO donor dose rather than increasing the lock solution concentration to 75 mg mL^{-1} as was evaluated in the bacterial adhesion studies. However, a minor decrease in cell viability such as that observed with 50 mg mL^{-1} DETA/NO is unlikely to be a problem in vivo due to the continuous flow of fluid (i.e., blood) outside the catheter within the body.

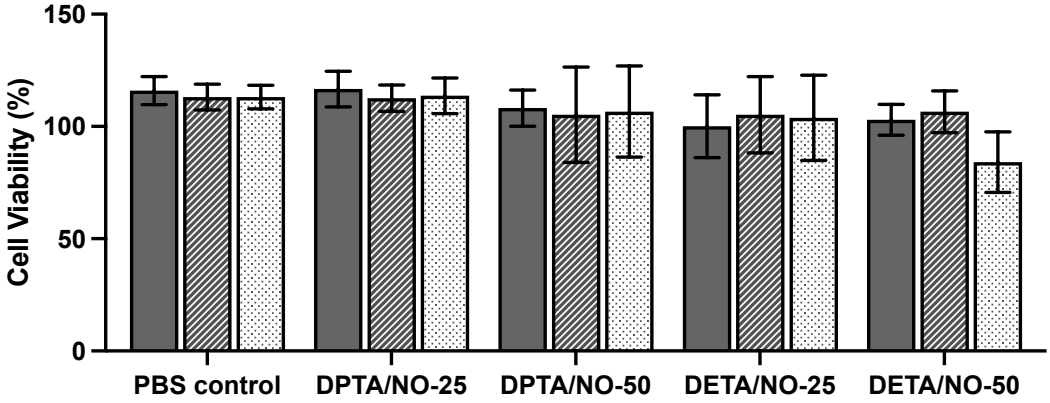

Figure 4.11 Cytotoxicity of catheter extract solutions against Vero cells. Catheters filled with lock solutions, including a PBS control and 25 mg mL^{-1} or 50 mg mL^{-1} of DPTA/NO or DETA/NO in PBS, were soaked in DMEM for 72 h. Aliquots of the external DMEM solutions were taken at 24 (solid), 48 (striped), and 72 h (dotted), and cells were exposed to catheter extract solutions for 24 h. Cell viability is calculated relative to cells treated with fresh, non-extract DMEM. Each bar represents the average ± standard deviation from $n \geq 3$ separate experiments.

4.4. Conclusions

Nitric oxide-releasing lock solutions represent a promising strategy for mitigating catheter-related complications, especially in decreasing incidences of infection. Two NO donor systems, DPTA/NO and DETA/NO, were utilized to develop NO-releasing lock solutions varying in release profile, with DPTA/NO demonstrating a burst-release profile and DETA/NO providing low and sustained levels of NO. The DETA/NO-based lock solutions investigated herein with sustained NO flux were most efficacious in preventing bacterial and protein adhesion to catheters, minimizing the potential for biofilm and thrombus formation. Further, the DETA/NO-based lock solutions were able to reduce the adhesion of pre-adhered bacteria (i.e., bacteria adhered to the catheter prior to treatment), indicating that the solutions can serve as both preventative and treatment strategies. Negligible toxicity was observed following exposure of mammalian cells to catheter extract solutions, highlighting the tolerable nature of these lock solutions to mammalian cells. An extensive evaluation of the best-performing lock solution candidate (50 mg mL^{-1} DETA/NO) is ongoing in a porcine model to determine the role of NO release on preventing infection, thrombosis, and stenosis simultaneously.

REFERENCES

(1) Dougherty, M. J.; Troutman, D. A.; Maloni, K. C. Management of Difficult Dialysis Access Issues for Dialysis Patients. *Adv. Surg.* **2019**, *53*, 83–101.

(2) National Kidney Foundation. *Hemodialysis Access: What You Need to Know*; 2006.

(3) Lok, C. E.; Foley, R. Vascular Access Morbidity and Mortality: Trends of the Last Decade. *Clin. J. Am. Soc. Nephrol.* **2013**, *8*, 1213–1219.

(4) Arciola, C. R.; Campoccia, D.; Montanaro, L. Implant Infections: Adhesion, Biofilm Formation and Immune Evasion. *Nat. Rev. Microbiol.* **2018**, *16*, 397–409.

(5) Donlan, R. M.; Costerton, J. W. Biofilms: Survival Mechanisms of Clinically Relevant Microorganisms. *Clin. Microbiol. Rev.* **2002**, *15*, 167–193.

(6) Wo, Y.; Brisbois, E. J.; Bartlett, R. H.; Meyerhoff, M. E. Recent Advances in Thromboresistant and Antimicrobial Polymers for Biomedical Applications: Just Say Yes to Nitric Oxide (NO). *Biomater. Sci.* **2016**, *4*, 1161–1183.

(7) Delistefani, F.; Wallbach, M.; Müller, G. A.; Koziolek, M. J.; Grupp, C. Risk Factors for Catheter-Related Infections in Patients Receiving Permanent Dialysis Catheter. *BMC Nephrol.* **2019**, *20*, 1–7.

(8) Donlan, R. M. Biofilm Formation: A Clinically Relevant Microbiological Process. *Clin. Infect. Dis.* **2001**, *33*, 1387–1392.

(9) Costerton, A. J. W.; Stewart, P. S.; Greenberg, E. P. Bacterial Biofilms : A Common Cause of Persistent Infections Published by : American Association for the Advancement of Science Linked References Are Available on JSTOR for This Article : Bacterial Bioflims : A Common Cause of Persistent Infections. *Science.* **1999**, *284*, 1318–1322.

(10) Barraclough, K. A.; Hawley, C. M.; Playford, E. G.; Johnson, D. W. Prevention of Access-Related Infection in Dialysis. *Expert Rev. Anti. Infect. Ther.* **2009**, *7*, 1185–1200.

(11) Kusminsky, R. E. Complications of Central Venous Catheterization. *J. Am. Coll. Surg.* **2007**, *204*, 681–696.

(12) Schwab, S. J.; Beathard, G. The Hemodialysis Catheter Conundrum: Hate Living with Them, but Can't Live without Them. *Kidney Int.* **1999**, *56*, 1–17.

(13) Agarwal, A. K. Central Vein Stenosis: Current Concepts. *Adv. Chronic Kidney Dis.* **2009**, *16*, 360–370.

(14) Ramanathan, V.; Darouiche, R. O. Prevention and Management of Hemodialysis Catheter Infections. *Expert Rev. Anti. Infect. Ther.* **2012**, *10*, 1447–1455.

(15) Goto, T.; Nakame, Y.; Nishida, M.; Ohi, Y. In Vitro Bactericidal Activities of Betalactamases, Amikacin, and Fluoroquinolones against Pseudomonas Aeruginosa Biofilm in Artificial Urine. *Urology* **1999**, *53*, 1058–1062.

(16) Dogra, G. K.; Herson, H.; Hutchison, B.; Irish, A. B.; Heath, C. H.; Golledge, C.; Luxton, G.; Moody, H. Prevention of Tunneled Hemodialysis Catheter-Related Infections Using Catheter-Restricted Filling with Gentamicin and Citrate: A Randomized Controlled Study. *J. Am. Soc. Nephrol.* **2002**, *13*, 2133–2139.

(17) McIntyre, C. W.; Hulme, L. J.; Taal, M.; Fluck, R. J. Locking of Tunneled Hemodialysis Catheters with Gentamicin and Heparin. *Kidney Int.* **2004**, *66*, 801–805.

(18) Nori, U. S.; Manoharan, A.; Yee, J.; Besarab, A. Comparison of Low-Dose Gentamicin With Minocycline as Catheter Lock Solutions in the Prevention of Catheter-Related Bacteremia. *Am. J. Kidney Dis.* **2006**, *48*, 596–605.

(19) Kim, S. H.; Song, K. I.; Chang, J. W.; Kim, S. B.; Sung, S. A.; Jo, S. K.; Cho, W. Y.; Kim, H. K. Prevention of Uncuffed Hemodialysis Catheter-Related Bacteremia Using an Antibiotic Lock Technique: A Prospective, Randomized Clinical Trial. *Kidney Int.* **2006**, *69*, 161–164.

(20) Poole, C. V.; Carlton, D.; Bimbo, L.; Allon, M. Treatment of Catheter-Related Bacteraemia with an Antibiotic Lock Protocol: Effect of Bacterial Pathogen. *Nephrol. Dial. Transplant.* **2004**, *19*, 1237–1244.

(21) Safdar, N.; Maki, D. G. Use of Vancomycin-Containing Lock or Flush Solutions for Prevention of Bloodstream Infection Associated with Central Venous Access Devices: A Meta-Analysis of Prospective, Randomized Trials. *Clin. Infect. Dis.* **2006**, *43*, 474–484.

(22) Saxena, A. K.; Panhotra, B. R.; Sundaram, D. S.; Al-Hafiz, A.; Naguib, M.; Venkateshappa, C. K.; Abu-Oun, B. A.; Hussain, S. M. N.; Al Ghamdi, A. M. A. A. Tunneled Catheters' Outcome Optimization among Diabetics on Dialysis through Antibiotic-Lock Placement. *Kidney Int.* **2006**, *70*, 1629–1635.

(23) Betjes, M. G. H.; van Agteren, M. Prevention of Dialysis Catheter-Related Sepsis with a Citrate-Taurolidine-Containing Lock Solution. *Nephrol. Dial. Transplant.* **2004**, *19*, 1546–1551.

(24) Weijmer, M. C.; Van Den Dorpel, M. A.; Van De Ven, P. J. G.; Ter Wee, P. M.; Van Geelen, J. A. C. A.; Groeneveld, J. O.; Van Jaarsveld, B. C.; Koopmans, M. G.; Le Poole, C. Y.; Schrander-Van Der Meer, A. M.; Siegert, C. E. H.; Stas, K. J. F. Randomized, Clinical Trial Comparison of Trisodium Citrate 30% and Heparin as Catheter-Locking Solution in Hemodialysis Patients. *J. Am. Soc. Nephrol.* **2005**, *16*, 2769–2777.

(25) Power, A.; Duncan, N.; Singh, S. K.; Brown, W.; Dalby, E.; Edwards, C.; Lynch, K.; Prout, V.; Cairns, T.; Griffith, M.; McLean, A.; Palmer, A.; Taube, D. Sodium Citrate Versus

Heparin Catheter Locks for Cuffed Central Venous Catheters: A Single-Center Randomized Controlled Trial. *Am. J. Kidney Dis.* **2009**, *53*, 1034–1041.

(26) Allon, M. Prophylaxis against Dialysis Catheter-Related Bacteremia with a Novel Antimicrobial Lock Solution. *Clin. Infect. Dis.* **2003**, *36*, 1539–1544.

(27) Metcalf, S. C. L.; Chambers, S. T.; Pithie, A. D. Use of Ethanol Locks to Prevent Recurrent Central Line Sepsis. *J. Infect.* **2004**, *49*, 20–22.

(28) Dannenberg, C.; Bierbach, U.; Rothe, A.; Beer, J.; Körholz, D. Ethanol-Lock Technique in the Treatment of Bloodstream Infections in Pediatric Oncology Patients With Broviac Catheter. *J. Pediatr. Hematol. Oncol.* **2003**, *25*, 616-621.

(29) Carpenter, A. W.; Schoenfisch, M. H. Nitric Oxide Release: Part II. Therapeutic Applications. *Chem. Soc. Rev.* **2012**, *41*, 3742–3752.

(30) Hetrick, E. M.; Shin, J. H.; Stasko, N. A.; Johnson, C. B.; Wespe, D. A.; Holmuhamedov, E.; Schoenfisch, M. H. Bactericidal Efficacy of Nitric Oxide-Releasing Silica Nanoparticles. *ACS Nano* **2008**, *2*, 235–246.

(31) Privett, B. J.; Broadnax, A. D.; Bauman, S. J.; Riccio, D. A.; Schoenfisch, M. H. Examination of Bacterial Resistance to Exogenous Nitric Oxide. *Nitric Oxide* **2012**, *26*, 169–173.

(32) Rouillard, K. R.; Novak, O. P.; Pistiolis, A. M.; Yang, L.; Ahonen, M. J. R.; McDonald, R. A.; Schoenfisch, M. H. Exogenous Nitric Oxide Improves Antibiotic Susceptibility in Resistant Bacteria. *ACS Infect. Dis.* **2021**, *7*, 23–33.

(33) Vaughn, M. W.; Kuo, L.; Liao, J. C. Estimation of Nitric Oxide Production and Reaction Rates in Tissue by Use of a Mathematical Model. *Am. J. Physiol.* **1998**, *274*, 2163–2176.

(34) Brisbois, E. J.; Kim, M.; Wang, X.; Mohammed, A.; Major, T. C.; Wu, J.; Brownstein, J.; Xi, C.; Handa, H.; Bartlett, R. H.; Meyerhoff, M. E. Improved Hemocompatibility of Multilumen Catheters via Nitric Oxide (NO) Release from S-Nitroso-N-Acetylpenicillamine (SNAP) Composite Filled Lumen. *ACS Appl. Mater. Interfaces* **2016**, *8*, 29270–29279.

(35) Yang, Y.; Qi, P. K.; Yang, Z. L.; Huang, N. Nitric Oxide Based Strategies for Applications of Biomedical Devices. *Biosurface and Biotribology* **2015**, *1*, 177–201.

(36) Frost, M. C.; Reynolds, M. M.; Meyerhoff, M. E. Polymers Incorporating Nitric Oxide Releasing/Generating Substances for Improved Biocompatibility of Blood-Contacting Medical Devices. *Biomaterials*. Elsevier May 2005, pp 1685–1693.

(37) Hou, Z.; Wu, Y.; Xu, C.; Reghu, S.; Shang, Z.; Chen, J.; Pranantyo, D.; Marimuth, K.; De, P. P.; Ng, O. T.; Pethe, K.; Kang, E. T.; Li, P.; Chan-Park, M. B. Precisely Structured Nitric-

Oxide-Releasing Copolymer Brush Defeats Broad-Spectrum Catheter-Associated Biofilm Infections in Vivo. *ACS Cent. Sci.* **2020**, *6*, 2031–2045.

(38) Brisbois, E. J.; Major, T. C.; Goudie, M. J.; Meyerhoff, M. E.; Bartlett, R. H.; Handa, H. Attenuation of Thrombosis and Bacterial Infection Using Dual Function Nitric Oxide Releasing Central Venous Catheters in a 9 Day Rabbit Model. *Acta Biomater.* **2016**, *44*, 304–312.

(39) Wo, Y.; Brisbois, E. J.; Wu, J.; Li, Z.; Major, T. C.; Mohammed, A.; Wang, X.; Colletta, A.; Bull, J. L.; Matzger, A. J.; Xi, C.; Bartlett, R. H.; Meyerhoff, M. E. Reduction of Thrombosis and Bacterial Infection via Controlled Nitric Oxide (NO) Release from S-Nitroso-N-Acetylpenicillamine (SNAP) Impregnated CarboSil Intravascular Catheters. *ACS Biomater. Sci. Eng.* **2017**, *3*, 349–359.

(40) Pant, J.; Goudie, M. J.; Chaji, S. M.; Johnson, B. W.; Handa, H. Nitric Oxide Releasing Vascular Catheters for Eradicating Bacterial Infection. *J. Biomed. Mater. Res. - Part B Appl. Biomater.* **2018**, *106*, 2849–2857.

(41) Goudie, M. J.; Pant, J.; Handa, H. Liquid-Infused Nitric Oxide-Releasing (LINORel) Silicone for Decreased Fouling, Thrombosis, and Infection of Medical Devices. *Sci. Rep.* **2017**, *7*, 1–13.

(42) Homeyer, K. H.; Goudie, M. J.; Singha, P.; Handa, H. Liquid-Infused Nitric-Oxide-Releasing Silicone Foley Urinary Catheters for Prevention of Catheter-Associated Urinary Tract Infections. *ACS Biomater. Sci. Eng.* **2019**, *5*, 2021–2029.

(43) Kumar, R.; Massoumi, H.; Chug, M. K.; Brisbois, E. J. S-Nitroso- N-Acetyl- l -Cysteine Ethyl Ester (SNACET) Catheter Lock Solution to Reduce Catheter-Associated Infections. *ACS Appl. Mater. Interfaces* **2021**, *13*, 25813–25824.

(44) IUL. Eddy Jet 2 User's Guide. 2012, pp 1–50.

(45) Sutton Scott. Accuracy of Plate Counts. *J. Valid. Technol.* **2011**, *17*, 42–46.

(46) Hrabie, J. A.; Keefer, L. K. Chemistry of the Nitric Oxide-Releasing Diazeniumdiolate ("nitrosohydroxylamine") Functional Group and Its Oxygen-Substituted Derivatives. *Chem. Rev.* **2002**, *102*, 1135–1154.

(47) Keefer, L. K.; Flippen-Anderson, J. L.; George, C.; Shanklin, A. P.; Dunams, T. M.; Chrisodoulou, D.; Saavedra, J. E.; Sagan, E. S.; Bohle, D. S. Chemistry of the Diazeniumdiolates. 1. Structural and Spectral Characteristics of the [N(O)NO]- Functional Group. *Nitric Oxide* **2001**, *5*, 377–394.

(48) Suchyta, D. J.; Schoenfisch, M. H. Controlled Release of Nitric Oxide from Liposomes. *ACS Biomater. Sci. Eng.* **2017**, *3*, 2136–2143.

(49) Dunne, W. M. Bacterial Adhesion: Seen Any Good Biofilms Lately? *Clin. Microbiol. Rev.* **2002**, *15*, 155–166.

(50) Lindsay, D.; von Holy, A. Bacterial Biofilms within the Clinical Setting: What Healthcare Professionals Should Know. *J. Hosp. Infect.* **2006**, *64*, 313–325.

(51) Charville, G. W.; Hetrick, E. M.; Geer, C. B.; Schoenfisch, M. H. Reduced Bacterial Adhesion to Fibrinogen-Coated Substrates via Nitric Oxide Release. *Biomaterials* **2008**, *29*, 4039–4044.

(52) Sigma-Aldrich. *Fetal Bovine Serum*; 2011.

(53) Lindl, T. *Zell- Und Gewebekultur*; Spektrum Akademischer Verlag, 2002.

CHAPTER 5: SUMMARY AND FUTURE DIRECTIONS

5.1. Summary of dissertation research

My dissertation research involved developing NO-based strategies for the prevention and treatment of infections. Chapter 1 described strategies by which bacteria can evade antibiotic treatment, including the acquisition of resistance mechanisms, formation of biofilms, or co-infection with other pathogens. Current limitations of conventional antibiotics in treating abiotic- and biotic-surface based infections were described to establish the immediate need for novel therapeutics. Exogenous NO was proposed as an alternative antibacterial agent for the treatment of resistant, biofilm-based, and/or polymicrobial infections due to the multiple mechanisms of action exerted by NO that are responsible for its broad-spectrum antibiofilm action. In addition, NO has roles in modulating inflammation, angiogenesis, thrombosis, and stenosis, motivating its use as a multimodal therapy for both wound and catheter-based infections. As exogenous NO exists in a gaseous form that is difficult to directly use for such therapies, strategies for the localized delivery of exogenous NO through small molecule NO donors and macromolecular scaffolds were discussed.

Chapter 2 detailed the development of a novel NO-releasing polysaccharide for wound healing applications through amine modification and subsequent *N*-diazeniumdiolation of HA, from which NO is then released. One NO-releasing amine modification of HA in particular, DPTA, facilitated bactericidal action at small doses against common wound pathogens, such as *E. coli*, *P. aeruginosa*, *S. aureus*, and *E. faecalis*. Both HA6-DPTA/NO and HA90-DPTA/NO were superior

to the conventional antibiotic neomycin sulfate at eradicating antibiotic-resistant pathogens (i.e., MDR-PA and MRSA). The investigation regarding antibiofilm efficacy determined HA6-DPTA/NO to be the stronger antibiofilm agent compared to both HA90-DPTA/NO and neomycin sulfate, highlighting the benefit of low molecular weight HA in biofilm penetration as well as NO's ability to eradicate biofilm-based bacteria. It was demonstrated that amine modification and NO donor loading did not sacrifice the innate biodegradability of HA as confirmed by in vitro studies where amine-modified and NO-releasing HA derivatives were degraded by the endogenous enzyme hyaluronidase. Lastly, treatment with HA6-DPTA/NO outperformed treatment with the PEG control and non-NO-releasing HA6-DPTA in an infected murine wound model regarding wound healing and bacterial clearance, highlighting the benefit of both the HA biopolymer and active NO release.

The promise of NO-releasing HA as a dual-action antibacterial wound therapeutic motivated the development of NO-releasing CS in Chapter 3, as CS is another endogenous GAG involved in wound healing. Properties of the two GAGs, including GAG identity (i.e., HA vs. CS), HA molecular weight, CS sulfation pattern, alkylamine modification, and NO-release properties, were investigated through in vitro antibacterial and wound healing assays. While DETA-modified GAGs were found to best inhibit bacterial growth for three strains each of *P. aeruginosa* (PAO1, MDR-PA, and AR-0239) and *S. aureus* (ATCC *S. aureus*, MRSA, AR-0565), DPTA-modified GAGs were the most bactericidal against the same six strains. In vitro, the alkylamine modification, GAG identity, and NO-release capability were all found to influence cell adhesion to ECM components and proliferation of human dermal fibroblasts and human epidermal keratinocytes. Furthermore, NO-release properties demonstrated decreased activation of the inflammatory receptor TLR4, suggesting that the NO-releasing GAGs may elicit anti-

inflammatory actions in the wound environment. Lastly, the most promising GAG candidates, including HA6-HEDA/NO, CSC-HEDA/NO, and CSC-DPTA/NO, were evaluated in an infected murine model. In comparing an NO-releasing HA derivative versus an NO-releasing CS derivative, it was found that CS facilitated faster wound closure. Further, it was demonstrated that the alkylamine attached to CS (i.e., HEDA or DPTA) did not impact wound closure rate. HEDA- and DPTA-modified CS (without NO) also exhibited significantly accelerated wound closure compared to control PEG-treated wounds, albeit less than the initial acceleration observed with NO-releasing CS, indicating the role that the CS backbone plays in the multi-action wound therapeutic.

Finally, Chapter 4 detailed the development of NO-releasing lock solutions for the prevention/treatment of infection and thrombosis associated with hemodialysis catheters. Two NO donor systems were utilized to investigate the role of the NO-release profile on antibacterial efficacy and protein adhesion. The slow, sustained NO release from DETA/NO-based lock solutions, when compared to the high initial NO flux profile of DPTA/NO-based solutions, was found to be most effective at preventing bacterial and protein adhesion as well as removing pre-adhered bacteria. Nitric oxide was found to readily diffuse through the catheter surface, whereas the NO donor (DPTA or DETA) demonstrated negligible leaching through the surface. As such, minimal toxicity to Vero cells was observed upon treatment with catheter leachate solutions. These studies demonstrated the efficacy of small molecule NO donor-based lock solutions in mitigating catheter-related complications, with an emphasis on preventing and treating infection.

5.2. Future directions

The investigations described in this dissertation established the utility of multi-action NO-release systems for the prevention and treatment of infections and associated complications for two distinct biomedical applications. While the results herein demonstrate the promise of these systems in treating chronic wounds and preventing catheter-related complications, substantial work is necessary before these NO-release systems could be employed in a clinical setting. In this section, an expansion of available NO-releasing systems and their formulations for clinical application as well as further in vitro and in vivo analyses for assessing therapeutic potential will be described. In addition, the exploration of these NO-release systems will be proposed for additional biomedical applications, including dermatological and dental therapies.

5.2.1. Expanding the library of NO-releasing GAGs

Nitric oxide-releasing HA and CS were both shown to exhibit antibacterial action and pro-wound healing activities in Chapters 2 and 3. These efficacies motivate the development of additional NO-releasing GAG derivatives either varying in GAG identity or alkylamine modification. Heparin and heparan sulfate, both within the GAG family, have been widely studied for their anticoagulant activity and ability to prevent thrombosis.[1] These biopolymers thus represent attractive scaffolds for modification with NO donors to prevent catheter-related infections and thrombosis. In a similar manner, dermatan sulfate, another member of the GAG family, has strong antithrombotic activity that is similar to heparin and HS.[1,2] In fact, danaparoid sodium, the active ingredient in the non-heparin antithrombotic and anticoagulant drug Orgaran, is composed of a mixture of three GAGs: heparan sulfate (84%), dermatan sulfate (12%), and chondroitin sulfate (4%).[3] As such, the modification of HS and DS to release NO represents an

attractive strategy for further developing an antibacterial and antithrombotic agent for use in catheter lock solutions. In addition to its roles in thrombosis, it has been proposed that DS is involved in wound healing, as it is a major constituent of the skin and exhibits roles in coagulation, cell growth, and immune defense.[4] These actions further motivate the modification of DS to release NO, as it could be useful for wound healing applications as well. The development of a larger library of NO-releasing GAGs will allow for a side-by-side comparison of the role of GAGs in infection control, thrombosis mitigation, and wound healing acceleration.

In addition to evaluating new GAG backbones, expanding the list of alkylamine substituents that can be added to GAGs for NO donor formation represents an interesting avenue to pursue. It has been well-supported in the literature that the presence of a terminal primary amine facilitates enhanced stabilization of *N*-diazeniumdiolate NO donors and thus extends NO release.[5,6] It has also been proposed that this positively charged terminal amine may assist in localizing the therapeutic to the bacteria given the negative charge of bacterial membranes.[7–9] In this dissertation research, the alkyl chain length between the NO donor location (i.e., secondary amine) and terminal primary amine was also hypothesized to impact antibacterial efficacy via NO donor stabilization and/or bacterial localization. However, a systematic study to fully elucidate the role of alkylamine substituents on the bacterial localization properties of NO-releasing biopolymers has not yet been performed.

Using the alkylamines displayed in Figure 5.1, such study could be initiated. The alkylamines vary in either: (1) terminal functional group, including methyl (Figure 5.1A), tertiary amine (Figure 5.1B), hydroxyl (Figure 5.1C-D), and primary amine (Figure 5.1E-H) functional groups; (2) alkyl chain length between the NO donor site and the terminal functional group, including ethyl (Figure 5.1A, C, E, G) and propyl (Figure 5.1B, D, F, H) spacing; or (3) number

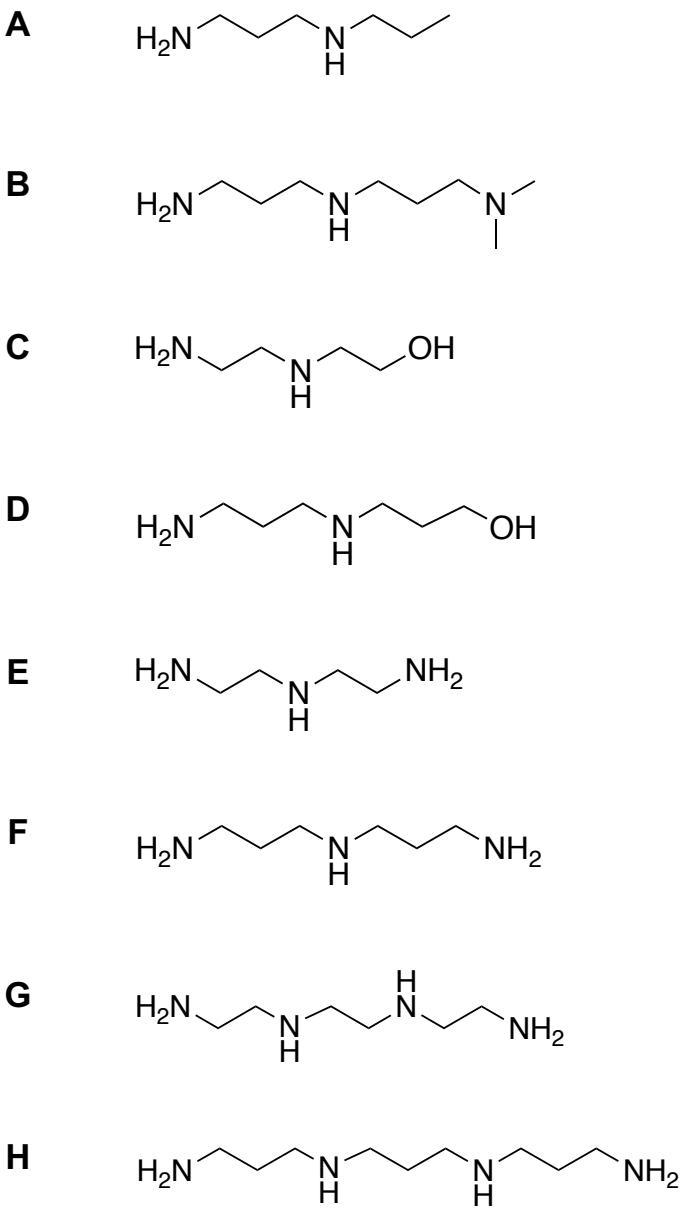

Figure 5.1 Structures of alkylamines for modification of GAGs, including **(A)** *N*-propyl-1,3-propanediamine, **(B)** *N,N*-dimethyldipropylenetriamine, **(C)** *N*-(2-hydroxyethyl) ethylenediamine, **(D)** 3-[(3-aminopropyl)amino]-1-propanol, **(E)** diethylenetriamine, **(F)** bis(3-aminopropylamine), **(G)** triethylenetetramine, and **(H)** *N,N*'-bis(3-aminopropyl-1,3-propanediamine).

of secondary amines, including alkylamines with one (Figure 5.1A-F) or two (Figure 5.1G-H) secondary amines. The role of this alkylamine moiety should be evaluated against mammalian cells to determine how it affects the toxicity profile of the material. Additionally, evaluation against relevant bacterial pathogens should be performed to determine how the alkylamine influences bacterial association and killing. To establish bacterial association properties, the GAGs can be readily labeled with fluoresceinamine at backbone hydroxyl groups using an established protocol.[10] Bacteria treated with the fluorescently tagged-GAG derivatives can then be imaged using confocal microscopy to monitor how the structural modifications affect localization of the biopolymer to the bacterial surface and whether localization is affected solely by terminal functional group or if other variables (e.g., bacteria strain, alkyl chain length) contribute to this property. In a following study, an NO-sensitive fluorescent probe, 4,5-diaminofluorescein diacetate (DAF-2 DA), should be employed to determine whether association between the NO-releasing GAGs and both Gram-negative and Gram-positive bacteria results in greater local concentrations of NO and more efficient delivery of NO to the bacterial cells.[11] These studies will provide insight into which structural properties are most effective at enhancing NO-based bacterial eradication and will investigate the mechanisms involved in their success.

5.2.2. In vitro evaluation of the role of NO-releasing GAGs on polymicrobial infections

As described in Chapter 1, infections, especially those found in chronic wounds, are rarely due to colonization by a single pathogen.[12–15] Indeed, 75-95% of chronic wounds evaluated across two studies were reported to be polymicrobial.[14,16,17] As conventional antibiotics typically exhibit antibacterial action through a single mechanism, they are often not able to eradicate the broad spectrum of bacteria that may be present in a wound.[18] Nitric oxide's multi-mechanistic

antibacterial action makes it a promising candidate in eradicating many different bacterial species simultaneously.[11,19] In Chapters 2 and 3, NO released from GAGs was utilized to eradicate a range of wound-relevant pathogens with varying resistance profiles, indicating that it is effective against both Gram-negative and Gram-positive bacteria that could exist in a chronic wound. However, it has not yet been investigated whether NO-releasing GAGs are able to eradicate multiple species of bacteria that are cultured together. Using in vitro polymicrobial bacteria solutions, this efficacy can be evaluated. The combination of *P. aeruginosa* with either *S. aureus* or *E. faecalis* is frequently observed in chronic wounds and would therefore be a relevant model.[17,20]

While bacteria were the focus of this dissertation work, other pathogens are frequently found in chronic wounds. A study published by Chellan et al. reported that of 518 diabetic patients with infected lower-limb wounds, 21.4% of the wounds contained both bacterial and fungal species.[21] In a separate study that evaluated 100 non-healing diabetic foot ulcers with more sensitive testing techniques, it was discovered that fungal species were present in up to 80% of the wounds, with many colonized by *Cladosporium herbarum* (41%), *Candida albicans* (22%), and *Aspergillus cibarius* (12%).[20,22] Specifically, *S. aureus* and *C. albicans*, which interact cooperatively, are often co-isolated from burn wounds and diabetic foot ulcers. Infections with *C. albicans* lead to physical damage to organ walls, allowing *S. aureus* to penetrate into internal organs more easily. In turn, *S. aureus* secretes proteases that assist *C. albicans* in adhering to the mucosal layer, increasing difficulty in eradication.[20] As NO has been shown to act as an antifungal agent,[23,24] it is likely that NO-releasing GAGs would be able to treat co-infections with bacterial and fungal species. The culture and treatment of co-pathogens, such as *S. aureus* and *C. albicans*, are necessary to elucidate whether this hypothesis holds true.

5.2.3. Preparation of GAG-based nanoparticles

The formation of NO-releasing GAG-based nanoparticles represents a new strategy for developing a wound healing therapeutic. While retaining the beneficial properties of the NO-releasing GAGs as discussed in Chapters 2 and 3, the use of nanoparticles could further increase these benefits, such as by slowing endogenous degradation and increasing tissue penetration. Previously, nanoparticles have been prepared using CS, heparin, or HA.[25–29] A straightforward method involves the use of carbodiimide chemistry to crosslink the carboxyl groups on GAGs with adipic acid dihydrazide. Using this method, HA nanoparticles varying in diameter from 90-190 nm were prepared.[28] Amine modification and NO donor formation could be included in a similar synthetic process to develop NO-releasing GAG nanoparticles.

One issue frequently reported with in vivo use of linear GAGs is rapid degradation by enzymes such as hyaluronidase.[30] While maintaining biodegradability is important when modifying the GAG structure, altering the kinetics of such biodegradation could be beneficial. By crosslinking the GAGs to form nanoparticles, degradation could be slowed, allowing for improved retention time. Degradation kinetics could be determined via studies in which GAG nanoparticles are exposed to enzymes (e.g., hyaluronidase) with subsequent analysis via gel permeation chromatography. It is hypothesized that HA molecular weight and CS/HS/DS sulfation pattern may affect particle size for the NO-releasing GAG nanoparticles. A systematic study of how these parameters affect nanoparticle size as well as properties such as skin permeability and tissue adhesion should be performed. Lastly, it will be necessary to elucidate how the formation of these nanoparticles affects interaction with endogenous receptors. As one example, HEK-Blue™ mTLR4 reporter cells could be used to assess how well the nanoparticles interact with the

inflammatory receptor TLR4. A large body of work could be established for the preparation and characterization of NO-releasing GAG-based nanoparticles.

5.2.4. Development of delivery strategies for NO-releasing GAGs in wound applications

The preliminary in vivo studies described in Chapters 2 and 3 involved NO-releasing GAG delivery via suspension of the biopolymer in PEG 400. While effective, further formulation development is necessary to optimize delivery of the GAG and allow for increased retention in the wound environment. To achieve this, the NO-releasing GAGs or NO-releasing GAG nanoparticles can be incorporated into hydrogels, wound dressings, or ointments. Hydrogels represent a promising strategy to increase cell adhesiveness and slow degradation.[31] In one study, Feura reported a method to prepare crosslinked hydrogels containing amine-modified HA with oxidized dextran via imine formation.[32] These hydrogels exhibited excellent swelling properties, with a swollen mass approximately 75-fold greater than the dry mass of the hydrogel, and demonstrated slow degradation in pH 7.4 and 5.4 buffers over 14 d.[32] Hyaluronic acid has also been utilized in the preparation of wound dressings. Uppal et al. reported the development of fibrous HA wound dressings via electrospinning that exhibited increased air permeability and enhanced wound healing in a porcine model as compared to gauze.[33] Similar techniques for the preparation of the described hydrogels and wound dressings could be employed for NO-releasing GAGs. Alternatively, NO-releasing GAG biopolymers or nanoparticles could be incorporated into gels formed from high molecular weight HA (<1 MDa) to prepare spreadable, easy-to-apply ointments. For all strategies, the long-term stability of NO would need to be evaluated. All of these methods may benefit clinical translatability in offering simple and effective ways to deliver the antibacterial wound healing agents.

5.2.5. Further in vivo evaluation of NO-releasing GAGs on murine wound healing using healthy and diabetic models

The preliminary in vivo studies described in this dissertation utilized a single concentration of NO-releasing GAG (50 mg kg^{-1} body weight) as a starting point. The assessment of additional concentrations (e.g., 25 and 100 mg kg^{-1}) in the same model would be useful to determine whether there is a concentration dependence on the benefits of the NO-releasing GAG and identify the optimal treatment dosage. Further, NO-releasing GAGs or NO-releasing GAG nanoparticles within the formulations prepared in Section 5.2.4 should be analyzed for their effect on in vivo wound healing to identify an optimal delivery formulation. The murine wound models utilized in Chapters 2 and 3 were primarily used to assess wound closure rates and endpoint bacterial burden. A time-based study is imperative to understand how the GAGs with or without NO affect infections and wound healing at the different stages (e.g., inflammation vs. proliferation phases). In Chapter 3, it was reported that active NO release was most influential during the initial days following wounding (days 1-4 post-wounding), whereas the non-NO-releasing CS derivatives were as effective as the NO-releasing derivatives at later time points (days 5-8 post-wounding). For this evaluation, mice should be sacrificed and wound tissue harvested at multiple time points post-wounding (i.e., 1, 3, 5, and 7 d post-wounding) for analysis via Nanostring to determine the gene profile,[34] Luminex assay to determine the cytokine profile,[35] and qPCR to determine the bacterial burden.[36] These data will give a more complete understanding of how the GAGs and NO-releasing GAGs affect wound healing to prepare for translation into clinical trials.

Additional models will be useful to fully evaluate the potential of NO-releasing GAGs as a wound healing therapeutic. Two of the major benefits of NO as an antimicrobial agent involve its broad-spectrum action and its unhindered action toward antibiotic resistant bacteria.[11,19,37,38]

Coupling the biopsy punch wound model with a polymicrobial infection composed of *P. aeruginosa* and *E. faecalis*, as described previously, would allow for evaluation of a complex infected murine wound.[39] Further, in an orthogonal study, an antibiotic-resistant pathogen, such as MDR-PA or MRSA, could be utilized to evaluate NO-releasing GAG's ability to enhance wound healing in a drug-resistant environment. These models will challenge NO's antimicrobial efficacy and truly evaluate whether these complications can be overcome by NO-releasing GAG therapy.

Lastly, it is of utmost importance to evaluate how the NO-releasing GAGs affect diabetic wounds. Diabetes is the disease that contributes to the greatest number of diagnosed chronic wounds and represents an unmet need in chronic wound therapy.[40] Diabetic individuals exhibit hyperglycemia and hypoxia, both of which contribute to an increase in ROS, impaired angiogenesis, dysfunction of key cells in wound healing (i.e., keratinocytes and fibroblasts), higher concentrations of MMPs, and decreased host immunity.[40–42] All of these complications, in turn, lead to decreased success in wound healing. Many of the factors associated with diabetic wound healing are influenced by NO, making treatment with NO-releasing GAGs especially intriguing for diabetic chronic wounds. For this study, streptozotocin (STZ) should be used to produce a murine model of type I diabetes via pancreatic islet β-cell destruction.[43,44] Wounding, infection, and treatment can then occur as optimized from earlier studies to assess the role of NO-releasing GAGs in diabetic wound healing. Similar biomarkers, such as genes and cytokines, can be used to monitor successful treatment of these wounds.

5.2.6. NO-releasing GAGs for additional applications

The work described herein focused on the development of NO-releasing GAGs for wound healing applications. However, these biopolymers represent attractive therapies for additional

applications. One application in particular is the treatment of melanoma, which is responsible for 80% of all skin cancer-related deaths.[45] Large concentrations of NO (i.e., μM) exhibit tumoricidal effects via oxidative and nitrosative stresses, which lead to DNA deamination, enzyme nitrosylation, impaired cellular function, enhanced inflammatory reactions, inhibited mitochondrial respiration, and cell apoptosis.[19,46] Nitric oxide therefore represents a promising strategy for the treatment of various cancers. A key receptor of both HA and CS, CD44, is overexpressed in many tumors.[47] The delivery of NO with a GAG backbone thus represents a localization strategy for the treatment of melanoma while minimizing off-target effects. The use of these materials should be evaluated against A375 human malignant melanoma cells as well as representative healthy skin cells (e.g., HDF and HEK) to evaluate whether the NO-releasing GAGs are selectively cytotoxic to cancerous cells as compared to healthy cells. Further, CD44 binding activity can be monitored to assess whether modification of GAGs with alkylamines and NO donors alters the CD44 binding affinity and thus localization potential.[48,49] Lastly, the use of fluorescently tagged NO-releasing GAGs in treatment of a 3-D MatTek melanoma model (consisting of A375 malignant melanoma cells, normal human-derived epidermal keratinocytes (NHEK), and normal human-derived dermal fibroblasts (NHDF)) will allow for visualization of this targeted therapy.[50]

The roles of NO-releasing GAGs on antibacterial activity and inflammation make these biopolymers attractive candidates for dental applications. Hyaluronic acid, for example, has been utilized in clinical studies for the treatment of periodontal disease as an HA-containing gel or mouthwash in addition to physical scaling and root planing procedures. HA-based treatments have demonstrated promising results in mitigating papillary bleeding,[51,52] gingival inflammation,[51,53] clinical attachment loss,[54–56] and bleeding on probing,[56,57] supporting the role of GAGs such as

HA, CS, and DS in tissue repair.[4,47,58] Through NO's antibacterial efficacy and inflammation modulation properties as well as the tissue repair properties of the GAGs, NO-releasing GAGs have the potential to be a beneficial treatment for periodontal disease. Pertinent activities can be evaluated through in vitro antibacterial assays against prominent periodontal pathogens, such as *Porphyromonas gingivalis* and *Aggregatibacter actinomycetemcomitans*,[59] in vitro cytotoxicity assays using human gingival fibroblasts (HGF) and human oral keratinocytes (HOK), and inflammation reporter cell assays (e.g., HEK-Blue™ mTLR2 or mTLR4). Eventual evaluation of top candidates in a murine periodontal model[60,61] will facilitate elucidation of therapeutic utility.

5.2.7. Evaluation of NO-releasing lock solutions in a porcine model

The NO-releasing catheter lock solutions developed in Chapter 4 exhibited successful prevention of bacterial and protein adhesion in vitro, supporting their use in preventing biofilm formation and thrombosis in vivo. To confirm these properties, as well as assess the role of the lock solutions on stenosis, a porcine model should be employed. For this analysis, silicone hemodialysis catheters can be implanted in pigs mimicking how they are implanted in humans. Pigs should either receive a conventional heparin lock solution (1000 units mL^{-1})[62,63] or an NO-releasing lock solution (50 mg mL^{-1} DETA/NO in PBS, pH 7.4) every 2-3 days to mimic catheter use in dialysis patients. Throughout the study, pigs should be monitored for infection, with a body temperature >103 °F indicating potential infection. Upon culturing of a blood sample, infected pigs should be treated with antibiotics. If antibiotic therapy is unsuccessful, pigs will be sacrificed. This process of treating and monitoring body temperature can be repeated for 28 d, upon which the pigs will be sacrificed, and the catheter, heart, placement vein, and surrounding tissues can be harvested for the analysis of thrombosis and stenosis. This model will be essential in determining

whether NO-releasing lock solutions represent a prevention and treatment strategy for catheter-related complications.

5.2.8. Exploration of additional catheter lock solutions

Chapter 4 detailed the development of NO-releasing catheter lock solutions using the NO donors DPTA/NO and DETA/NO. However, many previous NO-based catheter therapies have utilized a small molecule *S*-nitrosothiol NO donor, SNAP.[64–67] A side-by-side in vitro and in vivo comparison of lock solutions prepared from *N*-diazeniumdiolate and *S*-nitrosothiol NO donors would be useful prior to further development of these solutions. *N*-diazeniumdiolate NO donors have the benefit of high NO payloads, due to the storage of two moles of NO per mole of secondary amine, and less stringent storage conditions; however, *S*-nitrosothiols are often regarded as more biocompatible.[68] While the use of SNAP would result in approximately half of the NO payload of DETA/NO, SNAP's biocompatibility would likely allow greater NO donor doses to be utilized without exhibiting toxicity concerns. Evaluation of how these properties affect overall efficacy in mitigating catheter-related complications would inform further lock solution research and development. Of note, the development of NO-releasing lock solutions is not limited to small molecule NO donors. As such, NO-releasing macromolecular scaffolds should be evaluated as a means to maximize tissue compatibility at the catheter tip, as macromolecular scaffolds have been reported to be less cytotoxic to mammalian cells than small molecule *N*-diazeniumdiolate NO donors.[11] The development of NO-releasing heparan sulfate, heparin, or dermatan sulfate, as described in Section 5.2.1, represents a series of promising macromolecular scaffold systems for catheter applications due to the role of these GAGs in anticoagulation and antithrombosis.[1,2]

5.3. Conclusions

The dissertation work described herein highlights the importance of preventing and treating infections associated with chronic wounds and hemodialysis catheters. Due to NO's multi-mechanistic antibacterial properties and unlikelihood of developing bacterial resistance, particular focus was given to developing NO-based strategies for infection control. The synthesis of NO-releasing GAGs for the treatment of chronic wound infections yielded promising results in eradicating infection and accelerating wound closure using both in vitro and in vivo models. The design and implementation of NO-releasing lock solutions facilitated a decrease in protein and bacterial adhesion to silicone intravenous catheters as well as the ability to remove pre-adhered bacteria from the catheter surface. Both of these applications highlight the versatility of NO and the ability to harness NO for the development of strategies to address complex problems. Future studies of multi-action NO-release systems using murine wound models and porcine catheter models are necessary to fully elucidate their potential and translation to clinical use.

REFERENCES

(1) Volpi, N. Therapeutic Applications of Glycosaminoglycans. *Curr. Med. Chem.* **2006**, *13*, 1799–1810.

(2) Soares Da Costa, D.; Reis, R. L.; Pashkuleva, I. Sulfation of Glycosaminoglycans and Its Implications in Human Health and Disorders. *Annu. Rev. Biomed. Eng.* **2017**, *19*, 1–26.

(3) Acostamadiedo, J. M.; Iyer, U. G.; Owen, J. Danaparoid Sodium. *Expert Opin. Pharmacother.* **2000**, *1*, 803–814.

(4) Trownbridge, J. M.; Gallo, R. L. Dermatan Sulfate: New Functions from an Old Glycosaminoglycan. *Glycobiology* **2002**, *12*, 117R-125R.

(5) Hrabie, J. A.; Keefer, L. K. Chemistry of the Nitric Oxide-Releasing Diazeniumdiolate ("nitrosohydroxylamine") Functional Group and Its Oxygen-Substituted Derivatives. *Chem. Rev.* **2002**, *102*, 1135–1154.

(6) Keefer, L. K. Fifty Years of Diazeniumdiolate Research: From Laboratory Curiosity to Broad-Spectrum Biomedical Advances. *ACS Chem. Biol.* **2011**, *6*, 1147–1155.

(7) Silhavy, T. J.; Kahne, D.; Walker, S. The Bacterial Cell Envelope. *Cold Spring Harb Perspect Biol* **2010**, *2*, 1–16.

(8) Jin, H.; Yang, L.; Ahonen, M. J. R.; Schoenfisch, M. H. Nitric Oxide-Releasing Cyclodextrins. *J. Am. Chem. Soc.* **2018**, *140*, 14178-14184.

(9) Ahonen, M. J. R.; Suchyta, D. J.; Zhu, H.; Schoenfisch, M. H. Nitric Oxide-Releasing Alginates. *Biomacromolecules* **2018**, *19*, 1189–1197.

(10) Arnosti, C. Fluorescent Derivatization of Polysaccharides and Carbohydrate-Containing Biopolymers for Measurement of Enzyme Activities in Complex Media. *J. Chromatogr. B* **2003**, *793*, 181–191.

(11) Hetrick, E. M.; Shin, J. H.; Stasko, N. A.; Johnson, C. B.; Wespe, D. A.; Holmuhamedov, E.; Schoenfisch, M. H. Bactericidal Efficacy of Nitric Oxide-Releasing Silica Nanoparticles. *ACS Nano* **2008**, *2*, 235–246.

(12) Murray, J. L.; Connell, J. L.; Stacy, A.; Turner, K. H.; Whiteley, M. Mechanisms of Synergy in Polymicrobial Infections. *J. Microbiol.* **2014**, *52*, 188–199.

(13) Percival, S. L.; Thomas, J. G.; Williams, D. W. Biofilms and Bacterial Imbalances in Chronic Wounds: Anti-Koch. *Int. Wound J.* **2010**, *7*, 169–175.

(14) Peters, B. M.; Jabra-Rizk, M. A.; O'May, G. A.; William Costerton, J.; Shirtliff, M. E. Polymicrobial Interactions: Impact on Pathogenesis and Human Disease. *Clin. Microbiol.*

Rev. **2012**, *25*, 193–213.

(15) Price, L. B.; Liu, C. M.; Melendez, J. H.; Frankel, Y. M.; Engelthaler, D.; Aziz, M.; Bowers, J.; Rattray, R.; Ravel, J.; Kingsley, C.; Keim, P. S.; Lazarus, G. S.; Zenilman, J. M. Community Analysis of Chronic Wound Bacteria Using 16S RRNA Gene-Based Pyrosequencing: Impact of Diabetes and Antibiotics on Chronic Wound Microbiota. *PLoS One* **2009**, *4*, e6462.

(16) Citron, D. M.; Goldstein, E. J. C.; Merriam, C. V.; Lipsky, B. A.; Abramson, M. A. Bacteriology of Moderate-to-Severe Diabetic Foot Infections and in Vitro Activity of Antimicrobial Agents. *J. Clin. Microbiol.* **2007**, *45*, 2819–2828.

(17) Gjødsbøl, K.; Christensen, J. J.; Karlsmark, T.; Jørgensen, B.; Klein, B. M.; Krogfelt, K. A. Multiple Bacterial Species Reside in Chronic Wounds: A Longitudinal Study. *Int. Wound J.* **2006**, *3*, 225–231.

(18) Brogden, K. A.; Guthmiller, J. M.; Taylor, C. E. Human Polymicrobial Infections. *Lancet* **2005**, *365*, 253–255.

(19) Carpenter, A. W.; Schoenfisch, M. H. Nitric Oxide Release: Part II. Therapeutic Applications. *Chem. Soc. Rev.* **2012**, *41*, 3742–3752.

(20) Nair, N.; Biswas, R.; Götz, F.; Biswas, L. Impact of Staphylococcus Aureus on Pathogenesis in Polymicrobial Infections. *Infect. Immun.* **2014**, *82*, 2162–2169.

(21) Chellan, G.; Shivaprakash, S.; Ramaiyar, S. K.; Varma, A. K.; Varma, N.; Sukumaran, M. T.; Vasukutty, J. R.; Bal, A.; Kumar, H. Spectrum and Prevalence of Fungi Infecting Deep Tissues of Lower-Limb Wounds in Patients with Type 2 Diabetes. *J. Clin. Microbiol.* **2010**, *48*, 2097–2102.

(22) Kalan, L.; Grice, E. A. Fungi in the Wound Microbiome. *Adv. Wound Care* **2018**, *7*, 247–255.

(23) Regev-Shoshani, G.; Crowe, A.; Miller, C. C. A Nitric Oxide-Releasing Solution as a Potential Treatment for Fungi Associated with Tinea Pedis. *J. Appl. Microbiol.* **2013**, *114*, 536–544.

(24) Stasko, N.; McHale, K.; Hollenbach, S. J.; Martin, M.; Doxey, R. Nitric Oxide-Releasing Macromolecule Exhibits Broad-Spectrum Antifungal Activity and Utility as a Topical Treatment for Superficial Fungal Infections. *Antimicrob. Agents Chemother.* **2018**, *62*, 1–11.

(25) Shi, X.; Yang, X.; Liu, M.; Wang, R.; Qiu, N.; Liu, Y.; Yang, H.; Ji, J.; Zhai, G. Chondroitin Sulfate-Based Nanoparticles for Enhanced Chemo-Photodynamic Therapy Overcoming Multidrug Resistance and Lung Metastasis of Breast Cancer. *Carbohydr. Polym.* **2021**, *254*, 117459.

(26) Abdullah, T. A.; Ibrahim, N. J.; Warsi, M. H. Chondroitin Sulfate-Chitosan Nanoparticles for Ocular Delivery of Bromfenac Sodium: Improved Permeation, Retention, and Penetration. *Int. J. Pharm. Investig.* **2016**, *6*, 96.

(27) Almalik, A.; Donno, R.; Cadman, C. J.; Cellesi, F.; Day, P. J.; Tirelli, N. Hyaluronic Acid-Coated Chitosan Nanoparticles: Molecular Weight-Dependent Effects on Morphology and Hyaluronic Acid Presentation. *J. Control. Release* **2013**, *172*, 1142–1150.

(28) Fakhari, A.; Phan, Q.; Berkland, C. Hyaluronic Acid Colloidal Gels as Self-Assembling Elastic Biomaterials. *J. Biomed. Mater. Res. - Part B Appl. Biomater.* **2014**, *102*, 612–618.

(29) Khaliq, N. U.; Park, D. Y.; Lee, H. J.; Oh, K. S.; Seo, J. H.; Kim, S. Y.; Hwang, C. S.; Lim, T.-H.; Yuk, S. H. Pluronic/Heparin Nanoparticles for Chemo-Photodynamic Combination Cancer Therapy through Photoinduced Caspase-3 Activation. *ACS Appl. Nano Mater.* **2018**, *1*, 2943–2952.

(30) Kenne, L.; Gohil, S.; Nilsson, E. M.; Karlsson, A.; Ericsson, D.; Helander Kenne, A.; Nord, L. I. Modification and Cross-Linking Parameters in Hyaluronic Acid Hydrogels - Definitions and Analytical Methods. *Carbohydr. Polym.* **2013**, *91*, 410–418.

(31) Freudenberg, U.; Liang, Y.; Kiick, K. L.; Werner, C. Glycosaminoglycan-Based Biohybrid Hydrogels: A Sweet and Smart Choice for Multifunctional Biomaterials. *Adv. Mater.* **2016**, *28*, 8861–8891.

(32) Feura, E. S. Polysaccharide Formulations for Localized Nitric Oxide Delivery, University of North Carolina at Chapel Hill, 2020.

(33) Uppal, R.; Ramaswamy, G. N.; Arnold, C.; Goodband, R.; Wang, Y. Hyaluronic Acid Nanofiber Wound Dressing-Production, Characterization, and in Vivo Behavior. *J. Biomed. Mater. Res. - Part B Appl. Biomater.* **2011**, *97*, 20–29.

(34) Malkov, V. A.; Serikawa, K. A.; Balantac, N.; Watters, J.; Geiss, G.; Mashadi-Hossein, A.; Fare, T. Multiplexed Measurements of Gene Signatures in Different Analytes Using the Nanostring NCounterTM Assay System. *BMC Res. Notes* **2009**, *2*, 80.

(35) Barclay, D.; Zamora, R.; Torres, A.; Namas, R.; Steed, D.; Vodovotz, Y. A Simple, Rapid, and Convenient Luminex™-Compatible Method of Tissue Isolation. *J. Clin. Lab. Anal.* **2008**, *22*, 278–281.

(36) Maloney, S. E.; McGrath, K. V.; Ahonen, M. J. R.; Soliman, D. S.; Feura, E. S.; Hall, H. R.; Wallet, S. M.; Maile, R.; Schoenfisch, M. H. Nitric Oxide-Releasing Hyaluronic Acid as an Antibacterial Agent for Wound Therapy. *Biomacromolecules* **2021**, *22*, 867–879.

(37) Privett, B. J.; Broadnax, A. D.; Bauman, S. J.; Riccio, D. A.; Schoenfisch, M. H. Examination of Bacterial Resistance to Exogenous Nitric Oxide. *Nitric Oxide* **2012**, *26*, 169–173.

(38) Rouillard, K. R.; Novak, O. P.; Pistiolis, A. M.; Yang, L.; Ahonen, M. J. R.; McDonald, R. A.; Schoenfisch, M. H. Exogenous Nitric Oxide Improves Antibiotic Susceptibility in Resistant Bacteria. *ACS Infect. Dis.* **2021**, *7*, 23–33.

(39) Dalton, T.; Dowd, S. E.; Wolcott, R. D.; Sun, Y.; Watters, C.; Griswold, J. A.; Rumbaugh, K. P. An In Vivo Polymicrobial Biofilm Wound Infection Model to Study Interspecies Interactions. *PLoS One* **2011**, *6*, 1–10.

(40) Malone-Povolny, M. J.; Maloney, S. E.; Schoenfisch, M. H. Nitric Oxide Therapy for Diabetic Wound Healing. *Adv. Healthc. Mater.* **2019**, *8*, 1801210.

(41) Guo, S.; DiPietro, L. A. Factors Affecting Wound Healing. *J. Dent. Res.* **2010**, *89*, 219–229.

(42) Blakytny, R.; Jude, E. The Molecular Biology of Chronic Wounds and Delayed Healing in Diabetes. *Diabet. Med.* **2006**, *23*, 594–608.

(43) Furman, B. L. Streptozotocin-Induced Diabetic Models in Mice and Rats. *Curr. Protoc.* **2021**, *1*, 1–21.

(44) Breyer, M. D.; Böttinger, E.; Brosius, F. C.; Coffman, T. M.; Harris, R. C.; Heilig, C. W.; Sharma, K. Mouse Models of Diabetic Nephropathy. *J. Am. Soc. Nephrol.* **2005**, *16*, 27–45.

(45) Miller, A. J.; Mihm, M. C. Melanoma. *N. Engl. J. Med.* **2006**, *355*, 51–65.

(46) Choudhari, S. K.; Chaudhary, M.; Bagde, S.; Gadbail, A. R.; Joshi, V. Nitric Oxide and Cancer: A Review. *World J. Surg. Oncol.* **2013**, *11*, 1–11.

(47) Fallacara, A.; Baldini, E.; Manfredini, S.; Vertuani, S. Hyaluronic Acid in the Third Millennium. *Polymers* **2018**, *10*, 701.

(48) Bhattacharya, D.; Svechkarev, D.; Souchek, J. J.; Hill, T. K.; Taylor, M. A.; Natarajan, A.; Mohs, A. M. Impact of Structurally Modifying Hyaluronic Acid on CD44 Interaction. *J. Mater. Chem. B* **2017**, *5*, 8183–8192.

(49) Bhattacharya, D. S.; Svechkarev, D.; Bapat, A.; Patil, P.; Hollingsworth, M. A.; Mohs, A. M. Sulfation Modulates the Targeting Properties of Hyaluronic Acid to P-Selectin and CD44. *ACS Biomater. Sci. Eng.* **2020**, *6*, 3585–3598.

(50) MatTek Life Sciences. *Melanoma Data Sheet*.

(51) Sahayata, V. N.; Bhavsar, N. V; Brahmbhatt, N. A. An Evaluation of 0.2% Hyaluronic Acid Gel (Gengigel ®) in the Treatment of Gingivitis: A Clinical & Microbiological Study. *Oral Health Dent. Manag.* **2014**, *13*, 779–785.

(52) Jentsch, H.; Pomowski, R.; Kundt, G.; Göcke, R. Treatment of Gingivitis with Hyaluronan.

J. Clin. Periodontol. **2003**, *30*, 159–164.

(53) Gontiya, G.; Galgali, S. R. Effect of Hyaluronan on Periodontitis: A Clinical and Histological Study. *J. Indian Soc. Periodontol.* **2012**, *16*, 184–192.

(54) El-Sayed, K. M. F.; Dahaba, M. A.; Aboul-Ela, S.; Darhous, M. S. Local Application of Hyaluronan Gel in Conjunction with Periodontal Surgery: A Randomized Controlled Trial. *Clin. Oral Investig.* **2012**, *16*, 1229–1236.

(55) Kandil, I.; Khashaba, O.; Eldaker, M.; Anes, M. Evaluation of Topical Subgingival Application of Hyaluronic Acid (Ha) Gel Adjunctive To Scaling and Root Planing (Srp) in the Treatment of Chronic Periodontitis. *Int. J. Adv. Res.* **2017**, *5*, 450–459.

(56) Polepalle, T.; Srinivas, M.; Swamy, N.; Aluru, S.; Chakrapani, S.; Chowdary, B. A. Local Delivery of Hyaluronan 0.8% as an Adjunct to Scaling and Root Planing in the Treatment of Chronic Periodontitis: A Clinical and Microbiological Study. *J. Indian Soc. Periodontol.* **2015**, *19*, 37–42.

(57) Johannsen, A.; Tellefsen, M.; Wikesjö, U.; Johannsen, G. Local Delivery of Hyaluronan as an Adjunct to Scaling and Root Planing in the Treatment of Chronic Periodontitis. *J. Periodontol.* **2009**, *80*, 1493–1497.

(58) Zou, X. H.; Foong, W. C.; Cao, T.; Bay, B. H.; Ouyang, H. W.; Yip, G. W. Chondroitin Sulfate in Palatal Wound Healing. *J. Dent. Res.* **2004**, *83*, 880–885.

(59) Yang, L.; Jing, L.; Jiao, Y.; Wang, L.; Marchesan, J. T.; Offenbacher, S.; Schoenfisch, M. H. In Vivo Antibacterial Efficacy of Nitric Oxide-Releasing Hyperbranched Polymers against Porphyromonas Gingivalis. *Mol. Pharm.* **2019**, *16*, 4017–4023.

(60) Oz, H. S.; Puleo, D. A. Animal Models for Periodontal Disease. *J. Biomed. Biotechnol.* **2011**, *2011*, 754857.

(61) Marchesan, J.; Girnary, M. S.; Jing, L.; Miao, M. Z.; Zhang, S.; Sun, L.; Morelli, T.; Schoenfisch, M. H.; Inohara, N.; Offenbacher, S.; Jiao, Y. An Experimental Murine Model to Study Periodontitis. *Nat. Protoc.* **2018**, *13*, 2247–2267.

(62) Chu, G.; Fogarty, G. M.; Avis, L. F.; Bergin, S.; McElduff, P.; Gillies, A. H.; Choi, P. Low Dose Heparin Lock (1000 U/ML) Maintains Tunnelled Hemodialysis Catheter Patency When Compared with High Dose Heparin (5000 U/ML): A Randomised Controlled Trial. *Hemodial. Int.* **2016**, *20*, 385–391.

(63) Moran, J. E.; Ash, S. R. Locking Solutions for Hemodialysis Catheters; Heparin and Citrate - A Position Paper by ASDIN. *Semin. Dial.* **2008**, *21*, 490–492.

(64) Wo, Y.; Brisbois, E. J.; Wu, J.; Li, Z.; Major, T. C.; Mohammed, A.; Wang, X.; Colletta, A.; Bull, J. L.; Matzger, A. J.; Xi, C.; Bartlett, R. H.; Meyerhoff, M. E. Reduction of

Thrombosis and Bacterial Infection via Controlled Nitric Oxide (NO) Release from S-Nitroso-N-Acetylpenicillamine (SNAP) Impregnated CarboSil Intravascular Catheters. *ACS Biomater. Sci. Eng.* **2017**, *3*, 349–359.

(65) Goudie, M. J.; Pant, J.; Handa, H. Liquid-Infused Nitric Oxide-Releasing (LINORel) Silicone for Decreased Fouling, Thrombosis, and Infection of Medical Devices. *Sci. Rep.* **2017**, *7*, 1–13.

(66) Pant, J.; Goudie, M. J.; Chaji, S. M.; Johnson, B. W.; Handa, H. Nitric Oxide Releasing Vascular Catheters for Eradicating Bacterial Infection. *J. Biomed. Mater. Res. - Part B Appl. Biomater.* **2018**, *106*, 2849–2857.

(67) Homeyer, K. H.; Goudie, M. J.; Singha, P.; Handa, H. Liquid-Infused Nitric-Oxide-Releasing Silicone Foley Urinary Catheters for Prevention of Catheter-Associated Urinary Tract Infections. *ACS Biomater. Sci. Eng.* **2019**, *5*, 2021–2029.

(68) Riccio, D. A.; Schoenfisch, M. H. Nitric Oxide Release: Part I. Macromolecular Scaffolds. *Chem. Soc. Rev.* **2012**, *41*, 3731–3741.